Computationally Efficient Modelling of Compound Flooding due to Tropical Cyclones with the Explicit Inclusion of Wave-Driven Processes

Research into the required processes and the implementation within the SFINCS model

T.W.B. Leijnse

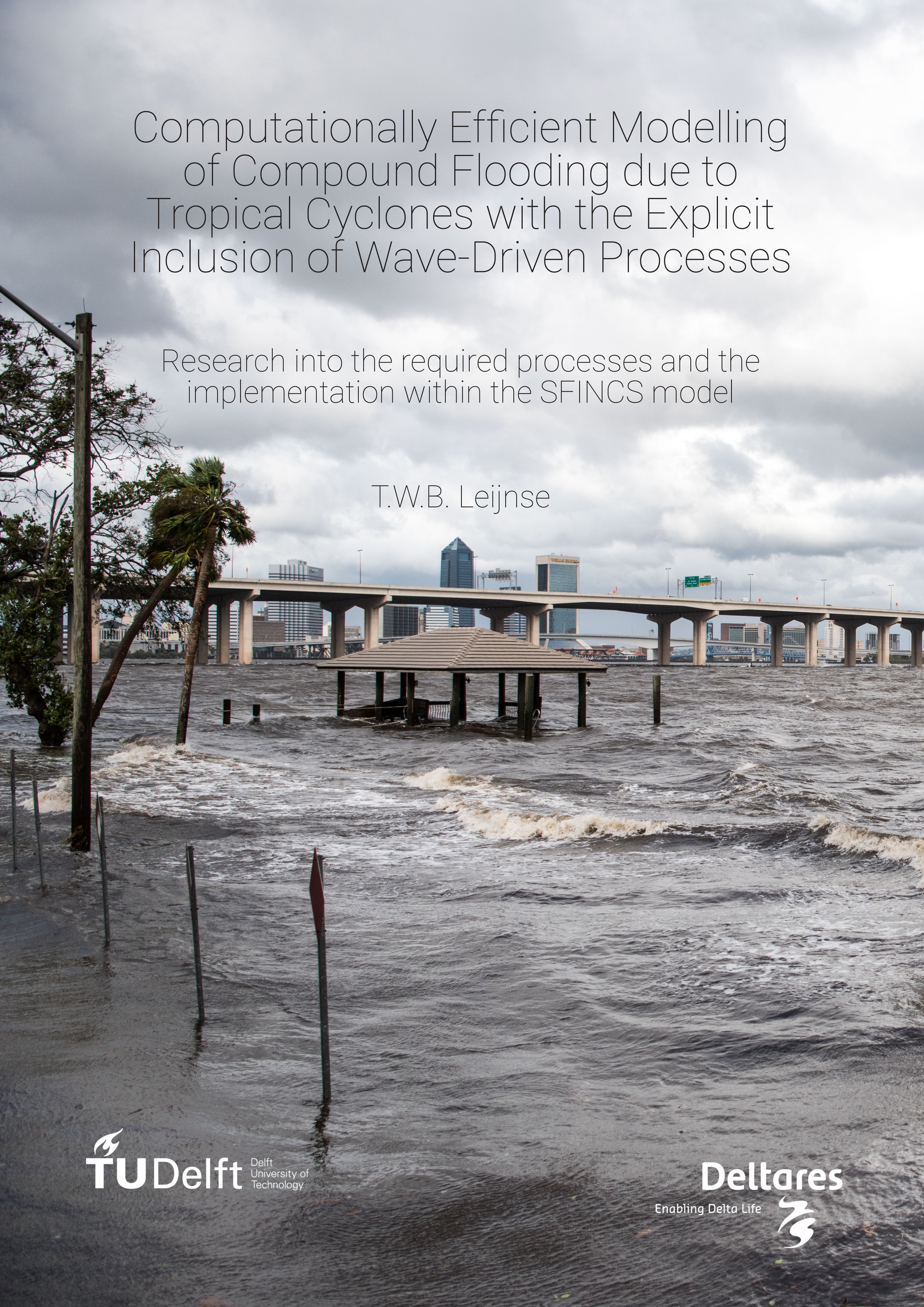

TU Delft Delft University of Technology

Deltares
Enabling Delta Life

Computationally Efficient Modelling of Compound Flooding due to Tropical Cyclones with the Explicit Inclusion of Wave-Driven Processes

Research into the required processes and the implementation within the SFINCS model

by

T.W.B. Leijnse

in partial fulfilment of the requirements for the degree of

Master of Science
in Hydraulic Engineering

at the Delft University of Technology (TU Delft),
to be defended publicly on Friday June 29, 2018 at 10:00 AM.

Student number:	4224035	
Chair committee:	Prof. dr. ir. A. J. H. M. Reniers,	TU Delft
Committee members:	Dr. ir. J. D. Bricker,	TU Delft
	Dr. ir. R. J. Labeur,	TU Delft
	Ir. C. M. Nederhoff,	Deltares
	Ir. M. van Ormondt,	Deltares

An electronic version of this thesis is available at `http://repository.tudelft.nl/`.

Cover: Powerful Hurricane Irma Slams Into Florida - Sean Rayford

Preface

This thesis completes the master of Hydraulic Engineering at the Delft University of Technology. The research has been carried out at Deltares in Delft, their cooperation is hereby gratefully acknowledged.

I want to thank my entire committee for their interest, feedback and time spend regarding my thesis. Thanks Ad for sharing your expertise regarding the project and leading the last meetings. Robert-Jan, thanks for all the feedback and keeping me sharp and thanks Jeremy for your interest in my work. Also many thanks to Kees as my daily supervisor, your everlasting enthusiasm to answer all my questions and reading my report is highly appreciated. And of course many thanks to you Maarten, for letting me work on your inspiring project regarding the SFINCS model and building stuff into the model even without having to ask for it. It was great to work with you all.

Furthermore I want to thank Ap at Deltares for your interest and motivation regarding compound flooding and the Jacksonville case study. Also thanks to you Robert, for sharing your knowledge regarding XBeach. In general I want to thank Deltares for the opportunity to carry out my thesis in their inspiring environment. On a related note, I want to thank my fellow graduate students at Deltares. Thanks for all the coffee breaks, distractions, student drinks and good times during my thesis, with as highlight winning the football tournament.

Last but definitely not least, special thanks to my friends, brother and parents for their support throughout this thesis and the many years before.

Tim Leijnse
Delft
June 2018

Abstract

Introduction

Tropical cyclones have a tremendous impact on coastal communities in terms of damage due to flooding and high wind velocities, as shown by the recent hurricane season of 2017. Coastal flooding due to tropical cyclones can be contributed to different types of forcing (e.g. high offshore water levels, rainfall, etc.), or multiple at the same time (i.e. compound flooding). Generally speaking, compound flooding is described as extreme events occurring in coastal areas where the interaction of high sea levels and large river discharges due to precipitation causes flooding (Wahl et al., 2015). However, in coastal areas, wave-driven flooding can also have a large contribution to flooding events (Roeber and Bricker, 2015).

Since a large part of the population lives in coastal areas, there is the need for accurate but fast flood forecasts and early warning systems. However, several days before landfall of a tropical cyclone, there is a lot of uncertainty in the forecast. Ideally, this uncertainty is taken into account in a probabilistic flood forecast, which requires fast models. Current modelling options are static models (e.g. bathtub approach), which are computationally inexpensive but simplistic because the dynamic aspects of flooding are not accounted for. Furthermore, there are advanced process-based models (e.g. Delft3D-FLOW (Lesser et al., 2004) or XBeach (Roelvink et al., 2009)), which are capable of hindcasting the dynamic process of compound flooding but are computationally expensive. An intermediate approach is the use of a semi-advanced model which solves all relevant processes in a computationally efficient manner. The SFINCS model is an example of such a model and is currently under development.

This research assesses how compound flooding due to tropical cyclones can be modelled in an accurate and computationally efficient way. Besides assessing the relevant physical processes, the implementation in the semi-advanced SFINCS model is tested. Also, the accuracy and efficiency is compared to advanced models for different types of compound flooding.

Relevant processes

For a traditional compound flooding event at Jacksonville, Florida, during Hurricane Irma (2017), the processes of high offshore water levels, wind and precipitation all have a significant influence in terms of flooding. For this case study, it is shown that the atmospheric pressure, Coriolis and viscosity terms of the momentum equation do not necessarily need to be solved to simulate the flooding accurately. The advection term needs to be solved when super-critical flow phenomena occur, but otherwise, it can be neglected. This is expected to be the case in case studies of compound flooding, as the case study of Jacksonville confirmed.

For a wave-driven flooding event at Hernani, the Philippines, during Typhoon Haiyan (2013), wave-driven processes have to be explicitly solved to simulate the flooding accurately. In order to simulate wave-driven flooding, the advection term needs to be included in the momentum equation. The non-hydrostatic pressure term needs to be solved when the spectrum of the incoming waves is incident wave-dominated, otherwise wave runup is underestimated.

Numerical implementation

These processes can be implemented in a semi-advanced model like SFINCS by using a first order explicit scheme based on LISFLOOD-FP (Bates et al., 2010). Combined with a simple drying and flooding mechanism, accurate results can be obtained. When including the advection term, this is the case under the conditions of a Froude number $Fr < 3$ and Manning friction coefficient $n > 0.02 s/m^{1/3}$. For lower friction values or higher Froude numbers, SFINCS becomes unstable. However, this does not limit the model application in the performed case studies were these conditions do not occur. Moreover, by using a swash zone modelling approach, realistic runup characteristics can be obtained while increasing computational efficiency by solving fewer grid cells. Using an indirect random wave forcing based on the wave spectra of incoming waves, similar realistic runup characteristics as with real water level time-series can be achieved. This has the advantage that time-series do not need to be supplied by a more advanced model. In the wave spectrum at the swash zone, the infragravity as well as the incident part of the wave spectra have to be included in order to achieve realistic runup characteristics.

Accuracy and efficiency

For the compound flooding event at Jacksonville, the semi-advanced SFINCS model is able to predict the flooding accurately. Comparing the modelled maximum water levels to the advanced Delft3D-FLOW model, a root mean squared difference (RMSD) of 6.4 cm is achieved. The computational efficiency meanwhile is 2 orders of magnitude faster in favour of SFINCS (i.e. +/- 100 times faster). For the wave-driven flooding event at Hernani, a similar speedup factor compared to the advanced XBeach model is obtained. Although, the accuracy is still less in this case compared to an advanced XBeach model. There is a negative bias in the predicted maximum water depths in the order of 20% with a RMSD in the order of 50 cm. The mean water depths are modelled without negative bias with a RMSD of 7 cm. The negative bias of the maximum water depths is mainly caused by an underestimation of the wave heights at the boundary of the swash zone model. At this location, only infragravity waves are still present and a combination of the swash zone modelling approach and numerical dissipation seems to cause the underestimation for this fringing reef type coast.

Conclusion

In this study, it is shown that using a semi-advanced model, like SFINCS, reasonable to good accuracy compared to more advanced models can be achieved in modelling compound flooding due to tropical cyclones. Meanwhile, the semi-advanced model is 2 orders of magnitude faster. Hereby the computational efficiency seems to get in the right range as needed for probabilistic flood forecasting within early warning systems while solving all relevant processes. Regarding the wave-driven processes, additional research is needed to improve the implementation within a semi-advanced model.

Contents

List of Figures

List of Tables

List of Acronyms and Symbols

Acronyms	Description
ADCIRC	ADvanced CIRCulation model
BTCS	Backward in Time, Central difference in Space
CFL	Courant-Friedrichs-Lewy
CPU	Central Processing Unit
CRM	Coastal Relief Model
DEM	Digital Elevation Model
DW	Deep Water
GEBCO	General Bathymetric Chart of Oceans
GLOFFIS	GLObal Flood Forecasting Information System
GLOSSIS	GLObal Storm Surge Information System
GPU	Graphics Processing Unit
IG	Infragravity
JONSWAP	JOint North Sea WAve observation Project
FINEL	Finite Elements model
LFP	LISFLOOD-FP
LIE	Local Inertia Equations
MPI	Message Passing Interface
MSL	Mean Sea Level
NARR	North American Regional Reanalysis
NED	National Elevation Dataset
NetCDF	Network Common Data Form
NH	Non-Hydrostatic
NHC	National Hurricane Centre
NHSSWE	Non-Hydrostatic Simplified Shallow Water Equations
NHSWE	Non-Hydrostatic Shallow Water Equations
NS	Navier-Stokes
OET	Open Earth Tools
OpenMP	Open Multi Processing
PPWL	Points Per Wave Length
RMS	Root Mean Squared
RMSD	Root Mean Squared Difference
RMSE	Root Mean Squared Error
SFINCS	Super-Fast INundation of CoastS
SI	Scatter Index
SLR	Sea Level Rise
SW	Shallow Water
SWAN	Simulating Waves Nearshore
SWASH	Simulating Waves till Shore
SSWE	Simplified Shallow Water Equations
SWE	Shallow Water Equations
SWL	Still Water Level
TC	Tropical cyclone
XBeach	Extreme Beach behaviour model
XBSB	XBeach SurfBeat model
XBNH	XBeach Non-Hydrostatic model
XBNH+	XBeach Non-Hydrostatic+ quasi 2-layer model

Roman symbols	Description	Unit
adv,x	Advection term in x-direction	$[m^2/s]$
adv,y	Advection term in y-direction	$[m^2/s]$
c	Wave celerity	[m/s]
C	Chezy friction coefficient	$[m^{1/2}/s]$
C_d	Drag coefficient	$[-]$
d	Bottom depth	$[m]$
dx	Grid resolution in x-direction	$[m]$
dy	Grid resolution in y-direction	$[m]$
eps	Flow depth limiter in XBeach	$[m]$
E	Wave energy in the water column	$[J/m^2]$
f	Frequency	$[Hz]$
f_s	Sampling frequency	$[Hz]$
f_p	Peak frequency	$[Hz]$
Fr	Froude number	$[-]$
Fr,x	Froude number of the flow in x-direction	$[-]$
Fr,y	Froude number of the flow in y-direction	$[-]$
g	Gravitational acceleration	$[m^2/s]$
h	Water depth	$[m]$
$h_{u,thresh}$	Flow depth limiter in SFINCS	$[m]$
H_s	Significant wave height	$[m]$
H_{m0}	Spectral significant wave height	$[m]$
$H_{m0,ig}$	Spectral significant infra-gravity wave height	$[m]$
$H_{m0,inc}$	Spectral significant incident wave height	$[m]$
H_0	Deep water wave height	$[m]$
k	Wave number	$[rad/m]$
L	Wave length	$[m]$
L_0	Deep water wave length	$[m]$
n	Ratio of group velociy and phase velocity	$[-]$
n	Manning friction coefficient	$[s/m^{1/3}]$
q_{inf}	Infiltration discharge	$[m^3/s]$
q_{src}	Point discharge	$[m^3/s]$
q_x	Momentum flux in x-direction	$[m^2/s]$
q_y	Momentum flux in y-direction	$[m^2/s]$
$rugdepth$	Runup gauge flow depth threshold value in XBeach	$[m]$
R_{max}	Maximum runup elevation	$[m]$
$R_{2\%}$	Two percent exceedance value of runup elevation	$[m]$
s	JONSWAP directional spreading coefficient	$[-]$
S_{ig}	Significant infra-gravity swash	$[m]$
S_{inc}	Significant incident swash	$[m]$
t	Time	$[s]$
T_p	Peak wave period	$[s]$
u	Flow velocity in x-direction	$[m/s]$
v	Flow velocity in y-direction	$[m/s]$
w	Flow velocity in z-direction	$[m/s]$
W	Wind speed	$[m/s]$
x	Location in x-direction	$[m]$
y	Location in y-direction	$[m]$
z_b	Bed level	$[m]$
z_s	Surface elevation	$[m]$
$z_{s,b}$	Surface elevation at the boundary	$[m]$

Greek symbols	Description	Unit
α	Heuristic time step reduction factor	$[-]$
β	Offshore slope	$[-]$
$\overline{\eta}$	Mean setup	$[m]$
γ	Breaker index	$[-]$
μ	Mean value of sample	$[-]$
ϕ	Random phase	$[rad]$
ρ_a	Density of air	$[kg/m^3]$
ρ_w	Density of water	$[kg/m^3]$
σ	Standard deviation	$[-]$
τ	Shear stress	$[N/m]$
θ	Numerical weighing factor	$[-]$
ξ	Irribarren number	$[-]$
ζ	Free-surface elevation	$[m]$

1

Introduction

1.1. Background

Tropical cyclones (TCs) have a tremendous impact on coastal communities in terms of damage due to flooding and high wind velocities, as shown by the recent hurricane season of 2017 (Harvey: 125 billion USD, Irma: 50 billion USD, Maria: 90 billion USD (NOAA, 2018)). Tens of millions of people around the world are exposed to coastal flooding from TCs (Mousavi et al., 2011). This is expected to increase due to a combination of projected TC intensity and frequency (Emanuel, 2013), sea level rise (Stocker, 2014) and expected population expansion along low-lying coastal areas (Curtis and Schneider, 2011). Coastal flooding and inundation during TCs can be contributed to different types of forcing or multiple at the same time (i.e. compound flooding).

Generally speaking, compound flooding is described as extreme events occurring in coastal areas where the interaction of high sea level and large river discharge due to precipitation causes extreme flooding (Wahl et al., 2015). However, in coastal areas, wave-driven flooding can also have a large contribution to occurring flooding events. An example is the village of Hernani, the Philippines, which was severely flooded during Typhoon Haiyan (2013) solely because of dynamic wave processes (Roeber and Bricker, 2015).

Early warning systems (EWS) are widely accepted as one of the components of effective flood risk management. These systems can greatly reduce the adverse consequences of flooding and they are relatively inexpensive compared to structural measures. Operational forecasting systems that predict river discharges and/or coastal water levels have therefore become common practice. In order to forecast the impacts of TCs, different models are needed and therefore a model train as depicted in Figure 1.1 is used. Apart from the compound flooding modelling, also models for the prediction of hurricane tracks, corresponding hydrodynamics and the translation towards the nearshore are needed.

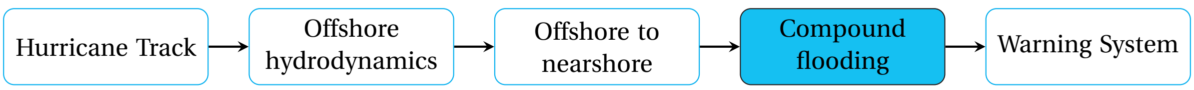

Figure 1.1: Model train of an early warning system for compound flooding, this thesis focusses on the flooding part

When modelling the impact of TCs, there has to be accounted for involved uncertainties. In every step of the model train, there is uncertainty regarding the input and output of the corresponding model. One of the largest uncertainties in forecasting the impacts of TCs is the actual path and intensity of a TC, this uncertainty can be significant (Powell and Aberson, 2001). The larger the lead time before landfall, the larger this uncertainty is. By modelling TC ensembles (i.e. different TC tracks and intensities), a probabilistic flood forecast can be given. In order to do this, the model train should be fast enough. Currently, it is often not possible to accurately forecast the impacts of extreme weather events, mainly because of computational limitations.

1.2. Problem description

This thesis focusses on modelling the flooding part of the model train. Currently, advanced process-based models like Delft3D-FLOW (Lesser et al., 2004) and XBeach (Roelvink et al., 2009) are capable of accurately modelling the flooding in hindcasting studies. However, the main downside of these advanced models is that they are computationally expensive and can therefore often not be used in real-time forecasting applications. Moreover, flood forecasting should be accomplished with enough lead time to allow people to take measures to protect themselves from flooding or take appropriate actions.

On the other hand, there are static models using the Planar Surface Projection Method (i.e. bathtub method), which are computationally inexpensive and can, therefore, be used in real-time applications and probabilistic flood calculations. However, the downside of these types of models is that the dynamic aspects of flooding are not accounted for. Therefore static models are generally not very accurate in the description of flood events. Accuracy in flat areas is for instance often low because landscape roughness effects are not included (Ramirez et al., 2016). Also, precipitation, relevant for compound flooding, is not included.

An intermediate approach that aims to combine the best of both types of models is the semi-advanced model. The relevant processes for modelling compound flooding due to TCs are solved, but this is done in a computationally efficient way. An example of such a computationally efficient model is LISFLOOD-LP (Bates et al., 2010). The downside of this model is that wave-driven processes are not included. A model aimed to fill this research gap is SFINCS (Super-Fast INundation of CoastS), but this is still in its development phase. The model is developed with computationally efficiency in mind while solving all processes relevant for compound flooding with the explicit inclusion of wave-driven processes.

1.3. Research objectives

The objective of this thesis is to assess the accuracy and efficiency of a semi-advanced model, like SFINCS, in simulating compound flooding due to TCs. In other the obtain reliable results, all relevant physical processes (e.g. precipitation, wave-driven processes) should be identified and taken into account in the model. The computational time should be as limited as possible in order to apply the model in an EWS, ensuring enough lead time and/or to take uncertainties in TCs into account. These research objectives can be formulated into the main research question:

> *How can compound flooding due to tropical cyclones be modelled in an accurate and efficient way?*

As sub-questions the following is stated:

1) *What are the relevant physical processes of compound flooding due to tropical cyclones?*

2) *How can the relevant physical processes be implemented in a semi-advanced model like SFINCS?*

3) *What is the accuracy and efficiency of a semi-advanced model like SFINCS compared to advanced models for different types of compound flooding?*

1.4. Methodology

In this thesis, the methodology as presented in Figure 1.2 will be followed. At first, the relevant processes for compound flooding due to TCs are identified via a literature review. Thereafter the relevant flow and wave processes are individually tested in conceptual tests. Thereby, the focus is on what the implication is of simplifying the shallow water equations (SWE; e.g. by neglecting advection) on flow- and wave-related processes. For these tests, the implementation of the semi-advanced SFINCS model is compared with the advanced XBeach model. To assess the accuracy and efficiency of a semi-advanced model like SFINCS compared to an advanced model for real flooding events, two case studies will be carried out. The first case study focusses on the wave-driven flooding at Hernani, the Philippines, during Typhoon Haiyan (2013). For this event, the results of SFINCS are compared with the advanced XBeach model. The second case study focusses on the compound flooding at Jacksonville during Hurricane Irma (2017). Here the accuracy and efficiency of SFINCS are compared to the advanced Delft3D-FLOW model.

1.5. Report outline

This report starts with a literature review in Chapter 2 that discusses the relevant processes for compound flooding and gives a comparison of how these are modelled by different models. In Chapter 3 a description is given of the semi-advanced SFINCS model. This includes the numerical implementation, the model

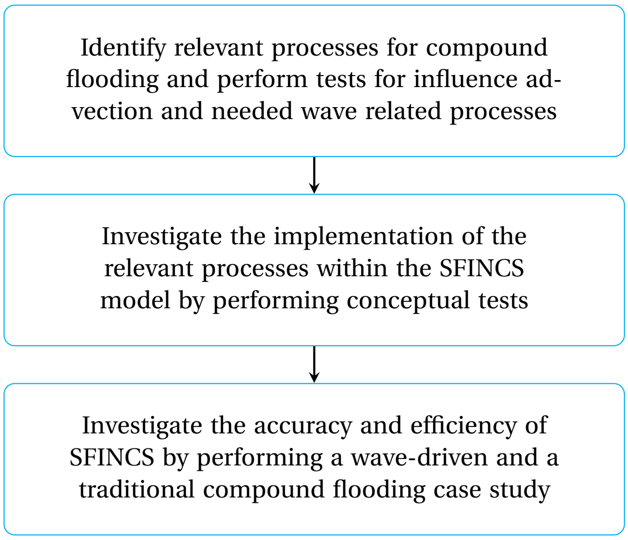

Figure 1.2: Flow chart of the methodology

limitations and the computational efficiency. Thereafter in Chapter 4 the results of multiple conceptual tests regarding relevant flow- and wave-related processes are discussed. In Chapter 5 the results of the case studies at Hernani and Jacksonville are discussed. The discussion, conclusions and recommendations are discussed in Chapters 6, 7 and 8. Appendices A to F provide more information regarding the setup of the different models and tests. Also, additional results are included that are not presented in the main report. More information regarding the models of Chapters 2 and 3 is given in Appendix A. For the flow- and wave related tests of Chapter 4 this is included in Appendices B and C respectively. Also other processes like precipitation are tested in simple tests in Appendix D. For the Hernani and Jacksonville case studies of Chapter 5 this is included in Appendices E and F.

2

Literature review

This literature review describes which different processes are important for compound flooding due to TCs and how this is implemented in different models. At first a description is given about the characteristics of compound flooding due to TCs and the relevant processes in Section 2.1. This is then used to explain the complication in modelling these processes and how different models deal with this in Section 2.2.

2.1. Relevant processes for compound flooding

2.1.1. Introduction

The first step into modelling compound flooding due to TCs is understanding what happens during such an event and what processes are important. This section first describes what tropical cyclones are and which corresponding causes for compound flooding do occur. Thereafter the relevant physical processes are discussed separately. This is done by distinguishing offshore, wave, flow and other related processes, see Figure 2.1. Hereby flow is important for all the processes, but for convenience it is discussed in a separate section.

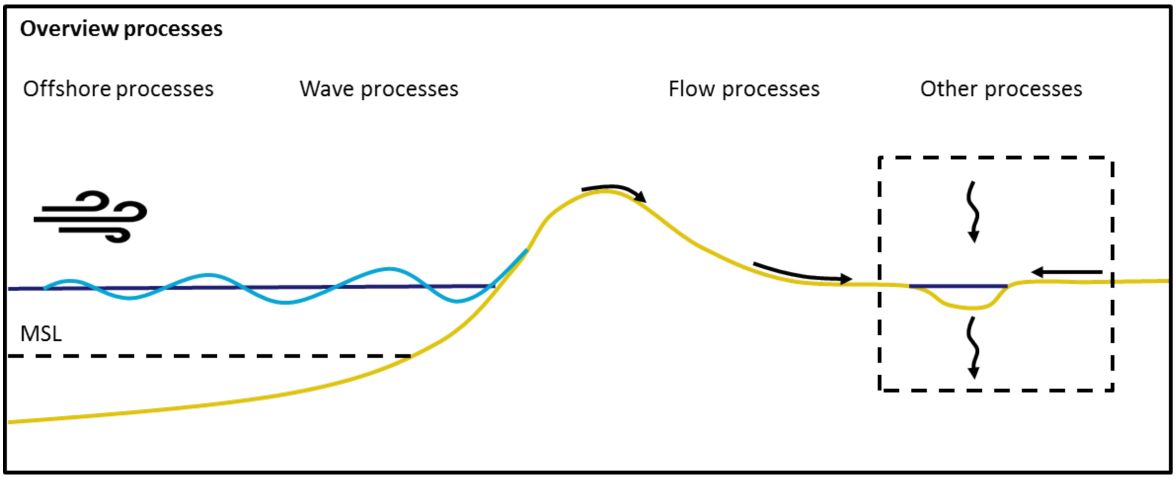

Figure 2.1: Schematic overview of the relevant processes for compound flooding due to TCs

2.1.2. Tropical cyclones

TCs are rotating low-pressure systems that develop over warm waters of oceans. They are classified as a TC when cyclonic storms have 1-minute averaged maximum wind speeds over 64 knots, measured at the standard measuring height of 10 m. TC usually have a diameter of around 320 km (Graham and Riebeek, 2006) and have three specific parts which can be distinguished, see Figure 2.2. The eye, the centre of the storm, is typically 30-60 km in diameter. Here the winds are only moderate but with the lowest pressure, which can drop to 880 mbar compared to the normal average of 1020 mbar (Holland, 1980). Further from the eye there is the 'eyewall', from about 15 to 50 km from the centre. This part is the most destructive part of the

TC where the precipitation is highest and the wind the strongest. Even further there is the region called the 'rainbands', which is the most outer part of the TC and can extend about 160 km from the eye. Precipitation rates associated with TC can be surpass 250 mm in one day (Zehnder, 2015). Due to the low pressure in the eye, a pressure gradient develops between the eye and the surrounding air. This leads to an air flow away from the eye, which can become very strong and is subjected to the Coriolis force. Sustained winds can be as high as 240 km/hr, with wind gusts which can exceed 320 km/hr.

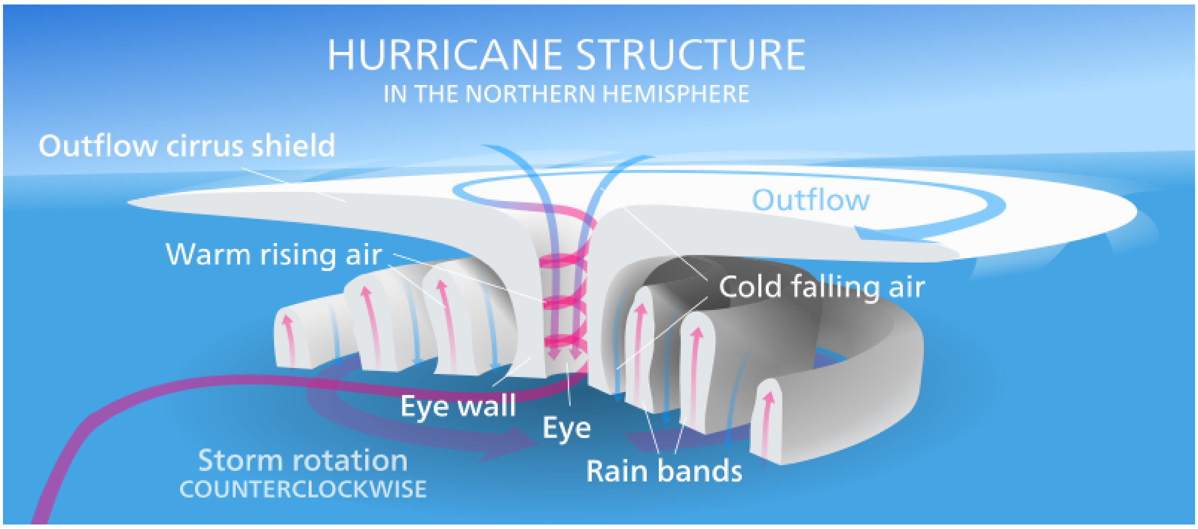

Figure 2.2: Schematic overview of the structure of a tropical cyclone, courtesy of Wikimedia (2018) (CC BY 3.0)

2.1.3. Compound flooding due to tropical cyclones

Compound flooding due to TCs can occur because of different types of forcing. For instance it can be dominated by offshore processes like storm surge in combination with tides. Hereby the spatial scales are in the order of 100 km and the time scale in the order of days. That storm surge can have a large impact on coastal flooding could for instance be seen during Hurricane Katrina, where the storm surge exceeded 10 m in several locations along the Mississippi coastline (Fritz et al., 2007). It can also be the case that the generated wave field by the TC is so extreme that wave related processes like runup and overtopping are the dominant cause of inundation. These processes have much smaller spatial and time scales. The first is in the order of metres to kilometres and the latter in the order of hours. The relevance of the wave-driven processes can be indicated using the town of Hernani, the Philippines, during the Typhoon Haiyan. Here large infragravity (IG) waves hit the coast, which was not accounted for by forecasting surge models but did heavily damage the coast (Roeber and Bricker, 2015). Apart from the forcing coming from the seaside, also other processes originating from the land can be dominant. Extreme precipitation events associated with TC can also lead to inundation in coastal zones, whereby large river discharges can occur as well. Hereby the spatial scale can be in the order of 100 km and the time scale of the river run-off in the order of a week. In some extreme cases, rainfall totals of 760 mm in a five-day period have been reported (Zehnder, 2015). When catchments are large enough, a significant amount of water can be transported towards the rivers.

Furthermore local effects like wind induced setup and seiches can be important. Both can for instance play a role in estuaries or shallow bays, with spatial scales of tens of kilometres and time scales of hours. In Tacloban, the Philippines, during Typhoon Haiyan the storm surge was in the order of 6 m, with a significant contribution of the seiche oscillation of the water surface inside Leyte Gulf (Mori et al., 2014). Apart from there being only one dominant forcing, a combination of multiple types of forcing at the same time can occur. This compound flooding can significantly increase the extend of flooding. Hereby non-linear interactions make it a dynamic phenomena. At that moment different types of forcing with different spatial and time scales meet. Because there are different types of forcing that can occur within one TC, it can vary spatially which process is dominant. For instance during the mentioned Typhoon Haiyan, the most casualties were in Tacloban where storm surge in combination with seiches were the dominant forcing. But further east in Hernani, wave-driven processes were the dominant forcing.

This overview shows that the different types of causes for compound flooding have different spatial and time scales, which can make the situation complex when multiple types of forcing occur at the same time. Additionally there are processes on larger time and spatial scales like sea level rise and climate systems such as El Niño which can contribute to coastal flooding, but these are not considered. Also the discussed processes can lead to overwash and breaching of dune coasts (e.g. De Vet et al. (2015)). However, morphology is not considered in this thesis. After this general overview of the types of compound flooding, the individual types of relevant processes are discussed.

2.1.4. Offshore processes

Although this thesis focusses on modelling compound flooding, an understanding of the offshore processes is important. Various processes play a role offshore, which have to be modelled as well. The output of these offshore models is then used for the input of the coastal flooding models. The relevant processes discussed can be seen in Figure 2.3.

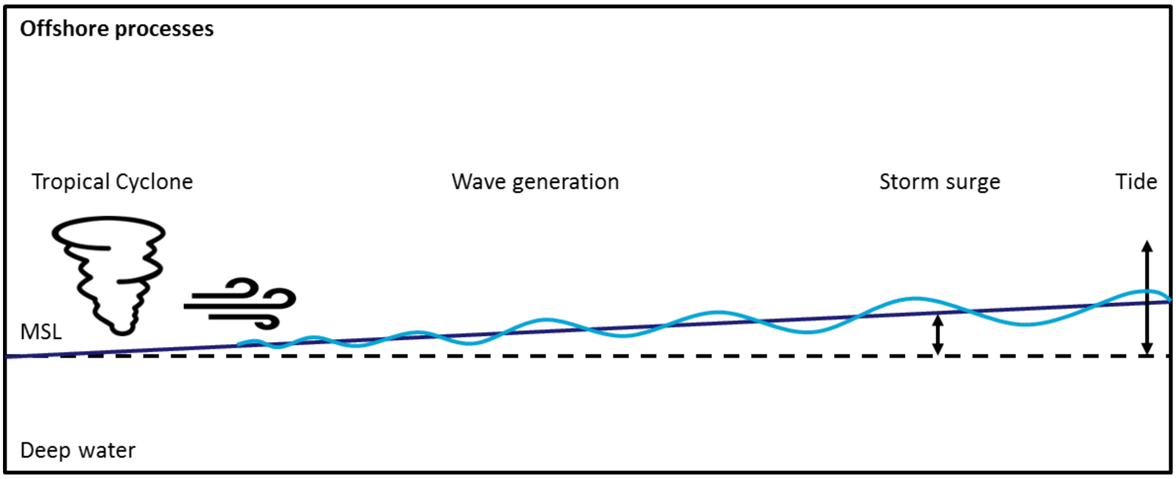

Figure 2.3: Schematic overview of the relevant offshore processes for compound flooding

Wave generation

Wave generation depends on the sustained wind speeds in combination with a fetch. The wind field of a TC can be described relative to the position, direction and velocity of the eye of the cyclone. The atmospheric pressure at the sea surface in the eye with respect to the ambient pressure and the radius to the maximum wind (Holthuijsen, 2010). The wave field is then only a function of these parameters. Thereafter the main factor for the development of extreme waves is the fetch from the eye to the considered coast. The longer this fetch is, the more waves can develop towards a fully developed sea state. With enough fetch the significant wave heights associated with TC can exceed 20 m in Deep Water (DW) (Caires and Sterl, 2005). Therefore, extreme wave heights due to TCs can have a significant impact on coastal flooding, when the majority of the wave energy is maintained when travelling into Shallow Water (SW).

Storm surge

Another significant factor in coastal flooding is storm surge. This is caused by the pressure drop due to the TC or can be wind-driven. The low pressure in and around the eye of a TC leads to an elevation of the local water level for a limited area. Generally the effect is mostly offshore and smaller compared to the wind-driven storm surge (NHC, 2018). For instance during Typhoon the pressure-driven storm surge was approximately 1 m while the total storm surge was more than 5 m (Mori et al., 2014). Also the effect of the pressure-driven storm surge was limited to within 50 km from the eye.

During wind-driven storm surge momentum from the atmosphere is transferred to the ocean results in the generation of storm surge (Vatvani et al., 2012). Hereby the wind exerts a stress onto the water surface, resulting in flow in the direction of the main wind direction. Near the coast the water can be piled up and lead to elevated water levels. These can be in the order of several meters and can thereby cause coastal flooding. Especially in (shallow) bays the storm surge can build up extremely because the wind setup is inversely related to the water depth, leading to strong surge levels. For instance during hurricane Ike the maximum storm surge was in the order of 4-5 m (Rego and Li, 2010). The orders of magnitude can thus be significantly, but storm surge is a very dynamic and complex phenomena. Depending on the exact track of the TC, wind direction, the bathymetry and local situation with shielding by for instance islands, the magnitudes can vary heavily.

Tides

Usually the areas where TC occur are also prone to tidal elevations of a few meters. The mean spring tidal range in TC dominated areas is in the range of 0-4 m (Davies, 1977), locally this can be even higher. When storm surge coincides with the occurrence of an elevated water level due to tides, the extend of coastal flooding increases significantly. Especially if there is a spring tide during the peak of a storm, the maximum water levels can become dangerously high. The most important factor here is timing. When the peak of the storm surge coincides with the peak of a spring tide, the results can be catastrophic.

2.1.5. Wave-driven processes

Apart from these offshore causes for inundation of storm surge in combinations with tides, also wave-driven processes can have an impact on coastal flooding. For instance, Stockdon et al. (2007) modelled that for hurricanes Bonnie (1998) and Floyd (1999), storm surge and wave runup both accounted for ~48% of the maximum total water levels. The remaining 4% was attributed to astronomical tides. This indicates that wave-driven processes can be a significant contributor to compound flooding during TC. Therefore, an understanding of the relevant processes (e.g. wave propagation from DW-SW and wave-driven runup) are vital in order to simulate coastal flooding due to waves correctly. To comprehend the processes of runup and overtopping, also the transformation of waves from DW to SW needs to be understood. This transformation is different for sandy- and reef-type coasts. For sandy-type coasts various processes change the characteristics of the offshore generated wave fields when moving from DW to coastal zones with SW. Shoaling and wave breaking affect the waves, wave-induced setup elevates the mean water level and in the swash zone lead to runup. The discussed processes are illustrated in Figure 2.4. For reef-type coasts IG waves are generated at the reef crest, which is discussed afterwards.

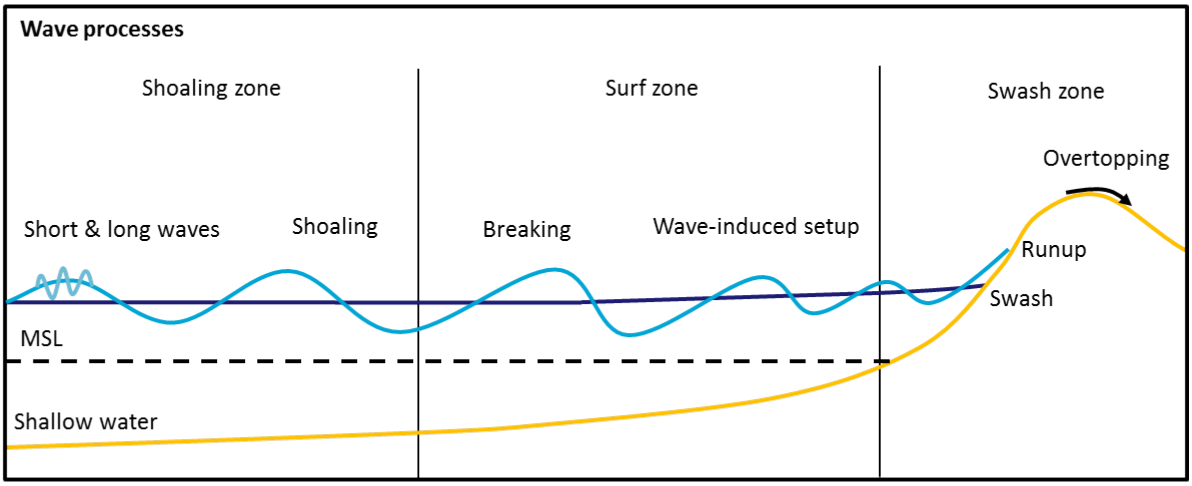

Figure 2.4: Schematic overview of the relevant wave-driven processes for compound flooding

Shoaling zone

Incident waves are generated offshore and as they travel their wave spectrum shifts because of frequency and direction dispersion. Also there are the IG wave motions that are generated by wave groups (Roelvink, 1993), which is also referred to as 'surf beat'. Spatial variations of wave energy density on the scale of wave groups result in gradients in radiation stresses, which act as a force on the water column. This force is then balanced by an opposing water-level gradient, which leads to local variations of the mean water level that are bound to the wave groups. Because they are bound, these IG waves travel with the wave group velocity. The relation is such that the IG water level is highest under the lowest wave group radiation stresses. Therefore the bound long waves are 180 degrees out of phase with the incident wave envelope. Generally IG waves have wave periods around 25 and 250 s.

Entering from offshore, the first zone waves encounter after the deep water region is the shoaling zone where the waves start to feel the bottom. Due to the decreasing water depth the wave speed and length of the wave decrease according to the dispersion relationship. Thereby the wave height increases, in theory it can become infinitely high. In reality, however, the increase of wave height in the shoaling zone is limited by dissipation due to wave breaking, which is discussed next.

Surf zone

In the surfzone, waves start to break when a certain critical steepness is reached, after which wave energy is dissipated through white-capping. It has been found that the bed slope plays an important role on the way the process of breaking takes place. Depending on the Iribarren parameter $\xi = \frac{tan(\beta)}{\sqrt{H_0/L_0}}$ (Battjes, 1974), which represents the ratio of the bed slope and the wave steepness. With this parameter ξ different breaker types like surging, collapsing, plunging and spilling breaker types can be distinguished.

Propagating waves do not only carry energy across the ocean surface but momentum as well. Using the concept of radiation stress, the depth-averaged and wave-averaged flux of momentum (Longuet-Higgins and Stewart, 1964), wave-induced setup and set-down can be explained. The cross-shore gradient of radiation stress increases in landward direction which means that at the water column a resulting force due to radiation stresses is acting in offshore direction. Balancing this leads to a small water level difference called set-down, which is present up to the point where the waves break. Thereafter the magnitude of the cross-shore gradient of radiation stress decreases rapidly due to wave breaking and the process reverses (Bosboom and Stive, 2015). This leads to an increased water level in the surf and swash zone called wave-induced setup. The amount of setup can build up to be in the order of a few meters and can therefore be of influence for coastal flooding.

Swash zone

In the swash zone waves eventually reach the coast and cause the waterline to be varying in time. Here swash is often referred to as vertical fluctuations around a temporal mean of the location of the moving waterline (Stockdon et al., 2006). The highest location in cross-shore direction is referred to as runup. The swash and the runup signal can both be split in contributions by incident and IG components. It is found that often IG wave energy dominates close to the shoreline and that thereby the amount of runup is largely influenced by IG waves, see for example Thornton and Guza (1982). It is also known that this IG wave runup has a significant influence on for instance morphological changes due to avalanching of dunes during extreme events (Roelvink et al., 2009). Besides the importance of the IG wave dominance, runup is also dependent on the beach slope and therefore grain size (e.g. gravel or fine sandy beach). This determines dissipative (mild slopes) of more reflective conditions (steep slopes). For the damage at coasts because of TC, runup can also be directly important when buildings are present close to or on the beach.

During extreme conditions a large runup can lead to overtopping of dunes or dikes. Sequentially, overtopping can lead to coastal flooding. Overtopping is possible when the dunes/dike crest height is lower than the runup. Sallanger (2000) defines four different storm regimes. During the swash and collision regime, runup doesn't overtop the dunes/dikes. During the overwash and inundation regime waves are able to overtop the dunes/dikes. The amount of overtopping is usually measured in discharges and can differ between soft (dunes) and hard (revetments) types of coast. The resulting overwash and inundation by overtopping consequently also changes the morphology of dunes, but this is not considered in this research.

Reef hydrodynamics

For reef-type coasts the hydrodynamic response is different than for a sandy-type coasts, which results in different wave characteristics in the swash zone. The bottom slope in front of a reef is generally much steeper than of a sandy-type coast. Due to this steep slope there is a narrow breaking zone at the crest of the reef where most waves break, see Figure 2.5. Wave breaking at the crest leads to an increase of the mean water level on the reef flat due to wave-induced setup (Gerritsen, 1980). When the location of the breakpoint at the reef crest oscillates due to wave groups, IG waves are generated in offshore and onshore directions (Péquignet et al., 2009). These IG waves generally do not break when travelling over the reef flat and are the dominant waves in the swash zone. Besides wave breaking, also energy is dissipated because of friction due to the limited water depth at the reef flat. The exact response of a reef is dependent on the width of the reef flat, the bottom slope in front of the reef, bottom roughness at the reef flat, water levels and offshore wave conditions (Quataert et al., 2015).

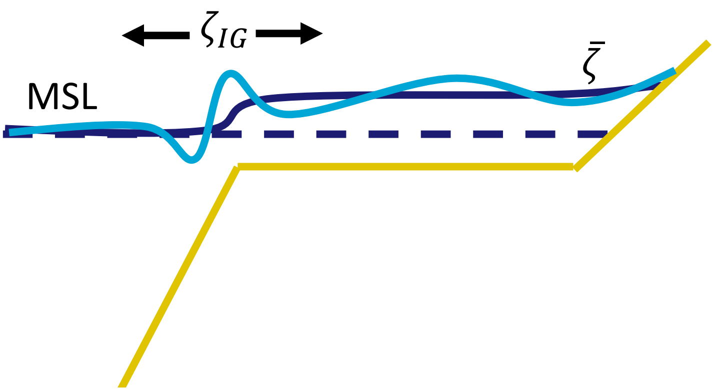

Figure 2.5: Schematic overview of the reef hydrodynamics, based on De Ridder (2018). Indicated is MSL (Mean Sea Level) with the dashed line, the mean wave-induced setup with the dark line and the generation of IG waves in both directions at the reef crest by the light blue line.

2.1.6. Flow related processes

Here the flow related processes are discussed from the perspective of wave overtopping. However, flow is also important in most other discussed processes. The flow of water in shallow water depths is described by the Shallow Water Equations (SWE), hereby assuming a hydrostatic pressure distribution. This assumption can be made for flows where the vertical scale is significantly smaller compared to the horizontal scale. Generally this is valid for the occurring phenomena, the validity of the assumption is further discussed in Section 3.5.4. If the hydrostatic static pressure assumption is not valid, the flow can be described by adding the non-hydrostatic (NH) pressure term giving the NHSWE (Non-Hydrostatic SWE). The flow related to the overtopping discharges can flow over land or water, which results in slightly different characteristics. Also sudden transitions like small canals or weirs can have an influence on the flow, as well as large objects like buildings. The relevant processes discussed can be seen in Figure 2.6.

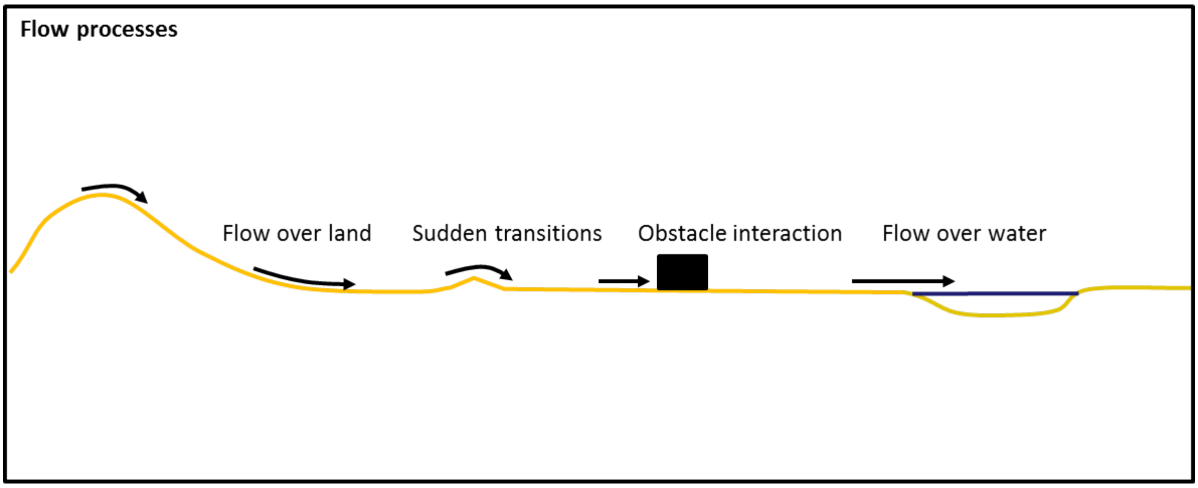

Figure 2.6: Schematic overview of the relevant flow related processes for compound flooding

Flow over land

The SWE can be written as follows (Liang et al., 2006):

$$
\begin{aligned}
&\frac{\partial \zeta}{\partial t} + \frac{\partial q_x}{\partial x} + \frac{\partial q_y}{\partial y} = 0 \\
&\underbrace{\frac{\partial q_x}{\partial t}}_{local\,inertia} + \underbrace{\frac{\partial u q_x}{\partial x} + \frac{\partial v q_x}{\partial y}}_{advection} - \underbrace{f q_y}_{Coriolis} - \underbrace{\upsilon_h\left(2\frac{\partial^2 q_x}{\partial x^2} + \frac{\partial^2 q_x}{\partial y^2} + \frac{\partial^2 q_y}{\partial x \partial y}\right)}_{horizontal\,viscosity} + \underbrace{gh\frac{\partial \zeta}{\partial x}}_{gradient} = \underbrace{F_x}_{friction} \\
&\underbrace{\frac{\partial q_y}{\partial t}}_{local\,inertia} + \underbrace{\frac{\partial u q_y}{\partial x} + \frac{\partial v q_y}{\partial y}}_{advection} + \underbrace{f q_x}_{Coriolis} - \underbrace{\upsilon_h\left(\frac{\partial^2 q_y}{\partial x^2} + 2\frac{\partial^2 q_y}{\partial y^2} + \frac{\partial^2 q_x}{\partial x \partial y}\right)}_{horizontal\,viscosity} + \underbrace{gh\frac{\partial \zeta}{\partial y}}_{gradient} = \underbrace{F_y}_{friction}
\end{aligned}
\tag{2.1}
$$

The top row is the continuity equation and the two below the momentum equations in x- and y-direction respectively. Hereby 'gradient' stands for the water level gradient. The momentum equations are of the conservative form with $q_x = hu$ and $q_y = hv$ for the momentum fluxes in x- and y-direction, with u and v as the flow velocities in x- and y-direction. Furthermore h is the water depth $h = \zeta + d$, where ζ is the free-surface elevation with respect to the reference level $z = 0$ and d the bottom depth. Furthermore υ_h is the horizontal viscosity, g the gravitational acceleration and f the Coriolis coefficient. F_x and F_y are the friction terms in x- and y-direction. This right hand side can also include external forcing.

Apart from the full SWE there are also simplified versions of the SWE by neglecting certain terms. Neglecting the horizontal viscosity terms gives the Simplified Shallow Water Equations (SSWE), which is the inviscid version of the Saint-Venant equations in 1D (Barre de Saint Venant, 1871). Further neglecting the advection terms gives the Local Inertial Equations (LIE) and then neglecting the local acceleration gives a quasi-steady approximation called the Diffusive Wave Equations (DWE). Finally neglecting the pressure gradient within the water level gradient and linearising the terms gives the Kinematic Wave Equations (KWE). At that point a balance between the bed gradient and the friction slope remains. In case you neglect the whole momentum equations, you are basically left with a bathtub model. For this research into modelling compound flooding, the Coriolis term is not important for flow in the swash zone and on land. The validity of this assumption is discussed in Section 3.5.2.

Other situations

The SWE are also applicable in other types of situations. For flow over wetlands or already inundated areas the influence of friction is small since the bed is wet, so that the dynamical forces are dominant (Stelling and Duinmeijer, 2003). This means that the roughness of the underground, dependent on for instance rural or urban areas, plays a smaller role. Also related is whether the underground is spatially uniform or full of sudden transitions. Flow transitions occur around weirs, small dams or canals and can lead to hydraulic jumps because of flow contraction and expansion. This results in super-critical flow conditions, analogous to dam break type situations. This gives challenges for model formulations because these only locally occurring fast flow conditions have to be modelled (Stelling and Duinmeijer, 2003). In urbanised areas, also the interaction with structures becomes important. In these urbanised areas there is not only wave/flow impact against buildings, but the flow is also diverted around these building. The flow is then confined and led through streets, increasing the flow velocities. Also man-made structures like bridges or large dams can influence the flow, as well as local channels and sewage systems. In general the same SWE can be used in these types of situations.

2.1.7. Other processes

Besides the inundation in coastal areas caused by processes originating from the sea, there are also other processes which can contribute to the extend of flooding. Besides the impact from the sea you can have the presence of high precipitation, river discharge and wind-induced setup, or even a combination of these. The considered processes are shown in Figure 2.7.

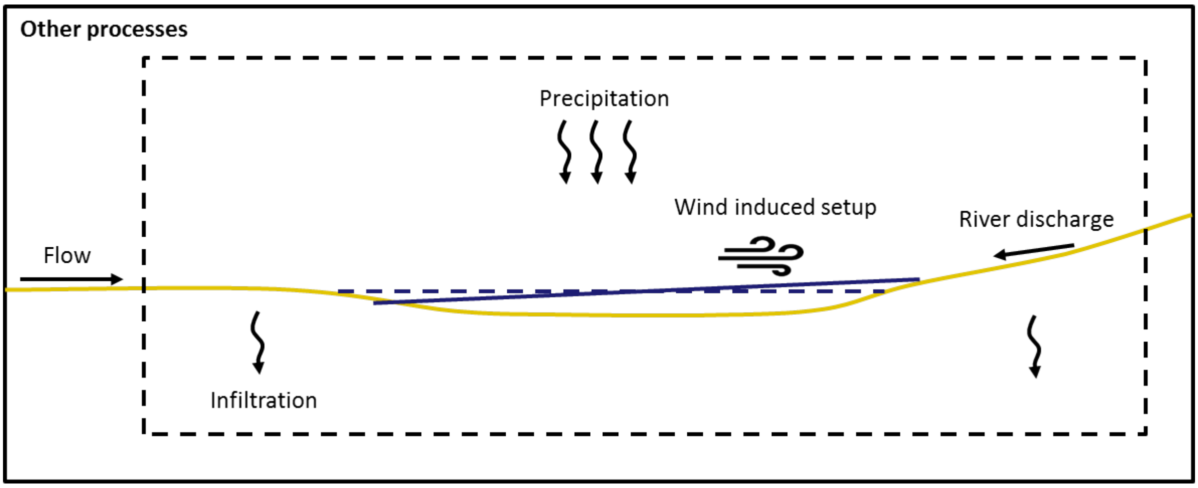

Figure 2.7: Schematic overview of the relevant compound flooding related processes

Infiltration

Once there is flow or precipitation over an area, a part of this water infiltrates into the soil. The infiltration rates are usually an order smaller than for instance the peak rainfall rates during a storm, but especially for longer storm durations the infiltration of water can become important for the total water balance. The infiltration rate can for instance be described using the Horton's equation (Horton, 1941). Maximum initial infiltration rates are in the order of 5 to 125 mm/hr (Moynihan and Vasconcelos, 2014) depending on soil type, moisture level and vegetation. During high intensity precipitation events, the soil can however become saturated limiting the infiltration rates. Spatial variance is hereby also important. It does matter whether the underground consists of soil or concrete. In the case of urban areas, infiltration rates ar a lot smaller than for rural areas. However, the water associated with precipitation is transported using sewer systems, as long as the systems can cope with the amount of water. These sewer systems can therefore become relevant for compound flooding in urban areas, but to limit the scope this is not considered in this thesis.

Precipitation

Besides destructive wind forcing, a TC often also results in a high cumulative rainfall. These quantities can be extreme, for instance during the recent hurricane Harvey 660 mm of rain fell in 24 hours in the Houston area (Kimmelman, 2017). Such a large amount of precipitation combined with for instance storm surge plays a significant role in the occurrence of compound flooding. Therefore it is relevant to include the process of precipitation when modelling these types of problems. Generally there is a correlation between the intensity of TCs and precipitation rates (Knutson and Tuleya, 2004). There is also stated that it is likely that in the future average precipitation rates within 100 km of the storm centre will increase. Associated with the precipitation is runoff to rivers and corresponding river discharge. The runoff coefficient is a widely used and often reported parameter describing basin response, on either an annual or an event basis (Blume et al., 2007). The related field of hydrology is hereby relevant, but falls outside the scope of this research. Global precipitation and runoff will increase 5.2 and 7.3 % respectively by 2050 (Wetherald and Manabe, 2002).

Wind-induced setup

Apart from the storm surge and wave generation associated with the wind forcing of tropical cyclones, also in the coastal region and the hinterland the wind can have an effect. In these areas there can be larger water bodies like lakes and estuaries or inundated lands because of compound flooding. Because these are shallow areas in general, wind-induced setup can be significant because of the inverse relation to the water depth, see Equation 2.2. Here the relation for the mean wind-induced setup for a basin of length L is shown.

$$\Delta\bar{\eta} = 0.5L \cdot \frac{\tau_{wind}}{\rho_w g h} \quad \text{with} \quad \tau_{wind} = C_d \rho_a W^2 \tag{2.2}$$

Hereby ρ_w and ρ_a are the densities of water and air, g the gravitational acceleration, h the water depth, C_d the drag coefficient and W the wind speed. Because the resulting setup can be significant wind forcing should not only be included in offshore models, but also in the compound flooding models closer to and around the shore.

2.2. Modelling compound flooding due to tropical cyclones

To illustrate how these relevant processes can be modelled, it is discussed how these are implemented in different models. At first an introduction regarding the complication of modelling compound flooding is given in Section 2.2.1. Thereafter the modelling approaches of different types of static/semi-advanced/advanced models is discussed in Sections 2.2.2 to 2.2.4. There is concluded with a discussion regarding the different modelling approaches in Section 2.2.5.

2.2.1. Introduction

Modelling compound flooding due to TC can be quite complex because multiple processes with different time and spatial scales are important. As was shown in Figure 1.1, multiple steps have to be taken before compound flooding can be modelled. At first the track of the TC has to be predicted with a large scale meteorological model. Multiple models exist, which will try to model the 'best track' as good as possible. This includes also the associated wind, pressure and precipitation fields. Then the wind and pressure data are fed into a model capable of modelling offshore hydrodynamics. This is also a large scale model capable of modelling surge and wave generation. Usually a coupled flow and wave model is used. This gives the hydrodynamic conditions relatively close to the coast, but still outside of the surf zone. When waves are significantly high, their transformation through the surf zone has to be modelled by a nearshore model. The output of these models is then used as input for the compound flooding model, or solved within the same model.

For the compound flooding model the difficulty is that the multiple processes that can be important require different approaches. This is, for example, related to the different spatial and time scales of the different processes as mentioned before. For instance for the adequate modelling of runup along the coast, grid resolutions in the order of 50 PPWL (Points Per Wave Length) are needed (Zijlema, 2015). For situations where only surge is important such a small resolution along the coast is not needed. When rivers or estuaries are present in the area of interest the resolution of the model should be in the order of tens or hundreds of meters so that their bathymetry is properly accounted for. When the area of interest contains cities or other urban areas, the grid resolution is also important. When flooding needs to be modelled on the scale of streets, the grid resolution should be accordingly small.

In terms of time scales, the needed time-steps for modelling compound flooding are apart from the spatial scales dependent on the type of flow occurring. For instance the flow during surge events is deemed similar as that of tidal flow. This is normally sub-critical flow, where the time-steps do not need to be extremely small. For wave-driven processes however, the local flow in the swash zone can become super-critical. To model this correctly you need shorter time-steps than for surge-driven flooding. River and precipitation runoff can generally be described as sub-critical, but at local contractions or dams the flow can become super-critical. Infiltration and wind-induced setup are relatively slow processes.

Different types of static/semi-advanced/advanced models, model the relevant processes in different ways. To gain insight multiple models are discussed, thereby comparing what processes are solved. As a static model the bathtub approach is considered. For the semi-advanced models LISFLOOD-FP, SFINCS and 3Di are considered. As advanced models ADCIRC, Boussinesq-type (here Funwave), Delft3D, FINEL, MIKE, SWASH and XBeach are considered. All models can be run in 1D mode, which is not considered. The results are summarised in Table A.1 of Appendix A.

2.2.2. Static models

The bathtub approach, also known as the Planar Surface Projection Method, is a fast and static approach to model coastal flooding. It simply compares a flood water elevation level and the bathymetry of the land to determine what areas get flooded. Hereby the dynamic aspects of flooding are not accounted for. The flood elevation level can for instance be estimated using empirical relations for wave setup and runup or storm surge levels from offshore models. The advantage of this approach is that it is really fast because it is not process-based, but there are some limitations performance and functionality wise. For instance flow velocities related to safety of people cannot be calculated. Also roughness effects of different landscapes on flooding cannot be captured (Ramirez et al., 2016). It is also stated that especially for topographically flat regions large errors can occur, which negatively influences the correctness of the predicted impacts. Also other processes like precipitation, river discharges or wind-induced setup cannot be taken into account. Nowadays there is shifted more to dynamic over static modelling approaches, but in the past it has been applied regularly (e.g. Barnard et al. (2009)).

2.2.3. Semi-advanced models

LISFLOOD-FP (LFP, Bates et al. (2010)) is a fast model especially designed for modelling rivers and flood plain inundation. As flow processes the normal solver consists of the LIE, so neglecting advection and viscosity. In terms of compound flooding it is only able to model river discharge. Precipitation or wind-induced setup is not possible as far as known to the author. Therefore it does not include offshore or wave related processes. However, the possibility to nest a LFP model within an XBeach model has been established.

SFINCS is a computationally efficient semi-advanced process-based model that is capable of simulating compound flooding in coastal areas. By default, the model resolves the LIE equations and includes simple implementations for infiltration, river discharge, rainfall and wind stresses. The model can be forced with water level time-series to include offshore water levels and waves. Hereby it only solves the swash zone to improve computational efficiency. To model wave-driven runup, overtopping and flooding correctly, advection can be included (SFINCS-SSWE). The numerical side of the model is further optimised by using for instance single precision and a limited overhead. The SFINCS model is explained much more elaborately in Chapter 3.

The model 3Di (Schuurmans and Leeuwen, 2017) has a slightly different angle on the modelling of flooding and inundation. Using a subgrid and quadtree approach it makes it possible to calculate flooding with high-resolution results in a short timespan. It is merely developed for water management and river flooding and can even model sewer systems during high precipitation events. As far as known to the author it is not possible to include offshore or wave related processes. For the flow it uses the SSWE and apart from wind-induced setup it can accurately account for the other relevant processes, especially in urban areas.

2.2.4. Advanced models

For the advanced models a distinction is made between SWE-models that use the hydrostatic pressure assumption, Boussinesq-models and NHSWE-models

SWE-models

ADCIRC (ADvanced CIRCulation model, Luettich et al. (1992) is a SWE-model that is used for applications like the prediction of storm surge and tides. It can be used in 2DH or 3D mode, can be coupled with SWAN (Simulating WAves Nearshore, Booij et al. (1999)) and has an unstructured grid. In terms of offshore processes it can model cyclones, storm surge and tides. It solves most wave processes in the nearshore and most other processes are implemented as well.

Delft3D (Lesser et al., 2004) is an advanced model to model multiple types of problems in coastal systems. It can be used in 2DH or 3D mode, contains the Delft3D 4 and Flexible Mesh suite, Furthermore it includes long-term morphology and has many added processes. It is capable of modelling offshore processes using SWAN in Delft3D-WAVE for the wave generation. For the wave processes nearshore it solves some of the processes like wave-induced setup, however it does not solve individual (incident) waves. For the flow processes it uses the SWE and all the other processes can be modelled.

MIKE (Warren and Bach, 1992) is another model for 2DH (MIKE 21) and 3D modelling (MIKE 3) of flow and waves. Both have a combination of different modules regarding flow- and wave modelling as well as other functionalities. There can for instance be chosen between boussinesq (MIKE BW) or spectral (MIKE SW) wave solvers. Furthermore unstructured grids and for parallel processing Graphics Processing Units (GPU) are possible to speed up the computations. Normally the model has a SWE-solver and most other processes are included.

Boussinesq-models

Boussinesq-type models, like Funwave (Bruno et al., 2009), can be seen as an extension of the SWE (Bosboom and Stive, 2015). Boussinesq-models account, to some extend, for the NH pressure distribution and have thereby as an advantage over the SWE that frequency dispersion is included. Wind forcing and all wave processes are included, but generally not other processes like precipitation and infiltration.

Non-hydrostatic SWE-models

FINEL (Finite Elements model, Labeur and Pietrzak (2005)) is a model similar to Delft3D in terms in functionalities, but then it uses a finite element method in combination with an irregular triangular/tetrahedral mesh. FINEL2D is the 2DH version capable of modelling morphology changes and FINEL3D is the 3D non-hydrostatic flow solver without morphology. Using SWAN it can also model wave-induced flows, individual waves are not solved in the model. The flow processes solve the NHSWE for the 2D version and the complete NS (Navier-Stokes) equations for the 3D version. As far as known to the author processes like precipitation and infiltration or not included in the model.

SWASH (Simulating Waves till Shore, Zijlema et al. (2011)) is a model capable of simulating different types of flow problems. It is a 3D non-hydrostatic model capable of simulating most offshore and wave processes. In terms of flow it uses the NHSWE, in a similar way as XBeach. The model does not include other processes like precipitation or infiltration.

XBeach (Extreme Beach behaviour, Roelvink et al. (2009)) is an advanced, process-based model which is suited to model processes close to the shore. As a major difference with the other models it can not only model morphological changes due to sediment transport, but also due to avalanching by dune impact during extreme conditions. The model is also successfully applied at more steep and coral reef types of coast (e.g. Quataert et al. (2015)). The model can be run in a 2DH SurfBeat (XBSB) mode solving the IG waves, a 2DH Non-Hydrostatic (XBNH) mode additionally solving incident waves (Roelvink et al., 2017) and a quasi 2-layer Non-Hydrostatic-plus (XBNH+) mode with an added hydrostatic second layer for better dispersive behaviour. The model cannot resolve offshore processes since it is designed for nearshore conditions, but there it solves all the relevant wave processes. Hereby including the incident waves (by using XBNH/XBNH+) improves the ability of the model to predict swash and runup for intermediate and reflective beaches (De Beer, 2017). In terms of flow it uses the SWE for XBSB and NHSWE for XBNH(+). It contains a part of the other relevant processes. For instance river discharge included, wind only spatially uniform and infiltration only when using the non-hydrostatic groundwater model. A process like precipitation is not yet included.

2.2.5. Discussion

Comparing these models it is clear that there are different models for different purposes, although they are all related to modelling compound flooding. Static models are the fastest option, but do not account for the dynamic aspects of flooding. On the other hand there are numerous advanced models that are process-based and take the dynamic aspects into account. There can be observed that are generally two types of models: large scale circulation models and nearshore wave models. The former are models like ADCIRC, Delft3D, FINEL and MIKE which are able to model the offshore processes as well as most other processes like wind-induced setup and precipitation. The latter are models like Boussinesq-type, SWASH and XBeach which are more suitable for nearshore modelling by solving individual waves. Usually they solve IG as well as incident waves using the NHSWE. These nearshore models do generally lack the relevant other processes which the circulation models solve, or do it in a very simplified way. For additional information regarding methods, recent advances and uncertainty analysis in flood inundation modelling see Teng et al. (2017).

All these advanced models have showed in numerous papers to be capable of hindcasting compound and wave-driven flooding. However, the exact computational efficiency of all these models is hard to assess. It is known from personal experience that advanced models like Delft3D and XBeach are too computationally expensive to use for probabilistic forecasting. The SWASH model is quite similar to the XBNH model and therefore also assumed to be too expensive as well. According to Zijlema (2018) Boussinesq-type models are several times slower than SWASH, while MIKE is similarly fast. Since FINEL and ADCIRC are similar models to Delft3D and MIKE, their computational efficiency is deemed to be similar.

Semi-advanced models can fill the research gap of computationally inexpensive models, that however do include the dynamics of flooding. There are semi-advanced models available for modelling river inundation like LFP and 3Di, but these do not include the needed processes relevant for coastal flooding. To model all types of compound flooding there is the need for a nearshore-type model that includes waves and all relevant other processes like wind stresses and precipitation. Thereby the large scale circulation flow is modelled using one of the other models, whose output is forced as boundary conditions in the semi-advanced model. Additionally, this model should also be developed with efficient modelling in mind. Therefore there is the research gap, which the semi-advanced SFINCS model tries to fulfil. In order to make this semi-advanced model an accurate and efficient one, more research is needed on what processes are really relevant and how they should be implemented.

3

The SFINCS Model

This chapter gives an overview of the current state of the SFINCS model. At first a general description is given regarding the approach of the model in Section 3.1. Thereafter the implementation of the flow, wave and other processes is discussed in Sections 3.2 to 3.4. This is followed by a discussion of the model limitations regarding the made assumptions and simplifications in Section 3.5. There is concluded with how the computational efficiency is achieved in Section 3.6.

3.1. Modelling approach

SFINCS is a computationally efficient semi-advanced process-based model that is capable of simulating compound flooding in coastal areas. The model is developed by Maarten van Ormondt and based on the LFP model as described in Bates et al. (2010). The desired application is to use SFINCS to model compound flooding for coastlines of hundreds to thousands of kilometres in an computationally inexpensive way. By doing so ensemble forecasting and quick hazard assessments regarding compound flooding become within reach, which is currently not possible. The computational efficiency is achieved by including only the needed processes of compound flooding in a simple and fast numerical solver. By default, the model resolves the LIE equations (SFINCS-LIE) and includes simple implementations for infiltration, river discharge, rainfall and wind stresses. The model can be forced with water level time-series to include offshore water levels and waves. Hereby it only solves the swash zone and the hinterland to improve computational efficiency. To model wave-driven runup, overtopping and flooding correctly, advection can be included (SFINCS-SSWE). The numerical side of the model is further optimised by using for instance single precision and a limited overhead.

3.2. Flow-related processes

At first the implementation of the flow related processes is discussed, starting with the SWE in general form and numerical grid as implemented in SFINCS in Section 3.2.1. Thereafter the order of calculating the different equations within SFINCS is used to discuss the implementation of the numerical grid and flooding and drying mechanism, the momentum equations, the addition of advection, the continuity equation and the stability condition in Sections 3.2.2 to 3.2.6.

3.2.1. Shallow water equations

The original implementation of the depth-averaged SWE in SFINCS consists of a decoupled system with a 2D continuity equation and two 1D momentum equations. The system has three equations and three unknowns, water level ζ and fluxes in x- and y-direction q_x and q_y. Neglecting the advection, Coriolis and viscosity terms, specifying the friction component and using linearised terms gives the LIE in conservative form (Bates et al., 2010):

$$\frac{\partial \zeta}{\partial t} + \frac{\partial q_x}{\partial x} + \frac{\partial q_y}{\partial y} = 0 \tag{3.1}$$

$$\frac{\partial q_x}{\partial t} + gh\frac{\partial \zeta}{\partial x} + \frac{gn^2 q_x^2}{h^{7/3}} = 0 \tag{3.2}$$

$$\frac{\partial q_y}{\partial t} + gh\frac{\partial \zeta}{\partial y} + \frac{gn^2 q_y^2}{h^{7/3}} = 0 \tag{3.3}$$

With $h = \zeta + d$, where ζ is the free-surface elevation $[m]$ with respect to the reference level $z = 0$, h is the water depth $[m]$ and d the bottom depth $[m]$. q_x and q_y are the fluxes in x- and y-direction $[m^2/s]$. n is the Manning roughness coefficient $[s/m^{1/3}]$ and g is the gravitational acceleration $[m/s^2]$. The $\frac{\partial \zeta}{\partial t}$ term replaces $\frac{\partial h}{\partial t}$ because the bottom level is constant in time (no morphology). Apart from the equations of LFP, the implementation in SFINCS has been expanded with a wind forcing term, as well as an advection term. The latter is added to the numerical implementation as an user option, see Section 3.2.4 for more information. For more information on the validity of the made assumptions, see Section 3.5.

3.2.2. Numerical grid

Numerically, SFINCS uses a staggered equidistant rectilinear grid in Cartesian coordinates (a so-called Arakawa C-grid (Arakawa and Lamb, 1977)). The free-surface elevation and bed level are defined in the cell centres, as shown in Figure 3.1. Contrastingly, the flow depths and fluxes are described on the cell edges. The use of this staggered grid is beneficial for the implementation of the boundary conditions. It also requires the interpolation of the water and bed levels to the cell edges for the computation of the flow depth difference between two adjacent cells.

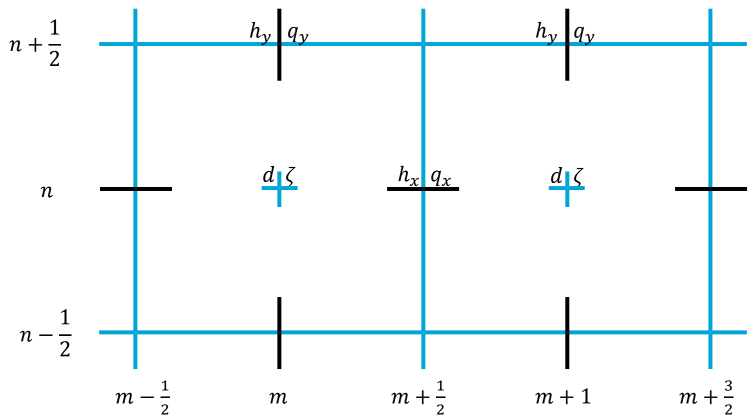

Figure 3.1: Numerical staggered grid of SFINCS with variables and locations. Fluxes between cells are shown in black.

The first step in the loop of the numerical solver is calculating the water depths in the cell edges (see Figure A.1 of Appendix A.4). For SFINCS this is based on the implementations in the Delft3D-FLOW model (Lesser et al., 2004). For the water and bed levels only the mean option is possible:

$$h^{t-\Delta t}_{x,m+\frac{1}{2},n} = \frac{\zeta^{t-\Delta t}_{m,n} + \zeta^{t-\Delta t}_{m+1,n}}{2} - \frac{d^{t-\Delta t}_{m,n} + d^{t-\Delta t}_{m+1,n}}{2} \tag{3.4}$$

Which is set not to become lower than zero. For $h^{t-\Delta t}_{y,m,n+\frac{1}{2}}$ a similar expression is used. The advection terms and momentum fluxes are only updated if this water depth h at the cell edge is larger than a certain flux limiter, $h_{u,thresh} = 0.05m$(default). This criteria therefore acts as a flooding and drying mechanism. There is no separate flooding and drying scheme as used in some other models.

3.2.3. Momentum equations

After the water depths in the cell edges are known, the momentum fluxes can be calculated as in Equations 3.5 and 3.6. An explicit scheme for both momentum equations is used, which is first order accurate in space and time and inherent (conditionally) stable. The descritisation of the momentum equations has some additional smoothing with respect to Bates et al. (2010), using a Lax-scheme to improve stability of the numerical solution. The state is smoothed by using a weighted average of the flux at the previous time level and the average of the fluxes in the adjacent cells also at that time level, controlled by a factor θ (default: $\theta = 0.9$). $\tau^t_{x,m+\frac{1}{2},n}$ and $\tau^t_{y,m,n+\frac{1}{2}}$ are the wind stresses in x- and y- direction acting on the water (see Section 3.4.4). Also the advection term 'adv' is added when specified by the user, which is explained in Section 3.2.4. Combined the momentum equations are:

$$q^t_{x,m+\frac{1}{2},n} = \frac{\left[\theta \cdot q^{t-\Delta t}_{x,m+\frac{1}{2},n} + (1-\theta) \cdot \frac{q^{t-\Delta t}_{x,m+\frac{3}{2},n} + q^{t-\Delta t}_{x,m-\frac{1}{2},n}}{2}\right] - \Delta t \cdot g \cdot h^{t-\Delta t}_{x,m+\frac{1}{2},n}\left[\frac{\zeta^{t-\Delta t}_{m+1,n} - \zeta^{t-\Delta t}_{m,n}}{\Delta x}\right] + \tau^t_{x,m+\frac{1}{2},n} \cdot \Delta t - adv_x \cdot \Delta t}{1 + \Delta t \cdot g \cdot n^2 \frac{\left|q^{t-\Delta t}_{x,m+\frac{1}{2},n}\right|}{\left(h^{t-\Delta t}_{x,m+\frac{1}{2},n}\right)^{7/3}}} \tag{3.5}$$

$$q^t_{y,m,n+\frac{1}{2}} = \frac{\left[\theta \cdot q^{t-\Delta t}_{y,m,n+\frac{1}{2}} + (1-\theta) \cdot \frac{q^{t-\Delta t}_{y,m,n+\frac{3}{2}} + q^{t-\Delta t}_{y,m,n-\frac{1}{2}}}{2}\right] - \Delta t \cdot g \cdot h^{t-\Delta t}_{y,m,n+\frac{1}{2}}\left[\frac{\zeta^{t-\Delta t}_{m,n+1} - \zeta^{t-\Delta t}_{m,n}}{\Delta y}\right] + \tau^t_{y,m,n+\frac{1}{2}} \cdot \Delta t - adv_y \cdot \Delta t}{1 + \Delta t \cdot g \cdot n^2 \frac{\left|q^{t-\Delta t}_{y,m,n+\frac{1}{2}}\right|}{\left(h^{t-\Delta t}_{y,m,n+\frac{1}{2}}\right)^{7/3}}} \tag{3.6}$$

3.2.4. Advection

In case the user specifies that the advection terms should be included in the momentum equations, the terms are calculated prior to the momentum equations. The user is given the option to add only the 1D advection term (SFINCS-SSWE 1D) for modelling in 1D, or the 2D advection term (SFINCS-SSWE 2D) for modelling in 2D. The former saves some computational time when calculating in 1D, since the 2D term is known to be zero beforehand. Per direction you then have an expression for the advection term, see Equation 3.7.

$$adv_x = adv_{x,1D} + adv_{x,2D} \quad \text{and} \quad adv_y = adv_{y,1D} + adv_{y,2D} \tag{3.7}$$

The 1D advection term is included using the Upwind scheme:

$$adv_{x,1D} = \frac{\left[\frac{q^{t-\Delta t}_{x,m+\frac{1}{2},n} q^{t-\Delta t}_{x,m+\frac{1}{2},n}}{h^{t-\Delta t}_{x,m+\frac{1}{2},n}} - \frac{q^{t-\Delta t}_{x,m-\frac{1}{2},n} q^{t-\Delta t}_{x,m-\frac{1}{2},n}}{h^{t-\Delta t}_{x,m-\frac{1}{2},n}}\right]}{\Delta x} \quad \text{for} \quad q^{t-\Delta t}_{x,m+\frac{1}{2},n} > 0 \tag{3.8}$$

$$adv_{x,1D} = \frac{\left[\frac{q^{t-\Delta t}_{x,m+\frac{3}{2},n} q^{t-\Delta t}_{x,m+\frac{3}{2},n}}{h^{t-\Delta t}_{x,m+\frac{3}{2},n}} - \frac{q^{t-\Delta t}_{x,m+\frac{1}{2},n} q^{t-\Delta t}_{m+\frac{1}{2},n}}{h^{t-\Delta t}_{x,m+\frac{1}{2},n}}\right]}{\Delta x} \quad \text{for} \quad q^{t-\Delta t}_{x,m+\frac{1}{2},n} < 0 \tag{3.9}$$

With a similar expression for $adv_{y,1D}$, but then varying in y-direction. Secondly the 2D advection term can be added using the Central Difference scheme:

$$adv_{x,2D} = v^{t-\Delta t}_{y,m+\frac{1}{2},n} \frac{\left[q^{t-\Delta t}_{x,m+\frac{3}{2},n} - q^{t-\Delta t}_{x,m-\frac{1}{2},n}\right]}{2\Delta y} \tag{3.10}$$

With for the flow velocity in y-direction, since this was not yet calculated at this point:

$$v^{t-\Delta t}_{y,m+\frac{1}{2},n} = \frac{\left[q^{t-\Delta t}_{y,m,n+\frac{1}{2}} + q^{t-\Delta t}_{y,m,n-\frac{1}{2}} + q^{t-\Delta t}_{y,m+1,n+\frac{1}{2}} + q^{t-\Delta t}_{y,m+1,n-\frac{1}{2}}\right]}{4h^{t-\Delta t}_{x,m+\frac{1}{2},n}} \tag{3.11}$$

For $adv_{y,2D}$ and $u^{t-\Delta t}_{x,m,n+\frac{1}{2}}$ there are similar expressions.

3.2.5. Continuity equation

After calculating the momentum fluxes, the water levels can be updated using the continuity equation. The continuity equation is discretised using first order explicit time-stepping with a first order central difference approximation of the spatial derivatives (Van Engelen, 2016):

$$\zeta^{t}_{m,n} = \zeta^{t-\Delta t}_{m,n} - \Delta t \left[\frac{q^{t}_{x,m+\frac{1}{2},n} - q^{t}_{x,m-\frac{1}{2},n}}{\Delta x} + \frac{q^{t}_{y,m,n+\frac{1}{2}} - q^{t}_{y,m,n-\frac{1}{2}}}{\Delta y} \right] \tag{3.12}$$

This scheme is also known as the BTCS-scheme, which is first order accurate in space and time and subjected to the CFL-condition (Courant-Friedrichs-Lewy, Courant et al. (1928)). In case other processes as precipitation, discharge or infiltration are specified, the changes in water level are added after the momentum but before this continuity equation. See Section 3.4 for the implementation of these processes.

3.2.6. Stability condition

As stated before the numerical scheme of SFINCS is subjected to the CFL-condition. This condition is used to determine the required time-step:

$$\Delta t < \alpha \cdot \frac{\Delta x}{\sqrt{g h_{max}}} \tag{3.13}$$

where h_{max} is the maximum value of the water depth in the computational domain at that time-step. The CFL-condition alone is not sufficient to ensure model stability. The assumption of small amplitude in calculating the wave celerity is not always valid and because of the inclusion of friction terms in the model (Bates et al., 2010). Therefore a heuristic time step reduction factor α-factor was advised for using this scheme, by default this is $\alpha = 0.75$. When fast flow conditions occur, the flow velocities are more in the order of $|u| + c$ than only c. The time-step can then be further limited by using a smaller α-factor for better stability. The minimum value is $\alpha = 0.1$.

3.3. Wave-driven processes

In SFINCS the swash zone is modelled by forcing the model at the boundary with an incoming wave velocity u_b using a weakly reflective generating-absorbing boundary condition, see Figure 3.2. This uses a varying water level ζ with a IG or incident wave signal. Additionally, a parametrisation for the wave-induced setup from DW to SW is applied (ζ_b), which can also account for the incident wave setup within the swash zone. This is further investigated in Chapter 4. Once the waves are created in the model because of the incoming velocity, they move freely into the domain. Because of the shallow water assumptions there is not accounted for frequency dispersion, the waves travel with $c = \sqrt{gh}$. Therefore larger waves can overtake smaller ones, whereby wave bores can merge. This inclusion of waves in SFINCS makes that processes in the swash zone like runup can be modelled. In this section at first the swash zone modelling approach is discussed in Section 3.3.1. Thereafter the boundary condition and the wave signal implementation are discussed in Sections 3.3.2 and 3.3.3. Finally the parametrisation for the wave-induced setup is discussed in Section 3.3.4.

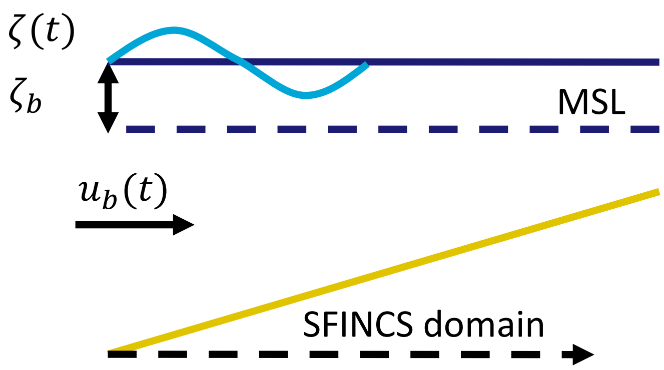

Figure 3.2: Illustration of the implementation of the wave processes in SFINCS

3.3.1. Swash zone modelling approach

According to Van Engelen (2016) the best location for the seaward boundary of the SFINCS model is in the nearshore at 2 m water depth. This depth is chosen so that most of the incident wave energy is dissipated. SFINCS does not account for wave breaking, so it is necessary that the boundary is at sufficient distance from the breaker line. This swash zone modelling approach is for instance also used in De Beer (2017) and Reniers et al. (2013). Based on the 2 m water depth criteria, there is determined in pre-processing which cells are inactive, boundary or normal active cells. Hereby the flux directions at the boundary are identified as in the blue lines of Figure 3.3. There is not accounted for wave-directions, every flux location is treated as a 1D flux. Therefore the implementation is not a full 2D boundary, this will be called a quasi-2D boundary from now. The consequences of this assumption are discussed in Chapter 5. For the input water level time-series, multiple input locations can be specified (yellow dots in Figure 3.3). For every flux location along the boundary there is linearly interpolated between the two closest input locations using a weighted average of both water levels at every input time-level. Every boundary flux location is forced with a velocity based on this water level using a weakly reflective generating-absorbing boundary condition (see Section 3.3.2). Hereafter the fluxes between the other active cells are calculated as described in Section 3.2.3.

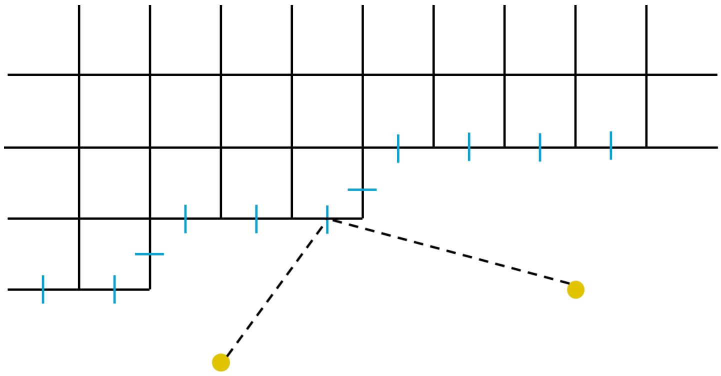

Figure 3.3: Illustration of the 2D implementation of the boundary implementation in SFINCS. The blue lines are the flux locations within the grid and the yellow dots the input water level time-series locations.

3.3.2. Weakly reflective generating-absorbing boundary condition

At every boundary flux location as showed in Figure 3.3, a 1D weakly reflective generating-absorbing boundary condition is applied in a similar way as in XBeach ('abs_1d', Roelvink et al. (2009)). The implementation is based on linear wave theory and can be applied at all four boundaries of the rectilinear grid. The formula of the Riemann-type boundary is:

$$u_b(t) = 2u^+ - \sqrt{\frac{g}{h(t)}}\zeta(t) + \bar{u} \tag{3.14}$$

With u_b as the velocity in [m/s] as imposed on the boundary of SFINCS, u^+ as the velocity of the incoming wave components and $\bar{u}$ as the residual currents. An elaborate description of the numerical implementation and two tests of the boundary condition regarding artificial reflection in 1D and 2D can be found in Chapter 4 of Van Engelen (2016).

3.3.3. Proposed boundary implementation including incident waves

One of the important aspects of SFINCS is that it simulates waves in the swash zone in a computationally efficient way. Therefore processes of the shoaling and surf zone are accounted for only in a simplified way. Initially this was implemented using a single sinusoid as an IG wave, see Equation 3.15.

$$\zeta(t) = n \cdot H_s \cdot cos\left(\frac{2\pi t}{T_{ig}}\right) \tag{3.15}$$

Here the water level of the IG wave ζ depends on a factor 'n' times the offshore significant wave height Hs. In the argument of the cosine a peak IG wave period T_{ig} is included. The created wave signal hereby only contains one cosine, which means that after every T_{ig} seconds the signal is repeated. This leads always to approximately the same runup values, which is not realistic and therefore not wanted. In Section 4.3 a new boundary implementation for SFINCS is investigated, of which the proposed implementation for the boundary water level is already given here in Equation 3.16. Hereby an indirect random water level time-series is created based on the spectrum of incoming waves at the boundary of SFINCS in 2 m water depth. The generation of a water level time-series from a wave spectrum is based on the implementation in XBeach (Van Dongeren (2003), Roelvink et al. (2009)), but applied for SW instead of DW.

$$\zeta(t) = \sum a_i \cdot cos(\frac{2\pi t}{T_i} + \phi_i) \quad \text{with} \quad a_i = \sqrt{2 \cdot E_i \cdot df} \quad \text{and} \quad T_i = \frac{1}{f_i} \tag{3.16}$$

Where df is the width of a bin within the variance density spectrum, E_i the energy within that bin, a_i the amplitude per bin and ϕ_i a random phase between $[-\pi, \pi]$. For an illustration of the definitions regarding the spectrum, see the left panel of Figure 3.4.

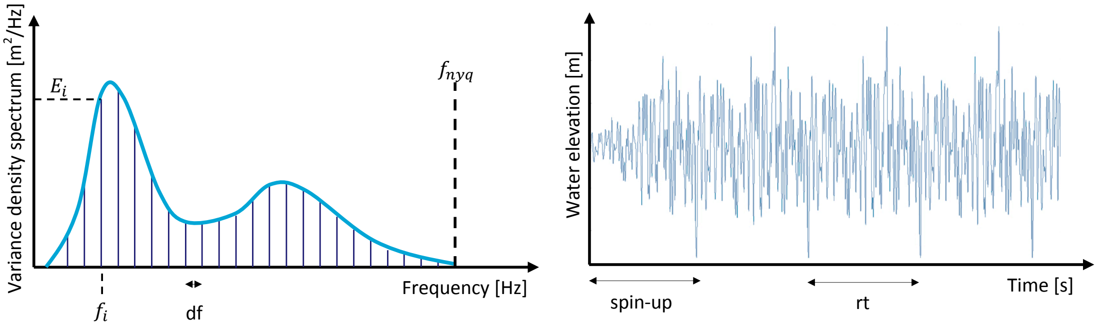

Figure 3.4: Illustration of the generation of an indirect random water level time-series

The variance density spectrum that is specified as input is read out until the Nyquist frequency of $f_{nyq} = f_s/2 = 0.5Hz$. This uses a time-series sampling frequency of $f_s = 1/dt = 1s$ with an appropriate time-step 'dt' of 1 second (e.g. default in XBeach). If the random phases per bin are created once, the signal repeats itself after a certain time (see the right panel of Figure 3.4). A signal return period of $rt = 1800s$ is chosen to contain multiple IG wave motions (analogous with the parameter 'rt' within XBeach, Roelvink et al. (2009)). Therefore the required number of bins when solving the whole spectrum is $nf = rt \cdot f_{nyq} = 900$ bins. When only the IG part of the spectrum is included ($f < 0.04Hz$) this becomes $nf = rt \cdot f_{nyq} = 72$ bins. In both cases the frequency bin width is $df = f_{nyq}/nf = 5.56 \cdot 10^{-4}Hz$.

After every 'rt' seconds the random signal begins to repeat itself and the water level is set to zero. For a good statistical representation of runup characteristics it is not wanted that the signal is repeated, so the random phases of all the bins are updated after 1800 seconds. Setting the water level to zero between the different time-series does not create too large shocks at the transition when making an incident wave signal. The total created signal always begins with a zero, then within the first 600s of model spin-up time gradually grows towards the full wave signal amplitudes (spin-up time as in Section 4.3.2). The random phase per bin is important not to create large peaks within the boundary water level time-series. Because the signal is made completely random, this also means that there is not necessarily a correlation between the IG and incident waves. This may not be fully corresponding with reality, but is a very fast and simple way to make a wave signal from a variance-density spectrum. The influence of the lack of correlation is investigated in Section 4.3.5. The random water level time-series are always created in pre-processing, after which they are given as input for SFINCS as a varying boundary water level signal.

3.3.4. Wave-induced setup

To still account for wave-induced setup within the swash zone modelling approach, a parametrised representation for the mean water level at the boundary of SFINCS was developed in Van Engelen (2016). This mean water level is a parametrisation for the wave-induced setup from DW to SW and the incident-wave induced setup from the SFINCS boundary to the shoreline. This incident-wave induced setup needs to be parametrised because in Van Engelen (2016) only the IG waves are included, thereby neglecting the incident waves and the corresponding setup. See Equation 3.17 for the expression of the mean water level at the boundary of SFINCS at 2 m water depth ζ_b:

$$\zeta_b = 0.36 \cdot H_s^{1.15} \cdot \xi^{0.290} \tag{3.17}$$

Which is added to the water level at the boundary of SFINCS. It uses the offshore significant wave height H_s, peak period T_p and slope β for Irribarren number $\xi = \frac{\beta}{\sqrt{H_s L_0}}$ and the deep water wave length $L_0 = \frac{g T_p^2}{2\pi}$. Instead of solving the wave processes, this parametrisation makes it possible to skip the surf zone and still account for wave-induced setup. For more information about the derivation of the formula there is referred to Chapter 5 of Van Engelen (2016). Whether this parametrisation is still valid when incident waves are solved as well, is investigated in Chapter 4 of this report.

3.4. Other processes

In order to apply SFINCS for real compound flooding cases, other processes should be included as well. Besides the discussed offshore water levels and waves, infiltration (Section 3.4.1), precipitation (Section 3.4.2), river discharge (Section 3.4.3) and wind forcing (Section 3.4.4) is included in the model. In the sequential paragraphs these processes and their implementation is discussed. The wind forcing is a term that is added to the momentum equations as explained before. The water level changes due to infiltration, precipitation and discharge points are updated after the momentum equation but before the continuity equation. These processes are tested in simple conceptual tests in Appendix D.

3.4.1. Infiltration

In SFINCS infiltration is included in a simple way by changing the water level per grid cell due to infiltration:

$$if \quad \zeta_{m,n}^{t-\Delta t} - d_{m,n} > h_{u,thresh}: \quad \zeta_{m,n}^{t} = \zeta_{m,n}^{t-\Delta t} + q_{inf}^{t} \cdot \Delta t \tag{3.18}$$

Here q_{inf}^t is the infiltration in $[m^3/s]$. As can be seen in the formula a negative value for q_{inf} should be specified in order for water to infiltrate immediately out of the model. Also a limiter is applied so that only water can infiltrate if there is a minimum water depth of $h_{u,thresh}$ meters in the velocity points, default $h_{u,thresh} = 0.05m$. However the water level can in theory still become lower than the bed level if more than 0.05 m of water is taken out of a cell. Although this is not very probable within one time-step of a few second.

3.4.2. Precipitation

In SFINCS precipitation is included in a simple way by raising the water level per grid cell due to rainfall:

$$\zeta_{m,n}^{t} = \zeta_{m,n}^{t-\Delta t} + w_{prcp}^{t} \cdot \Delta t \tag{3.19}$$

The rainfall w_{prcp}^t is specified in the input as $[mm/hr]$, which is converted to $[m/s]$ and is independent of the cell size. The rain input from meteorological models can be supplied spatially varying using the spiderweb approach or on a grid. Alternatively this can be specified in a spatially uniform way. The input is always time-varying, where there is linearly interpolated in time between two input time-levels.

3.4.3. Discharge points

In SFINCS discharge points are implemented as:

$$\zeta_{m,n}^{t} = \zeta_{m,n}^{t-\Delta t} + \frac{q_{src}^{t} \cdot \Delta t}{\Delta x \cdot \Delta y} \tag{3.20}$$

Where q_{src}^t is the discharge in $[m^3/s]$. A source point affects one cell, where the water level is raised accordingly for every time-step. This simple implementation means that no momentum is transferred. Only the water level gradient is changed, which leads to a momentum flux. Therefore for large discharges one could expect that the occurring momentum flux is less than if the flux of the discharge is forced directly.

3.4.4. Wind forcing

Wind forcing is included in the momentum equations of SFINCS. The wind speed can be supplied spatially varying using the spiderweb approach or on a grid. Alternatively it can be specified in a spatially uniform way. These wind speeds are then transferred to stresses acting on the water surface using the following formula for the x-direction:

$$\tau_{x,m+\frac{1}{2},n}^{t} = C_d \cdot \rho_a \cdot u_{wind}^2 \tag{3.21}$$

Where u_{wind} is the wind speed in $[m/s]$ in x-direction. The density of air ρ_a is included, as well as the drag coefficient C_d. The drag coefficient varies with the wind speed, consistent with the specification in Delft3D (Lesser et al., 2004). The values are as found by Vatvani et al. (2012): linearly increasing from $C_d = 0.001 - 0.0028[-]$ for wind speeds between $u_{wind} = 0 - 25[m/s]$, linearly decreasing from $C_d = 0.0028 - 0.0015[-]$ for wind speeds between $u_{wind} = 25 - 50[m/s]$ and thereafter with a constant value of $C_d = 0.0015[-]$. There is a similar expression for $\tau^t_{y,m,n+\frac{1}{2}}$. Note that in SFINCS the wind stresses are reduced for water depths smaller than 0.25 m, to prevent the wind-induced setup to become unnaturally high. This is not done in Delft3D, but is for instance done in ADCIRC as well.

3.5. Model limitations

Here the limitations of the model regarding the made assumptions are discussed. Included are the assumptions of neglecting advection, Coriolis, non-hydrostatic pressure, incident wave forcing and viscosity in Sections 3.5.1 to 3.5.5. There is discussed why the assumptions are made and under what conditions they are justified by theory. Whether this actually is the case, is investigated in Chapters 4 and 5.

3.5.1. Advection

An important simplification of the SWE initially made in SFINCS is neglecting the advective transport of momentum. Whether this is justified depends on the flow conditions. In Van Engelen (2016) it was argued that advection only becomes important for relatively short incident waves in shallow water. There the approach was to model only the IG part of the wave spectrum, which would justify neglecting the advection term. Using a dimensional analysis an indication was given of what terms are dominant for incident and IG waves. The concluding figure is reproduced here, showing the result for a 1 m high wave in Figure 3.5. For more information regarding the dimensional analysis there is referred to Chapter 4 of Van Engelen (2016). There has to be noted that the applied friction factor of that analysis of $c_f = 0.003[-]$ is low compared to the default friction factor in SFINCS. Therefore the influence of the advection and friction term in the figure might be overestimated.

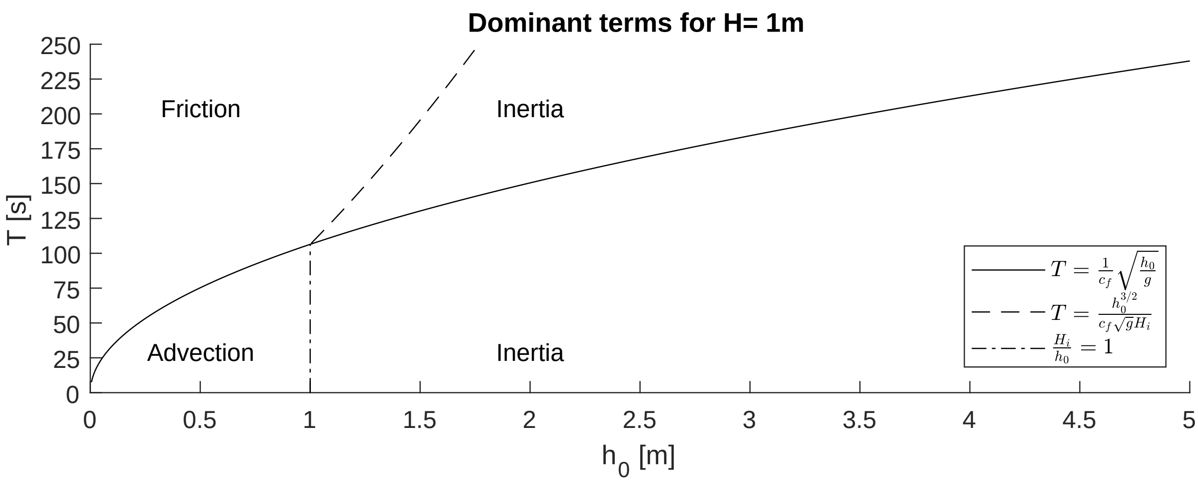

Figure 3.5: Dominant terms for a 1m high wave, made after Van Engelen (2016)

Figure 3.5 shows the dominant terms for a 1 m high wave for various wave periods T and water depths h_0. For this wave height the advection term becomes dominant for water depths smaller than 1 m and wave periods smaller than 100 s. When an IG wave of $T = 50s$ is taken as example, it can be seen that up to a water depth of about 0.25 m friction is the dominant term of the momentum equation. Then until a water depth of 1 m advection is the dominant term and further offshore inertia dominates. For IG waves (T>25 s) it can be seen that most of the time advection is not the dominant term. Van Engelen (2016) therefore argued that for solving only IG waves the advection term is not needed. While modelling IG waves with SFINCS-LIE by Van Engelen (2016), the general observations were that the model was able to come up with appropriate runup characteristics as long as the wave spectrum was IG wave dominated. It was also observed that during certain conditions the rundown velocities were overestimated, the exact reason was not known. In this research also incident waves are included to investigate their influence on the wave-driven inundation during TC. The influence of advection on modelling incident as well as IG waves is hereby investigated. Based on the dimensional analysis, it seems that advection might become important for incident waves ($T < 25s$). Therefore it might differ per situation whether neglecting the advection terms can be justified. This is further investigated in Chapter 4, since this is not fully known yet for modelling compound flooding.

Apart from the influence of advection for modelling waves, advection is important for modelling super-critical flow conditions. For instance during dam break type situations the local flow velocities can increase significantly. Then the advection term is important in smoothing out the steep water front. De Almeida and Bates (2013) showed for LFP as LIE model that in the lower range of sub-critical flows (Fr<0.5) a LIE model has good agreements with a full SWE model. For increasing Froude numbers the error by neglecting the advection term increased. How big the influence is of the advection term for super-critical flow conditions during a dam break is investigated in Chapter 4.

3.5.2. Coriolis

For large scale flows the rotation of the earth can start influencing the motion of the water. This Coriolis effect becomes stronger the larger the spatial scales are. Using the Rossby number $R_o = \frac{advection}{Coriolis} = \frac{U}{fL}$ the influence of the Coriolis term compared to the advection term can be quantified (Pietrzak, 2016). Take a spatial scale of 100 km for larger scale flows and flow velocities in the order of $U = 1m/s$ during a TC. Using the f-plane approximation the Coriolis parameter is $f = 2\Omega \sin\phi$. At a latitude of 30 degrees North this becomes $f = \Omega = 7.29 \cdot 10^{-5} s^{-1}$. Therefore the Rossby number becomes $R_o = 0.14[-]$. Thus for modelling the large scale flows before the coast during a TC, Coriolis can become important. If SFINCS would also be used as a larger scale circulation model like Delft3D, Coriolis should be included. Since SFINCS is used as a swash zone and inland model, with $L < 1km$ you get $R_o > 14[-]$, indicating that Coriolis can be neglected. In a case study in Chapter 5 there is reflected on this.

3.5.3. Incident wave forcing

Originally in Van Engelen (2016) the process of incident wave forcing was neglected in SFINCS. This has as a consequence that no incident waves are present in the model. A deviation of the mean water level at the coast can occur by not including the incident wave-induced setup. Also the incident wave forcing on the IG waves is not present and a deviation in the mean current can occur. To overcome the inability to capture incident wave-induced setup and set-down, a parametrised expression is added to SFINCS in Van Engelen (2016). What the actual influence of the lack of incident wave-forcing is, is investigated in Chapter 4. Also there is investigated whether SFINCS would be able to also model the incident waves.

3.5.4. Non-hydrostatic pressure

The SWE in SFINCS are used in depth-averaged form, thereby assuming a hydrostatic pressure distribution. Accordingly the vertical variations of the horizontal flow are assumed to be negligible. These assumptions can be made for flows where the vertical scale is significantly smaller compared to the horizontal scale. This assumption is often justified for IG waves. For incident waves the horizontal scales are much shorter, and therefore the assumption of a hydrostatic pressure might become invalid. Therefore the non-hydrostatic and wave resolving version of XBeach (XBNH) for instance uses the NHSWE with the inclusion of the NH pressure to solve incident waves (Roelvink et al., 2017). Additionaly, Zijlema (2015) for instance states: "Simulation of short waves is only possible with the addition of NH pressure to the SWE". In this thesis there is investigated whether it is also possible to model incident waves while still using the hydrostatic pressure assumption. It is expected that the incident waves cannot be modelled fully accurate, or that runup characteristics might be underestimated.

As a first indication a simple analysis is done based on Battjes and Labeur (2014). Here a quantitative criterion is given for the validity of the hydrostatic assumption of 'long waves'. Long waves have a wave length that is far greater than the depth in which they occur. Consequently, vertical accelerations are negligible so that the pressure can be considered hydrostatic. To assume a hydrostatic pressure distribution, also the wave-induced pressure variation must be almost uniform over the water depth. Using a sinusoidal motion of the water level, the following condition for the validity of the approximation of hydrostatic pressure was found:

$$\frac{\omega^2 h_0}{g} << 1 \tag{3.22}$$

When using $\omega = \frac{2\pi}{T}$, this is re-written to $T = \frac{2\pi}{\sqrt{\frac{g}{h_0}}}$. Calculating this for various wave periods and water depths gives Figure 3.6. Here the factor $\frac{\omega^2 h_0}{g}$ is shown for values of 1, 0.1 and 0.01. For IG waves with a wave period over 15 s, the approximation of hydrostatic pressure is valid for the water depths occurring in the swash zone modelling approach of SFINCS. For incident waves however, depending on the water depth the hydrostatic pressure assumption may not be fully valid any more. What role this plays in the swash zone is investigated in Chapter 4.

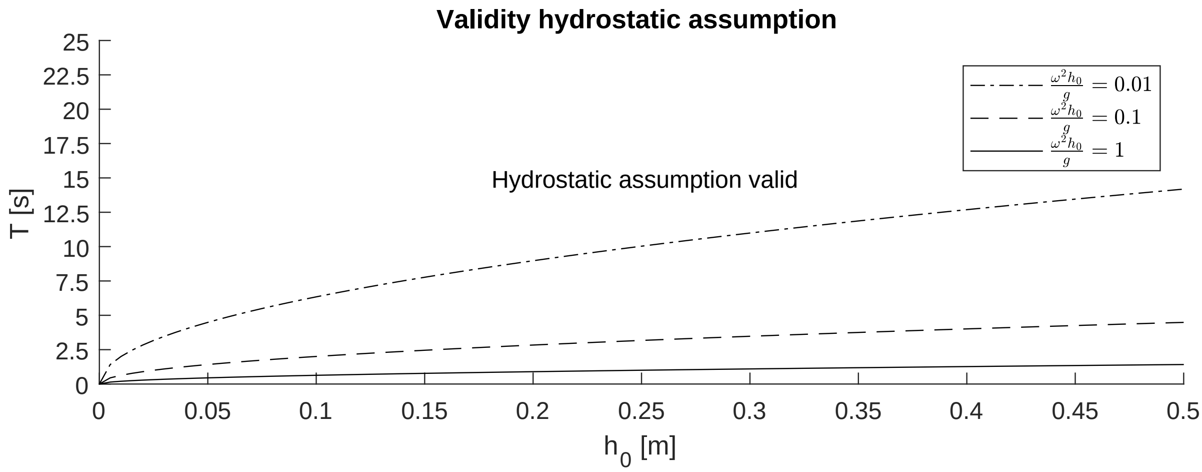

Figure 3.6: Validity hydrostatic assumption

3.5.5. Viscosity

At last the viscosity effects, momentum loss due to horizontal gradients in velocities, are neglected in SFINCS. In depth-integrated shallow-water models this viscosity is usually a representation of the turbulent motions that are not solved by the model. This viscosity usually has a smoothing effect on the calculated solution. There is not found in literature what the actual effect of the viscosity term is in the swash zone, where turbulence may occur because of wave breaking. In SFINCS the boundary is located shallow enough so that most wave energy is already dissipated. This could mean that the amount of turbulence present in the swash zone model could be low, but this is not known yet. For occurring flow conditions one would assume that turbulence does not play a large role and that therefore this does not need to be accounted for using a viscosity term. In general the viscosity term can have a smoothing effect on the numerical solution. Whether the viscosity term plays a role is investigated in Chapter 4.

3.6. Computational efficiency

All these physical assumptions and simplifications are made with the idea of a fast model in mind. Compared to advanced models who do include more of the processes, this will lead to a lower accuracy in some cases. When applied correctly the accuracy is still sufficient, and the gain in computational efficiency significantly. Apart from neglecting and simplifying certain processes, the gain in speed is also achieved by optimising the numerical implementation of the model. For instance an explicit scheme is chosen for the momentum equation. When time-steps are small compared to relevant time scales, explicit schemes are sufficient and they are usually cheaper per time step than implicit schemes (Zijlema, 2015). The descretisations are also first instead of second order accurate and linearised. Furthermore single precision instead of double precision is chosen, possibly introducing slight mathematical rounding errors.

Additionally, the use of OpenMP (Open Multi Processing) is used. This allows for the parallel computation of loops and thereby increases the speed of the model. The parallelisation method is described in Bates et al. (2010) and Neal et al. (2009). Another addition is the use of vectorisation within the loops instead of two-directional grid point calculation. All these physical and numerical choices together should make SFINCS faster than current advanced models. What the actual accuracy and efficiency of SFINCS is regarding the modelling choices is investigated in the rest of this thesis.

4

Conceptual Tests

In this chapter the results of several performed conceptual tests are discussed, which focusses on the assumptions made in the SFINCS model. Hereby the performance and numerical implementation of different processes in the SFINCS model is tested as well. At first, an overview is given regarding what is tested (and why) in Section 4.1. Thereafter the flow related tests are discussed in Section 4.2. Finally, the wave related tests are discussed in Section 4.3.

4.1. Introduction

As described in Chapter 3, a large part of the computational efficiency of SFINCS is obtained by making assumptions regarding what processes need to be solved. Based on theory, it is assumed that these simplification are valid. However, situations can occur which are on the limit of their validity. Therefore some of the assumptions and their validity are tested in multiple conceptual tests. These are split into flow and wave related tests. The outcomes can then by applied to SFINCS.

For the flow related processes, first the implementation of the drying and flooding mechanism is validated. Moreover, the importance of advection (or the inaccuracy of neglected it) is analysed in several dam break tests by applying respectively SFINCS-LIE and SFINCS-SSWE. Hereby also the implementation in the SFINCS model is tested. For all flow-related conceptual test the semi-advanced SFINCS model is compared to the advanced XBeach model.

For the wave related tests, there is investigated how SFINCS can be used for wave-driven flooding without using an advanced nearshore model like XBeach. First it is tested what terms of the momentum equations are important for a swash zone model. Hereby there is focussed on the assumptions regarding advection, incident wave forcing, NH pressure and viscosity. Hereafter it is then investigated in what way it would be possible to use SFINCS with an indirect forcing, while still having realistic runup characteristics. This is then used for the SFINCS model and tested for different types of wave spectra.

4.2. Flow related tests

At first the non-breaking wave propagation over a horizontal plane is investigated in Section 4.2.1. Thereafter there is focussed on the 1D dam break tests with dry and wet bed in Section 4.2.2. This is followed by the 2D dam break tests with dry and wet bed to investigate at 2D effects in Section 4.2.3. Finally, the results of the Carrier and Greenspan test is discussed in Section 4.2.4 and the conclusions in Section 4.2.5.

4.2.1. Non-breaking wave propagation over a horizontal plane

The first conceptual flow-related test models non-breaking wave propagation over a horizontal plane, based on Bates et al. (2010) and Hunter et al. (2005). The test is performed to analyse the ability of a model to capture floodplain 'wetting' and reproduce the correct flow velocity. Initially the 5 km long domain is completely dry, after which a boundary condition with a constant flow velocity of $u = 1 m/s$ and a rising water level according to an analytical solution is introduced. This causes a non-breaking wave to propagate into the domain, which has sub-critical flow. The model performances is compared with the analytical solution and the results of LFP of Bates et al. (2010). Also the computational efficiency is considered. For the analytical solution and numerical setups of SFINCS-LIE and XBeach (XBNH) see Appendix B.1.

Accuracy

Both the semi-advanced SFINCS-LIE and advanced XBNH model are capable of reproducing the main hydrodynamic patterns of a non-breaking wave over a horizontal plane (Figure 4.1). Generally speaking, SFINCS overestimates the water level close to the boundary and has a slightly lower propagation speed compared to the analytical solution (order of 3%). In the XBNH simulations the water level is reproduced more accurately (Table 4.1). The RMSE (Root Mean Squared Error) of LFP and SFINCS-LIE compared to the analytical solution is in the same order for the different grid sizes, while the volume error is smaller for SFINCS. Note that the analytical solution is not a true analytical solution to the LIE as solved by the models, it is therefore not expected that the model results will fully converge to the analytical solution (Bates et al., 2010). Although, at fine grid resolutions the differences should be small. This also explains why the shape at the tip of the wave, as showed in Figure 4.1, does not fully correspond with the dam break type shape that can be observed in reality. Also it turned out that XBeach does not work when all the grid points are initially dry, a low initial water level of $z_{s0} = 0.01m$ is specified to overcome this. This influences the result slightly, but otherwise SFINCS cannot be compared with XBeach. In general, the simple flooding and drying mechanism of SFINCS gives sufficient results for this simple case.

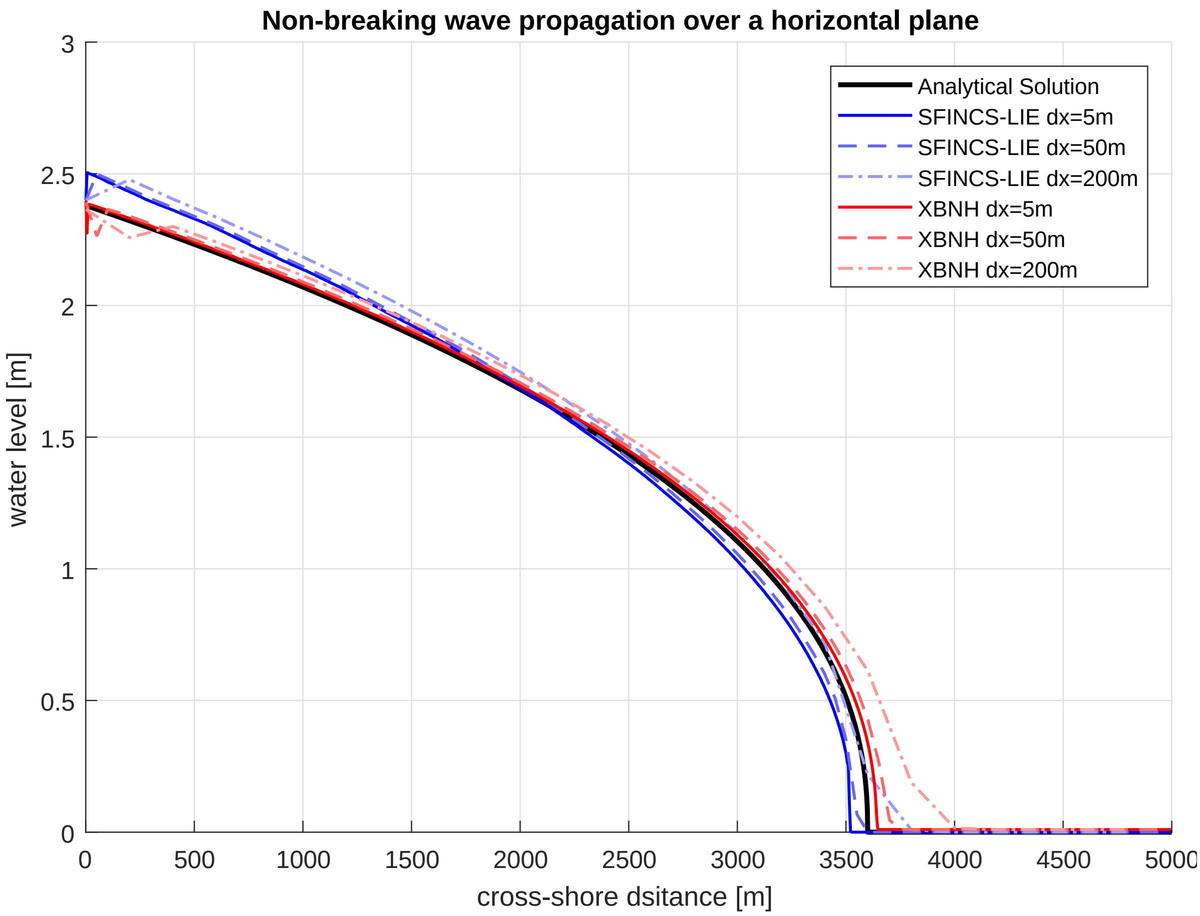

Figure 4.1: Analytical and numerical solution for SFINCS-LIE and XBNH for different grid sizes after 3600 seconds. With $n = 0.012 s/m^{1/3}$ for both models.

Efficiency

The expected patterns that smaller grid sizes lead to smaller time-steps, longer computation times and better accuracy can be observed from Table 4.1. Furthermore it can be seen that although SFINCS solves the same set of LIE, it is considerably faster then LFP. In this case SFINCS does use parallel processing with 4 processors where LFP does not (resulting in a 3-4 times shorter runtime), but when taking this into account still SFINCS is an order of magnitude faster. The used computer for LFP back in the day was probably slower (see Appendix A.2), but with these short runtimes this is not expected to result in the large observed differences. With XBeach it can be seen that it has smaller average time-steps than SFINCS and the runtime is an order of magnitude longer, bearing in mind that XBeach was not run using parallel processing. In all the conceptual tests of this chapter, SFINCS is run with parallel processing using OpenMP with 4 processors (see Appendix A.2 for the exact computer characteristics). XBeach is run on the same computer, but without parallel processing. XBeach can model with parallel processing by splitting up the model domain (using MPI, Message Passing Interface). However, this only works well in 2D.

Table 4.1: Accuracy and efficiency comparison between LFP, SFINCS-LIE and XBNH for different grid sizes. The RMSE and volume error are compared to the analytical solution. For LFP only the minimal time-step is given in Bates et al. (2010), for SFINCS and XBeach only the average time-step is known.

	RMSE [m]				**Volume error** [-]		
dx [m]	5	50	200	dx [m]	5	50	200
LFP	0.07	0.03	0.11	LFP	-2.37	-1.25	2.95
SFINCS-LIE	0.08	0.07	0.09	SFINCS-LIE	0	0.01	0.05
XBNH	0.03	0.06	0.14	XBNH	0.02	0.03	0.06
	Minimal/average dt [s]				**Computation time** [s]		
dx [m]	5	50	200	dx [m]	5	50	200
LFP	0.73	7.25	29.04	LFP	139 .8	1.2	0.6
SFINCS-LIE	0.93	9.32	37.34	SFINCS-LIE	0.12	0.02	0.02
XBNH	0.3	3.06	10.37	XBNH	25.35	1.9	0.62

4.2.2. 1D dam break

As a second conceptual flow related test there is focussed at the classic dam break test, based on Chanson (2006), Cui (2013), Kroon (2009) and Stoker (1957). This test is widely used to validate the performance of wetting and drying procedures, as well as the performance of the advection terms. Also the large water level gradients and resulting high flow velocities test the ability of the model to handle the wetting of multiple cells per time-step. The thickness of the water depth at the front of the analytical solution becomes infinitely small. This is difficult in a numerical implementation, since usually a finite minimum flow depth to distinct dry from wet cells is used. Here first the results for the 1D dam break test with a dry bed are presented, the results with a wet bed are similar and only briefly discussed. For the analytical solutions and model setups of SFINCS and XBeach see Appendices B.2 and B.3.

Accuracy

Figure 4.2 presents the 1D dam break test with an initial dry bed after 5 seconds. On the x-axis the cross-shore dimension is shown and on the y-axis the water level is presented. The analytical solution in black starts with a water level of 1 m at the left and goes towards an infinite small water depth at the right. The different colours represent different versions of the SFINCS and XBeach models. In the left panel the grid resolution is 0.1 m and in the right panel the resolution is 0.5 m. For both resolutions XBSB and XBNH is capable of reproducing the main hydrodynamic pattern with (for RMSE values for different grid resolutions see Table 4.2). There is no difference between XBSB and XBNH, this gives an indication that the NH pressure term is not that important for this situation. For the same tests, SFINCS-LIE is not capable of reproducing the dam break test. This is related to the neglected advection term, which is of importance in this abrupt flow disruption. When advection is included (SFINCS-SSWE), results are much more in line with the analytical solution and XBeach results. However, instability can occur in SFINCS-SSWE for small grid sizes in combination with no roughness (left panel of Figure 4.2).

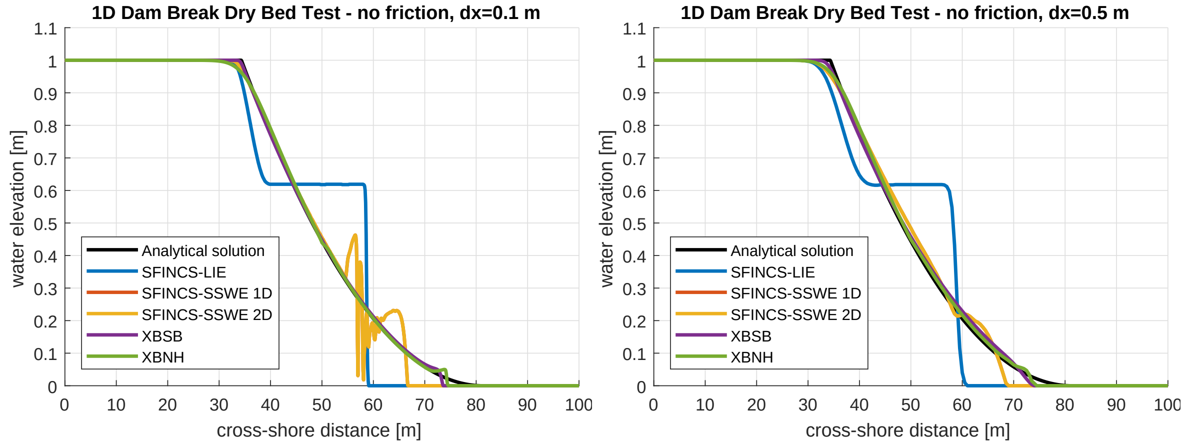

Figure 4.2: Analytical, SFINCS and XBeach solutions for the 1D dam break test with dry bed for different grid resolutions and without friction after 5 seconds. Left: dx=0.1m, Right: dx=0.5m

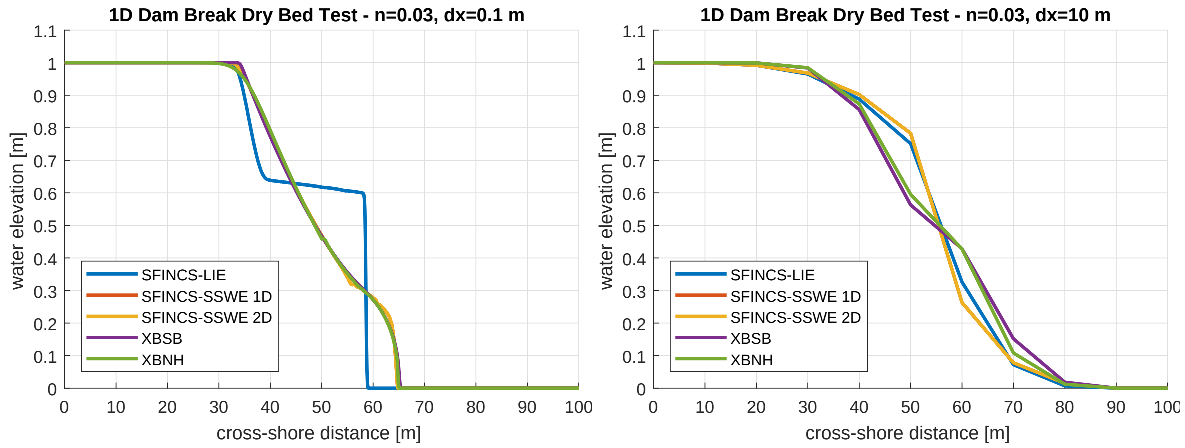

Figure 4.3: Analytical, SFINCS and XBeach solutions for the 1D dam break test with dry bed with a manning roughness coefficient of $n = 0.03s/m^{1/3}$ for different grid resolutions after 5 seconds. Left: dx=0.1m, Right: dx=10m

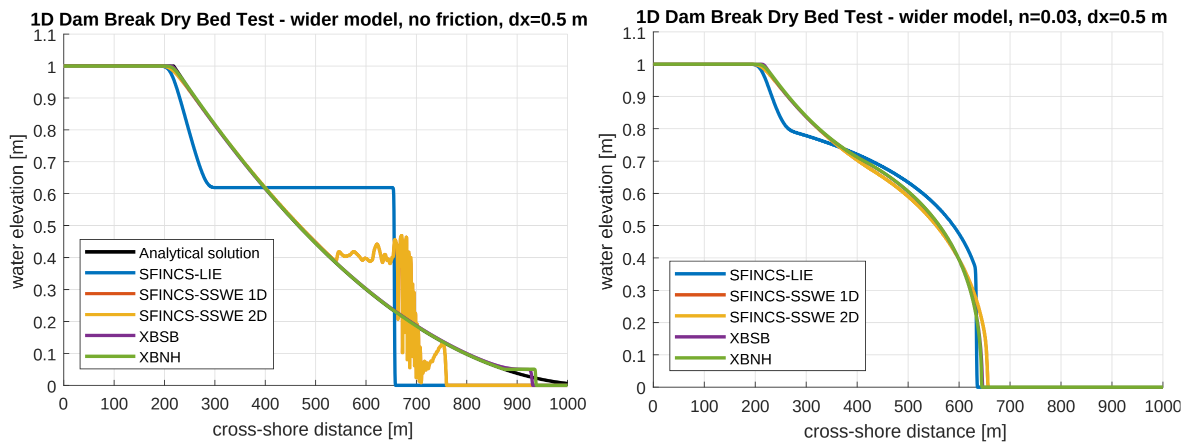

Figure 4.4: Analytical, SFINCS and XBeach solutions for the 1D dam break test with dry bed for a 1000m wide model with and without friction after 90 seconds. Left: without friction Right: $n = 0.03s/m^{1/3}$

In more practical cases, bed friction is of importance and should therefore be taken into account. Moreover, larger grid sizes are often applied in compound flooding cases. Bates et al. (2010) observed that LFP does not perform well for Manning friction values $n < 0.02s/m^{1/3}$ with small grid sizes, which seems to be the case for SFINCS as well. Therefore the same test with dx=0.1 m is run but then with $n = 0.03 s/m^{1/3}$, as in Section 4.2.1. Figure 4.4 presents the same 1D dam break test with a initial dry bed as Figure 4.2, however, in these cases bed friction is taken into account (for this case there is no analytical solution). Model resolution varies between 0.1 meter (left panel Figure 4.4) and 10 meter (right panel Figure 4.4). Model results show that SFINCS-SSWE with a small resolution and bed friction is in this case stable. Moreover, for larger grid cells, the inclusion of advection seems to be less of importance. This is related to numerical diffusion because of the larger grid cells.

To assess what happens after the first 5 seconds where the flow velocities are high, the model runtime and the domain size are increased. The runtime is increased to 90 seconds and the model is made 1 km wide with dx=0.5m, again the dam break is in the middle of the domain. Because of the sensitivity to friction the runs are performed with and without friction. The left panel of Figure 4.4 shows that while the model is stable in the first 5 seconds (Figure 4.2), in some later stage instabilities occur. This does not happen when including friction and then the result is quite close to that of XBeach (right panel of Figure 4.4). Interestingly, even the SFINCS-LIE does a good job regarding the propagation speed. This gives the impression that the advection term is most needed shortly after the dam break, when the velocities are highest.

Efficiency

To illustrate the differences in computational efficiency, the model runtimes are presented in Table 4.2. It can be seen that SFINCS generally is an order of magnitude faster than XBeach, bearing in mind that XBeach was not run using parallel processing. The speedup factor is larger for the smaller grid sizes. Turning on advection does make SFINCS-SSWE 1D a little bit slower than SFINCS-LIE, this is because more terms have to be calculated and stored. Similarly, SFINCS-SSWE 2D is generally slightly slower than SFINCS-SSWE 1D. Similarly, the computational efficiency of XBeach is lower because it even solves more terms. It has to be noted that the computation times can vary when repeating a test, because of the short run-times of less than a second.

Table 4.2: RMSE compared to the analytical solution and computation time for 1D dam break test dry bed without friction after 5 seconds for different models.

	RMSE [m]					**Computation time** [s]			
dx [m]	0.1	0.5	1	10	dx [m]	0.1	0.5	1	10
SFINCS-LIE	0.109	0.101	0.093	0.101	SFINCS-LIE	0.034	0.014	0.024	0.010
SFINCS-SSWE 1D	0.036	0.022	0.026	0.108	SFINCS-SSWE 1D	0.040	0.013	0.010	0.013
SFINCS-SSWE 2D	0.036	0.022	0.026	0.108	SFINCS-SSWE 2D	0.062	0.016	0.015	0.011
XBSB	0.005	0.011	0.017	0.084	XBSB	6.099	0.421	0.250	0.047
XBNH	0.007	0.009	0.013	0.087	XBNH	5.866	0.499	0.187	0.109

Wet bed

When the downstream bed is initially wet with 0.1 m of water, a different (analytical) solution is obtained (see Figure 4.5 and Appendix B.3). The main difference is that the flooding and drying mechanism is not tested because all cells are already wet. The wet bed also inflicts the shape of the solution as now a steep front and a horizontal section is observed. The ability of the model to reproduce the height of the hydraulic jump indicates whether the model is momentum conservative.

In general the same results regarding accuracy and efficiency are obtained compared to the test with the dry bed. However, Figure 4.5 shows that for the wet bed case the result of SFINCS-SSWE is already stable for dx=0.1 m when running without friction, which was not the case with the dry bed. The result is very close to that of XBeach and the analytical solution. That the solution is less sensitive to friction or small grid sizes than for the dry bed test is assumed to be the case because the flooding and drying mechanism does not play a role.

4.2.3. 2D dam break

To test the influence of advection, sudden transitions and the momentum conservation in 2D, the laboratory experiment by Stelling and Duinmeijer (2003) is reproduced. The difference with the 1D dam break test is that the water of the upstream part cannot flow freely to the downstream part because of a limited opening of 0.4 m wide, which is opened by a gate. Hereby there is strong flow contraction and an increase of the flow velocities leading to an even stronger shock wave. This propagating shock wave also results in a 2D flow pattern, which

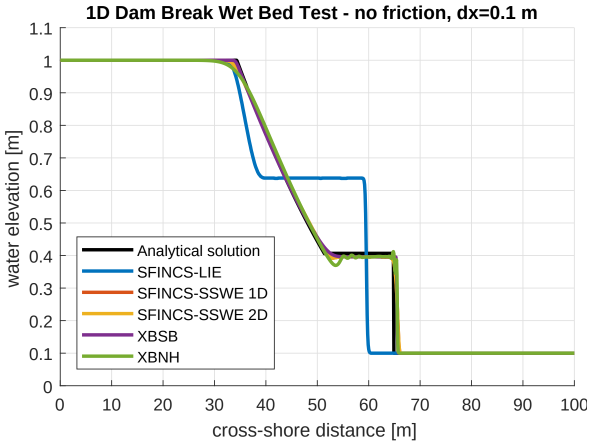

Figure 4.5: Analytical, SFINCS and XBeach solution for the 1D dam break with wet bed test without friction and $dx = 0.1m$ after 5 seconds.

tests the importance of the 2D advection term and the ability of the models to reproduce this. The upstream water level is set to 0.6 m and the downstream water level respectively 0 and 0.05 m for the dry and wet bed cases. The initial velocities are set to zero and the release of the water is instantaneous (in the experiment however a gate is opened with 16 cm/s). The difficult part is to correctly reproduce the propagation speed and flow pattern around the opening. Also the sudden flow transition and rapidly varying flow is important to model correctly. Because the original data of the experiments was not available, the SFINCS and XBeach results are plotted over the figures of the original paper. For the experimental and numerical setups of SFINCS and XBeach see Appendix B.4. Also some of the results are presented in that appendix. The results with a wet bed are similar to the dry bed case and only briefly discussed.

Accuracy

Figure 4.6 presents the water levels at different time-steps for a cross-section in the middle of the domain, for the different models. It can be seen in the upper left panel that with SFINCS-LIE the upstream water level drains too fast and that the created water front downstream is too high. The latter is similar to the results of the 1D dam break test. This is better with both SFINCS-SSWE models, but there model instabilities occur outside of the gate opening. In this area super-critical flow is present. Further downstream the flow velocities decrease and the flow becomes stable again. With XBSB and XBNH no instabilities occur and it can be seen that there is a hydraulic jump between the super- and sub-critical areas.

To assess why the result of SFINCS-SSWE is unstable, the dimensionless Froude number is calculated for the different models. Using the largest occurring flow velocity in x- and y-direction of the simulation and its corresponding water depth, the Froude numbers are calculated as follows:

$$Fr_x = \frac{u}{\sqrt{gh}} \quad \text{and} \quad Fr_y = \frac{v}{\sqrt{gh}} \tag{4.1}$$

The Froude numbers for SFINCS-LIE, SFINCS-SSWE and XBeach are presented in Table 4.3. It can be seen that in both the 1D and 2D dam break tests super-critical flow conditions occur ($Fr > 1$). For the 2D dam break tests the Froude numbers for SFINCS-SSWE are multiple times larger than XBeach. Because of the occurring instabilities in SFINCS-SSWE, the local water level gradients and corresponding flow velocities increase. This leads to far larger Froude numbers compared to XBeach. To assess why the model results of SFINCS-SSWE are unstable while for the same settings ($n = 0.03s/m^{1/3}$ and $dx = 0.1m$) the result of the 1D dam break test is stable, the maximum Froude numbers are also calculated for this test. It can be seen that the Froude numbers in that test are smaller, indicating that $Fr = 3$ seems to be the limit for SFINCS-SSWE in combination with the simple flooding and drying mechanism. For SFINCS-LIE the Froude number is in the order of magnitude of XBeach for the 2D dam break test and even lower for the 1D dam break test. SFINCS-LIE therefore is more stable than SFINCS-SSWE, but the result for dam break type situations is also less accurate.

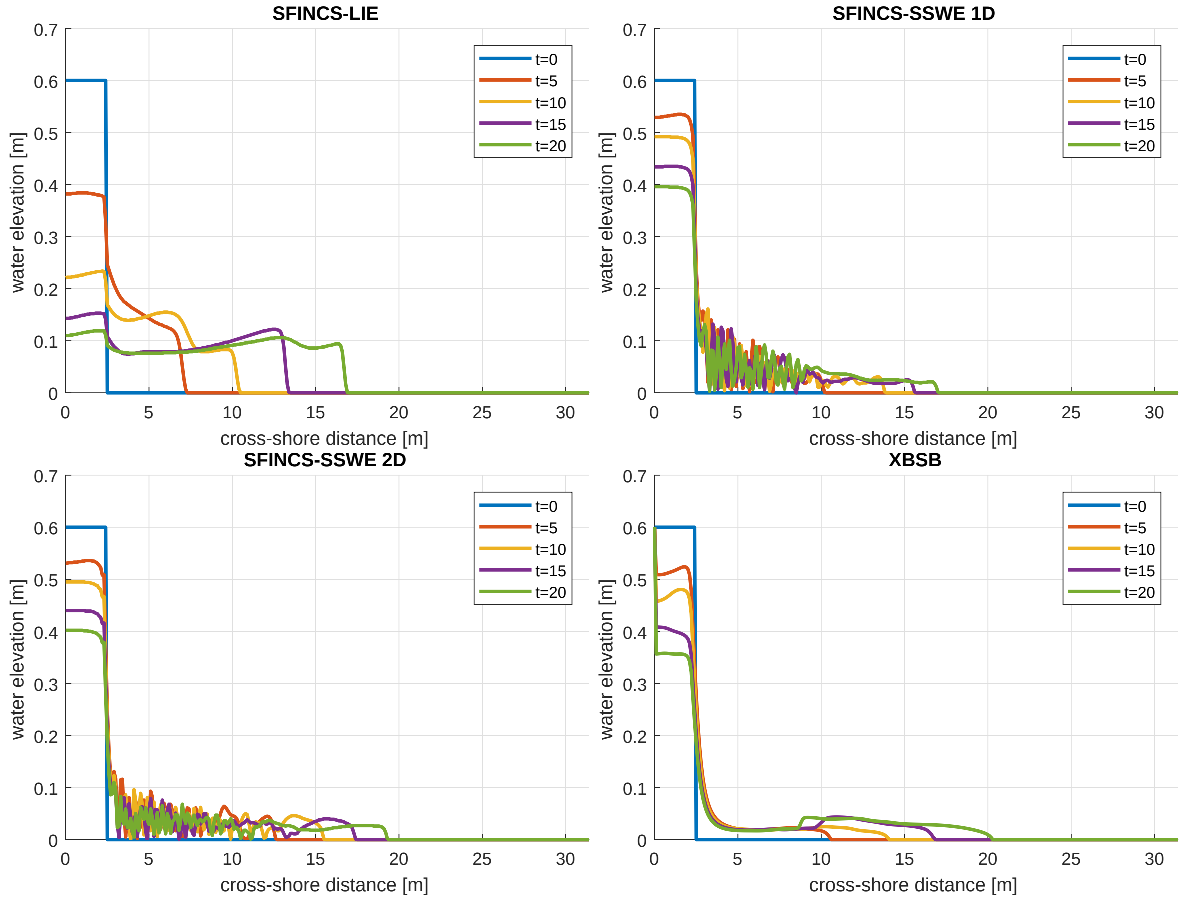

Figure 4.6: SFINCS and XBeach cross-sections for the 2D dam break test with dry bed. With $n = 0.012 s/m^{1/3}$ for XBeach and with $n = 0.03 s/m^{1/3}$ for SFINCS. Upper left= SFINCS-LIE, upper right= SFINCS-SSWE 1D advection, lower left= SFINCS-SSWE 2D advection, lower right= XBSB

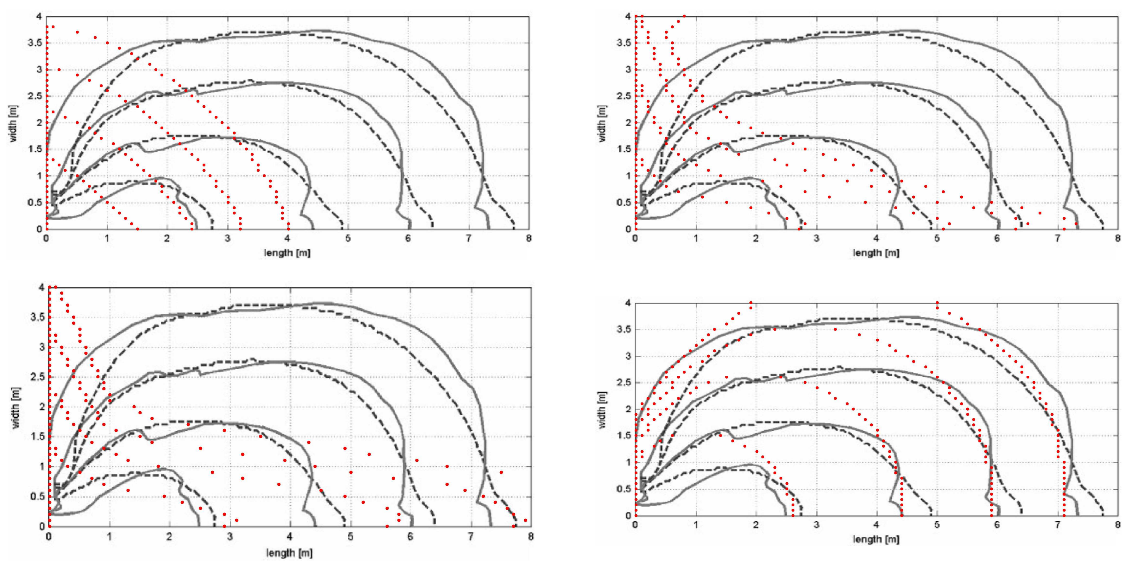

Figure 4.7: SFINCS and XBeach propagation fronts for the 2D dam break test with dry bed after 1-4 seconds. With $n = 0.012 s/m^{1/3}$ for XBeach and with $n = 0.03 s/m^{1/3}$ for SFINCS. Upper left= SFINCS-LIE, upper right= SFINCS-SSWE 1D advection, lower left= SFINCS-SSWE 2D, lower right= XBSB. Red dots are the results of the model runs by SFINCS/XBeach, the dashed and solid lines are the modelled and measured results of Stelling and Duinmeijer (2003).

Table 4.3: Froude number for 1D and 2D dam break tests with dry bed for SFINCS and XBeach. $F_{r,x}$ is the Froude number for the maximum flow in x-direction. $F_{r,y}$ is the same for the flow in y-direction

1D dam break	$F_{r,x}$ [-]	**2D dam break**	$F_{r,x}$ [-]	$F_{r,y}$ [-]
SFINCS-LIE	1	SFINCS-LIE	5	2.5
SFINCS-SSWE	3	SFINCS-SSWE	40	10
XBeach	3	XBeach	4	3

To assess the representation of the 2D flow pattern, the water front is plotted for different time-steps in Figure 4.7. These are plotted over the measured and modelled results of Stelling and Duinmeijer (2003). SFINCS-LIE is not able to reproduce the hydrodynamic pattern. With SFINCS-SSWE the forward propagation speed is more correct, but the lateral flow velocities are off. With XBeach the results are much better, but still not as good as modelled by Stelling and Duinmeijer (2003). It is not known why this is the case. The differences between the SFINCS and XBeach results are mainly numerically (viscosity does not seem important in the 1D dam break test). Since the flooding and drying scheme of SFINCS seems sufficient in the 1D test, the different descritisation of the momentum equations probably causes the differences. Where SFINCS uses a explicit first order scheme, XBeach uses a second order accurate implicit scheme (Warming and Beam, 1979) by default. This could be the reason that XBeach is more stable for these supercritical conditions.

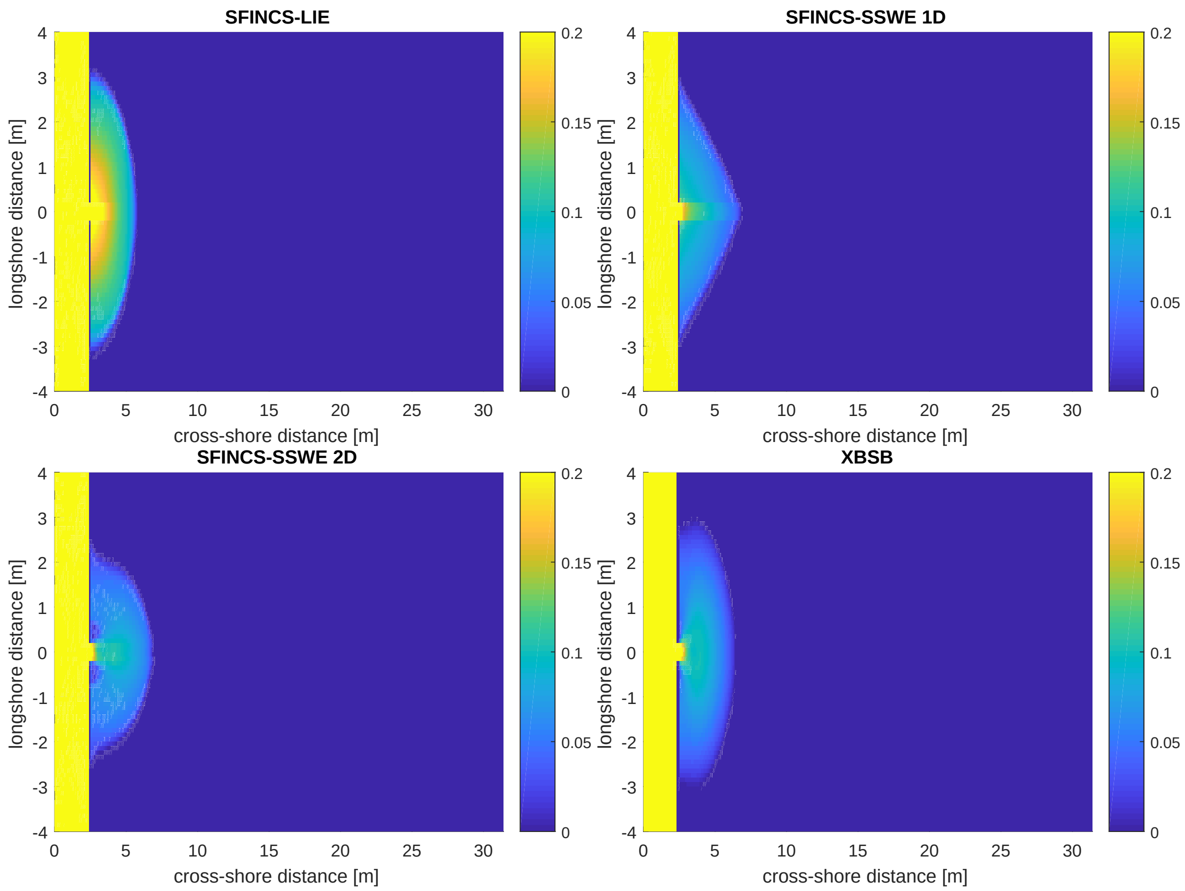

Figure 4.8: SFINCS and XBeach solutions for the 2D dam break test with dry bed with $n = 0.12 s/m^{1/3}$ after 4 seconds. Upper left= SFINCS without advection, upper right= SFINCS with 1D advection, lower left= SFINCS with 2D advection, lower right= XBSB, all after 4 seconds.

To assess the influence of the 2D part of the advection term in the momentum equation (see Section 3.2.4), the friction coefficient is increased until the solutions of SFINCS-SSWE are stable. This is with a Manning friction coefficient of $n = 0.12 s/m^{1/3}$, which is rather high. This is applied for SFINCS as well as XBeach and gives the 2D flow pattern of Figure 4.8. There can be seen that the 2D advection term of SFINCS-SSWE 2D improves the shape of the flow pattern compared to only using the 1D advection term in SFINCS-SSWE 1D. Therefore for 2D simulations where super-critical flow occurs, the full advection term should be included. Compared to XBeach the result is still not 'round' enough, but it definitely improves.

Efficiency
The computational efficiency of the initial runs without friction is shown in Table 4.4. SFINCS is faster since it solves less terms, but as displayed in the previous results you also loose quite some performance. Switching on advection in SFINCS makes the model slower, because it takes more time to calculate the momentum balance for every grid cell (since the time-step is the same). Therefore it not surprising that switching to 2D advection makes the model again a bit slower.

Table 4.4: RMSD (root mean squared difference) and SI (Scatter Index) compared to XBNH and the computation time over the whole simulation for the 2D dam break test with dry bed for SFINCS with $n = 0.03$ and XBeach with $n = 0.012$.

	RMSD [m]	**SI** [-]	**Computation time** [s]
SFINCS-LIE	0.069	0.710	2.215
SFINCS-SSWE 1D	0.032	0.240	3.478
SFINCS-SSWE 2D	0.031	0.232	4.087
XBSB	0.005	0.038	88.967
XBNH	0.000	0.000	137.000

Wet bed
The 2D dam break tests is performed again here but with a wet bed, by introducing an downstream water level of 0.05 m. In general the observations are the same as for the 2D dam break with dry bed. Because of the wet bed the friction forces become less dominant, which affects the outcome. For additional figures of the numerical solutions see Appendix B.5. For the wet bed the flow velocities are a little bit lower than for the dry bed case, but still too high for SFINCS-SSWE. Again XBeach performs a lot better than SFINCS, which sustains the hypotheses that the differences are because of the different numerical scheme and not because of the flooding and drying mechanism. However, the XBeach results are also in this case not as good as modelled in Stelling and Duinmeijer (2003)

4.2.4. Carrier and Greenspan
The flow related tests are concluded with the test best known as the Carrier and Greenspan test. It checks the ability of models to represent runup and rundown of non-breaking long waves. Hereby the wetting and drying capabilities are tested, as well as the correct representation of the nodes and the artificial dissipation within the model. The models results can be compared with an analytical solution derived by Carrier and Greenspan (1958). This describes the motion of a harmonic, non-breaking IG wave on a plane sloping beach without friction. The results of SFINCS are again also compared to XBeach as the advanced model. Hereby XBSB is used as a SWE model and since viscosity does not seem to play a significant role according to the dam break tests, the numerical solvers can be compared. The numerical setup of SFINCS and XBeach as well as a brief description of the analytical solution is given in Appendix B.6.

Accuracy
Figure 4.9 shows the results of SFINCS-LIE and -SSWE compared to the analytical solution of Carrier and Greenspan (1958) for the water levels and flow velocities. There can be seen that when advection is not included, the result differs significantly from the analytical solution. With the water levels the nodes of the standing wave pattern are not as clear as they should be. At the shoreline the water front during runup is too steep, similar to what is observed for the water front during the dam break tests. Therefore the runup is not high enough. This also visible with the flow velocities where the velocities during the uprush are underestimated. During the downrush the velocities on the other hand are overestimated. Including advection in the model (right panel of 4.9) makes the results significantly better. For SFINCS-SSWE the nodes seem correct compared to the analytical solution. Also the steep water fronts at the water line are much smoother. Hereby the maximum runup seems correct. The flow velocities during runup and rundown are also much better compared to the analytical solution than for SFINCS-LIE.

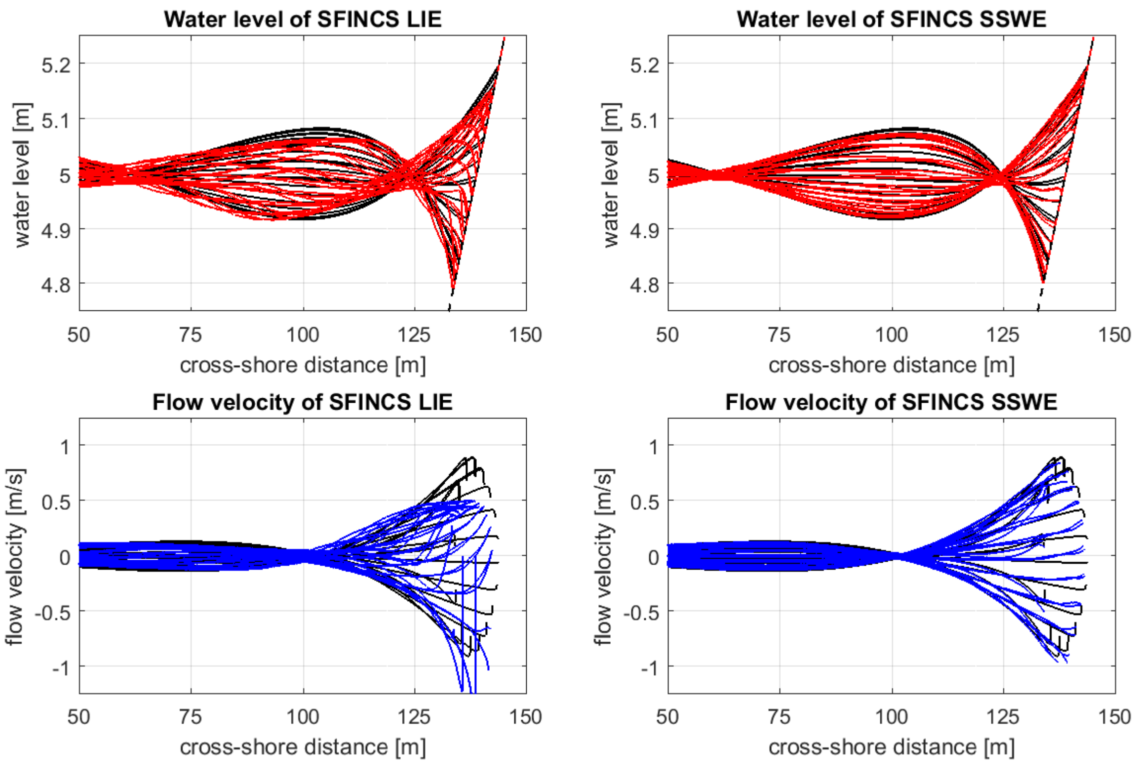

Figure 4.9: Water levels and velocities of the Carrier and Greenspan test compared to the analytical solutions. Black lines are of the analytical solution and the coloured ones of the SFINCS results. Left: SFINCS-LIE, Right: SFINCS-SSWE.

When the same figure is also made for XBSB in Figure B.11 of Appendix B.6.3, there can be seen that the results are not really better for XBeach compared to SFINCS-SSWE. The amplitude of the anti-node of the water level is a bit closer to the analytical solution and so are the maximum runup and rundown. However, the nodes are less 'sharp' than for SFINCS-SSWE. It is not clear why this is the case. In the same figure also differences between SFINCS and XBeach for the water levels at the offshore boundary are shown. Hereby the signal of XBeach is what is used as the input for SFINCS. For SFINCS-SSWE the most offshore grid cell still has the same water level signal as the XBeach input, but at one cell more into the domain differences occur. After the initial spin-up time, the water level is always a bit lower than the input. This does not occur in the XBeach results, which means that there is more artificial dissipation in SFINCS. This happens regardless whether the SFINCS-LIE or -SSWE version is used. Since the artificial dissipation is higher at the boundary, this also explains why the amplitude at the anti-node of the water levels is slightly lower in SFINCS compared to XBeach. Also the less expensive scheme in SFINCS can have a slight effect on this. Still, XBeach is not completely the same as the analytical solution as can be seen in Figure 4.10.

Table 4.5: RMSE compared to the analytical solution and computation time for SFINCS and XBeach for the Carrier and Greenspan test for t=328s (see Figure 4.10)

	RMSE [m]	**Computation time** [s]
SFINCS-LIE	0.013	20.561
SFINCS-SSWE	0.006	26.034
XBSB	0.019	65.786

Efficiency

In terms of efficiency, Table 4.5 is obtained. It can be seen that SFINCS is similarly fast as XBeach, bearing in mind the use of parallel processing. This is the case because SFINCS solves more grid cells (3001 as opposed to 801) and the average time-steps are smaller. Note that if the default α-value was chosen (see Appendix B.6), SFINCS would be about an order faster than XBeach. Although, then the results of SFINCS are less smooth and deviating a bit more from the analytical solution.

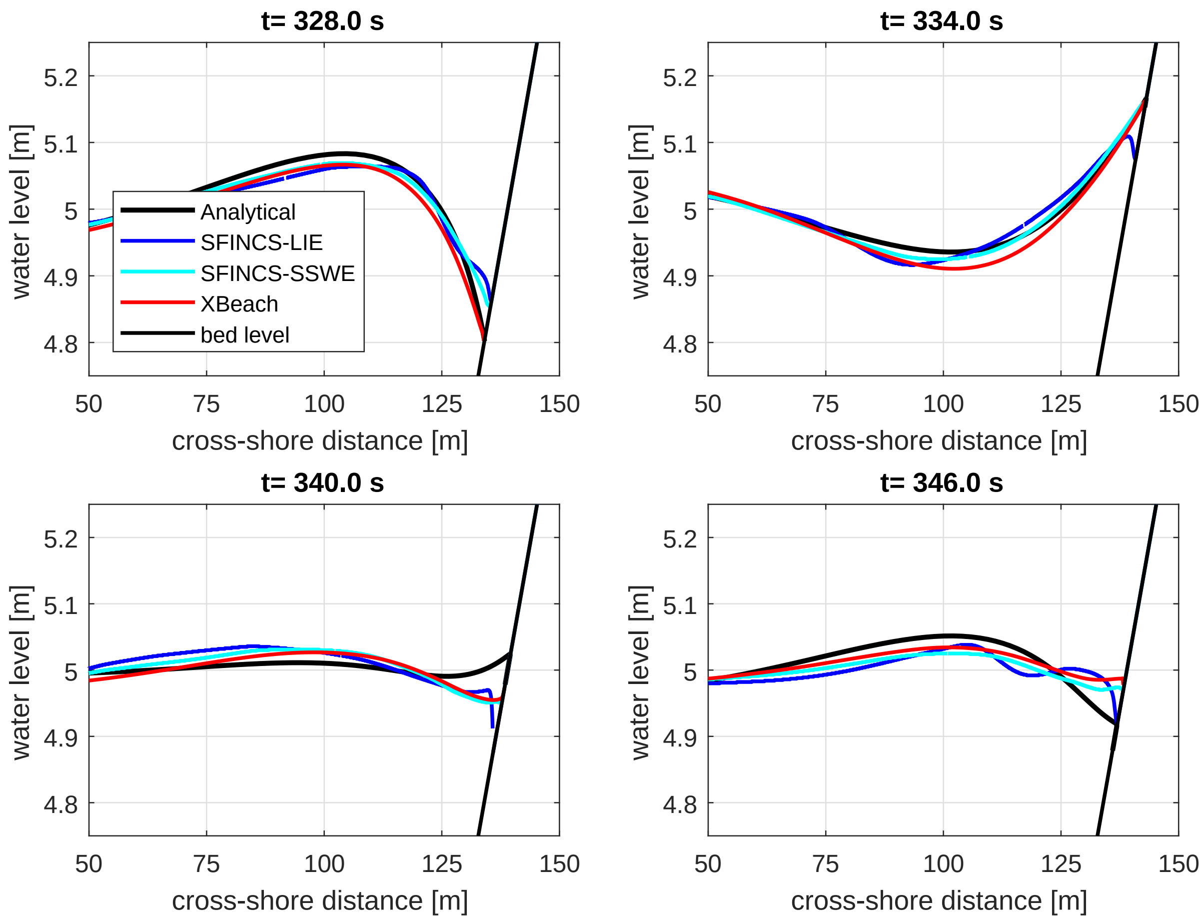

Figure 4.10: Comparison of the water levels of the analytical, SFINCS-LIE, SFINCS-SSWE and XBSB results of the Carrier and Greenspan test

4.2.5. Conclusion

The goal of the flow related conceptual tests is to analyse whether the flooding and drying mechanism of SFINCS works and what the influence of the advection term is. The models results indicate the following:

1. The simple drying and flooding method of the SFINCS model seems sufficient. For the Bates, Dam break as well as the Carrier and Greenspan tests similar results in drying and flooding performance compared to the advanced XBeach model are achieved, which contains a robust momentum-conserving drying/flooding formulation based on Stelling and Duinmeijer (2003) (Roelvink et al., 2009).

2. Advection is important when the flow is super-critical. As illustrated in the 1D dam break test, in the first phase after the dam break when the flow is super-critical the advection term is necessary to model the flow phenomena correctly. In a later phase the flow becomes sub-critical and without advection the results are similar.

3. The first order explicit scheme of SFINCS can handle super-critical flow when including advection within the limits of $Fr < 3$ in combination with a Manning friction of $n > 0.02 s/m^{1/3}$. Within those limits the results of the semi-advanced SFINCS model are comparable to that of the the second order implicit scheme of the advanced XBeach model. Outside of those limits the model results become unstable in the region of the super-critical flow, as seen in the 1D and 2D dam break tests.

4.3. Wave related tests

At first the goal of the wave related tests is explained in Section 4.3.1. Thereafter the numerical setup of XBeach and SFINCS is explained in Sections 4.3.2 and 4.3.3. Then the important swash zone processes are analysed in Section 4.3.4. Section 4.3.5 investigates the use of an indirect forcing and Section 4.3.6 the optimisation of the grid resolutions. Finally, in Section 4.3.7 all this is combined leading to the conclusions of Section 4.3.8.

4.3.1. Introduction

Ideally, in order to computationally efficient simulate compound flooding, including the effects of wave-driven flooding, the effects of waves are included directly in the SFINCS model without running a computationally expensive model like XBeach. This can be achieved with two steps. The first step is by parametrising the surf zone and imposing waves in shallow water as a swash zone model, see Figure 4.11. The second step is to apply SFINCS to simulate wave runup, overtopping and sequential wave-driven flooding (here only runup is tested, overtopping is a later step). In order to analyse the ability of a semi-advanced model (i.e. SFINCS-LIE or SFINCS-SSWE) to simulate wave-driven flooding, a series of conceptual runup tests is carried out. In these tests the semi-advanced model is compared to the advanced XBNH+ model. Due to limited observational data, it is assumed that the advanced model is 'the truth'. XBeach is used because it has proved to be capable of modelling waves in the surf and swash zone, see e.g. Roelvink et al. (2017). For more information on the choice between the different XBeach versions see Appendix C. The conceptual tests will start with different swash zone models directly forced from a full XBNH+ model (Section 4.3.4). Sequentially, an indirect forcing based on a wave spectrum is compared with the same full XBNH+ model (Section 4.3.5). All tests are still run in 1D, since first a good implementation in 1D has to be found.

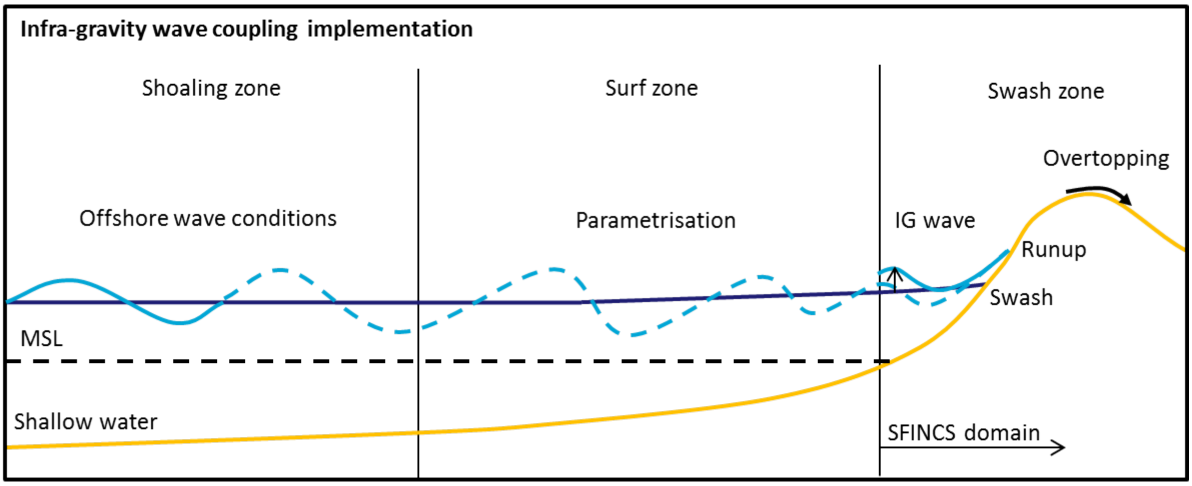

Figure 4.11: Schematic overview of the wave boundary implementation in SFINCS

For the conceptual tests, multiple XBeach models are run starting in DW and simulating the surf and swash zone. From these XBeach models the water level time-series at 2 m water depth (location of the SFINCS boundary) are retrieved, split into incoming and outgoing waves using the Guza-method (Guza et al., 1984) from which the variance-density spectra are created (see Appendix C). These wave signals and characteristics are put into different versions of swash zone models. These are SFINCS-LIE & -SSWE, XBNH and XBNH+. Thereafter the swash and runup characteristics of the full XBeach model are compared to the different swash zone models. Hereby the importance of the different terms of the momentum equation can be investigated. The test setup is illustrated in Figure 4.12.

Hereafter the wave spectra at 2 m water depth of the full XBeach model is used to make a water level signal, so that SFINCS can be run with an indirect forcing. The resulting swash and runup characteristics are then compared with those of the full XBeach model. Hereby the influence of IG and incident waves and the shape of the created signal are investigated. Finally the grid sizes are optimised in Section 4.3.6 leading to the proposed implementation in Section 4.3.7. For an overview of the different conceptual tests see Figure 4.13.

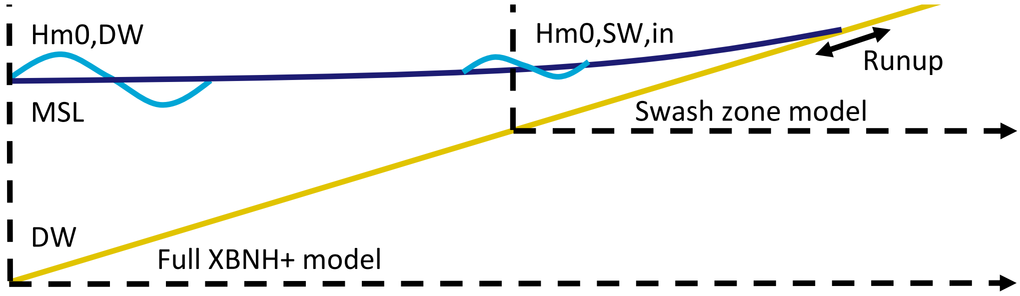

Figure 4.12: Illustration of the wave test setup with the full XBNH+ model and the smaller swash zone models, which use the incoming wave characteristics of the full model

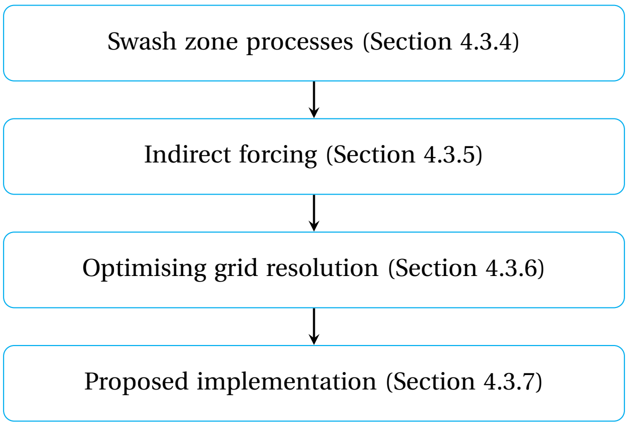

Figure 4.13: Flow chart of conceptual wave tests

4.3.2. Numerical setup XBeach

For the beach slopes the bathymetry has been kept simple using a linear slope for the entire profile. The dataset includes milder as well as steeper beach slopes ranging from $\beta = 0.01 - 0.1[-]$. The used grids are spatially varying and depend on the offshore conditions, see Appendix C. The number of PPWL is set to 40.

For the wave conditions a wide range of mild to more energetic offshore wave conditions is specified using a JONSWAP spectrum. The offshore wave steepness is kept below 0.14 according to the Miche criterion (Miche, 1944). Sections 4.3.4 through 4.3.6 use a small dataset of 64 runs with four slopes and $H_s = 6, 8, 10, 12[m]$ and $T_p = 10, 12, 14, 16[s]$. For testing the final proposed implementation a larger dataset is used in Section 4.3.7. This dataset consists of 540 runs with $H_s = 3 - 12[m]$ and $T_p = 9 - 17[s]$ in steps of one, with six different slopes. The corresponding Irribarren numbers ξ can be seen in Figure 4.14.

Within Figure 4.14 also the border between dissipative and more reflective conditions is shown, $\xi = 0.3[-]$ (Stockdon et al., 2007). This border is important because around this value the wave spectra characteristics change, with a larger amount of incident wave energy for increasing values of ξ. Within dissipative conditions most incident waves have broken in the surf zone, thereby dissipating energy. For more reflective conditions this is not necessarily the case, where more energy is present close to the coast and incident waves are more important or even dominant.

The models are run for six hours in order to accurately capture the effect of wave seeding on runup, for more details see Appendix C.1.2. Hereby the first 600 s are considered spinup and are not used in analysis. A constant Manning coefficient of $n = 0.02 s/m^{1/3}$ is used. This corresponds with the default value of XBeach and resembles sand. For additional information on used definitions, methods and model setup, see Appendix C. When XBNH(+) is used as a swash zone model, the incoming water level time series of the full XBNH+ model are imposed into the swash zone model. This model starts at 2 m water depth and has an equidistant 1 m grid. Because of constant grid size the exact number of PPWL varies per condition, but is in the same order as for the full XBNH+ model.

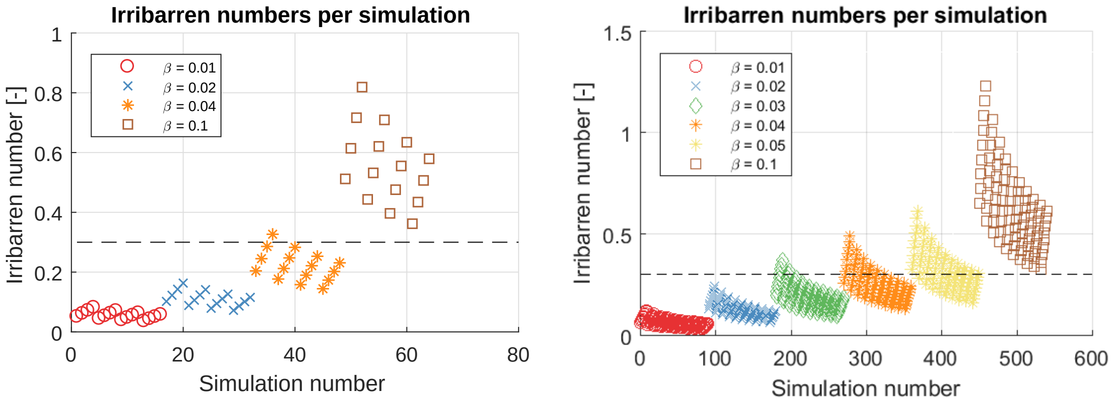

Figure 4.14: Irribaren numbers per slope, left: limited dataset, right: large dataset. The dashed line represents the border between more dissipative $\xi < 0.3$ or more reflective conditions $\xi > 0.3$. (Stockdon et al., 2007)

4.3.3. Numerical setup SFINCS

The grids of SFINCS are equidistant and start at 2 m water depth until MSL+15 m, which was also the maximum in XBeach. Initially, the used grid resolution for SFINCS is 1 m. Later in Section 4.3.6 this is increased to find the optimal grid sizes. This is has been done from a practical point of view (i.e. computationally efficient modelling). In cross-shore direction an additional 10 meters (of the same depth as the starting point) are added to the model bathymetry in order to overcome strong rundown peaks. During testing it turned out that it was needed during strong energetic conditions with a random wave forcing. This was applied for the SFINCS runs with indirect forcing with 10 additional meters. The amount of grid cells depended on the grid resolution and was rounded up, for more information see Appendix C.1.4. Also it is specified that the created boundary signal cannot drop below 0.5 m above the bed level, see the same Appendix.

The SFINCS model is forced with waves using different methods. At first the incoming water level time series of XBNH+ at 2 m water depth (including wave-induced setup) are imposed to analyse the accuracy of a semi-advanced model in simulating wave-driven runup. Thereafter this is changed into an indirect forcing, whereby the most accurate method is investigated. Then the forcing is based on the wave spectra of the incoming waves, rather than the actual water level time-series.

Furthermore the input for the wave boundary condition of SFINCS consists of a mean water level suitable for adding wave setup from DW to SW, tides and storm surge. For the SFINCS results with direct forcing this water level was set to zero (setup is included in the time series). For the SFINCS results with indirect forcing it was done using the parametrisation derived in Van Engelen (2016), see Equation 3.17.

4.3.4. Swash zone processes

In this first test, different swash zone models are directly forced with the incoming water level time series of the full XBNH+ model. Hereby every swash zone model is forced with exactly the same water level time series. Therefore the influence of the different terms within the momentum equations can be investigated. This gives insight in what model approximations of SFINCS, as explained in Section 3.5, are justified. Table 4.6 shows the six different used swash zone models and the solved terms. The XBNH+ NHSWE model is the most complete model with the including of viscosity, advection, non-hydrostatic pressure and a second layer. The XBNH model does not have a second layer. For both cases viscosity is also turned on and off (NHSWE and NHSSWE). Unfortunately it is not possible to force XBSB with the water level time series, therefore the true SWE are not tested. The results of the different swash zone models are shown in Figure 4.16 comparing the runup characteristic R2%. The results are discussed for the different terms.

Table 4.6: Terms of the momentum equations as tested with different swash zone models

	Local inertia, water level gradient & friction	Advection	Viscosity	NH pressure	2-layer
SFINCS-LIE	X				
SFINCS-SSWE	X	X			
XBNH NHSSWE	X	X		X	
XBNH NHSWE	X	X	X	X	
XBNH+ NHSSWE	X	X		X	X
XBNH+ NHSWE	X	X	X	X	X

Advection

Figure 4.16 shows a comparison in runup (R2%) as calculated by the full XBNH+ model on the x-axis and 6 other model configurations on the y-axis. Comparing the results of SFINCS-LIE and SSWE in Figures 4.16 a&d gives insight into the role of advection. It is clear that losing the advection term has a significant effect on the results. Especially for the steeper slopes SFINCS-LIE significantly underestimates the runup compared to the full XBeach model. This can best be explained with a cross-section when comparing the water levels with and without advection, which is illustrated in Figure 4.17. Both showed runs have exactly the same forcing at the boundary, so the cross-sections can be compared. It can be seen that during the uprush the bore without advection remains steeper and does not flow out as high as the bore with advection, leading to a lower runup peak. This is similar to the results of the 1D dam break and Carrier and Greenspan tests with and without advection of Section 4.2. During the downrush it can be seen that without advection the water flows down too fast. This leads to an overestimated rundown peak, similar to the results in the basin of the 2D dam break tests of Section 4.2. This means that without advection the rundown and therefore the swash signal is overestimated and that therefore the performance is less. This also explains the issue with overestimated rundown velocities that occurred in Van Engelen (2016), where no advection was used in SFINCS. Interestingly, SFINCS-LIE compares well to the full XBeach model for the runs with slope 1:100. It was shown in Section 3.5.1 that in theory for IG waves the flow is friction and inertia dominated and that therefore the advection term could be neglected. The incoming wave spectra for one condition for different slopes in Figure 4.15 shows that the steeper the slope becomes, the more incident wave energy becomes present. Also the peak frequency of the IG part shifts to higher frequencies. For the 1:10 slope the variance density peak in the incident wave part is even higher than the IG part. But for the milder slopes the swash zone is IG wave dominated. This leads to the notion that for IG wave dominated coasts without hardly any incident wave energy, the advection term can be neglected. For steeper coasts where incident waves become important, the advection terms should be included.

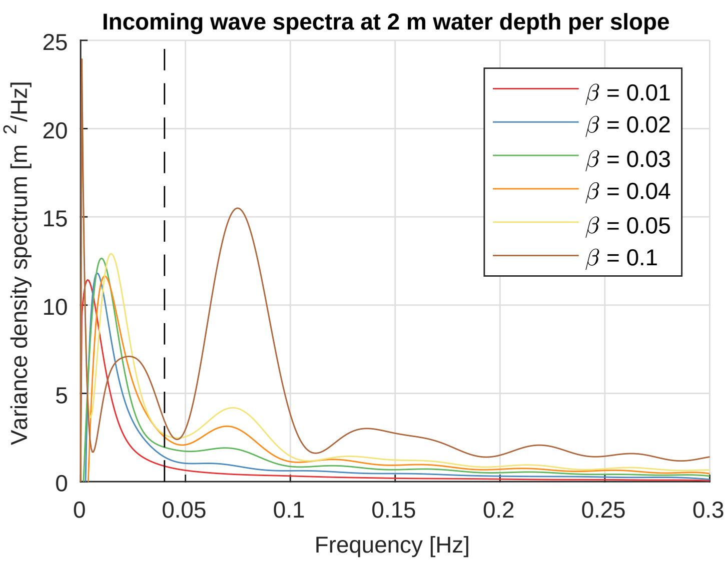

Figure 4.15: Illustration of the spectrum of the incoming waves per slope for the offshore condition $H_s = 10m$, $T_p = 12s$

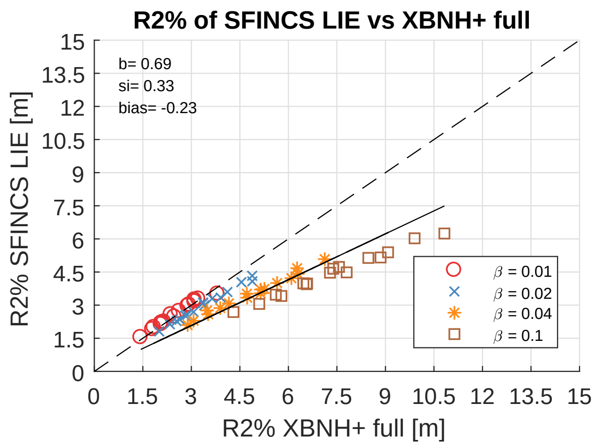

(a)

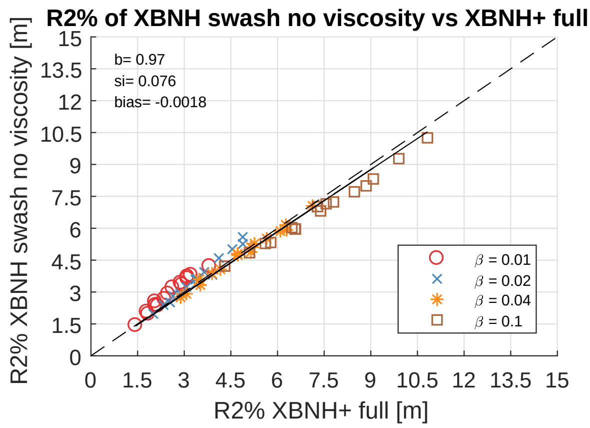

(b)

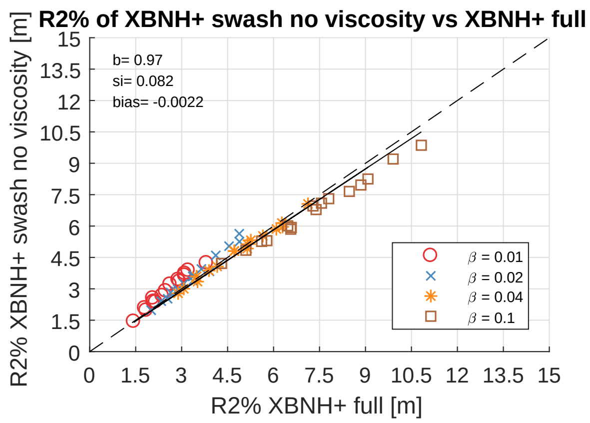

(c)

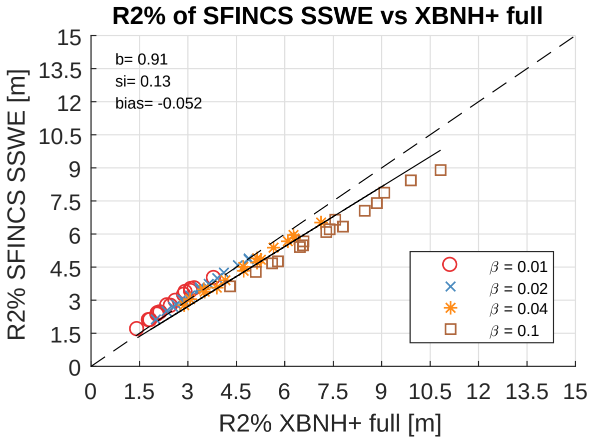

(d)

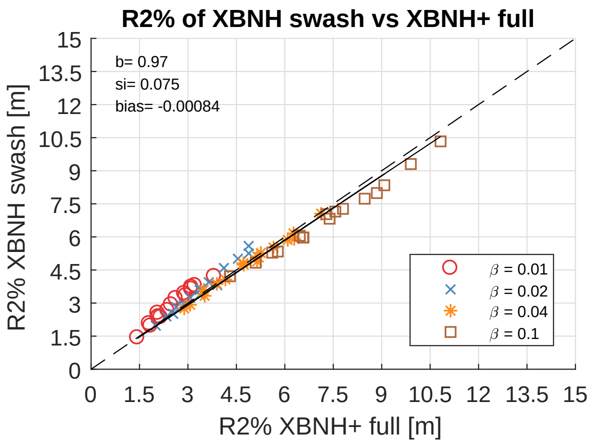

(e)

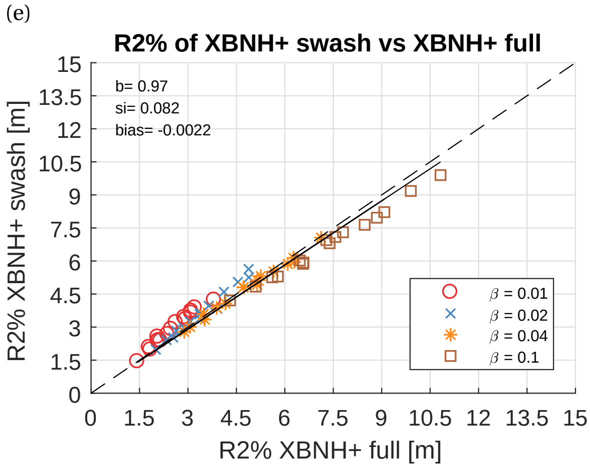

(f)

Figure 4.16: R2% of various swash zone models compared to the full XBNH+ model. a) SFINCS-LIE b) SFINCS-SSWE c) XBNH without viscosity d) XBNH e) XBNH+ without viscosity f) XBNH+. As statistical parameters the least-squared estimator 'b', Scatter Index 'si' and relative bias 'bias' are included, for more information see Appendix C

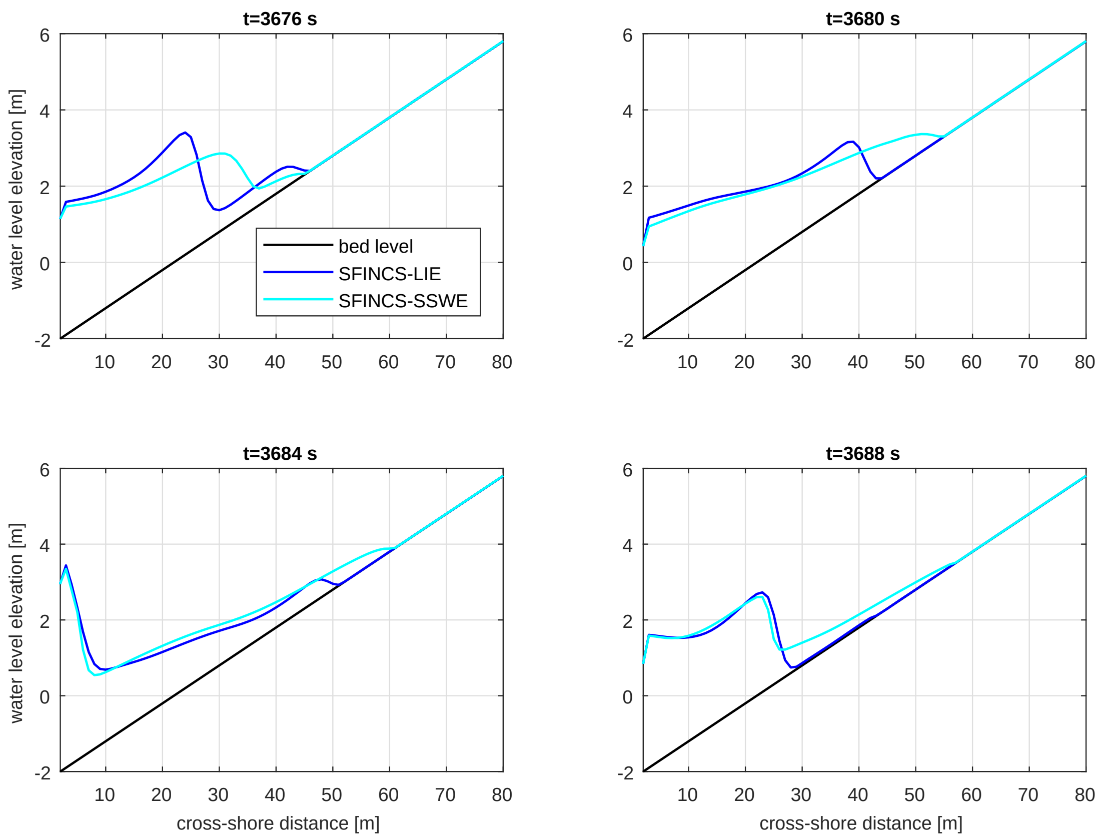

Figure 4.17: Comparison of the water levels of SFINCS with (-SSWE) and without advection (-LIE) for a condition with slope 1:10, $H_s = 10s$ and $T_p = 12s$

Viscosity

Although the influence of viscosity cannot be compared using a SSWE and SWE model, by turning on and off viscosity in XBNH(+) the role of viscosity can still be compared (NHSSWE vs NHSWE). Comparing XBNH with and without viscosity in Figures 4.16 b&e shows hardly any difference, although the results are not exactly the same. When comparing this for XBNH+ in Figures 4.16 c&f, the results are even smaller. That the viscosity term is not important for these types of flow conditions was also observed in Section 4.2, but a theoretical explanation is not known. The results give the notion that horizontal viscosity is in general not important in the swash zone and can therefore be neglected in SFINCS. The default setting for viscosity in XBeach is $0.1m^2/s$ (Roelvink et al., 2009).

Non-hydrostatic pressure

The influence of the hydrostatic pressure assumption can be investigated by comparing the results of SFINCS-SSWE and XBNH without viscosity. It can be seen by comparing Figures 4.16 b&d that the results including the NH pressure term are better than without the NH pressure term, although the difference is smaller than with the advection term. The runup prediction for the steeper slopes improves, which corresponds with theory. In Section 3.5.4 it was showed that for IG waves the hydrostatic pressure assumption should be valid, while for incident waves it can become invalid depending on the depth. That the runup prediction with SFINCS-SSWE without the NH pressure is not that far off for steep coasts, is good for SFINCS. This could for instance be solved by applying a water level correction at the boundary. For mild slopes XBNH overestimates the runup, this is further investigated later.

Two-layer model

For completeness, the influence of the second layer in the XBNH+ model is analysed. The 2-layer XBNH+ model is used for the improved dispersion (see Appendix C.1.1) and to decrease the possible existence of numerical wiggles. Comparing the results of XBNH (NHSSWE and NHSWE) and XBNH+ (NHSSWE and NHSWE) in Figure 4.16, adding the second layer does not have an effect in the swash zone. This is explained by the fact that in SW the velocity profile is depth-uniform. Therefore a second layer is not needed to represent the velocity profile accurately.

General observations

Apart from observations specific to the terms of the momentum equations, also some more general observations can be made. Comparing the results of the XBNH+ swash and full scale model in Figure 4.16 f, the runup characteristics should in theory be the same since the same model is used. However, it can be seen that for the mildest slope the runup is slightly overestimated in the swash zone model. For the steepest slope the runup underestimated. This difference could in theory occur because of the Guza-method of splitting the wave signal into the incoming and outgoing waves. In De Beer (2017) a similar swash zone model with XBNH was also used with the Guza-method. There also differences in runup were observed, but it was thought not to be because of the Guza-method. This pattern of over and underestimation can also be seen for the other SFINCS-LIE & SSWE and XBNH runs. It is assumed that this is an artefact of the swash zone model approach, also it is not known for sure. Opposed to the full XBeach model the imposing model boundary is a lot closer to the coast, where reflecting waves might have a stronger effect on the performance of the boundary implementation.

Efficiency

The efficiency is shown in Table 4.7, it can be seen that on average SFINCS is in the order of 5 times faster. The maximum speed-up is in the order of a factor 10. However, SFINCS was run using parallel processing so the actual speedup is lower. The comparison of the runtimes is a fair since all the models use the same grid and the same input. It is logical that the SFINCS models run for a shorter amount of time, since they solve less terms of the momentum equations. Interestingly, adding the 1D advection term (SFINCS-SSWE) increases the runtime on average only by 1% . Furthermore, differences in runtime between SFINCS and XBeach can occur because of the different numerical schemes. So although you can loose accuracy for incident wave dominated conditions, using SFINCS improves the computational efficiency. Hereby there has to be noted that for modelling convenience the α-value of Equation 3.13 was set to the minimum of 0.1 to ensure model stability. Section 4.3.6 shows that this value can be increased, which means that the numerical speedup factor will be larger than depicted in Table 4.7.

Table 4.7: Maximum, mean and minimum runtimes of the different swash zone models in seconds

Runtime [s]	SFINCS LIE	SFINCS SSWE	XBNH NHSSWE	XBNH NHSWE	XBNH+ NHSSWE	XBNH+ NHSWE
max	482	496	4105	4162	3970	4194
mean	380	384	1568	1701	1569	1551
min	223	280	389	387	391	379

Conclusion

For IG wave dominated conditions without hardly any incident wave energy left in the swash zone, a LIE model can still have realistic runup characteristics. Hereby the computational efficiency can be increased with an order of 5-10. For conditions where the amount of incident wave energy cannot be neglected, the advection term is needed for realistic runup predictions. If the incident wave energy is dominant with reflective coast conditions (as for slope $\beta = 0.1$), also the NH pressure term is needed. For those conditions the hydrostatic pressure assumption becomes invalid. Furthermore it is observed that the viscosity term does not play a role, although this cannot be theoretically explained. Also the 2-layer model of XBNH+ is not important in the swash zone. In general it is observed that there is a pattern that for the mildest slopes the runup is slightly overestimated and for the steepest slopes slightly underestimated. Comparing the full and swash zone model results of XBNH+, the results should be the same but this was not the case. This does not seem to occur because of the Guza-method of splitting the incoming and outgoing waves. Therefore the hypothesis is that it is an artefact of the swash zone model approach, although it is not known for sure.

While the results of SFINCS-SSWE are significantly better than SFINCS-LIE for steeper slopes and the added computational time is negligible, from here onwards only SFINCS-SSWE is used for the upcoming conceptual tests. For the incident wave dominated conditions there is a consistent underestimation of the runup because the NH pressure term is not solved, but this can be solved using an added water level correction at the boundary. It was not known yet that SFINCS could also be using for modelling incident waves

(Van Engelen (2016) only imposed IG waves), but it is shown that with a SSWE instead of a NHSWE model for modelling the swash zone still realistic runup predictions can be made. The direct forcing as used here is not wanted for the final implementation because it means that still an XBeach model has to been run from DW to 2m water depth, with the corresponding high computational load. Therefore there is tested whether an indirect forcing can be made in the next section.

4.3.5. Indirect forcing

After showing that it is possible to model realistic runup conditions using a semi-advanced model with a swash zone modelling approach, there is assessed whether the boundary water level time-series can also be made indirectly. Hereby the direct incoming water level time-series of the full XBNH+ model is not used any more, but only the wave spectrum of that time series. In a future setup this spectrum can be parametrised, saving computation time by not needing a nearshore model like XBeach to derive the wave characteristics at the boundary of SFINCS. The different investigated options to make a time-series from a spectrum are shown in Figure 4.18. The first step for an indirect forcing is to use a single sinusoid IG wave forcing. Thereafter a random IG wave signal is investigated and finally a random incident wave signal. Also the role of the parametrisation of the wave-induced setup is analysed.

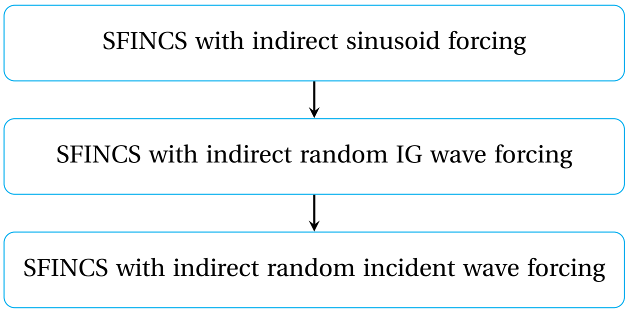

Figure 4.18: Flow chart of indirect forcing approaches

Sinusoid wave forcing

Initially, in the SFINCS model the boundary signal was based on a single sinusoid, see Eq 3.15 (Section 3.3.3). Hereby the wave energy $H_{m0,IG}$ is used as input for the significant wave height and the peak frequency for the wave period. However, the result of this forcing is as that after every wave period the time series repeats itself. This means that the maximum runup is approximately the same every wave period. Therefore the runup distribution is a single line, as opposed to reality where the swash signal is more random and the runup distribution approximately Gaussian. This means that the boundary signal is too simple to have realistic runup characteristics.

Infragravity wave forcing

To make the signal more realistic, a sum of multiple sinusoids with random phases is used as in Eq 3.16. The method to convert a wave spectrum into a random water level time-series is based on Van Dongeren (2003) (for more information see Section 3.3.3). The the wave spectrum of the incoming waves is divided in frequency bins with a certain amount of energy. Hereby only the IG part of the wave spectrum is used. The frequency is used for the wave period of every sinusoid and the energy for the amplitude. After giving every sinusoid a random phase, an indirect random wave signal is made. The random phase is important to get a varying boundary signal in time, which then also leads to a varying runup signal in time. It is found that the method is energy conservative, so that the energy of incoming wave spectra is well transferred to the created signal. This gives realistic runup characteristics for IG wave dominated conditions (i.e. slopes<1:50). However, for conditions where incident waves become important the runup is underestimated (i.e. slopes>1:50). This can be seen in the left part of Figure 4.21. For this steep slope, the runup distribution and R2% is far off when including only the IG part of the wave spectrum.

Incident wave forcing

To improve the runup representation for the steeper slopes, the incident part of the wave spectrum is included as well to make a random wave signal. Hereby the spectrum is used up to the Nyquist frequency of

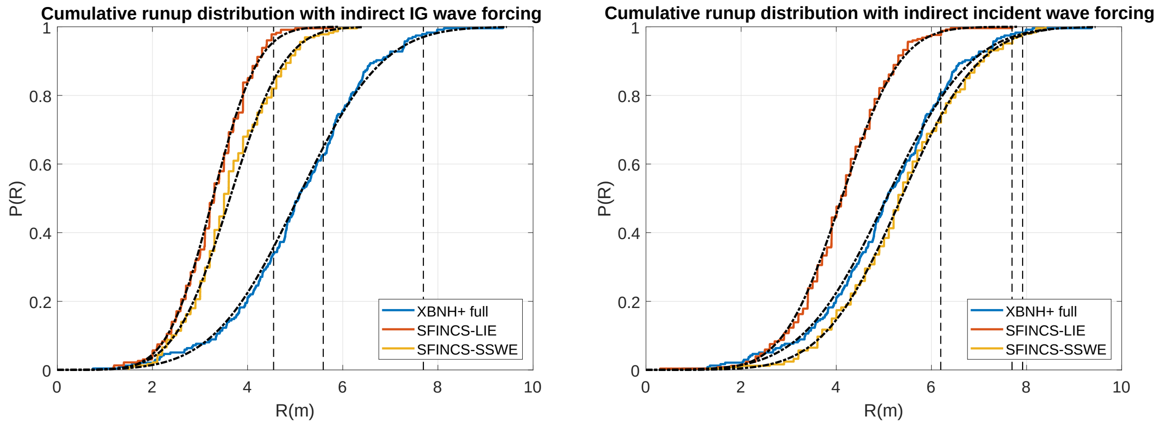

Figure 4.19: Cumulative runup distributions for with indirect IG and incident wave forcing, both with slope 1:10, $H_s = 10m$, $T_p = 12s$. Left: only IG wave energy, Right: full spectrum. Hereby the dashed lines through the distributions are the corresponding Gaussian fits. The vertical dashed lines are the R2% values

0.5 Hz, see Section 3.3.3. Since the signal is still made fully random, this means that there is no coherence between the IG and incident waves in the created signal. This is not observed in literature, but since it is the most simple (and thus fastest) way to create a wave signal it is applied here. When both incident and IG wave energy are included in the boundary of the swash zone SFINCS model, the runup distribution can be reproduced (right panel Figure 4.19). However, based on the difference between SFINS-LIE and SFINCS-SSWE it is clear that advection needs to be included when modelling runup.

Including the incident wave energy, the influence of the random forcing on the runup characteristics is shown in Figure 4.20. The applied mean boundary water level is based on the larger XBNH+ model and thus includes some wave-driven setup from DW to SW (-2 meter water depth). The varying water level itself is made with the random signal based on the incoming wave spectra. Compared to Figure 4.16d, the accuracy is only marginally less when using the random water level signal. The random signal therefore does not seem to reduce the R2% significantly.

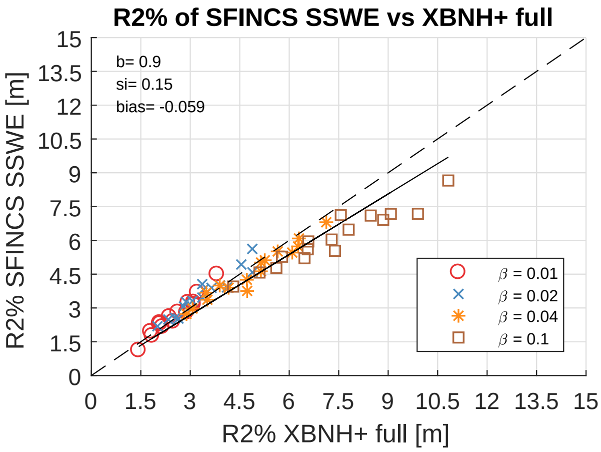

Figure 4.20: R2% of SFINCS-SSWE with the real wave-induced setup at the boundary of the full XBNH+ model combined with a random wave signal, compared to the full XBNH+ model.

In order to analyse the lack of differences in the runup distribution between the direct forced SFINCS model and the indirect forcing model, water level time series at different water depths are compared. Figure 4.21 shows in red the wave boundary signals as they are specified as input, whereby it is clear that the real signal has some skewness and asymmetry. Contrastingly the random signal shows no coherence between the waves whatsoever. The created water level signal in SFINCS at 2m water depth is exactly the same as the input, as it should be. More interestingly, the further from the boundary you come (so lower in the figure), the more asymmetric the waves become. This can be explained by the fact that the SWE do not account for frequency dispersion (Bosboom and Stive, 2015). Hence, shallow water waves travel with $c = \sqrt{g(h+\eta)}$, which means that larger waves can overtake smaller waves. This bore merging can be observed for the direct as well as the indirect forcing, but on the latter it is much more present because of the much more irregular boundary signal. The small very irregular waves are smoothed out because of advection. Combined with the merging of bores, the time-series at the shore (lower part of Figure 4.21) of the real and indirect forcing appear rather similar. For milder slopes boundary signal with direct forcing does not have such steep incident waves, since the signal is more IG wave dominated. In general these observations give the hypothesis that the lack of coherence in the boundary wave signal does not have a large effect on the asymmetry of the waves close to the shore.

In order to test the hypothesis that the lack of coherence at the boundary wave signal does not have a large effect on the skewness of waves, the skewness in model runs of SFINCS and XBNH+ is compared. The skewness is calculated using a Matlab script, with the definition: $s = \frac{E(x-\mu)^3}{\sigma^3}$. Figure 4.22 presents the skewness at the boundary (left panel) and of the swash signal (right panel). On the x-axis the model results from XBNH+ are shown and on the y-axis the model results from SFINCS. The symbols indicate different slopes of the bathymetry. As expected based on literature, at the boundary the XBNH+ model results indicate a skewness that seem to increase with the slope. In SFINCS this skewness is not present. This is due to the random phases applied when the indirect forcing was created. However, when the waves travel into the domain they become more skewed (see also Figure 4.21). Therefore, the differences between SFINCS and XBeach are much smaller for the skewness of the swash signal (right panel of Figure 4.22). In fact, the regression line is almost 1:1. The amount of scatter in skewness is however also significant. Moreover, when comparing the XBNH+ results from both panels in Figure 4.21, the amount of skewness reduces between the boundary and the shoreline.

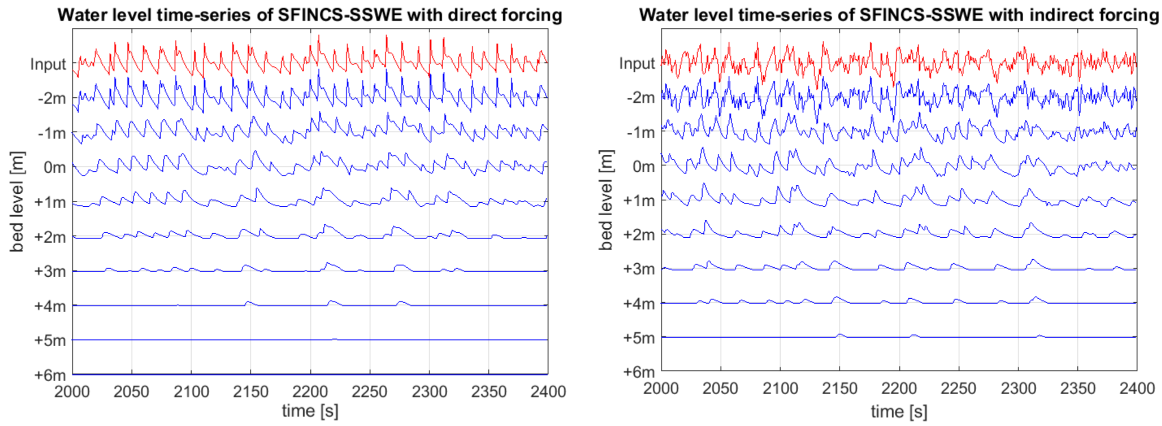

Figure 4.21: Comparison of water level time-series of SFINCS at different bed levels around their mean, Left: direct forcing, Right: with indirect forcing. In red the input time-series is shown. Both are with slope 1:10 and offshore condition $H_s = 10s$ and $T_p = 12s$

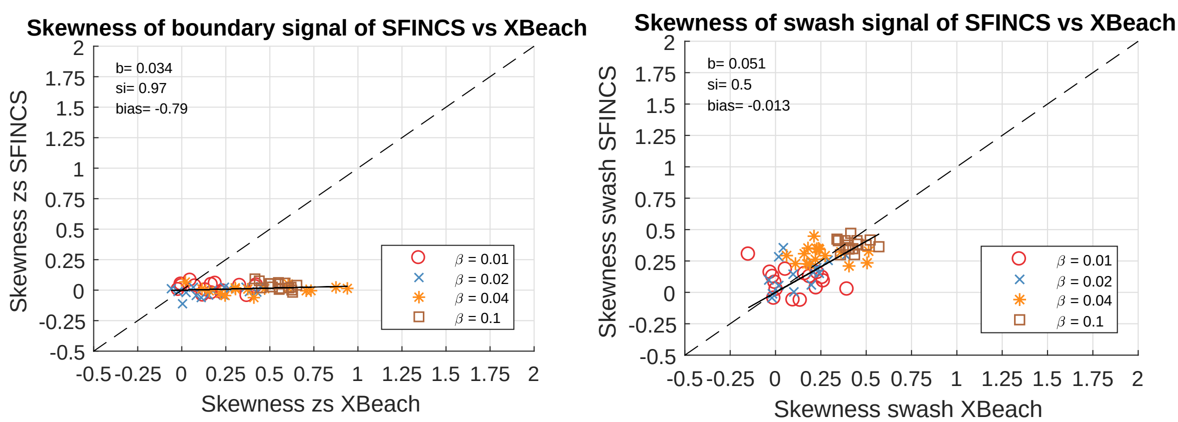

Figure 4.22: Skewness of SFINCS compared to XBeach, Left: skewness of the wave boundary signal, Right: skewness of the swash signal

Wave-induced setup

In the previous section, the mean wave-induced setup at the SFINCS boundary was taken from the realistic time-series of XBeach. With the idea of parametrising the surf zone in mind, this is done using a parametrisation of the wave-induced setup. A formula has been developed by Van Engelen (2016), the results with this parametrisation are shown in Figure 4.23. The original formula of Van Engelen (2016) (see Section 3.3.4) accounts for the setup from DW to SW as well as a setup correction for the incident wave-induced setup. The latter is not needed any more since incident waves are imposed in the model. This is showed in Figure 4.23b, where the original implementation is used. It is clear that using the whole setup correction of the formula leads to too high runup characteristics. The reason that also the runup for the IG wave dominates conditions is underestimated, can be because SFINCS-LIE instead of SSWE was used in developing the formula. Also it was made using milder energetic conditions than used here. On the other hand when not using a setup parametrisation at all (Figure 4.23a), the runup is underestimated. This is to be expected since then the wave-induced setup from DW to SW is not accounted for. In Appendix C.3.2 there is investigated how much the parametrisation should be reduced.

It is found that a reduction of 60% gives the best runup predictions. The 60% reduction of the setup formula that is used here, indirectly also accounts for the runup underestimation for using the SSWE without a NH pressure term. Comparing the runup characteristics of Figures 4.20 and 4.23b, shows that with the parametrised setup the runup is slightly better. This is mainly because of the higher water level at the boundary to counteract the lack of solving the NH pressure term. The slight overestimation is fully dependent on the exact percentage of reduction of the original formula. Also with this random wave forcing the pattern that the runup for milder slopes is overestimated and the runup for steeper slopes underestimated, can be seen. It is however a bit smaller, since the setup parametrisation takes into account the offshore slope. Hereby there has to be noted that the 60% reduction is a temporal solution. It is advised that the parametrisation of the wave-induced setup is altered completely. This can be like Eq 4.2, but this falls outside of the scope of this conceptual test.

$$\text{swash zone correction} = \text{setup DW to SW} + \text{NH pressure correction} + \text{(advection correction)} + \text{(incident wave correction)} \tag{4.2}$$

Conclusion

It is shown that with SFINCS-SSWE it is also possible to achieve realistic runup characteristics when using an indirect random wave forcing. This is done by making a random wave signal based on the wave spectrum of the incoming waves. For coasts where incident waves are more significant or even dominant, the incident part of the wave spectrum is necessary to achieve correct runup characteristics. For the rest of the conceptual wave tests, the incident wave energy is therefore included. Furthermore, the lack of asymmetry and skewness of the random boundary signal does not seem to harm the runup characteristics due to bore merging in the model. However, the wave-induced setup parametrisation has to be altered. The parametrisation as derived by Van Engelen (2016) also accounts for the incident wave-induced setup, which is now included in the model itself since the incident wave energy is included at the boundary. To move forwards this is done by reducing the parametrisation by 60%, but this is a temporal solution.

4.3.6. Optimising grid resolution

Up to now, the same model setup with a grid resolution of 1 meter is applied for all bathymetry slopes. However, from a practical point of view larger grid cells are preferred in order to reduce computational time. Therefore there is analysed if the grid size can be increased for certain conditions. Also it is investigated whether the time-step reducing factor α can be increased. Up to now the factor was set to the minimum value of $\alpha = 0.1$, to make sure that no instabilities occur in the model results affecting previous made conclusions.

Grid size increase

In order to estimate the the maximum grid resolution per slope, SFINCS-SSWE with an indirect incident wave forcing and 60 % setup reduction is run with grid resolutions of 1, 2, 5, 10, 20 and 50 m. A comparison for the Runup $R_{2\%}$ is shown in Figure 4.25. Additionally, the same is done for the mean setup, S_{ig} and S_{inc}. This is shown in Figures C.14, C.15 and C.16. The figures give an insight on how sensitive a parameter is on the used grid resolution per slope. The statistical parameters per slope are given in Table C.3. In general the result is

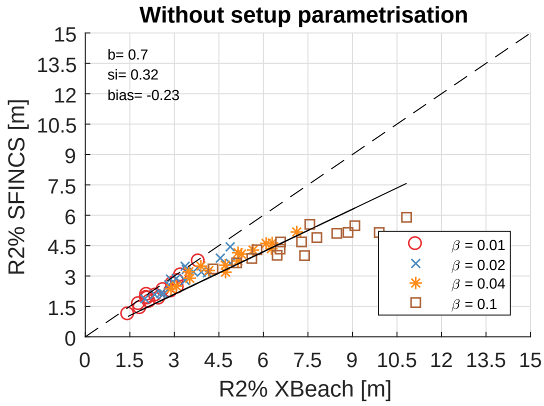

(a)

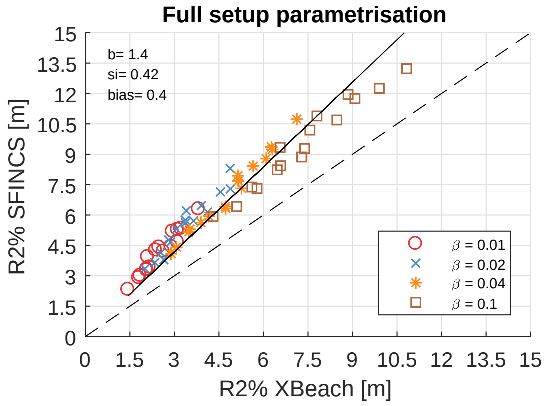

(b)

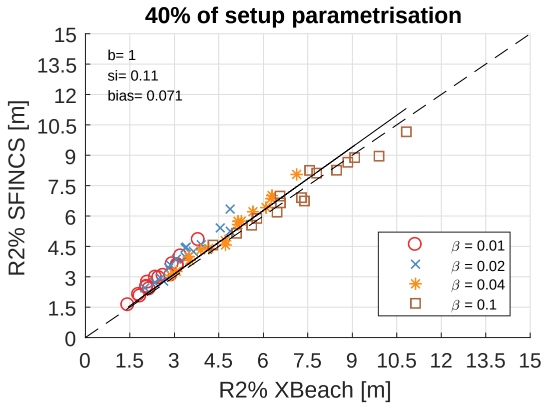

(c)

Figure 4.23: R2% of SFINCS with different amounts of wave-induced setup at the boundary compared to the full XBNH+ model. a) without any setup at the boundary b) 40% of setup parametrisation c) full setup parametrisation

that for R2% the mild slopes can have quite large grid sizes, but that the steeper slopes already differ using grid resolutions of 5m.

Finding the optimum for the grid sizes is done in Appendix C.3.3, where first per parameter and slope the grid size with the least scatter and bias is found. Thereafter the optimum grid sizes per parameter and slope are compared, giving the maximum advised grid resolution per slope as depicted in Figure 4.24. When also including 1:33 and 1:20 slopes, the general trend seems to be $dx_{max} = 0.2/\beta$, but this is only a general indication. There can be seen that increasing the slope exponentially decreases the maximum grid resolution, because of runup distribution accuracy and incident wave presence reasons as explained before. It is promising that for IG wave dominated coasts the grid resolution can be an order of magnitude higher then used so far. For incident wave dominated coasts the resolution has to remain rather small, although the order of magnitude is not smaller than common for an advanced model like XBNH. In general, the number of PPWL with these grid resolutions are in the order of 40 for the incident dominated coasts with a minimum of 20. This number is also applied in advanced nearshore models. For the IG dominated coasts the number of PPWL is higher, but the grid resolution cannot be further increased. Then the runup distribution is not reproduced correctly any more.

Time-step reduction

Since per slope the advised grid sizes are determined, the only step left is determining the maximum α-values per slope. So far this is run using $\alpha = 0.1$ (see Eq 3.13) for modelling convenience, but for computational efficiency it can probably be increased. This is tested by running the most energetic condition for all slopes and testing what the maximum value for α can be without having the model results to implode, see also Figure 4.24. It are these maximum values that are used for all the conditions within that slope in Section 4.3.7. This means that the α-values for milder slopes are a bit underestimated but this was much more effective for engineering practice when running 540 models. For completeness the maximum α-values for the weakest condition is also included in the figure, to give an idea of how much the α-values can be increased for mild energetic conditions. For information on the sensitivity of the SFINCS results, see Section C.1.5.

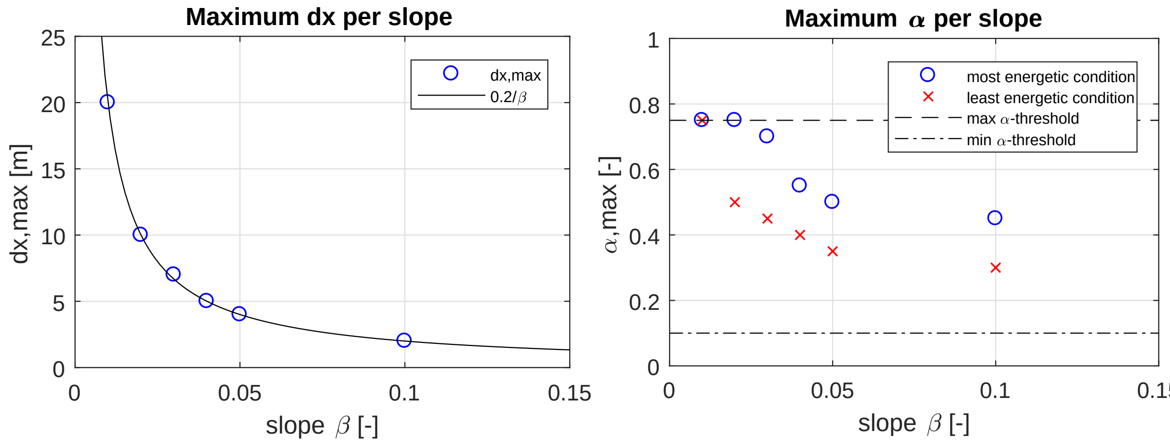

Figure 4.24: Maximum advised grid sizes and α-values. Left: maximum advised grid size per slope, Right: maximum α-value per slope for advised maximum grid size per slope

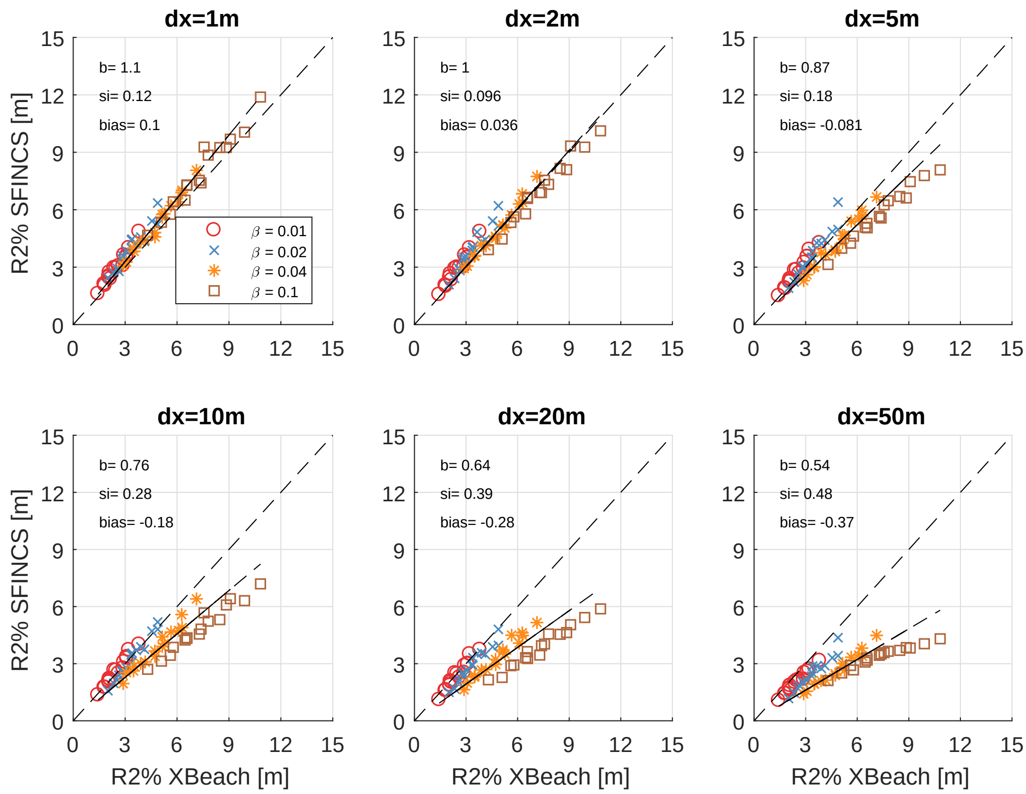

Figure 4.25: R2% of SFINCS compared to XBeach for the limited data set, per grid resolution

Conclusion

For computational efficiency the required minimal grid resolution and alpha-values were analysed. Model results indicate that the minimal grid resolution and α-values can be increased. Both can be increased the most for milder slopes with IG wave dominated conditions.

4.3.7. Results proposed implementation

Since the validity of the assumptions in the swash zone is discussed, a method for making an indirect forcing is introduced and the grid resolutions increased for practical use, the proposed implementation is further tested for additional swash zone parameters besides R2%. This is done using a larger dataset of 540 conditions including 2 more slopes and also some more less energetic conditions. At first the accuracy of the boundary implementation is shown, thereafter that swash zone characteristics and efficiency compared to modelling practice. The overall conclusions are discussed in Section 4.3.8.

Boundary implementation accuracy

When the incoming significant wave heights of XBNH+ and the significant wave heights of the created random signal at the SFINCS boundary are compared in Figure 4.26, it can be seen that the IG as well as the incident wave heights correspond well. The differences are small and therefore there can be concluded that the method of creating a random wave boundary signal is successful in containing the amount of energy of the initial spectrum. Furthermore there can be observed that the range of $H_{m0,ig}$ for all the different conditions is in the same order of magnitude. However, for $H_{m0,inc}$ there is the clear distinction that the steepest slopes have the most incident wave energy in the spectrum, as one would expect. This also means that the more reflective conditions have more energy left at 2m water depth (hence they are less dissipative).

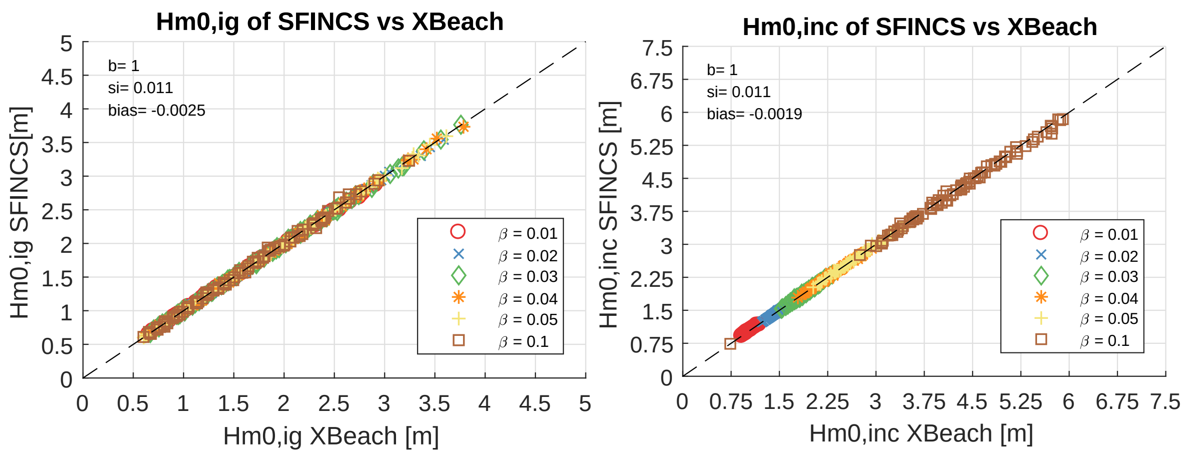

Figure 4.26: Significant wave heights of SFINCS compared to XBeach, Left: infra-gravity, Right: incident

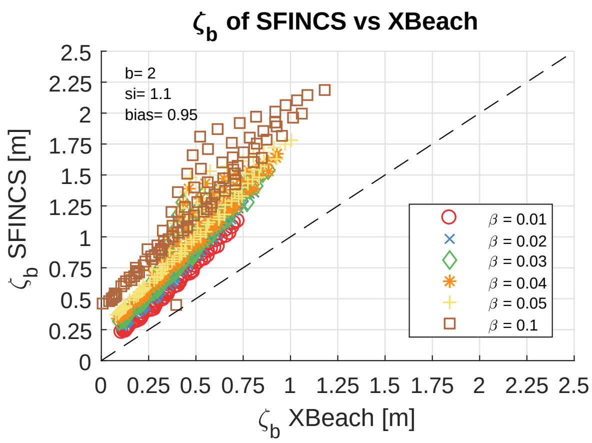

Figure 4.27: Mean water level at 2m water depth ζ_b of SFINCS compared to XBeach

Comparing the mean water level at the boundary ζ_b between SFINCS and XBNH+ in Figure 4.27, shows that SFINCS always overestimates the water level at the boundary. The water level is always bigger than zero because of the wave-induced setup from DW to SW. The additionally needed water level is mainly correction for not solving the NH pressure term. This term is important because of the local invalidity of the hydrostatic assumption when incident waves are present in the wave spectrum. That an additional water level is also present for IG wave dominated conditions, is partly because the wave-induced setup parametrisation is reduced indirect of the slope. Also the pattern of slightly overestimated runup for milder conditions was already seen in Section 4.3.4 and is thought to be a artefact of the swash zone modelling approach. That the water level at the boundary is higher then for XBNH+ is not a problem, as long as the corresponding runup predictions are correct.

Swash zone accuracy

Investigating the significant swash S_{ig} and S_{inc}, one notices that S_{ig} is slightly under- or overestimated depending on the slope (see Figure 4.28). Deviations compared to XBeach can occur because of the random wave boundary signal. Because the signal is more random than in reality, it can occur that the water level at the boundary drops quickly. This then results in a waterline that drops significantly and leads to a swash signal with a higher amplitude and therefore higher significant swash. This rundown overestimation seems to happen more for IG wave dominated conditions. Only for the 1:10 slope there is no over-prediction of S_{ig}. Then there is more energy in the incident wave part of the spectrum, which is why the amount of S_{inc} on its term is more overestimated compared to the other slopes.

To explain this a bit further, there is checked what happens with S_{ig} and S_{inc} when SFINCS-SSWE and XBNH+ swash are forced with a direct signal (runs from Section 4.3.4). The figures are showed in Appendix C.3. There can be seen that XBNH+ swash also overestimates S_{ig} compared to XBNH+ full for the mildest slope, it is not clear why. For the other slopes S_{ig} is correct. For S_{inc} it is correct, apart from the steepest slope which is slightly overestimated. It can be the case that during the Guza-method for splitting the incoming and outgoing waves, higher order frequencies are introduced in the boundary signal. This is not known for sure. SFINCS-SSWE on the other hand underestimates S_{ig} for the steepest slope and overestimates S_{ig} for the other slopes. For S_{inc} it overestimates when incident wave energy is present, where the strongest overestimation is for the 1:10 slope as in Figure 4.28. It seems that compared to XBNH+ full, that for the incident wave dominated coast the amount of S_{ig} is underestimated and S_{inc} overestimated. The specific swash spectra give the impression that not enough incident wave energy is 'transferred' to the IG waves and thereby to the IG swash. The hypothesis hereby is that because the NH pressure is not accounted for, less bore merging and IG generation within the model occurs. It is not known whether this is actually the case.

Coming back to the results of the final implementation with indirect wave forcing. There the amount of overestimation of S_{inc} is in the same order of magnitude as for the direct forcing. Therefore it does not seem to be because of the random forcing (also because the lack of asymmetry and skewness does not seem to influence the runup characteristics). It is also possible that the numerical solver of SFINCS introduces some instabilities at the water line since it is only first order accurate, while for the second order implicit solver of XBeach this is not the case. It is not known whether this actually happens.

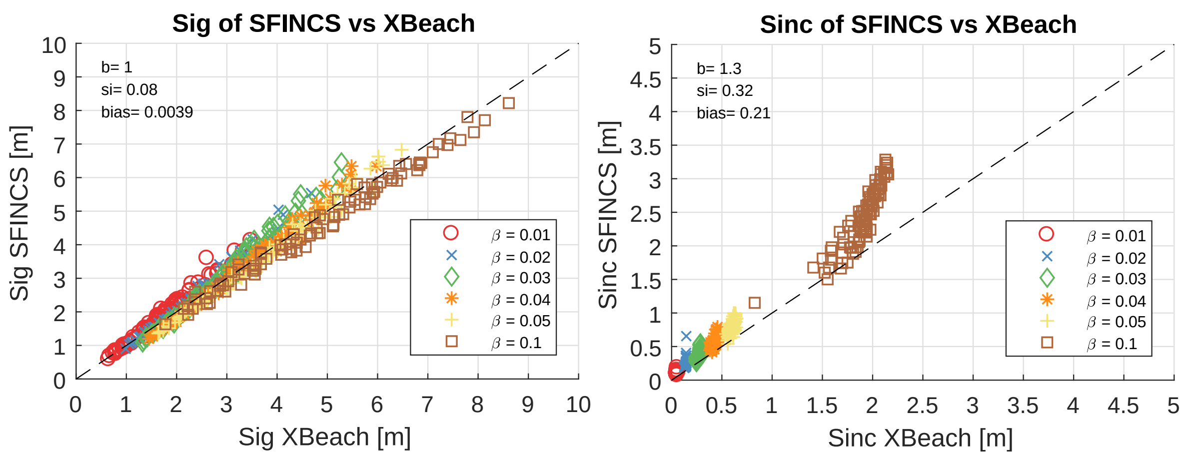

Figure 4.28: Significant swash of SFINCS compared to XBeach, Left: infra-gravity, Right: incident

A comparison of the setup, the mean value of the runup signal, in Figure 4.29 shows that still the amount of setup is generally underestimated compared to XBeach. It is found that with the proposed boundary implementation the rundown is overestimated for milder slopes, leading to a lower mean setup. When filtering the rundown from the swash signals it can be seen in the right plot that the trend of the predicted setup is correct, although there is scatter present. Here only the time-steps with a water level larger than the boundary water level ζ_b, are used when calculating the mean setup. This means that the rundown is not included in the averaging process. In terms of predicting overtopping, it is important that this setup at the coast and the runup characteristics are correct. Although it would be better when the 'full' setup would be correct as well. In general there can be noticed that the steeper slopes have a significant higher setup than the milder ones, since there is more energy left close to the coast.

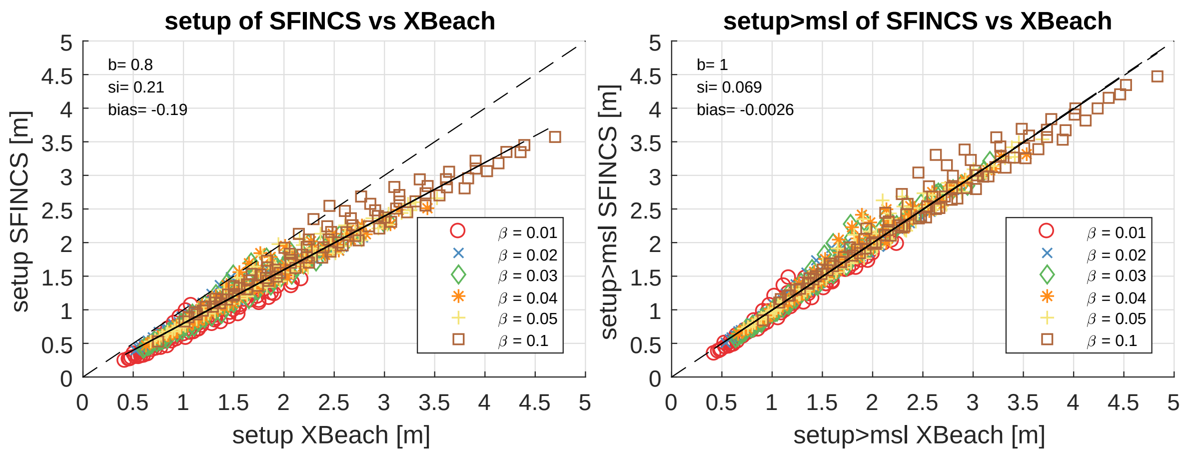

Figure 4.29: Mean setup at the shoreline of SFINCS compared to XBeach, Left: using the whole swash signal, Right: using the swash signal with zs>MSL

The runup characteristics $R_{2\%}$ and R_{max} in Figure 4.30 show that SFINCS-SSWE with the proposed implementation is well able to give realistic predictions regarding runup. The general trend is a slight underestimation of the runup, but this depends on the exact parametrisation of the boundary water level. For R_{max} there naturally is more scatter present because it is more dependent on the exact seeding of the boundary wave signal. This is also present in XBeach, see Figure C.1, where a 24 hour run did lead to a higher R_{max} than a 6 hour run. This is an uncertainty in seeding and is always present with modelling runup.

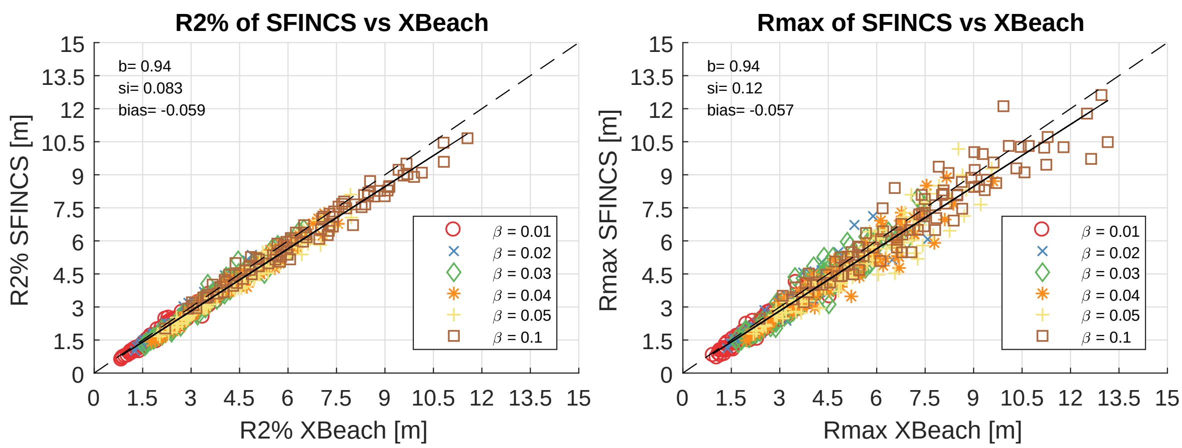

Figure 4.30: Runup characteristics of SFINCS compared to XBeach, Left: R2%, Right: Rmax

Modelling efficiency

Comparing the efficiency of the SFINCS swash zone model with the full XBNH+ model, shows that on average the speed-up factor is more then one order of magnitude bearing in mind the differences with parallel processing, see Table 4.8. This shows that with this implementation, the efficiency is significantly higher than the current modelling practice with a full advanced model. Hereby the future implementation with a parametrisation for the development of the wave spectra from DW to SW does not add additional computational time. The corresponding accuracy depends on the quality of the parametrisation of the wave spectrum from DW to

SW. The increased efficiency shows that with this approach the modelling efficiency significantly increases. Interestingly, the model runtimes compared to those of the direct forcing model runs of SFINCS-SSWE have reduced with an order of magnitude. This is because of the optimisation of the grid and α-values. In general the largest speed-up factors are achieved for the milder slopes.

Table 4.8: Maximum, mean and minimum runtimes of the final SFINCS SSWE implementation compared to the full XBNH+ runs

	Runtime [s]		Speed-up factor [-]
	SFINCS SSWE	XBNH+ full	
max	38	25733	1774
mean	19	2011	128
min	11	320	14

4.3.8. Conclusion

The goal of the performed wave conceptual tests is to investigate how wave-driven flooding can be modelled in an accurate and efficient way and what processes are important. The model results indicate the following:

1. The advection term is always needed to model wave runup. It is shown that with SFINCS-LIE the runup is strongly underestimated for steeper coasts. Because incident wave energy is present then, the advection term is needed. Including the viscosity term does not necessarily improve the results with XBeach, using the default value of $0.1 m^2 s^{-1}$. The NH pressure term as used in XBNH(+) is important when the wave spectrum is incident wave energy dominated. Excluding this term leads to an underestimation of the runup.

2. The incident wave part of the spectrum of the incoming waves needs to be included to model wave runup. It is shown that to be able to model runup accurately for dissipative and more reflective beaches, the incident waves (if present) are necessary to be included when modelling the swash zone. It is also shown that the semi-advanced SFINCS-SSWE model with a swash zone modelling approach is able to model this, although an underestimation of the R2% is present for incident wave dominated coasts by not solving the NH pressure term.

3. The current parametrisation of the wave-induced setup has to be changed. Since the incident wave energy is now included in the boundary condition, parametrising the incident wave-induced setup as in the formulation of Van Engelen (2016) is not needed any more. Only the wave-induced setup from DW to SW needs to be parametrised. Improving the parametrisation can be combined with making a correction term for not solving the NH pressure term. It is shown that the underestimation can be overcome by elevating the boundary water level.

4. Using an indirect random wave signal as a boundary condition based on the spectrum of the incoming waves can give realistic and similar runup characteristics to using the real water level time-series of an advanced model. As runup characteristics a R2% with a scatter index <10% can be achieved, for Rmax this is 12%. The swash zone characteristics are however effected by the random forcing. The rundown is overestimated because of the random forcing and corresponding lack of coherence between the IG and incident waves. Still the scatter index of S_{ig} is smaller than 10%. However S_{inc} is overestimated, the hypothesis is that this is mainly caused by the lack of solving the NH pressure term, but this is not known for sure.

5

Case Studies

In order to assess whether the conclusions of the conceptual tests also apply in more realistic cases, two case studies are performed. The first is regarding the wave-driven flooding at Hernani, which is discussed in Section 5.1. The second is regarding the traditional compound flooding at Jacksonville, which is discussed in Section 5.2.

5.1. Case study wave-driven flooding: Hernani

In order to access whether the results of the conceptual wave tests also apply in a real case with wave-driven flooding, a case study is performed regarding the flooding at Hernani, the Philippines, during Typhoon Haiyan (2013). There is tested whether SFINCS with the swash zone modelling approach is able to reproduce the flooding as good as an advanced model. Furthermore it is investigated whether the method of indirect forcing with a random phase signal gives similar results. At first an introduction into the flooding event is given in Section 5.1.1. Thereafter the model setup is discussed in Section 5.1.2. Then the results of modelling a 1D transect are showed in Section 5.1.3. Finally, the results of modelling a 2D model are given in Section 5.1.4 and the conclusions in Section 5.1.5.

5.1.1. Introduction

Under normal storm conditions the village of Hernani is protected by a fringing reef (see Figure 5.1) and 1 m high seawall in front of the village. However, Typhoon Haiyan was so extreme that this was not sufficient to protect the village. Although the surge offshore was only 0.7 m, still whole houses were swept away (see e.g. Roeber and Bricker (2015)). The offshore waves had an extreme significant wave height of 16 m, which generated large IG waves over the reef. When these waves reached the beach, they still contained a lot of energy and flooded the entire inland area. Existing surge models were not able to predict this destructive events since waves were not explicitly solved. This is the type of situation that triggered the development of the SFINCS model. To forecast such events EWSs are needed where waves are explicitly included. With this case study there is investigated whether this is possible with a semi-advanced model like SFINCS.

5.1.2. Model setup

To model this event an existing XBNH model is used as the advanced model, where the results of SFINCS are compared to. This model is based on Roeber and Bricker (2015), who modelled this with a Boussinesq-type model. The XBeach model has a 5 m grid resolution in cross-shore direction and 10 m in longshore direction. The model starts in deep water (80m-MSL) and models the entire reef slope, reef flat and inland area. With SFINCS there is started at the beach at the end of the reef flat (0m+MSL, see Figure 5.2), with the idea of a swash zone modelling approach where most of the energy dissipation has already happened. At this location the water level time-series are retrieved from the XBeach model and forced at the SFINCS boundary. This is done similarly to the conceptual wave tests. Hereby the Guza-method for splitting incoming and outgoing waves is not used in this case. The reason for this is that splitting waves can only be accurately carried out for 1D models and it is wanted to perform the Hernani case in 2D. The offshore conditions for the XBeach model are modelled by a Delft3D-FLOW & -WAVE model train. The surge is only 0.7 m, while the offshore wave characteristics are an extreme $H_s = 16m$ with $T_p = 17s$. The flooding event is modelled for 30 minutes. The

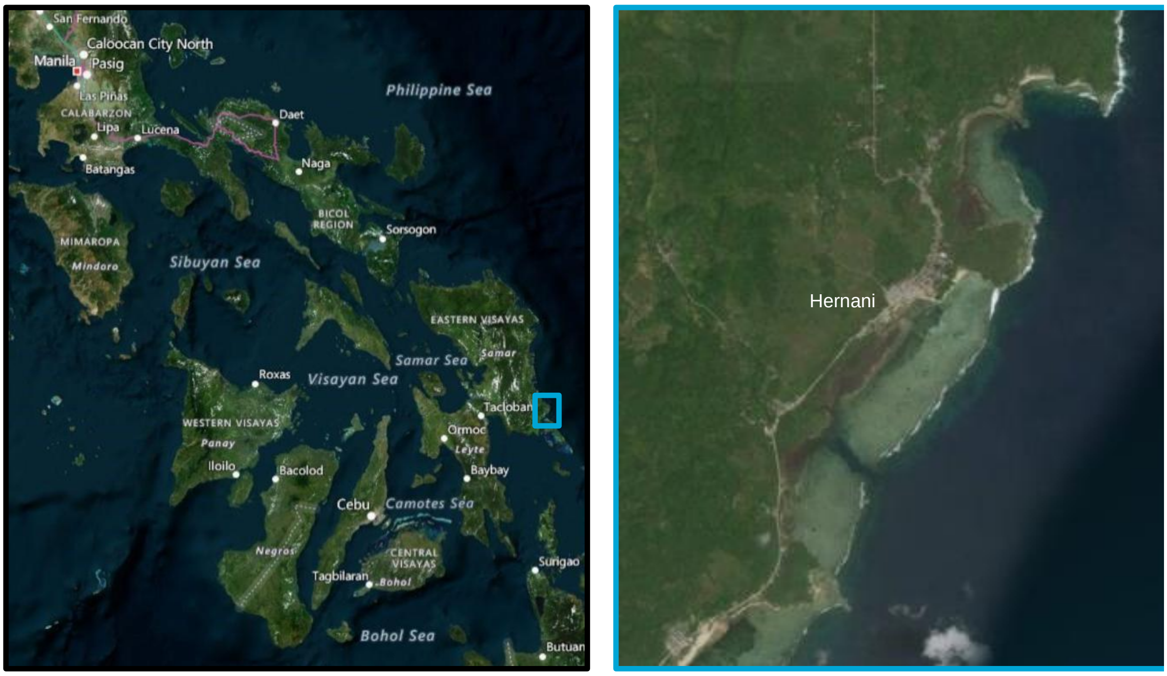

Figure 5.1: The location of Hernani in the Philippines, Eastern Samar Left: part of the Philippines with the location of Hernani in the box, Right: the village of Hernani with the reef in front of it

friction is set to a Manning value of $n = 0.028 s/m^{1/3}$. To keep the results of both models stable, the time-steps need to be reduced. In XBeach there is specified that $CFL = 0.2$ and in SFINCS that $\alpha = 0.1$.

First the flooding event is modelled in a 1D transect, to assess whether the swash zone modelling approach works also for this real case with a reef-flat type coast. The 1D transect is chosen at a similar location as in Roeber and Bricker (2015) (see Figure E.1 of Appendix E.1), where video images of a house swept away were taken. At the boundary of SFINCS still very large IG waves are present with a long peak period in the order of 300 s (see Figure E.2). The spectrum is similar to the 1D model of Roeber and Bricker (2015) and shows that at the beach there is no incident wave energy left. With SFINCS both the LIE and SSWE versions are tested, as well as the use of the real time-series of XBeach and an indirect random wave forcing. The latter is done the same way as for the conceptual tests, but then for the wave-induced setup the mean water level of XBeach is used. The parametrisation of Van Engelen (2016) is not made for a reef type coasts and can therefore not be used.

For the 2D model the setup of SFINCS is similar as the 1D transect, but then the spatial variability of the waves has to be captured. In order to do this the water level time-series of XBeach are retrieved from multiple locations instead of one. Along the shoreline an input location is used every 100 m, see Figure E.2. All these time-series are used as input for SFINCS, where internally there is interpolated for every boundary point between the time-series of the two closest input locations. Again also the use of a random wave signal is tested, this time in two different ways to assess the importance of a longshore coherence between the waves. The first is by making the time-series of every input location a random signal, where there is no coherence between the signals (called 'random phase'). The second is by keeping the random phases of all the bins the same between all the input locations, see Figure E.3 of Appendix E.2. Hereby only the amplitudes per bin differ between the different locations and a more longshore coherent signal is made (called 'uniform phase'). In the end the maximum water depths are compared between the XBeach and SFINCS models, as what is needed for an EWS.

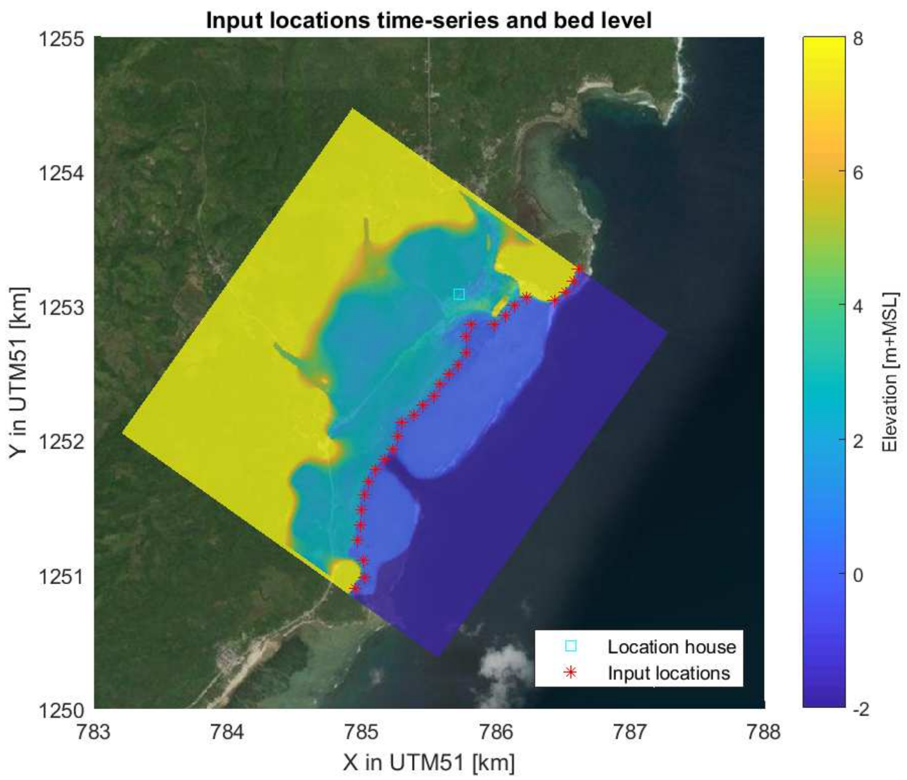

Figure 5.2: Input locations of water level time-series of SFINCS along the 0m+MSL shoreline for the 2D model. Also the location of the house that is swept away as described in Roeber and Bricker (2015) is shown.

5.1.3. 1D transect

In order to asses whether SFINCS can model the same extend of flooding as XBeach for a 1D transect, these are compared for the region from the beach and landwards. Figure 5.3 shows the maximum water levels for XBeach, SFINCS-LIE and SSWE. In the left figure SFINCS is forced with the real time-series of XBeach, nonetheless the maximum water levels are significantly underestimated. It can be seen that already at the boundary the maximum water levels are too low. Then the maximum water levels are constant until X=785.8km, where waves are overtopping and flow into the hinterland. To see what happens at the boundary, four snapshots of the instantaneous water levels are shown in Figure 5.4. It can be seen that the generated wave at the boundary is significantly lower in SFINCS than XBeach. This results in less overtopping and less flooding of the hinterland compared to XBeach. Based on the conceptual runup tests, the underestimation of wave runup can be caused by the lack of solving the NH pressure term or the swash zone modelling approach. The former is not likely because the spectrum contains only IG wave energy (see Figure E.2), so based on theory the hydrostatic pressure assumption should be valid. Therefore it is more likely that the underestimation is caused by the swash zone modelling approach. The forcing of the boundary of SFINCS is in this case very close to the seawall. The dissipation close to the boundary seems to be too large, which can also (partly) be artificial numerical dissipation. This dissipation is not noticed in the conceptual wave tests, but there more incident wave energy is present. It might be that the boundary implementation in SFINCS has difficulties producing low frequency IG waves with steep fronts. The differences between SFINCS-LIE and SSWE can be explained by that once overtopping occurs, the way they overflow is different. With SFINCS-LIE the wave bores remain steep, while with SFINCS-SSWE it is smoothed out more realistically. The steeper bores of SFINCS-LIE result in a higher maximum water level. With XBeach the maximum water levels inland are less smooth because more waves penetrate to the hinterland and influence the maximum water levels.

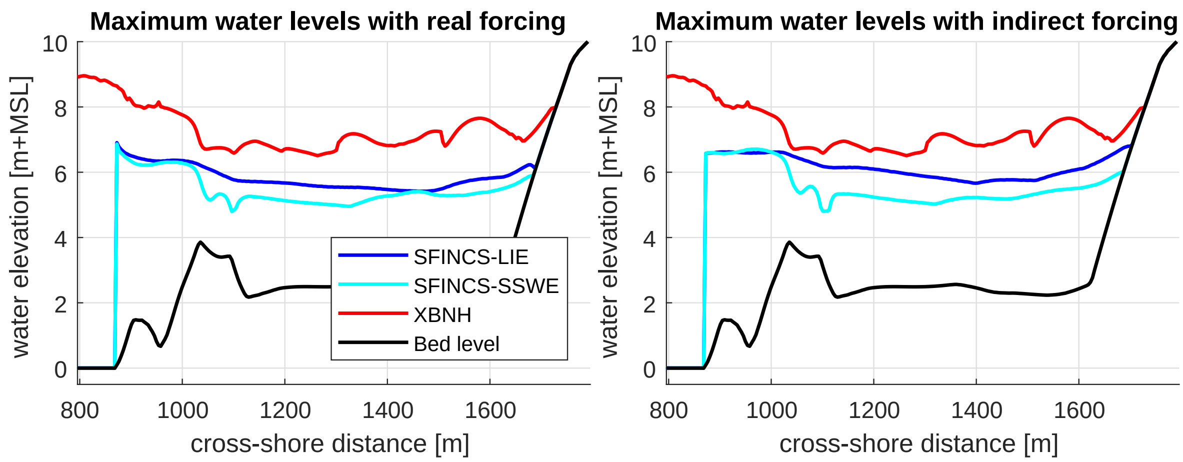

Figure 5.3: Maximum water levels of XBeach and SFINCS for the 1D transect. Left: results of SFINCS with the real water level time-series as input, Right: results of SFINCS with an indirect random forcing

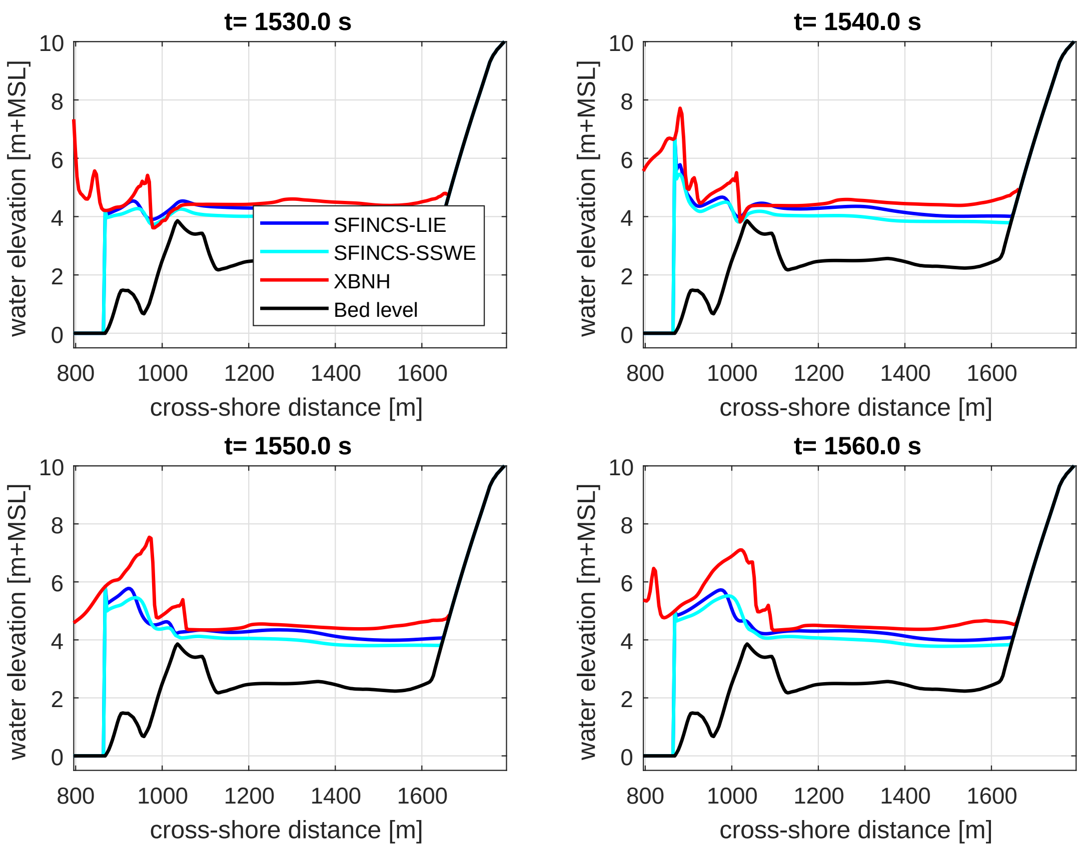

Figure 5.4: Instantaneous water levels of XBeach and SFINCS with real forcing for the 1D transect at 4 time-steps

On the right hand side of Figure 5.3 there can be seen that with an indirect forcing with SFINCS similar results can be achieved as with the real forcing, although it is still underestimated. The underestimation could again be solved by using an elevated water level as a correction term as in the conceptual tests, but since there is no physical explanation for the underestimation, this is therefore not done. Additionally, the times-series of the water depth, flow velocity and Froude numbers for SFINCS and XBeach at the location of the SFINCS boundary are showed in Figure 5.5. In the upper panel of Figure 5.5 there can be seen that large IG waves reach the boundary with a corresponding large wave setup, whereby the wave heights are underestimated by SFINCS. The middle panel shows that there are velocity peaks in the order of 5 m/s. The corresponding Froude numbers (lower panel) have a maximum value of 0.8, so the flow at the boundary is not super-critical.

In general it can be said that the waves and inland flooding is overestimated with the 1D transect modelling compared to reality, since there is no directional spreading in the incoming waves. Also there is no lateral outflow in the hinterland, which results more in an overwash and inundation event than an overtopping and flooding event. Therefore there is also modelled with a 2D model, which is described in the next section.

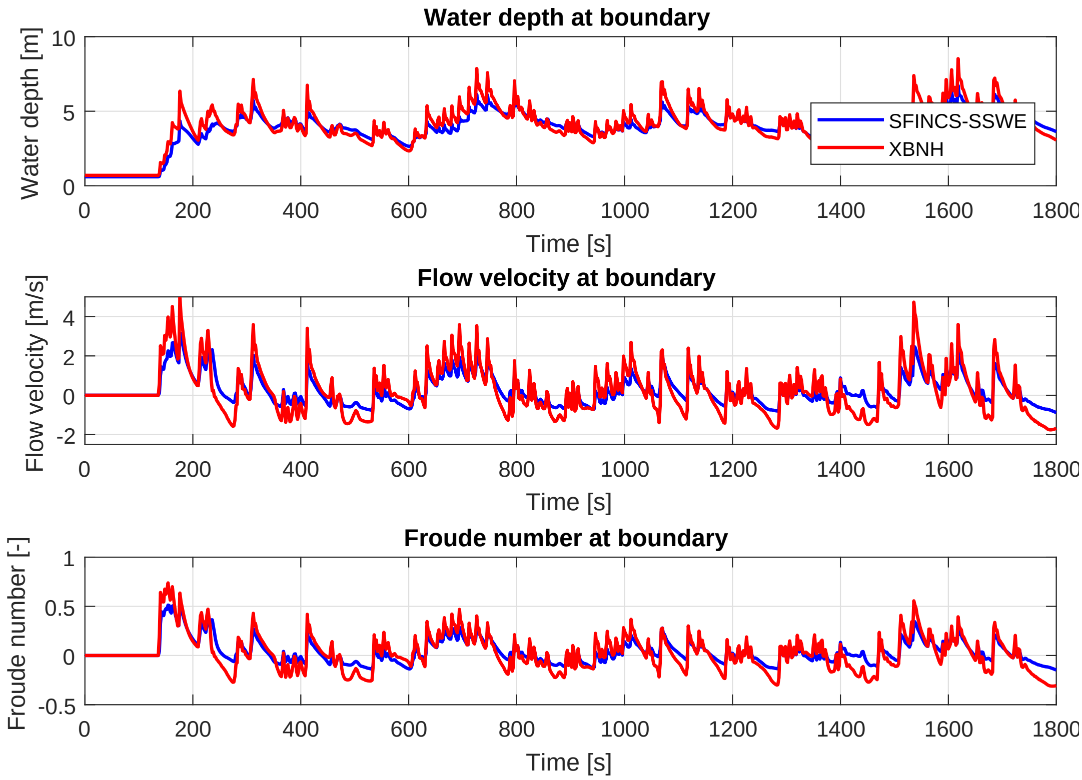

Figure 5.5: Comparison between SFINCS-SSWE and XBNH of the water depth, flow velocity and Froude numbers in time at the boundary of the 1D models with real forcing

5.1.4. 2D model

To compare the results of XBeach and SFINCS when directional spreading and a 2D bathymetry is taken into account, the same approach as for the 1D transect is done for a full 2D model. Hereby the flooding is a bit less extreme and more realistic compared to the 1D model. Also the ability of the swash zone modelling approach to capture the longshore variability of the waves with different input locations along the shoreline is tested. This is relevant for whether a spatial coherence for the wave input is needed for the indirect random forcing with SFINCS.

Influence swash zone modelling

At first the results of SFINCS with real forcing are compared with XBeach. Figures 5.7 a&e show that the maximum water depth in the hinterland is now in the order of 1.5-2 m, instead of the 4m for the 1D transect of Section 5.1.3. This can also be seen in the left picture of Figure 5.6. Therefore the directional spreading and lateral outflow is important for the model results. Furthermore it can be seen that the differences between the model results of XBeach and SFINCS are smaller than for the 1D transect. It can still clearly be seen that in the region close to the shoreline, SFINCS significantly underestimates the maximum water depths. In the hinterland there still is a slight under-prediction of the maximum water depth, but the order of magnitude is much better.

Influence advection

If the results of SFINCS-LIE are compared with SFINCS-SSWE (Figure 5.7 e&f), the results seem to be similar. In both models the water depths are underestimated close to the shoreline. In the hinterland the maximum water depths are more similar to XBeach. It can however be seen that in the north of the domain, where the village is situated, the results of SFINCS-LIE are relatively closer to XBeach than SFINCS-SSWE. This is the area that under normal circumstances is protected by the seawall. To assess this more closely, a transect of the 2D model results is made at the same location as in Section 5.1.3. The left panel of Figure 5.6 shows that the maximum water levels of XBeach and SFINCS-LIE are similar in the hinterland, but that for SFINCS-SSWE the maximum water level is lower there. From the boundary until X=785.8 km the maximum water levels of LIE and SSWE are the same, which seems to indicate that after the overtopping of waves the flow behaviour is different. In order to assess this the time-series of the water depths at the location of the house that is swept away is showed in the right part of the Figure 5.6. There can be seen that SFINCS-LIE follows the pattern of XBeach quite well, although there is a small phase lag and the peaks of the waves are underestimated. With SFINCS-SSWE the water depths are significantly lower, it seems that less water is overtopped. With SFINCS-LIE the wave bores remain steeper (as for instance seen in the dam break tests), while for SFINCS-SSWE they are more realistic and smoothed out. While the height of the waves is similar at the boundary of SFINCS, the steeper wave fronts of SFINCS-LIE help in overtopping more water. Therefore the maximum water depths are lower for SFINCS-SSWE. In the rest of the domain there is no presence of this seawall and the flooding is more an overwash than an overtopping event, with less differences between SFINCS-LIE and SSWE.

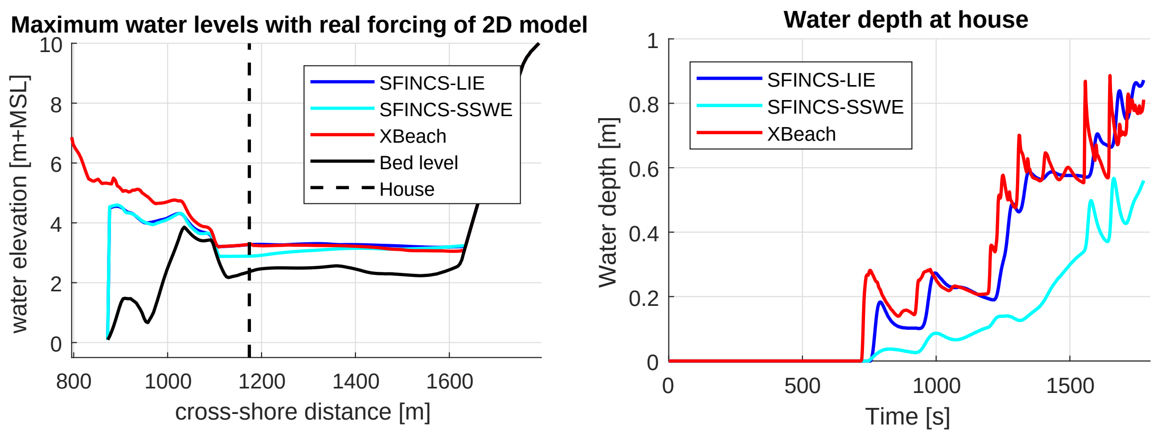

Figure 5.6: Maximum water levels at the transect of the house that is swept away (left) and corresponding time-series of water depths (right).

Real forcing compared to indirect forcing

There is also investigated whether similar results with SFINCS can be obtained by forcing the model with an indirect random wave signal. Hereby it is the question whether a spatial coherence between the input time-series is needed, which was not yet an issue in the 1D transect. This assessed by forcing one model with completely random time-series for every input location 'random phase' and one where the phases per bin are the same between the different input time-series 'uniform phase' (see also Appendix E.2). The results can be seen in Figures 5.7 c&g and 5.7 d&h respectively. With the completely random phases the maximum water depth is underestimated in the entire domain and the flooding extend is too small. However, if the phases per bin are kept the same between all input locations the results are much better. The flooding extend seems to be the same as with the real forcing (comparing Figures 5.7 f&h) This can better be explained by showing a snapshot of the instantaneous water levels for the different models. Figure 5.8 shows this for t=600s in the simulation of the models. Note that the spatial patterns of XBeach and SFINCS with real forcing are related to each other, but not with the indirect forcing since this is made random. The similar spatial patterns for Figures 5.8 a&c give the impression that the differences between XBeach and SFINCS at the beach are mainly caused by the swash zone modelling approach and the corresponding underestimation of the wave height as for the 1D transect. The way of forcing the waves with input every 100 m (see Figure 5.2) and normal to the coast (the incoming wave direction is not taken into account) seems to have a smaller influence on the results. The spatial variability of the wave energy seems to be correct, although the water levels are underestimated with SFINCS. The exact effect is not assessed separately.

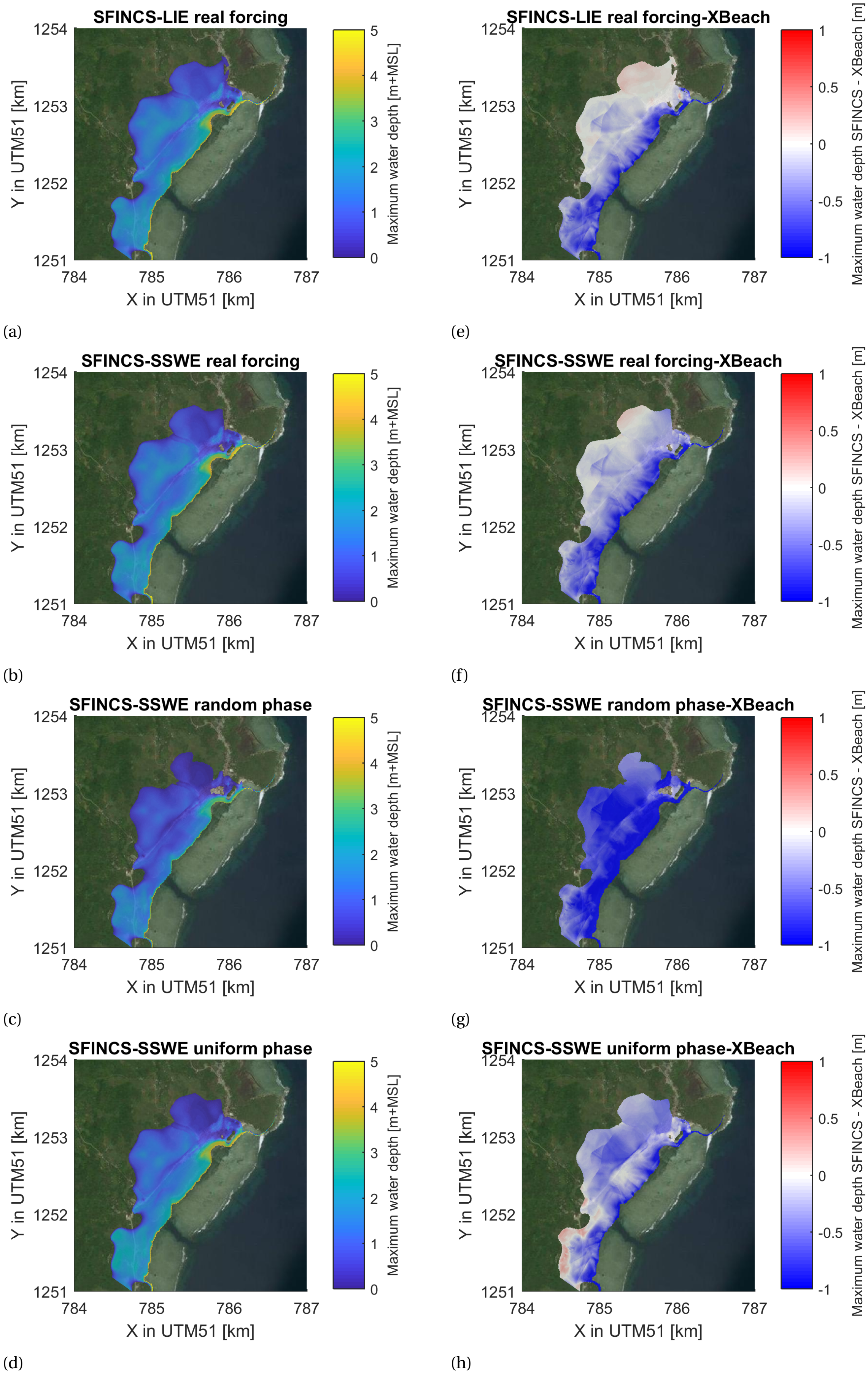

Figure 5.7: Maximum water depths SFINCS and compared to XBeach. a & e: SFINCS-LIE with real forcing, b & f: SFINCS-SSWE with real forcing, c & g: SFINCS-SSWE with completely random indirect forcing and d & h SFINCS-SSWE with random indirect forcing but equal phases.

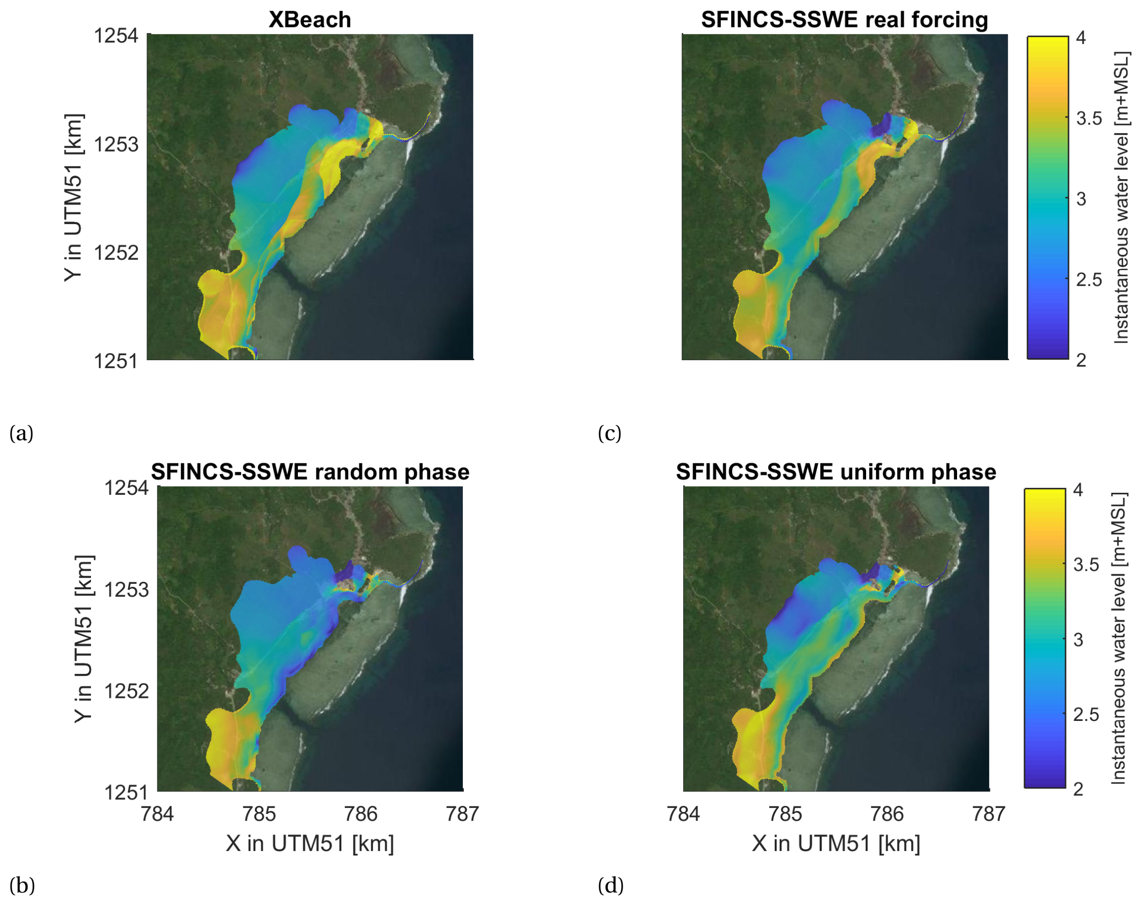

Figure 5.8: Instantaneous water levels at $t = 600s$ for different model runs. a) XBeach (XBNH), only the area landward of the beach is shown, b) SFINCS-SSWE with real forcing, c) SFINCS-SSWE with indirect forcing with random phase and d) SFINCS-SSWE with indirect forcing with uniform phase

Comparing Figures 5.8 b&d shows that for the 'uniform phase' run the spatial coherence between the waves is better. With the 'random phase' the water levels seem to vary more along the coast and 'work together' less, which explains why less water is overtopped and the flooding extend is smaller. Also there seems to be some wave focussing in the left and middle of the model and also at the village based on the XBeach result. The SFINCS run with 'uniform phase' seems to capture this better than the completely random version. Therefore it seems to be important to keep spatial coherence between the input water level time-series, which can be done by keeping the random phases per bin the same for all the input location time-series. In general with the random phase modelling the exact seeding of the signal is also important. In the conceptual wave tests it is shown that modelling for 6 hours gives a realistic cumulative runup distribution, but modelling only hour does not (see Appendix C.1.2). Here the event lasts only for 30 minutes, which means that the exact seeding of the boundary signal gives quite some uncertainty. This also applied to the XBeach results.

Accuracy and efficiency

To quantify the performance of the different SFINCS runs, statistics regarding the maximum, mean and root-mean-square (RMS) of the water depths per grid point compared are calculated. The regression line (least squared estimator) and root mean squared difference (RMSD) compared to XBeach are calculated. Table 5.1 shows that the SFINCS runs have a negative bias in the order of 20% compared to XBeach with a RMSD of 0.5 m for the maximum water depth. Hereby the performance of SFINCS-SSWE with the real and indirect forcing with uniform phase are similar. The results of the random phase run is clearly worse. The predicted mean water depth is better in all cases, mainly indicating that the incident water depths are underestimated. This corresponds with the underestimation of the waves in the region close to the shoreline. The RMS shows a slightly larger underestimation than the mean water depth. For spatial distributions of both parameters see Figure E.4 in Appendix E.2. Comparing the real and indirect forcing shows that with the indirect forcing there is slightly more uncertainty in the results. It is hereby clear based on Table 5.1 that the results of 'uniform phase' are better

Table 5.1: Performance of 2D SFINCS models compared to XBeach. The least-squared estimators regression line [-] and RMSD [m] is calculated for all maximum and mean water depths of SFINCS compared to XBeach, as well as the RMS of the water level time-series per grid point.

	Maximum water depth		**Mean water depth**		**RMS water depth**	
	regression line	RMSD	regression line	RMSD	regression line	RMSD
SFINCS LIE real forcing	0.80	0.44	0.99	0.07	0.9	0.16
SFINCS SSWE real forcing	0.78	0.47	0.99	0.07	0.89	0.17
SFINCS SSWE random phase	0.57	0.96	0.91	0.13	0.74	0.32
SFINCS SSWE uniform phase	0.78	0.51	0.89	0.12	0.79	0.25

In terms of efficiency the differences are again large. The SFINCS-LIE run took in the order of 20 seconds and the SFINCS-SSWE runs in the order of 40 seconds. Adding advection in this case thereby significantly increases the computational time. Still the model is considerably faster than XBeach. While XBeach solves 35% more cells and also solves the NH pressure and viscosity terms, the model runtime is 10.8 hours on the same computer. Taking into account the differences with parallel processing (1 vs 4 processors), the speedup factor is two orders of magnitude. However, the increased computational efficiency comes with a price regarding the accuracy.

5.1.5. Conclusion

The goal of this case study is to asses whether a semi-advanced model with a swash zone modelling approach is able to reproduce the wave-driven flooding at Hernani as well as an advanced model. The model results indicate the following:

1. The advanced model of XBeach is able to model the large impact at the village of Hernani during Typhoon Haiyan. The generation of large IG waves over the reef in front of the village is captured, which is not possible with a surge model. Using a semi-advanced model with swash zone modelling approach the flooding can be modelled in 2D in an efficient way (2 orders of magnitude faster), but in terms of accuracy there is a negative bias in the predicted maximum water depths. This is in the order of 20% with a RMSD in the order of 0.5 m. The mean water depths are modelled without a bias and with a RMSD of 0.07 m for the real forcing. The negative bias of the maximum water depths merely originates at the boundary of SFINCS where the wave heights already are underestimated directly at the boundary. This seems to be the case because of the swash zone modelling approach. Also too much artificial dissipation because of the first order explicit scheme might contribute. Or maybe something in the boundary does not work correctly. Therefore with the semi-advanced SFINCS model it is possible to predict serious flooding at the town of Hernani, but the magnitude is underestimated.

2. In this case, adding advection to the momentum equations with SFINCS-SSWE does not lead to better results than SFINCS-LIE. With the current results the overtopping discharges with SFINCS-LIE are slightly higher because the waves remain steeper. Thereby the maximum water depths are closer to XBeach. In case the wave heights at the boundary would not be underestimated, the hypothesis is that then the results with SFINCS-SSWE will be better than SFINCS-LIE. This is because including the advection term results in more realistic flow of water that is overtopped.

3. It is important to have a spatial coherence of the waves at the boundary in the swash zone. Using a quasi-2D approach (not accounting for wave direction) seems to be good enough in this case. Thereby it seems important that the grid is orientated so, that the cells are normal to the coast (because assumption normal to the coast). Also input time-series locations every 100 m with interpolation for boundary points in between seems to be good enough.

4. Using an indirect random forcing can give similar results for SFINCS as using a real time-series. Because it is a short event, the seeding of the boundary signal introduces uncertainty (also the case for XBeach). Spatial coherence can be kept by keeping the random phases per bin equal between the different created water levels input time-series. Hereby the alongshore variation of wave energy is kept.

5.2. Case study compound flooding: Jacksonville

This section discusses the results of the case study regarding the compound flooding at Jacksonville. At first the case is described in Section 5.2.1, thereafter the model setup is discussed in Section 5.2.2 and the results of the advanced Delft3D models shown in Section 5.2.3. Thereafter a description is given regarding the occurring flooding in Section 5.2.4, the results of Delft3D and SFINCS compared in Section 5.2.5 and the relevant processes discussed in Section 5.2.6. Finally the contributions of the different types of forcing to the inundation are discussed in Section 5.2.7 and the conclusions in Section 5.2.8.

5.2.1. Introduction

This case study focusses on the compound flooding at Jacksonville, Florida (Figure 5.9) during hurricane Irma in the beginning of September 2017. Due to a combination of surge, precipitation and wind-induced setup there was major compound flooding in and around the Jacksonville area. Flood waters rushed into the city's streets and reached up to 1.5 m deep in some locations (Cangialosi et al., 2018). The St. Johns river set record flood stages causing major flooding in the Jacksonville metropolitan area, where hundreds of people were rescued. The flooding in Jacksonville was record-breaking in some locations and overall Irma was responsible for one of the worst flooding events in the city's 225+ year history. The north-eastern portion of the state also experienced hurricane-force wind gusts and embedded tornadoes that caused structural damage to homes and businesses. There was also widespread tree and power line damage across the area. Since Irma is such a recent event, no hindcasting studies have been published yet. Therefore the results of an advanced Delft3D model are compared with measurements to get a good model setup.

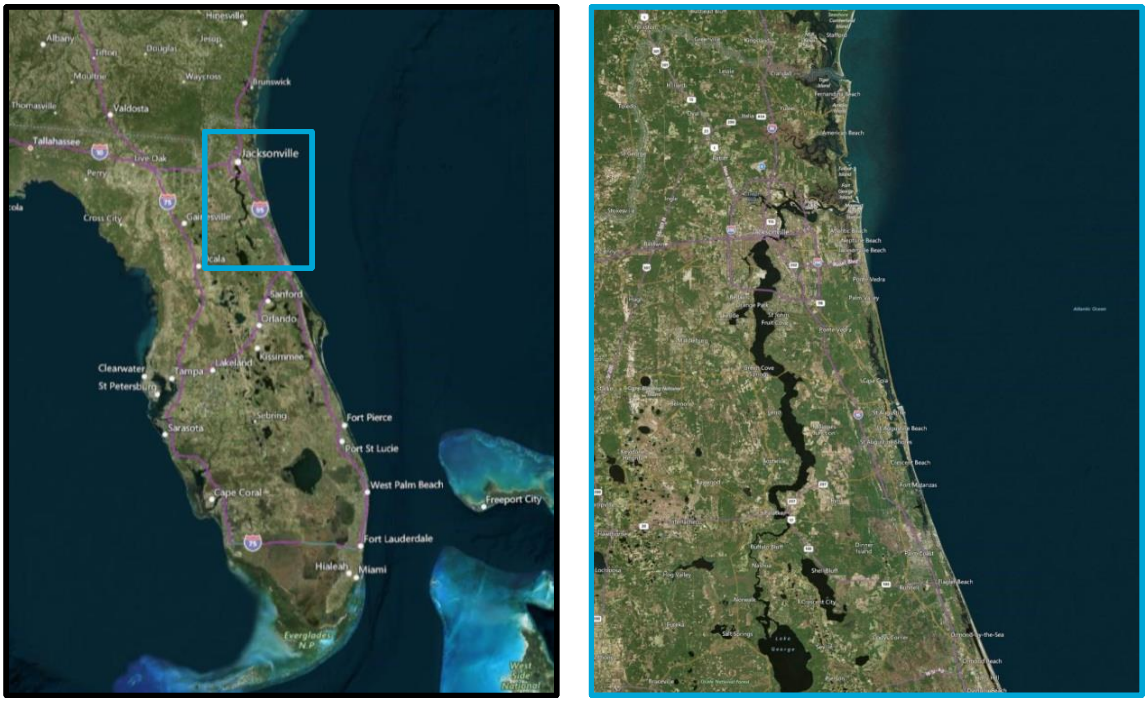

Figure 5.9: Overview of the site of the case study surrounding Jacksonville. Left: Florida with detailed model in box. Right: Jacksonville and surroundings with St.Johns river

5.2.2. Model setup

A model train of 3 Delft3D-FLOW and WAVE models is used to simulate the compound flooding in the region of Jacksonville (see Figure 5.10). The overall model and most coarse model covers Florida and a large part of the Caribbean. The intermediate covering the whole of Florida. The detailed model covers Jacksonville and a large part of the St. Johns river and is only a Delft3D-FLOW model. It is this detailed model where the performance of Delft3D and SFINCS will be compared. For Delft3D-FLOW, nesting is carried out by passing down Riemann boundary conditions from the coarse to the detailed model. For Delft3D-WAVE, nesting was carried out by passing down the 2D spectrum information via a so-called sp2 file. Both models are forced with spatially varying wind from the National Hurricane Centre (NHC, NHC (2018)). The used precipitation data of the NARR (North American Regional Reanalysis, Mesinger et al. (2006)) underestimated the rainfall compared to measurements, so 40% is added to the rainfall (see Section F.1.3). And as a third forcing, the tide and surge input is almost the same between Delft3D and SFINCS. This is done by taking the water level time-series at multiple points along and close to the coast from the detailed Delft3D model (see Figure F.1). These time-series are used as the boundary condition in SFINCS. Additionally, the inflow of water in the St. Johns river in the south because of rainfall from outside the model is accounted for by nesting the water level at that location from the intermediate model. Hereby SFINCS again uses the time-series of the detailed Delft3D model to keep the differences as small as possible. Also, a spatially uniform infiltration rate of $5mm/hr$ is used. Furthermore the grids, numerical settings and input are kept the same between Delft3D and SFINCS as much as possible. Hereby SFINCS is used without advection (SFINCS-LIE), the influence of this assumption is discussed later. For more details on the setup of Delft3D (all domains) and SFINCS see Section F.1.

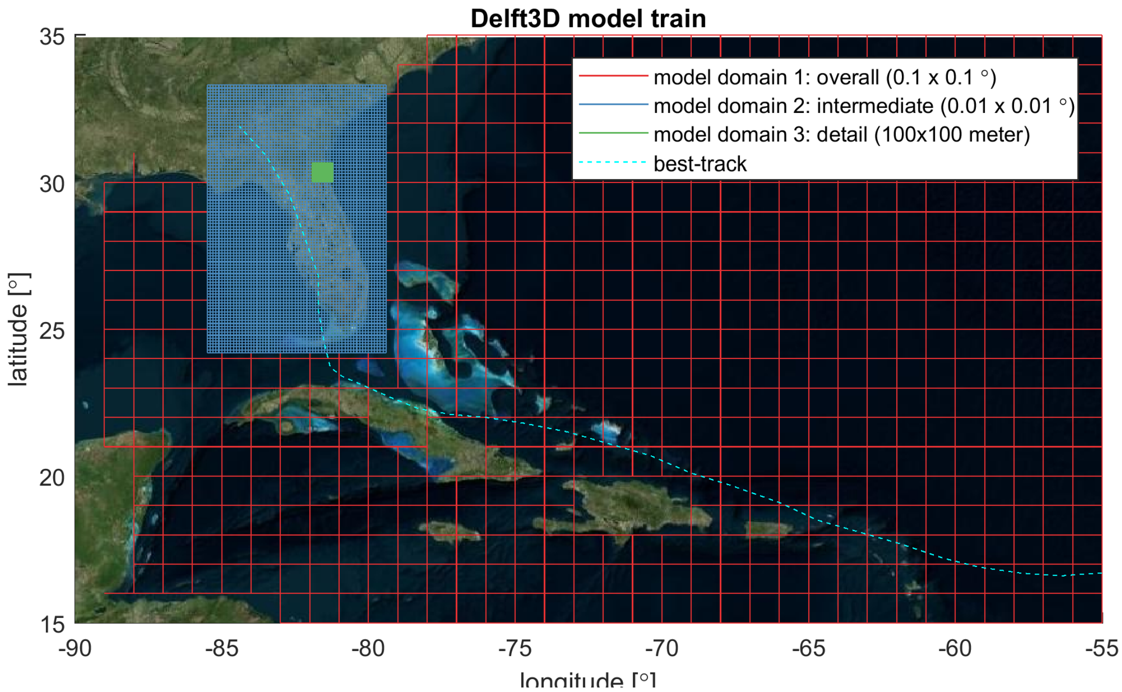

Figure 5.10: Delft3D model train. SFINCS results are compared with the 100 m detailed model of Jacksonville. Note, the real grid sizes are a factor 10 smaller.

5.2.3. Delft3D model results

The overall and intermediate models are validated using measurement stations. This is done for wind, atmospheric pressure, water level and waves data for both models, see Appendix F.2. The peaks of the wind speeds generally correspond well, as well as the timing of the peak and the wind directions. The pressure swath because of the TC is also modelled quite well. The same holds for the water levels along the coast with the tidal and surge components. At Fernandina Beach (close to the mouth of the St. Johns river), the surge is underestimated during the peak of the storm while the tide is modelled correctly. This underestimation of the surge will still be present in the models with the detailed domains. It is not known yet why this underestimation occurs. As said, the rainfall is calibrated upon the measured time-series and is therefore realistic as well. Although waves are not included in the detailed model, using SWAN they are accounted for in the larger models. Offshore of Jacksonville, the waves have a significant wave height in the order of 5 m. In general it is found that there is a reasonable to good representation of the compared types of forcing for both the overall and intermediate models. For the detailed Delft3D model it is found that the model can reproduce the hydrodynamic patterns of the flooding well, see Appendix F.3. Furthermore the results are better than that of the automatic storm surge hindcast of CERA (Coastal Emergency Risks Assessment CERA (2018)), based on ADCIRC, where the water levels in the St. Johns river are underestimated since precipitation is not taken into account.

5.2.4. Description of occurring flooding

To illustrate what happens at Jacksonville during hurricane Irma, Figures 5.11 and 5.12 show the water levels at four time-steps during high and low water at the peak of the storm. In Figure 5.11 the location of the hurricane with the direction of wind directions can be seen, as well as the combination of the surge and tide. Irma does not pass directly over Jacksonville, but still strong wind velocities are present causing surge.

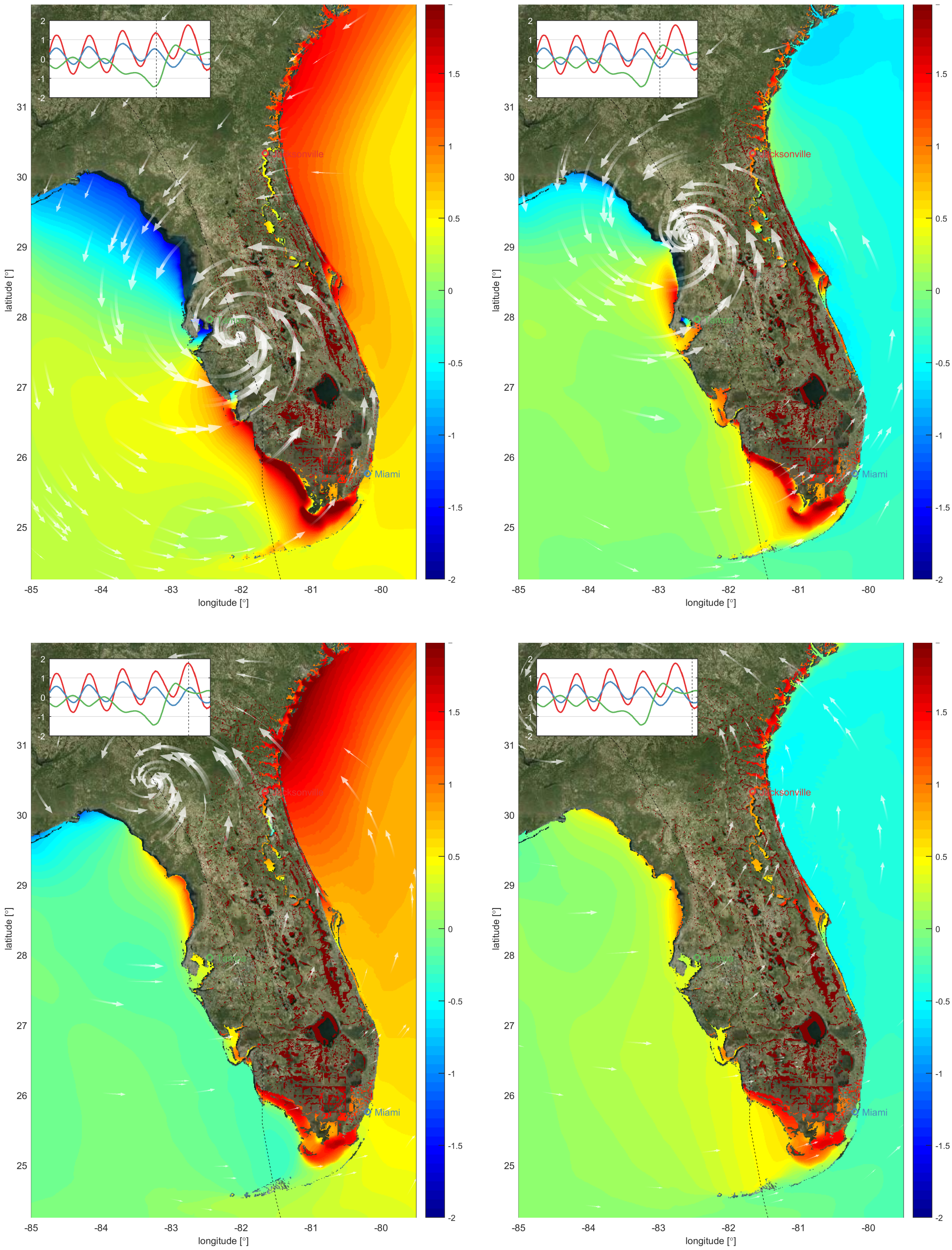

Figure 5.11: Water levels of intermediate Delft3D model at different time-steps

Figure 5.12 shows the tidal propagation within the St. Johns river, the significant wind-induced setup and the relaxation and flooding afterwards when the wind speeds drop. Additionally there is a significant amount of rainfall, which is transported towards the St. Johns river and elevates the water level. This is combined with the elevated water levels offshore because of the surge and tide, which limits the discharge into sea. At Jacksonville the river narrows and there significant elevated water levels and corresponding flooding occurs.

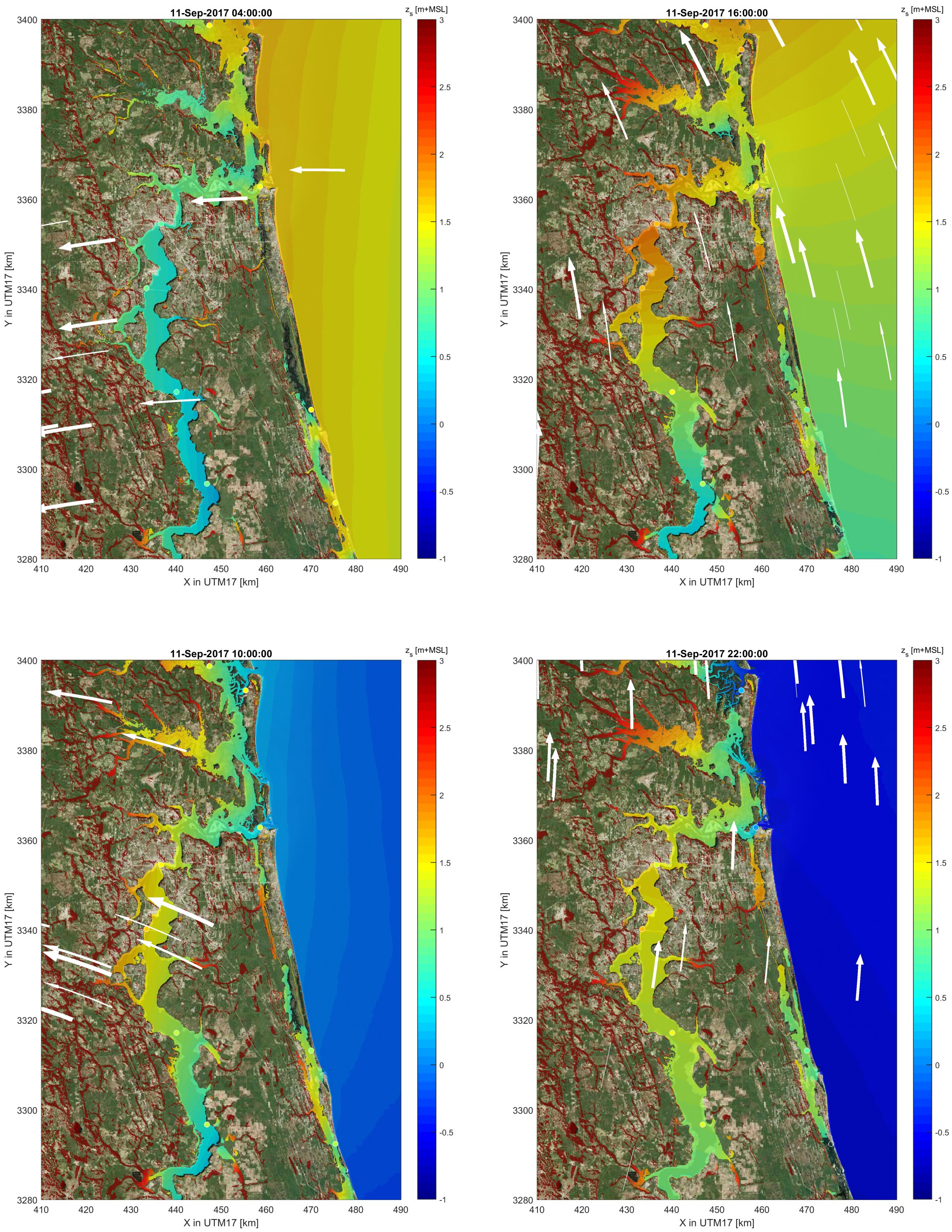

Figure 5.12: Water levels of detailed Delft3D model at different time-steps

5.2.5. Comparison results Delft3D and SFINCS

Since it is shown that the advanced Delft3D model is capable of reproducing the relevant hydrodynamic processes, there is investigated whether SFINCS can model this. Hereby there is compared with the results of the detailed Delft3D model to see how well the results match with a more advanced model, as well as with measurements to validate the results.

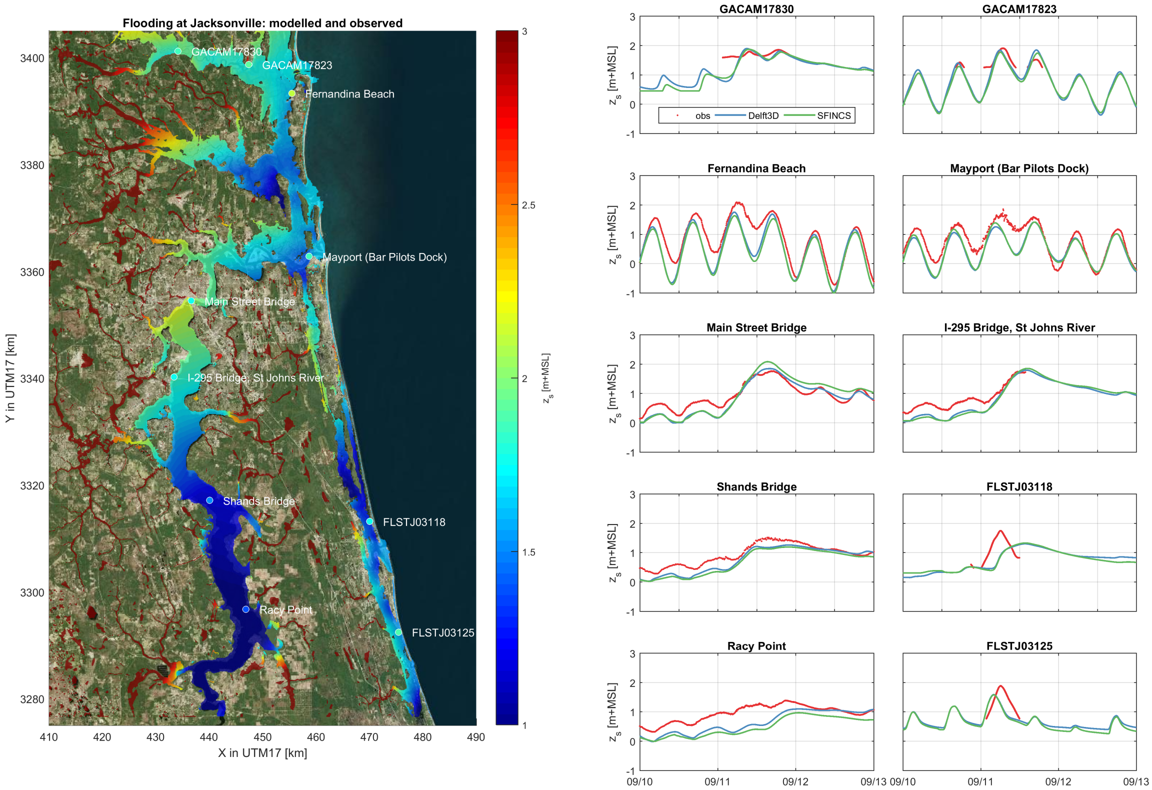

Figure 5.13: Maximum water levels of detailed Delft3D and SFINCS models compared to measurements. Left: maximum water level map of SFINCS for water depths over 0.5 m with maximum measured water levels as coloured dots, Right: water level time-series of Delft3D, SFINCS and measurements.

Figure 5.13 shows that SFINCS is very well capable of modelling the same water levels in the river as Delft3D. In the regions close to the coast the differences in maximum water levels are very small. The same holds for the southern part of the St. Johns river, the tidal amplitude as well as the water level peaks are similar. Closer to Jacksonville at Main Street Bridge the differences are slightly higher, SFINCS overestimates the peak. The differences between Delft3D and SFINCS are further investigated by spatially comparing the maximum water levels. Figure 5.14 shows that overall the differences in the modelled maximum water levels between Delft3D and SFINCS are small. A RMSD of 6.4 cm is good considering the fact that the model runtime of SFINCS is about 2 orders of magnitude faster than Delft3D (20 min vs 1.6 days, whereby Delft3D solves 45% more cells). For a discussion regarding the exact speedup factor see Section 6.1.3.

However, still some differences are visible. To be sure this is not caused by the implementation of infiltration, precipitation or wind stresses, these are tested in Appendix D. These processes are implemented correctly. The model results indicate that SFINCS releases the rain faster than Delft3D, especially in the western and north-western part of the domain. The hypothesis is that this is caused by the different flooding and drying criteria both models used. In Delft3D the ADI-scheme contains more restrictions regarding when water is released are present than the simple implementation in SFINCS. This could result in differences in how fast and how much water is released and flows to the river. In general the model results are quite sensitive to the exact value of the flow velocity threshold parameter. Therefore it is not possible to say whether the results of the flooding and drying mechanism of Delft3D are better than that of SFINCS. Another difference between both models is that in SFINCS the wind stresses for water depths smaller than 0.25 m are linearly reduced (see Section 3.4.4). This is also done for models like ADCIRC, but is not applied in Delft3D. It is not known whether resulting differences are significant, or which implementation is better. Additionally, some differences are present in the area at the southern boundary. Comparing the water level time-series in Figure F.18 in Appendix F.3 shows that differences are present close to the boundary in the south. At the boundary cell itself the water levels are the same for Delft3D and SFINCS. However, after September 11 at noon when the wind speeds significantly increase, in SFINCS the water level at one cell north of the boundary cell is underestimated about 0.2 m. It is not exactly clear why this happens, but the hypothesis is that it has something to do with a combination of the strong wind stresses and the boundary condition. This underestimation at the boundary has an effect in the rest of the river in the southern domain. Therefore also the maximum water levels of Figure 5.14 in this area are underestimated.

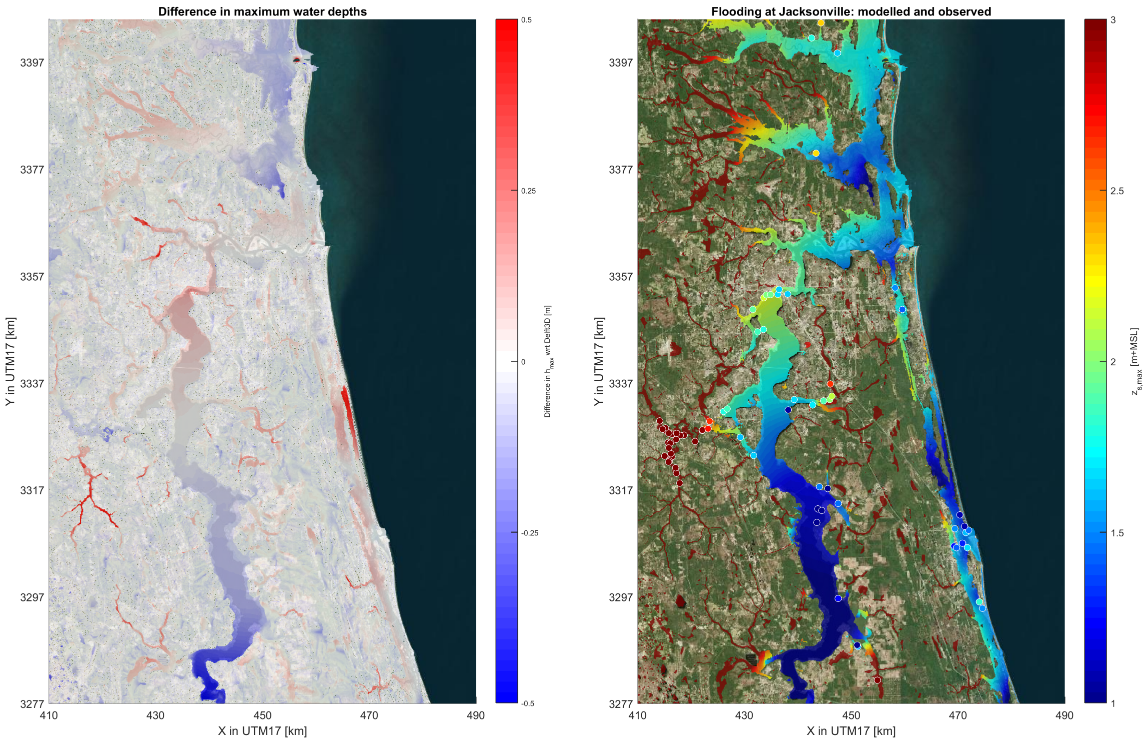

Figure 5.14: Comparison of maximum water depths and levels of the detailed Delft3D and SFINCS models. Left: difference in maximum water depths map of SFINCS, Right: maximum water level map of SFINCS with maximum measured water levels of high water marks in dots.

Furthermore differences with the measurements are present. At Mayport and Fernandina beach the maximum water levels are underestimated because of the underestimation within the intermediate and detailed Delft3D models (see Figure 5.13). The same holds for the FLSTJ-stations. At Acosta bridge differences occur because of uncertainty in the measurements. The measurement stations at Acosta and Main Street bridge are very close to one another, but the difference in measured maximum water levels is in the order of 40 cm. In the modelled results the water level differences between the two measurements points are much smaller, therefore it is assumed that the measured maximum water levels at Acosta bridge are underestimated. In both Delft3D as SFINCS, the water levels at Main Street Bridge are overestimated. This can occur because the wind-induced setup and/or the river run-off because of precipitation is overestimated. The RMSE of the maximum water levels at water level measuring stations between the results of SFINCS and the measurements is 0.37 m with a negative bias of 5%.

Additionally, measured high water marks are measured by USGS (United States Geological Survey, USGS (2017)) and can be used to validate the modelled results. Figure 5.14 shows that compared to the high water marks, the modelled results generally overestimate the maximum water levels. Along the St. Johns river this is mainly the case because the water levels in general are overestimated, as explained earlier. Furthermore there is more uncertainty in the comparison with the high water marks than with the water level time-series at the river. The high water marks are more local situations, which may not be always correctly represented with a 100 m resolution grid. Of the high water marks only the ones with the label 'fair' or better are used. The RMSE is with a value of 0.71 m rather high. Accordingly, there is a positive bias of 12 %.

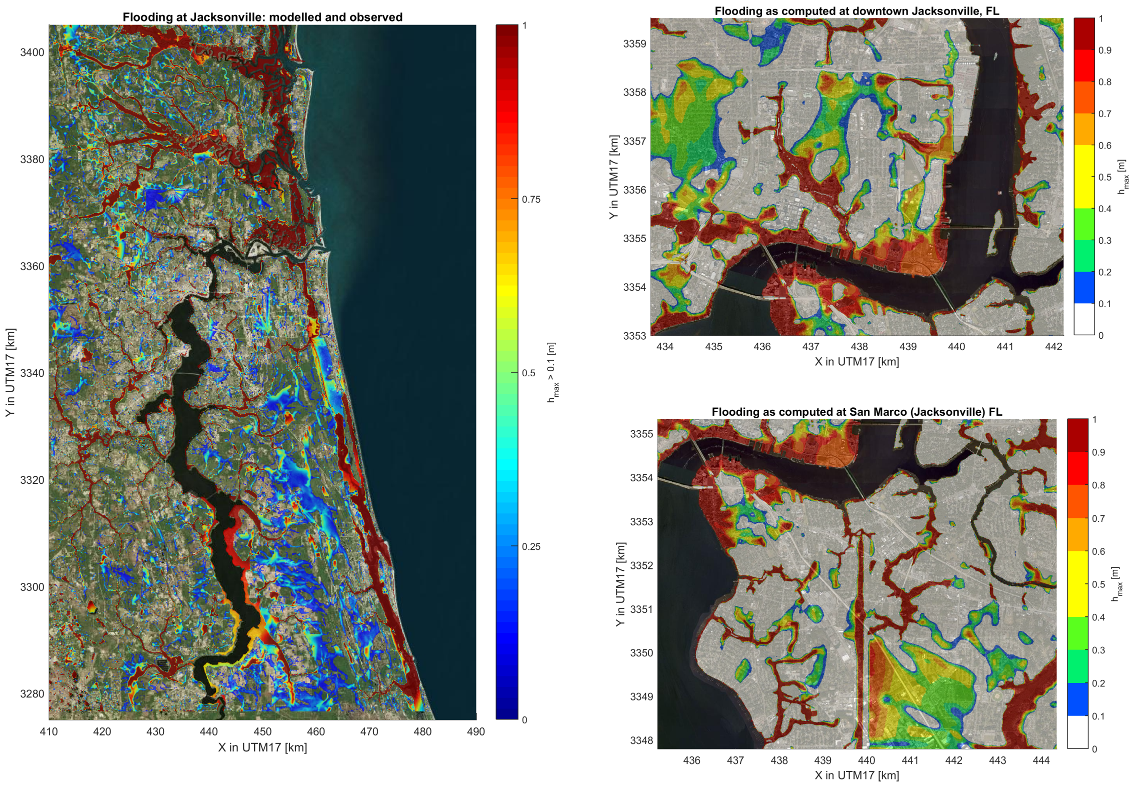

Figure 5.15: Maximum water depths of detailed SFINCS model for areas that are normally dry. Left: maximum water depth map of SFINCS for water depths larger than 0.1 m, Right: impression of the maximum water depth of SFINCS at downtown Jacksonville and San Marco using a sub grid approach using a more detailed DEM (Digital Elevation Model).

Figure 5.15 shows the actual maximum water depths at locations that normally are not covered with water and have a larger water depth than the flow velocity threshold. There can be seen that large areas along the St. Johns river and the two other small tidal rivers in the north have more than 1 m maximum water depth. Also a large area along the coast is flooded, as well as urban and rural areas with water depths in the order of 0.25 m. The two detailed plots show using a subgrid approach more detailed what areas along the St.Johns river in the centre of Jacksonville are flooded. Here a lot of damage was observed.

5.2.6. Relevant processes

Since the results of Delft3D and SFINCS are fairly similar, it seems no problem that SFINCS solves less processes. The lack of advection, atmospheric pressure, Coriolis and viscosity is further discussed in this section.

Advection

The showed results so far are all with the original SFINCS-LIE version without advection and since the model results are comparable to Delft3D (SWE model) this does not seem to lead to significant changes. To check whether the results would differ when including advection, the same model is also run with SFINCS-SSWE. The water level time-series hardly show any difference, the tidal propagation is for instance not better when including advection. The only thing that can be observed is that with SFINCS-SSWE the drop of the water levels after the peak of the storm takes slightly longer. Furthermore the flow in the river seems sub-critical everywhere. Dam break type situations therefore do not seem to occur. Theoretically one might also expect that advection would not be important in this case (see Section 3.5). However, solving the advection terms makes SFINCS about 40% slower. Therefore it seems that for this case it is best not to solve the advection terms. The accuracy is very similar while the efficiency is significantly higher.

Atmospheric pressure

Another difference between SFINCS and Delft3D is that Delft3D accounts for the change in water level height due to the atmospheric pressure drop by the TC. Since the differences of the model results are small, it seems that the effect on the results is small. This is checked by turning the pressure term on and off in Delft3D, but the differences are negligible. At Jacksonville the pressure drop is in the order of 25 mbar, where the maximum drop in the eye of the hurricane is 80 mbar. The pressure drop could thus have been higher, but even offshore the contribution to the surge of the pressure drop is generally low (Section 2). So with the inland modelling with SFINCS, the lack of the pressure does not seem to give a difference in this case.

Coriolis

In this case not accounting for the Coriolis term in SFINCS does not seem to have an effect on correctly modelling the extend of flooding. This is checked by doing runs with and without Coriolis in Delft3D, where no differences are noticeable. A low influence of the Coriolis effect on inland flooding corresponds with theory (Section 3.5). However, there can be cases where Ekman setup as a result of the Coriolis effect can be relevant (e.g. Chao et al. (2002) or Kennedy et al. (2011)). Although this might me more relevant for the intermediate model supplying the boundary conditions to SFINCS at 2 m water depth than the inland modelling of SFINCS.

Viscosity

Finally, the last difference is the viscosity term that is solved in Delft3D. Because of the results of the conceptual tests it is expected that the term does not make a large difference. This is tested by turning the viscosity term on and off in Delft3D, and the differences are negligible. For this case it seems therefore that it is not needed to solve the viscosity term. However, there can cases where the viscosity term should be higher (by default, the horizontal eddy viscosity in Delft3D is $1m^2/s$).

5.2.7. Contributions to compound flooding

To assess the contribution of the different types of forcing to the inundation (water levels, wind and rain), 3 additional runs have been performed with SFINCS. Hereby the models are run with the full forcing minus rain/offshore water levels/wind. Since one forcing at a time is turned off, the significance of that specific forcing can be shown. Figure 5.16 shows that all three types of forcing have a significant effect on the occurring flooding. Of course it varies spatially where which forcing is most dominant. There on the left hand side of the figure that the majority of the extend of inundation can be contributed to precipitation and the corresponding river run-off. This can also been seen at the time-series on the right hand side of the figure at for instance Racy Point. Here the water level is about 2 m underestimated when precipitation is not taken into account. Also the wind-induced setup at the narrowing St. Johns river at Jacksonville (Main Street Bridge) is significant (about 0.5m). The reasonably high surge and tidal water levels also prevent the water to easily flow out of the river. Also non-linear effects are important along the river, where the interaction between the different types of forcing elevates the water levels even more. At Main Street bridge this is in the order of 0.2 m. Concluding, all the three types of forcing needed to be modelled to come up with appropriate inundation predictions. Therefore it is not possible to use a static bathtub approach to model the flooding.

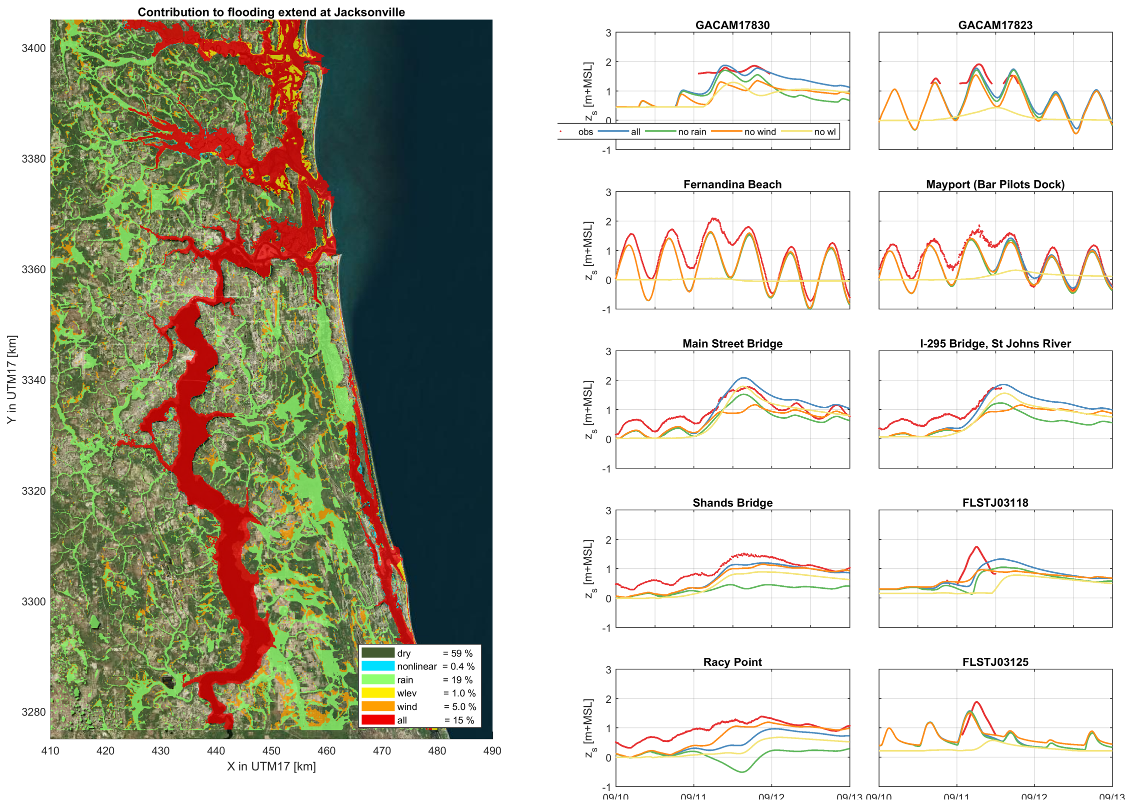

Figure 5.16: Contributions to compound flooding of the three different types of forcing and non-linear effects. Left: map of extend of flooding because of different types of forcing for water depths over 0.1 m, Hereby the dark red area is inundated in all cases. Right: water level time-series of SFINCS for different cases to verify the contribution of different types of forcing.

5.2.8. Conclusion

The goal of this case study is to asses whether a semi-advanced model is able to reproduce the compound flooding at Jacksonville as well as an advanced model. The model results indicate the following:

1. The hindcast of Hurricane Irma with a modelling train of three Delft3D-FLOW and WAVE models shows that advanced models are capable of simulating all the relevant hydrodynamic processes of compound flooding at Jacksonville.
2. A semi-advanced model like SFINCS is also capable of reproducing all the main hydrodynamic processes relevant for this case study, but with a fraction of the computational time (2 orders of magnitude faster). Hereby a similar accuracy is achieved for the maximum water levels with a RMSD of 6.4 cm.
3. The simplifications made within SFINCS-LIE (i.e. excluding advection, atmospheric pressure, Coriolis and viscosity terms) do not change the model results significantly.
4. The flooding experienced at Jacksonville during Hurricane Irma is the result of a combination of high offshore water levels, rainfall and wind-driven setup on the St. Johns river. It is thereby an example of a traditional compound flooding case.

6
Discussion

In this chapter a reflection is made regarding the work presented in this thesis. A discussion regarding the applied methods is given in Section 6.1. Thereafter the swash zone modelling approach is reflected on in Section 6.2. There is concluded with a discussion regarding the use of a semi-advanced model like SFINCS in an EWS in Section 6.3.

6.1. Applied methods

6.1.1. Model-model comparison

Throughout this thesis, the results of the semi-advanced SFINCS model are compared with advanced models like Delft3D and XBeach. The downside of such model-model comparisons is that there are uncertainties in the accuracy of the results of the base model. The fact that a more advanced model solves more processes, does not necessarily mean it can describe the occurring phenomena exactly according to reality. Therefore, a comparison to measurements is vital.

For the conceptual flow tests of Section 4.2 the results of the advanced and semi-advanced models are compared to analytical and experimental solutions, which reduces the uncertainty. In the conceptual wave tests of Section 4.3 this is not the case which increases the uncertainty. The advanced (uncalibrated) XBNH+ model is used, without comparing to measurements. XBeach has been shown to give realistic runup predictions (e.g. Roelvink et al. (2017)), but the XBSB and XBNH+ versions give different runup predictions for dissipative conditions (see Appendix C.1.1). This is also found by De Beer (2017), it is showed that the inclusion of incident waves in the XBNH(+) model gives better runup predictions for mild conditions on an intermediate beach. Furthermore, there is an overestimation in the computed runup characteristics when applying a 1D model schematisation due to the exclusion of directional spreading (e.g. Stockdon et al. (2014)). Since in practical use the semi-advanced model will be used in 2D, there is uncertainty whether the conclusions regarding the ability of SFINCS to accurately model runup still apply.

For the Hernani case study of Section 5.1 it was not possible to compare the model results to measurements. The used XBNH model seems to describe the hydrodynamic phenomena similar to Roeber and Bricker (2015), but there is uncertainty regarding the model results and what happened in reality. For instance, no data regarding wave heights on the reef was available to check the wave input for the SFINCS model. Also, measurements of maximum water or runup elevations to validate the advanced model was not present. At last for the case study of Jacksonville in Section 5.2, the modelled (maximum) water levels and model input compared reasonably well to measurements. In the comparison between Delft3D-FLOW and SFINCS model, small differences were observed and deemed inevitable since numerical implementations like the flooding and drying scheme are not the exact same in both models. However, based on the results it cannot be concluded that the implementation in the advanced Delft3D-FLOW model is preferred / better.

6.1.2. Splitting incoming and outgoing waves

In the conceptual wave tests the water level time-series of XBeach at 2 m water depth are retrieved, whereafter the signal is split into incoming and outgoing waves with the Guza method (Guza et al., 1984). Only the incoming wave signal is used to create the forcing of the different swash zone models. Theoretically, this will result in no differences between the results of the XBNH+ swash zone and XBNH+ full model, however, in practice, this was not the case. The hypothesis is that this is caused by the swash zone modelling approach in combination with a not perfect method for splitting the waves into incoming and outgoing. It could for example be the case that the Guza-method performs less for high-frequency incident wave energy (De Beer, 2017). In the Hernani case study, as opposed to the conceptual wave tests, waves were not split into incoming and outgoing contributions. The full time-series from XBeach were applied as boundary conditions. The reason for this is that splitting waves can only be accurately carried out for 1D models and the Hernani case is 2D. It is possible to specify the velocities for the Guza-method as $\sqrt{u^2+v^2}$ to account for 2D dimensions, but since the incoming and outgoing waves can have different wave directions, this is deemed to give inaccurate results. This approach for the Hernani case study introduces a boundary condition for SFINCS where not only the incoming waves are present. However, this can not be the reason why the high dissipation at the boundary is observed. The imposed wave height drops quickly all along the shore, also at locations where there is more an overwash than an overtopping event, where waves less waves are reflected.

6.1.3. Determining computational efficiency

Throughout this thesis the computational efficiency of different advanced models are compared with the semi-advanced SFINCS model. The comparisons in the different tests are not always completely fair. For instance, in the conceptual tests, SFINCS used OpenMP for parallel processing (with 4 processors). XBeach can model with parallel processing by splitting up the model domain (using MPI). However, this only works well in 2D, therefore SFINCS had a computational advantage for these 1D tests. Although, it can not be directly stated that running a model parallel on 4 processors instead of one makes the computation 4 times faster, the speedup is generally less (see e.g. Neal et al. (2009)). With the Hernani case study, XBeach is not run with MPI, but it is run on a faster CPU (Central Processing Unit) than SFINCS (see Section A.2). The SFINCS model is hereby even more than 2 orders of magnitude faster, so the described 2 orders of magnitude speedup is correct. With the Jacksonville case study, Delft3D-FLOW is used without parallel processing but run on a faster CPU than SFINCS. Also, Delft3D needs more grid cells for the computation because it is not possible to manually de-activate grid cells as in SFINCS (see Section 3.3.1). Therefore the described speedup in computational efficiency is in the right order of magnitude.

6.2. Swash zone modelling approach

6.2.1. Assumptions implementation

The swash zone modelling approach means that the boundary of the SFINCS model is located at the 2 m water depth contour. This water depth is determined in Van Engelen (2016), but is based on uncalibrated XBSB model results rather than measurements. Therefore the incident wave energy is underestimated, introducing uncertainty in the derivation of the optimal swash zone boundary water depth for SFINCS. However, during the conceptual wave tests in this thesis, this 2 m water depth value was still used and seemed to give good results while compared to a full XBNH+ model. Furthermore the optimal boundary water depth value is not tested for 2D runup, although the results are expected to be similar as in 1D.

With the Hernani case study the boundary is not chosen at 2 m water depth but at the shoreline because of the fringing reef. For a reef type coast the optimal boundary location can differ from a sandy beach type coast. It is assumed that the best location for these situations is to be close to the shoreline (still in the swash zone), because of the complex processes of IG wave generation and many reflected waves at the reef crest around 2 m water depth, but the optimal location is not tested. Another implication of the boundary depth is that for curved shorelines, a 'checker-board' boundary can occur. Hereby every side of the boundary cells is forced with a flux based on the input water level time-series. Because all waves are assumed to propagate shore-normal, the wave height in one boundary cell could be overestimated. Whether this leads to large overestimations is not known / tested. At last, not supplying every boundary grid cell with an individual water level time-series but interpolating linearly can lead to differences in alongshore wave energy. In the Hernani case study the effect seems to be limited, but this is not tested specifically.

6.2.2. Indirect random wave forcing

This thesis presented a method to introduce an indirect wave forcing into a swash zone modelling approach by making a random wave signal. Hereby there is a lack of coherence between the forced IG and incident waves. For the prediction of runup in 1D on a linear slope it is showed that the swash characteristics are affected by the random signal due to an overestimation of rundown. The latter seems not to be an issue for predicting runup. However, the effect on overtopping and the behaviour in 2D is not known. For the Hernani case study the random signal seems to give similar results to a real asymmetric wave signal for a overtopping/overwash type event, but the wave spectra in that case only contains IG wave energy. Whether similar results in a real 2D situation can be obtained when significant incident wave energy is present is not known. Another issue of the random wave forcing could occur when predicting maximum flow velocities. For an EWS it can be important to include velocities into the flood risk assessment, but it is not known whether the random waves negatively influence this prediction or not.

At last the proposed implementation for the indirect random wave forcing uses a large amount of bins (900) to make the signal. From a practical point of view where all these values have to be stored in memory and are possible slowing down the model, the number of bins and corresponding frequency bin width should probably be reduced. It is however not known what effect this will have on the results. The expectation is that a reduction of the number of bins is possible as long as the created wave spectra still resembles the input wave spectra. The amount of bins is also linked to how often the random phases should be updated. Within this thesis the phases are updated every 1800 s, but this number decreases if less bins are used. From a statistical point of view the best cumulative runup distribution is acquired when a wave signal of 1800 s, is thereafter not re-used. How much re-using the wave signal negatively influences the runup distribution is not known.

6.3. Implementation in an early warning system

The current SFINCS version including the traditional compound flooding related processes seems to be ready in terms of accuracy and efficiency to be applied in an EWS. It is however not known yet what the best grid resolution is to use in terms of efficiency and accuracy. In the Jacksonville case study using the 100 m grid resolution, good results are achieved, but it is not known whether this can even be improved by using a finer grid resolution. However, smaller grid cells will make SFINCS more computationally expensive due to more grid cells and smaller time steps. For a future version of SFINCS where wave-driven processes are explicitly included, the grid sizes in the coastal area of the beach need to be smaller. For the conceptual wave tests, the proposed grid resolutions varied between 2 and 20 m for more reflective and more dissipative coasts. Whether these guidelines can be used in 2D is not known. Since the smallest necessary grid resolution is one of the important limiting factors for the possible computational efficiency of an EWS and the number of ensembles that can be run, the required resolution is an important factor for the implementation within an EWS.

7

Conclusions

In this thesis, insight is obtained in how compound flooding due to TCs can be modelled in an accurate and efficient way with the semi-advanced SFINCS model. Thereby first the relevant physical processes are identified, second the implementation in the semi-advanced SFINCS model is tested and last the results of that semi-advanced model are compared to more advanced models. In this chapter first the conclusions regarding the sub-questions as stated in Chapter 1 are given. Thereafter the main research question is answered.

1) What are the relevant physical processes of compound flooding due to tropical cyclones?

Based on literature, multiple physical processes can by relevant during a compound flooding event due to TCs. This includes high offshore water levels, precipitation and corresponding river runoff, wind-induced setup and wave-driven processes like wave runup. In the case study of Jacksonville, Florida, during Hurricane Irma (2017), model results indicate that for this compound flooding event, offshore water levels and precipitation are most important for the extent of flooding. Wind-induced setup on the St. Johns River was also a relevant process for the occurring flooding. In this case study, the differences between the advanced and semi-advanced models are small. This indicates that the lack of solving the advection, atmospheric pressure, Coriolis and viscosity terms in the SFINCS model does not necessarily reduce the accuracy of the model. With the conceptual dam break tests, it is shown that advection needs to be included when the flow is super-critical. However, in real case studies of compound flooding (like the case of Jacksonville), super-critical flow does often not occur. With sub-critical flow conditions the advection term can be neglected, saving in the order of 40% of the computational time. Therefore it is preferred to neglect the advection term when super-critical flow conditions do not occur.

For the case study of Hernani, the Philippines, during Typhoon Haiyan (2013), it is shown that wave-driven processes have to be solved explicitly. Without these processes, the surge predicts no harm while in reality whole houses are swept away by massive IG waves. Based on conceptual runup tests, model results show that advection needs to be included within SFINCS in order to retrieve accurate runup values. Once the spectrum of the incoming waves is mainly incident wave dominated (at more reflective beaches), the lack of solving the NH pressure term leads to an underestimation of the runup. However, this can be corrected by using an elevated water level at the boundary. The lack of solving a viscosity term does not seem to have an impact on wave-driven flooding, but this cannot be concluded explicitly. For all conditions, the incident wave part of the spectrum of the incoming waves needs to be included to model wave runup accurately.

2) How can the relevant physical processes be implemented in a semi-advanced model like SFINCS?

In terms of the flow related processes, the first order explicit scheme of SFINCS seems sufficient for modelling the flow phenomena during compound flooding due to TCs. The limits of the scheme when including advection are super-critical flow with $Fr < 3$ and Manning friction values of $n > 0.02 s/m^{1/3}$. These limits are met in practical cases of compound flooding due to TCs and within those limits the results of the semi-advanced SFINCS model are comparable to that of advanced models. Furthermore, the simple flooding and drying mechanism of SFINCS seems to be sufficient.

In terms of the wave related processes, the swash zone modelling approach as applied in SFINCS, improves the computational efficiency while still producing reasonably accurate results. In performed conceptual runup tests, using this approach runup characteristics like R2% with a scatter index and relative bias smaller than 10% can be achieved. It is found that the approach slightly influences the runup characteristics, but the influence is smaller than for instance the uncertainty in the seeding of the boundary signal. For the flooding event at Hernani, the results with the swash zone modelling approach are less good. There is for example a negative bias in the prediction of the maximum water levels. This starts already in the first cells at the boundary where the wave height drops. It can however not be concluded whether this originates in the boundary implementation or the swash zone modelling approach itself.

Using an indirect random wave forcing based on the wave spectra at the boundary of a swash zone model can give similar results as forcing the time-series of an advanced model. With conceptual runup tests in 1D, a random forcing gives realistic and similar runup characteristics to an advanced model for a range of different offshore conditions. The swash zone characteristics are however affected by the random forcing. The rundown is overestimated because of the random forcing and corresponding lack of coherence between the IG and incident waves. With the Hernani case study also similar results are achieved when using an indirect random forcing. For the swash zone modelling approach, the wave-induced setup between DW and SW is parametrised, but the current formulation has to be improved. The lack of solving an NH pressure term leads to an underestimation of the runup for incident wave dominated conditions. Using a correction term at the boundary for the lack of solving the NH pressure, this underestimation can be overcome.

3) What is the accuracy and efficiency of a semi-advanced model like SFINCS compared to advanced models for different types of compound flooding?

The hindcast of Hurricane Irma with a model train of three Delft3D-FLOW & -WAVE models shows that advanced models are capable of simulating all the relevant hydrodynamic processes of compound flooding at Jacksonville. With the semi-advanced SFINCS-LIE model (without advection) a similar accuracy can be achieved. The RMSD of the maximum water levels compared to Delft3D-FLOW for the detailed model with the same input is 6.4 cm. The hindcast of Typhoon Haiyan reagarding the flooding at Hernani shows that the advanced XBeach model is capable of modelling the wave processes responsible for the wave-driven flooding event. With the semi-advanced SFINCS-SSWE model (including advection) there is a negative bias in the predicted maximum water depths in the order of 20% with a RMSD in the order of 50 cm when modelling in 2D. The mean water depths are modelled without negative bias with a RMSD of 7 cm. The negative bias of the maximum water depths is mainly caused by an underestimation of the wave heights at the boundary of the swash zone model. In both case studies, the semi-advanced SFINCS model is about 2 orders of magnitude faster than the respective advanced models (taking into account the inevitable differences).

How can compound flooding due to tropical cyclones be modelled in an accurate and efficient way?

For the modelling of compound flooding due to TCs, relevant physical processes as elevated offshore water levels, wind and precipitation have to be included. This can be done in a sufficiently accurate and efficient way by using a semi-advanced model. Hereby a first order explicit scheme and a simple flooding and drying mechanism give accurate results. Excluding physical processes like the atmospheric pressure, Coriolis and viscosity terms do not necessarily reduce the accuracy of the models' results. For the traditional event of compound flooding, the advection term only needs to be included when super-critical flow conditions occur. To be able to model wave-driven flooding, wave-driven processes have to be solved explicitly. Hereby the advection term always needs to be included. Using a swash zone modelling approach fewer grid cells have to be solved, while the accuracy can be similar to a model that starts in DW. The forcing at the boundary can be done using an indirect random wave forcing based on the nearshore wave spectra. The transformation of the offshore to nearshore wave spectra can be parametrised, just as the wave-induced setup. With all these assumptions and simplifications in mind, the accuracy of a semi-advanced model like SFINCS is still reasonable to good compared to an advanced model. In terms of computational efficiency, using a semi-advanced model can be about two orders of magnitude faster than an advanced model. Apart from the increased efficiency by solving less physical processes, the numerical side of the model is optimised by limiting the overhead of the model, using single precision, having linearised terms and using parallel processing. Hereby the computational efficiency seems to get in the right range as needed for ensemble forecasting within an EWS.

8

Recommendations

Based on the work presented in this thesis, recommendations are formulated on how to move forward regarding the semi-advanced SFINCS model with the goal of the implementation within an EWS in mind. At first recommendations regarding the used swash zone modelling approach are presented in Section 8.1. Thereafter in Section 8.2 the implementation of a semi-advanced model in an EWS is discussed. There is concluded with some proposed improvements of the SFINCS model in Section 8.3.

8.1. Swash zone modelling approach

8.1.1. Dissipation at boundary

In the Hernani case study it is found that there is too much dissipation at the boundary, causing the wave heights and correspondingly the maximum water depths to be underestimated. There needs to be investigated why this occurs. It is not clear whether this is caused by the swash zone modelling approach at the end of the reef. It can also be caused by too much artificial dissipation because of the first order explicit scheme or that something with the generating-absorbing boundary condition does not fully function. For the conceptual wave tests such problems were not noticed. For the Hernani case study the wave spectrum consists of very low frequency IG waves, where for the conceptual wave tests more incident wave energy is present and the peak of the IG wave energy has higher frequencies. For the Carrier and Greenspan test with a free long wave also some dissipation at the boundary is noticed. It might be that the boundary condition has difficulties reproducing (steep) low frequency IG wave, but more research on this is needed. For a range of conditions (also with incident wave energy) there can be tested whether this dissipation at the boundary occurs. Also, it is relevant to know whether it is related to the reef type coast of the case study, or that the dissipation also applies for sandy beach type coasts.

8.1.2. Sandy beach type coasts

For sandy beach type coasts like the conceptual wave tests the results of the swash zone modelling approach are good, but the value of 2 m water depth as boundary limit is not validated yet with measurements. When doing so, runup and overtopping may also be compared to measurements as for instance done in Roelvink et al. (2017), since this is not done yet with SFINCS. For the parametrisation of wave-induced setup from DW to SW a new formula is needed. For sandy beach type coasts it is probably better to derive such a formulation using a Dean-profile (Dean, 1977) rather than a linear slope. There can also be thought to use an analytical solution for the setup. For the proposed correction term for the lack of solving the NH pressure term, first more information is needed whether incident wave dominated conditions actually occur during TCs for steep beaches. Otherwise such a relation is maybe not really needed. When doing model runs to derive a parametrisation for the wave-induced setup, the same simulations can also be used to derive a parametrisation of the spectrum of incoming waves. It is showed that based on the nearshore wave spectra, realistic runup conditions can be achieved using an indirect random wave forcing. Using a parametrisation for the wave spectra, an advanced model like XBeach is not needed anymore to derive the wave spectra. Thereby precious computational time can be saved. To account for IG as well as incident wave energy, it is advised to derive separate relations for the IG and incident wave parts of the spectrum using the peak frequencies of both sides and the wave energy H_{m0}.

8.1.3. Fringing reef type coasts

The results of the Hernani case study suggest that maybe sandy beach and fringing reef type coasts should be handled differently. The fringing reef type coast is in this thesis handled similarly to the beach type by only modelling the swash zone, at the end of the reef. However in practice, still an advanced model is needed to give the wave spectra at this location. Or maybe it is possible to make separate parametrisations for the wave-induced setup and wave spectra, similarly to the relations for the sandy beach type coasts. However, there is not investigated yet whether it is possible to model the entire reef-flat with a semi-advanced model like SFINCS. At the reef crest a lot of waves reflect, which can make starting at 2 m water depth difficult. Although, by modelling the entire reef flat, spatial variability can be taken into account more accurately. Another possibility it so supply the conditions using the Bayesian network BEWARE of Pearson (2016).

8.1.4. Indirect random wave forcing

There is shown that with making an indirect random wave forcing, based on a wave spectrum as retrieved from an advanced model, realistic runup characteristics can be achieved. When changing this to a parametrisation of the wave spectra, the same methodology for making a random wave signal can still be used. However, the swash zone characteristics are affected by the random signal and lack of coherence between the IG and incident waves. Therefore if there is a fast way to make the shape of the signal more realistic while the energy of the wave spectrum is still maintained, this should be done. The signal can be made more asymmetric by using a sawtooth-shape, but the challenge thereby is to conserve the energy within the wave spectrum. Possible methods can be using a sum of saw-tooth signals, locking the phases of the random signals for multiplications of the base frequency, combining a random IG signal with an incident sawtooth signal and combining a random IG signal with a single sinusoid for the incident part with an amplitude based on the breaking steepness.

Although the method of making an random wave signal in this thesis is based on XBeach (Van Dongeren, 2003), the method when including incident waves is not exactly the same as in the XBNH model. There the random water level time-series from the wave spectrum including incident wave energy is not calculated directly, but in two steps. At first a time-series ζ_{inc} containing only the incident wave energy is constructed similarly as in Section 3.3.3. Second, from the incident wave time-series, an IG time-series ζ_{IG} is constructed using the difference-interaction coefficient D of Herbers et al. (1994). Both time-series are then added giving the total time-series $\zeta = \zeta_{IG} + \zeta_{inc}$. There can be investigated whether this slightly difference method is also applicable for constructing a random indirect time-series at the boundary of the swash zone and whether this results in an improved coherence between the IG and incident waves.

8.1.5. Wave direction at boundary

For curved coasts the boundary of SFINCS can result in a checker-board type pattern (see e.g. Section 3.3.1). This means that for a boundary cell on an edge, a velocity in x- as well as y- direction is imposed. Both velocities are hereby based on the same water level time-series, which means that the resulting wave height in that cell will most likely be overestimated. During the Hernani case study this is not noticed, but the grid is rotated so that the boundary is as parallel to the coast as possible. As a solution for more curved coasts, the imposed velocities can be reduced based on the input of a mean wave direction. This can be done using basic trigonometry, reducing the velocities based on the angle between the boundary cell flux and the mean wave direction.

8.2. Implementation in an early warning system

8.2.1. Required resolution

It is not known yet what the minimally required resolution is for traditional compound and wave-driven flooding events in order to give realistic enough predictions. Hereby both cases require different spatial scales. For the implementation in an EWS, this can done by using a finer grid for the coastal zone where waves are included (as well as the advection term) and a coarser grid for the inland zone where waves are excluded (just as advection). Both models can then be linked together, but then it has to be investigated how to do this. It is possible in SFINCS to nest water levels, but discharges might be more appropriate (see e.g. Ahmadian et al. (2018)). Another way to deal with the difference in spatial resolution is by using a spatially varying grid resolution (not yet possible with SFINCS). This can be done using a flexible mesh (e.g. Luijendijk et al. (2015)) or quad-tree techniques (e.g. Schuurmans and Leeuwen (2017)). There needs to be investigated what the best option is, having computational efficiency in mind. Different methods and grid resolutions can be tested by comparing different combinations for the same case study with measurements.

8.2.2. Required number of ensembles

Another question is how many number of ensembles are required in order to have a good probabilistic approach. When more is known regarding this subject, a better estimate can be made regarding the computational efficiency that is needed for the semi-advanced model. It might be that the current version of SFINCS is already fast enough. On the other hand it can also be the case that the model should still become a number of times faster. This can impact future decisions regarding the development of the model.

8.2.3. Model input

Furthermore there are also questions regarding the input for the EWS. It is shown in the Jacksonville case study that using an model train of advanced Delft3D-FLOW & -WAVE models, realistic input can be achieved for the detailed flooding model. However for practical applications with ensemble forecasting it is not possible to do multiple runs (or maybe even one) of these advanced models to produce this model input. Therefore real-time forecasting models like GLOSSIS (Verlaan et al., 2015) and GLOFFIS (Weerts et al., 2016) can be used for the surge and tidal input. It is however no known if these have sufficient accuracy to provide accurate enough model input during a TC. The same holds for wave inputs like WAVEWATCHIII (Tolman, 2002). Hurricane tracks can be provided by the NHC and wind as well as precipitation input by the NARR (Mesinger et al., 2006). During the Jacksonville case study the NARR data however underestimated the amount of rainfall. Therefore there can be quite some uncertainty for the model input of the EWS, with possibly worse model results. There can be accounted for this by using multiple ensembles of different scenarios, the amount is limited by the computational efficiency of the whole model train. In terms of model input, using spatially uniform instead of spatially varying precipitation and wind input can speed up the SFINCS model. For the Jacksonville case study, using a spatially uniform input, the model runtime reduces about 15%. However, the accuracy is then also slightly less. It is not known for what spatial scales the assumption of spatially uniform conditions is justified.

8.3. The SFINCS model

8.3.1. NetCDF output

To improve the post-processing of the results of SFINCS, it seems best to write the model output in the generic NetCDF (Network Common Data Form) format. Hereby the data output is more generic and similar to other advanced models. This also improves the applicability for EWSs.

8.3.2. Graphics Processing Unit

To speed up the SFINCS model even more, apart from the current OpenMP parallel processing the use of GPUs for parallel processing may be beneficial. The highly parallel structure of GPUs makes them more efficient than general-purpose CPUs (Central Processing Unit) for algorithms where the processing of large blocks of data is done in parallel. In SFINCS for every grid cell the same set of equations is solved. Therefore the use of GPU might make the model even faster without having to alter the physics.

8.3.3. Dynamic time-stepping

In SFINCS the determination of the time-step is dynamic and based on the CFL-condition using $c = \sqrt{gh}$. However, for modelling waves or dam break type situations, the flow propagation speed is more in the order of $c + v$. For these types of situations in the conceptual runup tests, the time-step limiter α often had to be reduced compared to the default value of 0.75. For practical use this is not optimal, therefore information regarding the maximum flow velocity in the determination of the needed time-step can be included. Calculating $c + v = \sqrt{gh} + \sqrt{u^2 + v^2}$ for the CFL-condition per grid cell and using the lowest time-step dt can be done(similar to the implementation of XBeach (Roelvink et al., 2009)). Or simply using the maximum water depth h (as is done now) and maximum flow velocity per time-step in the domain, thereby assuming a slightly too small time-step. However, for traditional compound flooding types of situations (without waves or supercritical flow), the current time-step determination seems sufficient. There can be implemented that with waves a more extended time-step determination is used, while without waves the original implementation is used.

Bibliography

Ahmadian, R., Falconer, R. A., and Wicks, J. (2018). Benchmarking of flood inundation extent using various dynamically linked one- and two-dimensional approaches. *Journal of Flood Risk Management*, 11:S314–S328.

Arakawa, A. and Lamb, V. R. (1977). Computational design of the basic dynamical processes of the UCLA general circulation model. *Methods in computational physics*, 17:173–265.

Barnard, P., O'Reilly, B., van Ormondt, M., Elias, E., Ruggiero, P., Erikson, L., Hapke, C., Collins, B., Guza, R., Adams, P., and Thomas, J. (2009). The Framework of a Coastal Hazards Model- A Tool for Predicting the Impact of Severe Storms. *U.S. Geological Survey Open File Report*, (October 2015):21.

Barre de Saint Venant, A. (1871). Theorie et Equations Generales du Mouvement Non Permanent des Eaux Courantes. *Comptes Rendus des seances de l'Academie des Sciences*, 73:237–240.

Bates, P. D., Horritt, M. S., and Fewtrell, T. J. (2010). A simple inertial formulation of the shallow water equations for efficient two-dimensional flood inundation modelling. *Journal of Hydrology*, 387(1-2):33–45.

Battjes, J. (1974). Surf similarity, paper presented at 14th International Conference on Coastal Engineering. *Am. Soc. of Civ. Eng., Copenhagen*.

Battjes, J. and Labeur, R. (2014). *Lecture notes Open Channel Flow*. Delft University of Technology.

Blume, T., Zehe, E., and Bronstert, A. (2007). Rainfall-runoff response, event-based runoff coefficients and hydrograph separation. *Hydrological Sciences Journal*, 52(5):843–862.

Booij, N., Ris, R. C., and Holthuijsen, L. H. (1999). A third-generation wave model for coastal regions: 1. Model description and validation. *Journal of Geophysical Research*, 104(C4):7649–7666.

Bosboom, J. and Stive, J. (2015). *Coastal Dynamics I*. Delft Academic Press, 0.5 edition.

Bruno, D., De Serio, F., and Mossa, M. (2009). The FUNWAVE model application and its validation using laboratory data. *Coastal Engineering*, 56(7):773–787.

Caires, S. and Sterl, A. (2005). 100-year return value estimates for ocean wind speed and significant wave height from the ERA-40 data. *Journal of Climate*, 18(7):1032–1048.

Cangialosi, J. P., Latto, A. S., and Berg, R. (2018). National Hurrican Center Tropical Cyclone Report, Hurricane Irma. (30 Augusut-12 September 2017).

Carrier, G. F. and Greenspan, H. P. (1958). Water waves of finite amplitude on a sloping beach. *Journal of Fluid Mechanics*, 4(01):97.

CERA (2018). Coastal Emergency Risk Assessment - https://cera.coastalrisk.live/.

Chanson, H. (2006). Analytical solutions of laminar and turbulent dam break wave. *River Flow*, (1955):465–474.

Chao, W. C., Chen, B., and Tao, W.-K. (2002). Sensitivities of Topical Cyclones to Surface Friction and the Coriolis Parameter in a 2-d Cloud-resolving Model.

Courant, R., Friedrichs, K., and Lewy, H. (1928). Uber die partiellen Differenzengleichungen der mathematischen Physik. *Mathematische Annalen*, 100(1):32–74.

Cui, H. (2013). *A new numerical model for simulating the propagation of and inundation by tsunami waves*. Master thesis, Delft University of Technology.

Curtis, K. J. and Schneider, A. (2011). Understanding the demographic implications of climate change: estimates of localized population predictions under future scenarios of sea-level rise. *Population and Environment*, 33(1):28–54.

Davies, J. L. (1977). *Geographical variation in coastal development.* Longman Publishing Group.

De Almeida, G. A. M. and Bates, P. (2013). Applicability of the local inertial approximation of the shallow water equations to flood modeling. *Water Resources Research*, 49(8):4833–4844.

De Beer, A. F. (2017). *The influence of incident waves on runup.* Master thesis, Delft University of Technology.

De Ridder, M. P. (2018). *Non-hydrostatic wave modelling of coral reefs with the addition of a porous in-canopy model.* Master thesis, Delft University of Technology.

De Vet, L., McCall, R., Den Bieman, J., Stive, M., and Van Ormondt, M. (2015). Modelling dune erosion, overwash and breaching at Fire Island (NY) during Hurricane Sandy. In *The Proceedings of the Coastal Sediments 2015.* World Scientific.

Dean, R. G. (1977). *Equilibrium beach profiles: US Atlantic and Gulf coasts.* Department of Civil Engineering and College of Marine Studies, University of Delaware.

Deltares (2018a). Open Earth Tools - https://publicwiki.deltares.nl/display/OET/OpenEarth.

Deltares (2018b). XBeach Skillbed Report - https://oss.deltares.nl/web/xbeach/skillbed. Technical report.

Duinmeijer, S. P. A. (2002). Verification of Delft FLS. (February).

Emanuel, K. A. (2013). Downscaling CMIP5 climate models shows increased tropical cyclone activity over the 21st century. *Proceedings of the National Academy of Sciences*, 110(30):12219–12224.

Fritz, H. M., Blount, C., Sokoloski, R., Singleton, J., Fuggle, A., McAdoo, B. G., Moore, A., Grass, C., and Tate, B. (2007). Hurricane Katrina storm surge distribution and field observations on the Mississippi Barrier Islands. *Estuarine, Coastal and Shelf Science*, 74(1-2):12–20.

Gerritsen, F. (1980). Wave Attenuation and Wave Set-Up on a Coastal Reef. In *Coastal Engineering 1980*, pages 444–461, New York, NY. American Society of Civil Engineers.

Graham, S. and Riebeek, H. (2006). Hurricanes: The Greatest Storms on Earth.

Guza, R. T., Thornton, E. B., and Holman, R. A. (1984). Swash on Steep and Shallow Beaches. In *Coastal Engineering 1984*, pages 708–723, New York, NY. American Society of Civil Engineers.

Herbers, T., Elgar, S., Guza, R., and O'Reilly, W. (1994). Infragravity-frequency (0.005–0.05 Hz) motions on the shelf. Part II: Free waves. *Journal of physical oceanography*, 25(6):1063–1079.

Holland, G. J. (1980). An analytical model of the wind and pressure profiles in hurricanes. *Monthly Weather Review*, 108(8)(8):1212–1218.

Holthuijsen, L. (2010). *Waves in Oceanic and Coastal Waters.* Cambridge University Press.

Horton, R. E. (1941). An Approach Toward a Physical Interpretation of Infiltration-Capacity 1. *Soil Science Society of America Journal*, 5(C):399—-417.

Hunter, N. M., Horritt, M. S., Bates, P. D., Wilson, M. D., and Werner, M. G. (2005). An adaptive time step solution for raster-based storage cell modelling of floodplain inundation. *Advances in Water Resources*, 28(9):975–991.

Kennedy, A. B., Gravois, U., Zachry, B. C., Westerink, J. J., Hope, M. E., Dietrich, J. C., Powell, M. D., Cox, A. T., Luettich, R. A., and Dean, R. G. (2011). Origin of the Hurricane Ike forerunner surge. *Geophysical Research Letters*, 38(8):1–5.

Kimmelman, M. (2017). Lessons From Hurricane Harvey: Houston's Struggle Is America's Tale.

Knutson, T. R. and Tuleya, R. E. (2004). Impact of CO2-induced warming on simulated hurricane intensity and precipitation: Sensitivity to the choice of climate model and convective parameterization. *Journal of Climate*, 17(18):3477–3495.

Kroon, A. (2009). *Implementation of a wetting and drying algorithm in a finite element model*. Master thesis, Delft University of Technology.

Labeur, R. J. and Pietrzak, J. D. (2005). A fully three dimensional unstructured grid non-hydrostatic finite element coastal model. *Ocean Modelling*, 10(1-2 SPEC. ISS.):51–67.

Lesser, G. R., Roelvink, J. A., van Kester, J. A., and Stelling, G. S. (2004). Development and validation of a three-dimensional morphological model. *Coastal Engineering*, 51(8-9):883–915.

Liang, D., Falconer, R. A., and Lin, B. (2006). Improved numerical modelling of estuarine flows. *Proceedings of the Institution of Civil Engineers - Maritime Engineering*, 159(1):25–35.

Longuet-Higgins, M. and Stewart, R. (1964). Radiation stresses in water waves; a physical discussion, with applications. *Deep Sea Research and Oceanographic Abstracts*, 11(4):529–562.

Luettich, R. A. J., Westerink, J. J., and Scheffner, N. W. (1992). ADCIRC: An Advanced Three-Dimensional Circulation Model for Shelves, Coasts, and Estuaries. Report 1. Theory and Methodology of ADCIRC-2DDI and ADCIRC-3DL. Technical Report 6, Coastal Engineering Research Center Vicksburg MS.

Luijendijk, A., Braat, L., Waagmeester, N., and Scheel, F. (2015). Pilot application of Delft3d Flexible Mesh: assisting field campaign at the sand engine. *36th IAHR World Congress*, (December):8.

Mesinger, F., DiMego, G., Kalnay, E., Mitchell, K., Shafran, P. C., Ebisuzaki, W., Jović, D., Woollen, J., Rogers, E., Berbery, E. H., Ek, M. B., Fan, Y., Grumbine, R., Higgins, W., Li, H., Lin, Y., Manikin, G., Parrish, D., and Shi, W. (2006). North American regional reanalysis. *Bulletin of the American Meteorological Society*, 87(3):343–360.

Miche, R. (1944). Mouvements ondulatoires des mers en profondeur constante on decroissante. *Ann. des Ponts et Chaussees*, 131.

Mori, N., Kato, M., Kim, S., Mase, H., Shibutani, Y., Takemi, T., Tsuboki, K., and Yasuda, T. (2014). Geophysical Research Letters. *Geophysical Research Letters*, 41:1–8.

Mousavi, M. E., Irish, J. L., Frey, A. E., Olivera, F., and Edge, B. L. (2011). Global warming and hurricanes: the potential impact of hurricane intensification and sea level rise on coastal flooding. *Climatic Change*, 104(3-4):575–597.

Moynihan, K. P. and Vasconcelos, J. G. (2014). SWMM Modeling of a Rural Watershed in the Lower Coastal Plains of the United States. pages 1–12.

Neal, J., Fewtrell, T., and Trigg, M. (2009). Parallelisation of storage cell flood models using OpenMP. *Environmental Modelling and Software*, 24(7):872–877.

NHC (2018). Storm Surge Overview - https://www.nhc.noaa.gov/surge/.

NOAA (2018). Costliest U.S. tropical cyclones tables updated. *NOAA Technical Memorandum NWS NHC-6*, page 3.

Pearson, S. G. (2016). *Predicting Wave-Induced Flooding on Low-Lying Tropical Islands*. Master thesis, Delft University of Technology.

Péquignet, A. C. N., Becker, J. M., Merrifield, M. A., and Aucan, J. (2009). Forcing of resonant modes on a fringing reef during tropical storm Man-Yi. *Geophysical Research Letters*, 36(3):20–23.

Pietrzak, J. D. (2016). An Introduction to Oceanography for Civil and Offshore Engineers.

Powell, M. D. and Aberson, S. D. (2001). Accuracy of United States tropical cyclone landfall forecasts in the Atlantic basin (1976-2000). *Bulletin of the American Meteorological Society*, 82(12):2749–2767.

Quataert, E., Storlazzi, C., Van Rooijen, A., Cheriton, O., and Van Dongeren, A. (2015). The influence of coral reefs and climate change on wave-driven flooding of tropical coastlines. *Geophysical Research Letters*, 42(15):6407–6415.

Ramirez, J. A., Lichter, M., Coulthard, T. J., and Skinner, C. (2016). Hyper-resolution mapping of regional storm surge and tide flooding: comparison of static and dynamic models. *Natural Hazards*, 82(1):571–590.

Rego, J. L. and Li, C. (2010). Storm surge propagation in Galveston Bay during Hurricane Ike. *Journal of Marine Systems*, 82(4):265–279.

Reniers, A. J. H. M., Gallagher, E. L., MacMahan, J. H., Brown, J. A., van Rooijen, A. A., van Thiel de Vries, J. S. M., and van Prooijen, B. C. (2013). Observations and modeling of steep-beach grain-size variability. *Journal of Geophysical Research: Oceans*, 118(2):577–591.

Ritter, A. (1892). Die fortpflanzung de wasserwellen. *Zeitschrift Verein Deutscher Ingenieure*, 36(33):947–954.

Roeber, V. and Bricker, J. D. (2015). Destructive tsunami-like wave generated by surf beat over a coral reef during Typhoon Haiyan. *Nature Communications*, 6:7854.

Roelvink, D. (1993). *Surf beat and its effects on cross-shore profiles.* PhD thesis, Delft University of Technology.

Roelvink, D., McCall, R., Mehvar, S., Nederhoff, K., and Dastgheib, A. (2017). Improving predictions of swash dynamics in XBeach: The role of groupiness and incident-band runup. *Coastal Engineering*, (February):1–21.

Roelvink, D., Reniers, A., Van Dongeren, A., Van Thiel de Vries, J., Lescinski, J., and McCall, R. (2010). XBeach model description and manual. *Unesco-IHE Institute for Water Education, Deltares and Delft University of Tecnhology. Report June*, 21:2010.

Roelvink, D., Reniers, A., van Dongeren, A., van Thiel de Vries, J., McCall, R., and Lescinski, J. (2009). Modelling storm impacts on beaches, dunes and barrier islands. *Coastal Engineering*, 56(11-12):1133–1152.

Sallanger, A. J. (2000). Storm Impact Scale for Barries Islands. *Journal of Coastal Research*, 16(3):890–895.

Schuurmans, W. and Leeuwen, E. V. (2017). 3Di : A new Dutch hydrological model.

Smit, P., Stelling, G. S., Roelvink, D., van Thiel de Vries, J., McCall, R., van Dongeren, A., Zwinkels, C., and Jacobs, R. (2010). non-hydrostatic_report_draft. Technical report, Delft University of Technology & Deltares, Delft.

Stelling, G. S. and Duinmeijer, S. P. (2003). A staggered conservative scheme for every Froude number in rapidly varied shallow water flows. *International Journal for Numerical Methods in Fluids*, 43(12):1329–1354.

Stockdon, H., Thompson, D., Plant, N., and Long, J. (2014). Evaluation of wave runup predictions from numerical and parametric models. *Coastal Engineering*, 92:1–11.

Stockdon, H. F., Holman, R. A., Howd, P. A., and Sallenger, A. H. (2006). Empirical parameterization of setup, swash, and runup. *Coastal Engineering*, 53(7):573–588.

Stockdon, H. F., Sallenger, A. H., Holman, R. A., and Howd, P. A. (2007). A simple model for the spatially-variable coastal response to hurricanes. *Marine Geology*, 238(14):1–20.

Stocker, T. (2014). *Climate change 2013: the physical science basis: Working Group I contribution to the Fifth assessment report of the Intergovernmental Panel on Climate Change.* Cambridge University Press.

Stoker, J. J. (1957). *Water Waves, The Mathemematical Theory with Applications.* Interscience Publishers Inc., New York.

Teng, J., Jakeman, A. J., Vaze, J., Croke, B. F., Dutta, D., and Kim, S. (2017). Flood inundation modelling: A review of methods, recent advances and uncertainty analysis. *Environmental Modelling and Software*, 90:201–216.

Thornton, E. B. and Guza, R. T. (1982). Energy saturation and phase speeds measured on a natural beach. *Journal of Geophysical Research*, 87(C12):9499.

Tolman, H. (2002). The 2002 release of WAVEWATCH III. *7th International Workshop on Wave Hindcasting*.

USGS (2017). About USGS - https://www.usgs.gov/about/about-us.

Van Dongeren, A. (2003). Numerical modeling of infragravity wave response during DELILAH. *Journal of Geophysical Research*, 108(C9):3288.

Van Engelen, T. (2016). *Towards a rapid assessment flood forecasting system for the Southern California coast*. Master thesis, Delft University of Technology.

van Ormondt, M., Nederhoff, K., and van Dongeren, A. (2017). Delft Dashboard: a quick setup tool for hydrodynamic models. *Not published yet*.

Vatvani, D., Zweers, N. C., Van Ormondt, M., Smale, A. J., De Vries, H., and Makin, V. K. (2012). Storm surge and wave simulations in the Gulf of Mexico using a consistent drag relation for atmospheric and storm surge models. *Natural Hazards and Earth System Science*, 12(7):2399–2410.

Verlaan, M., Kleermaeker, S. D., and Buckman, L. (2015). GLOSSIS : Global Storm Surge Forecasting and Information System. *Coast and Ports 2015*, 17(September):1–6.

Wahl, T., Jain, S., Bender, J., Meyers, S. D., and Luther, M. E. (2015). Increasing risk of compound flooding from storm surge and rainfall for major US cities. *Nature Climate Change*, 5(12):1093–1097.

Warming, R. F. and Beam, R. M. (1979). An extension ofA-stability to alternating direction implicit methods. *BIT*, 19(3):395–417.

Warren, I. R. and Bach, H. K. (1992). MIKE 21: a modelling system for estuaries, coastal waters and seas. *Environmental Software*, 7(4):229–240.

Weerts, A., Gijsberts, P., and Sperna Weiland, F. (2016). Global scale predictability of floods. *EGU General Assembly*, 18(April):15775.

Wetherald, R. T. and Manabe, S. (2002). Simulation of hydrologic changes associated with global warming. *Journal of Geophysical Research: Atmospheres*, 107(D19).

Wikimedia (2018). Hurricane structure - https://upload.wikimedia.org/wikipedia/commons/4/4f/Hurricane-en.svg - Attribution 3.0 Unported (CC BY 3.0).

Zehnder, J. (2015). Tropical Cyclone - https://www.britannica.com/science/tropical-cyclone.

Zijlema, M. (2015). *Computational Modelling of Flow and Transport January 2015*. Number January.

Zijlema, M. (2018). Comparison SWASH vs Boussinesq-type models - http://swash.sourceforge.net/features/perform.htm.

Zijlema, M., Stelling, G., and Smit, P. (2011). SWASH: An operational public domain code for simulating wave fields and rapidly varied flows in coastal waters. *Coastal Engineering*, 58(10):992–1012.

A

Additional model information

In this appendix additional information regarding the different used models is presented. Section A.1 summarises the characteristics of the different models as introduced in Chapter 2 in one table. In Section A.2 the characteristics of the different used computers in this thesis are given and in Section A.3 the specific versions of the used models. Finally, Section A.4 shows a simplified call graph of the source code of SFINCS.

A.1. Model comparison

Table A.1: Model comparison for the general characteristics and offshore, wave, flow and other processes. With 'sedtrans' the ability to model sediment transport is meant. MPI stands for parallel processing using Message Passing Interface. OpenMP stands for Open Multi Processing. GPU stands for Graphics Processing Units.

Model	General characteristics Dimensions	Grid type	Offshore proceses Parallelisation	Tropical cyclones	Wave generation	Wave processes Storm Surge	Tides	Wave resolving	Shoaling zone	Surf zone	Swash zone	Morphology
Static												
Bathtub	2D	no	no	no	no	no	no	no	no	no	no	no
Semi-advanced												
LFP	2DH	rectangular	OpenMP/no	no	no	no	no	no	no	no	no	no
SFINCS-LIE	2DH	rectilinear	OpenMP	no	no	input	input	only IG waves (under research)	simple	simple	yes	no
SFINCS-SSWE	2DH	rectilinear	OpenMP	no	no	input	input	all (under research)	simple	simple	yes	no
3Di	1D/2D	rectangular using quadtree and subgrids	unknown, cloud-based	no	no	no	no	no	no	no	no	no
Advanced												
ADCIRC	2DH/3D	unstructured	MPI/no	yes	yes (via SWAN)	yes	yes	yes	yes	yes	yes	no
Delft3D	2DH/3D	rectilinear/curvilinear/unstructured	MPI/no	yes	yes (via SWAN)	yes	yes	no	yes	yes	no	sedtrans
FINEL2D	2DH	unstructured	yes, type unknown	no	yes (via SWAN)	yes	input	no	yes	yes	no	sedtrans
FINEL3D	3D	unstructured	yes, type unknown	yes	yes (via SWAN)	yes	input	no	yes	yes	no	no
Funwave	2DH	rectilinear	MPI/no	yes	yes	yes	input	all	yes	yes	yes	no
MIKE 21/3	2DH/3D	rectilinear/unstructured	GPU/MPI/OpenMP/no	yes	yes	yes	yes	no/all	yes	yes	yes	sedtrans
SWASH	2DH/3D	rectilinear/curvilinear	MPI/no	yes	no	yes	input	all	yes	yes	yes	no
XBSB	2DH	rectilinear/curvilinear	MPI/no	no	no	input	input	only IG waves	yes	yes	yes	sedtrans+avalanching
XBNH	2DH	rectilinear/curvilinear	MPI/no	no	no	input	input	all	yes	yes	yes	sedtrans
XBNH+	2 layer 3D	rectilinear/curvilinear	MPI/no	no	no	input	input	all	yes	yes	yes	sedtrans

Model	Flow processes Equations	Viscosity	Advection	Coriolis	Other processes Infiltration	Precipitation	River discharge	Wind-induced setup
Static								
Bathtub	no	no	no	no	no	no	no	no
Semi-advanced								
LFP	LIE	no	no	no	no	no	yes	no
SFINCS-LIE	LIE	no	no	no	simple	yes	simple	yes
SFINCS-SSWE	SSWE	no	yes	no	simple	yes	simple	yes
3Di	SSWE	no	yes	no	yes	yes	yes	no
Advanced								
ADCIRC	SWE	yes	yes	yes	no	yes	yes	yes
Delft3D	SWE	yes	yes	yes	no	yes	yes	yes
FINEL2D	NHSWE	yes	yes	no	no	no	no	yes
FINEL3D	NS	yes	yes	yes	no	no	no	yes
Funwave	Boussinesq	yes	yes	yes	no	no	no	yes
MIKE 21/3	SWE/Boussinesq	yes	yes	yes	yes/simple	yes/simple	yes	yes
SWASH	NHSWE	yes	yes	yes	no	no	no	yes
XBSB	SWE	yes	yes	yes	no	no	yes	simple
XBNH	NHSWE	yes	yes	yes	yes	no	yes	simple
XBNH+	NHSWE	yes	yes	yes	yes	no	yes	simple

A.2. Used computers

Within this thesis different computers are used, which are stated here regarding the comparison in computational efficiency between different models.

For Delft3D runs:
cluster: 32 GB RAM, 2 cores (4 cores hyper-threading), 3.2 GHz, Intel Xeon E5-2667 v3

For SFINCS and XBeach runs:
wcf-project node: 16 GB RAM, 4 cores, 2.6 GHz, Intel Xeon E5-2670

For SFINCS runs of the Jacksonville case study:
wcp-project node: 16 GB RAM, 8 cores, 2.6 GHz, Intel Xeon E5-2670

LFP in Section 4.2.1 according to Bates et al. (2010):
3 GB RAM, 2 cores, 2.66 GHz, Intel Core2 Duo

A.3. Model versions

Throughout this research the models of Delft3D, SFINCS and XBeach are used. Their respect model versions are stated here:

Delft3D: Within this thesis there has been made use of the Delft3D 4 version without the use of flexible mesh.

XBeach: For XBeach, the XBeach X Beta release revision 5442 is used.

SFINCS: In the beginning of this thesis a subversion repository was created for SFINCS. Different versions of SFINCS have thereby been used, where most runs are performed using the latest V38 version. All used versions are backward compatible. SFINCS is always run with parallel processing using OpenMP. The amount of processors used depended on the amount of processors available (4 or 8).

A.4. SFINCS call graph

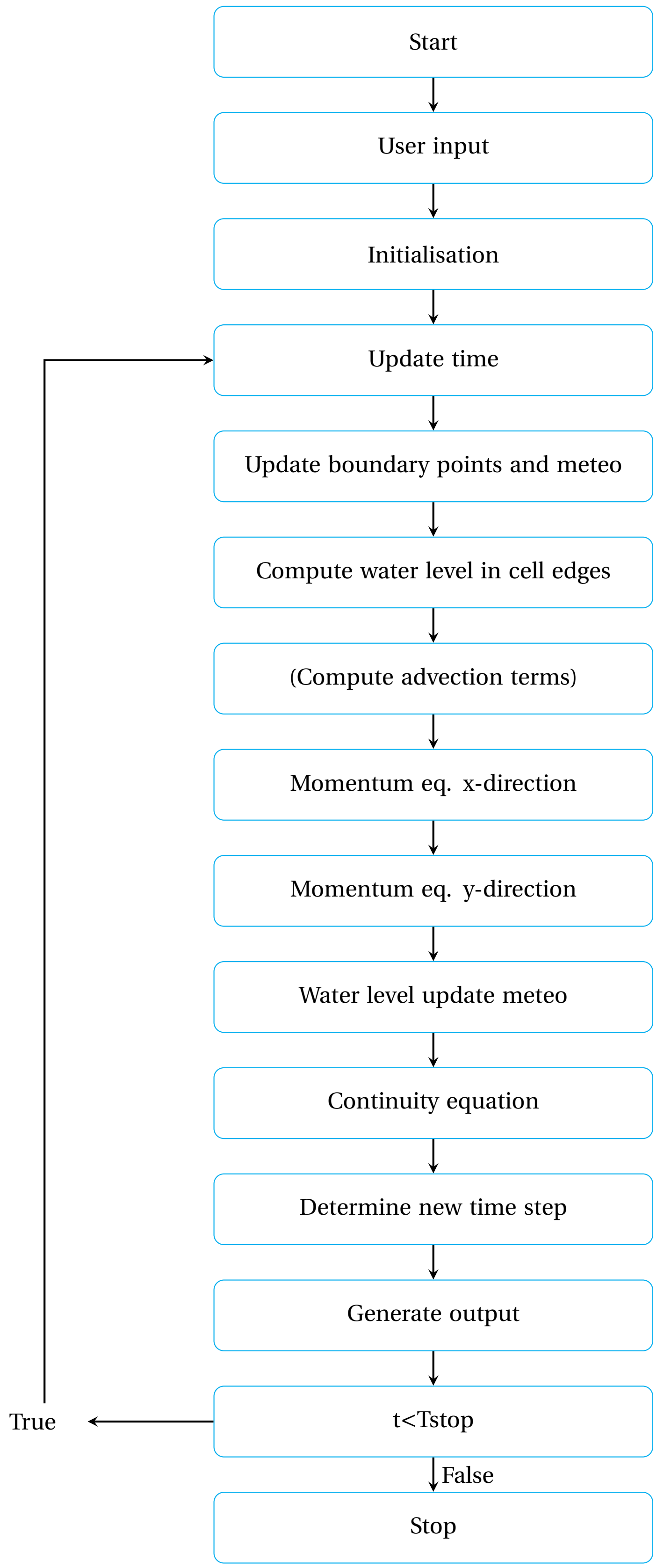

Figure A.1: Simplified call graph of the source code of SFINCS

B

Conceptual tests flow processes

This appendix discusses multiple details of the conceptual flow tests. Additional information regarding the analytical and experimental solutions and model setup is presented, as well as additional results. Section B.1 contains the Bates test, Sections B.2 and B.3 the 1D dam break tests and Sections B.4 and B.5 the 2D dam break tests. There is concluded with additional information regarding the Carrier and Greenspan test in B.6.

B.1. Non-breaking wave propagation over a horizontal plane

B.1.1. Analytical solution

There is a difference in the power coefficient for the analytical solution between Bates et al. (2010) and Hunter et al. (2005), therefore the latter is used since it is the original mention of the test. To get to the analytical solution the 1D form of the SWE for momentum and continuity equation are used for the flow over a planar surface, after Hunter et al. (2005):

$$\frac{\partial h}{\partial t} + \frac{\partial uh}{\partial x} = 0 \tag{B.1}$$

$$\frac{\partial u}{\partial t} + u\frac{\partial u}{\partial x} + g\left(\frac{\partial h}{\partial x} + S_0\right) + \frac{gn^2u^2}{h^{4/3}} = 0 \tag{B.2}$$

In these continuity and momentum equations, u is the component of the depth-averaged velocity in x-direction. S_0 is the bed slope, g the gravitational acceleration and h the water depth. If a constant flow condition $u(x=0,t) = constant$ is imposed, Equation B.1 becomes a pure advection equation in h as the following:

$$h(x,t) = h(x-ut) \tag{B.3}$$

The front of the wave propagates with the constant flow velocity while maintaining its shape. This also means that the velocity is uniform and therefore Equation B.2 becomes an ordinary differential equation:

$$S_0 + \frac{\partial h}{\partial x} + \frac{n^2u^2}{h^{4/3}} = 0 \tag{B.4}$$

For a horizontal plane $S_0 = 0$, where the remains can be integrated directly:

$$h(x,t) = \left[\frac{7}{3}(C - n^2u^3(x-ut))\right]^{3/7} \tag{B.5}$$

Here C is a constant of integration and is equal to $C = 0$. In general C can be set by referring to the initial conditions of the problem. Equation B.5 is the analytical solution to the non-breaking wave propagation over a horizontal plane problem. The solution is showed in Figure 4.1 of Section 4.2.1. There has to be noticed that this analytical solution is not a true analytical solution to the inertial equation as solved by the models and it is therefore not expected that the model results will fully converge to the analytical solution. Although at fine grid resolutions the differences should be small (Bates et al., 2010). The fact that the analytical solution is not the true solution to the DWE also explain why its shape at the tip of the wave, as showed in Figure 4.1, does not fully correspond with what is observed in reality.

B.1.2. Numerical setup SFINCS

The numerical input of SFINCS is based on Bates et al. (2010) because there the accuracy (volume error and RMSE) and efficiency (minimum time-step and total computation time) are calculated for different grid sizes. The main displayed test by LFP uses a Manning friction coefficient of $n = 0.03 s/m^{1/3}$ and grid size $\Delta x = 50m$, which are also used for SFINCS as well as XBeach. So therefore you have $\Delta x = 50m$, $\Delta y = 1m$, $mmax = 100$, $nmax = 1$, $n = 0.03$, $\alpha = 0.75$(default), $\theta = 0.9$(default), $bndtype = 3$(discharge velocity boundary). This discharge boundary condition is provided by inserting $x = 0m$ in Equation B.5 and calculating $h(0,t)$ per time-step, which is used as input in 'sfincs.bzs' (water depth times a velocity of 1 m/s gives a discharge). The bed level is $0m$ everywhere, just as the initial water level. Later also the grid resolutions of $\Delta x = 5m$ and $\Delta x = 200m$ ware modelled, with corresponding $mmax = 1000$ and $mmax = 25$.

B.1.3. Numerical setup XBeach

XBSB does not have an appropriate boundary condition for this situation, but XBNH does in the form of the 'boun_U.bcf' file option (wbctype = ts_nonh) (Roelvink et al., 2010) and is therefore chosen. Hereby the constant flow velocity and rising water level are introduced, leaving with the same input at the boundaries as SFINCS. It turned out that XBeach does not work when all the grid points are initially dry, so a low initial water level of $z_{s0} = 0.01m$ is specified. This influences the result slightly, but otherwise SFINCS cannot be compared with XBeach.

B.2. 1D dam break dry bed

B.2.1. Analytical solution

The analytical solution is based on Chanson (2006), as used in Cui (2013). Chanson (2006) describes the ideal fluid flow solution for a frictionless dam break in a wide horizontal channel. It yields the Ritter solution (Ritter, 1892):

$$U = 2\sqrt{gD} \tag{B.6}$$

$$\frac{x}{t\sqrt{gD}} = 2 - 3\sqrt{\frac{d}{D}} \tag{B.7}$$

With U as the wave front celerity, d as the water depth and D as the initial reservoir height. Equation B.7 was first derived in Barre de Saint Venant (1871). The equations give the wave front celerity and the free-surface profile for $t > 0$. When Equation B.7 is rewritten and presented in more consistent notation the following is obtained:

$$h(x,t) = h_0\left(\frac{2}{3} - \frac{x}{3tc_0}\right)^2 \tag{B.8}$$

With $c_0 = \sqrt{gh_0}$ as the propagation speed of the shock wave. This is the analytical solution between $x = -c_0 t$ and $x = 2c_0 t$, where $x = 0$ is the location of the dam break. Upstream the water depth is still 1m and downstream 0 m.

B.2.2. Numerical setup SFINCS

The numerical implementation is done as in Cui (2013) and Smit et al. (2010) with a 100 m long model, with the dam break interface in the middle and a water level of 1 m upstream. The model is run for 5 seconds to analyse at the capability of the models to capture the strong water level gradients just after the dam break. In SFINCS the dam break test input did require the option to use a spatially variant initial water level $zs_{0,x,y}$.Because of the sharp water level gradient the time-step should be reduced to get stable results, therefore α was set to the minimum advised setting of $\alpha = 0.1$. Furthermore the minimum flow depth for momentum flux 'huthresh' (also known as a flooding an drying threshold) was set to $huthresh = 0.01$. As grid resolutions there is varied between $\Delta = 0.1m$ and $\Delta = 10m$. Also no boundary conditions were specified so the boundaries were basically vertical walls. For SFINCS the test is run with the versions LIE, SSWE 1D and SSWE 2D.

B.2.3. Numerical setup XBeach

The initial water levels can be specified in XBeach using 'zsinitfile', which works the same as described for SFINCS. The boundaries are set to 'wall' (Roelvink et al., 2010), leaving with the same vertical walls as in

SFINCS. It is possible to implement this for XBSB as well as XBNH, which is done to illustrate the influence of the hydrostatic assumption on the results. Both XBeach versions are run including advection, where both numerical schemes are a little bit different. The CFL-condition parameter was set to $CFL = 0.4$ as in (Smit et al., 2010) and also a minimum flow depth for momentum flux was specified $eps = 0.001$. In (Smit et al., 2010) this was set to $10^{-10}m$, but in the current XBeach version the model did not run with such low values.

B.3. 1D dam break wet bed

B.3.1. Analytical solution

For the test with the wet downstream bed the analytical result is slightly different than for the dry bed. Four different zones h_i can be distinguished, as showed in Figure B.1.

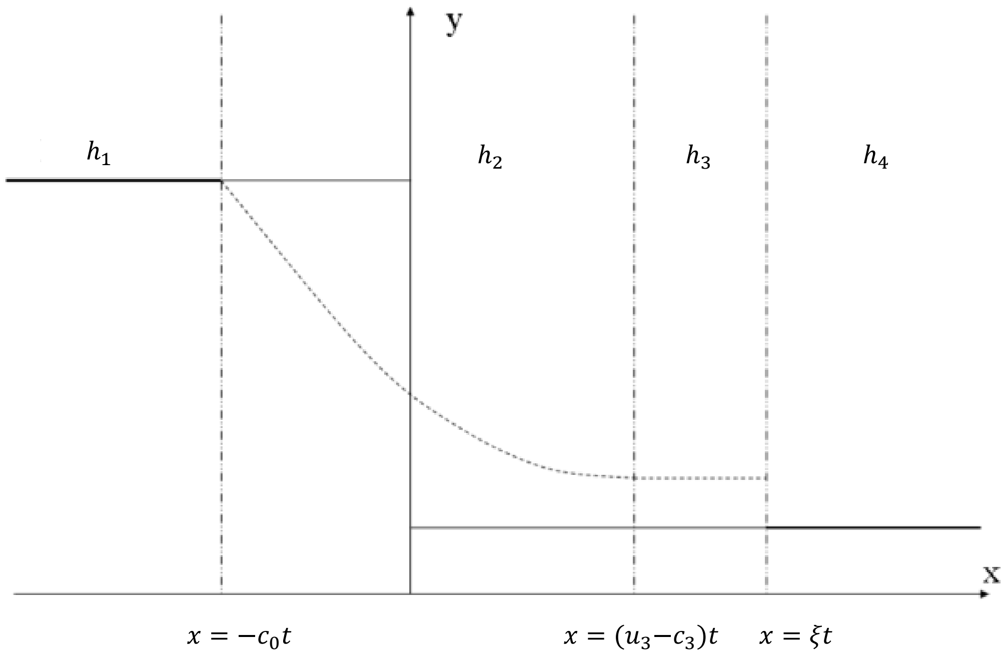

Figure B.1: Example of the 4 different zones for the 1D dam break test with wet bed, figure based on Kroon (2009)

The first zone is the upstream area, which is not affected by the dam break. Then there is the parabolic shaped area which is described in the same way as for the dry bed test. Then there is an area with a constant shock wave height and finally the unaffected downstream area. The solution in zone 3 is according to Kroon (2009):

$$h_3 = \frac{1}{g}\left[-\frac{1}{3}(u_3 - c_3) + \frac{2}{3}c_0\right]^2 \tag{B.9}$$

$$c_3 = \sqrt{gh_3} \tag{B.10}$$

$$u_3 = \xi(1 - \frac{d_4}{d_3}) \tag{B.11}$$

$$\xi = \sqrt{g\frac{h_3}{h_4}\frac{d_3 + d_4}{2}} \tag{B.12}$$

Where ξ is the propagation velocity of the front. Because $d_3 = d_4 = 0m$ and $h_{2,t=0} = h_{3,t=0} = h_{4,t=0} = 0.1m$ and $u_{3,t=0} = c_{3,t=0} = 0$ these equations can be solved.

B.3.2. Numerical setup SFINCS & XBeach

The only thing that is changed in the numerical setup of de models was that the initial downstream water depth was set to 0.1 m.

B.4. 2D dam break dry bed

B.4.1. Experimental solution

The physical experiment is designed to represent the flooding of a flat area after a dike breach. Hereby the lifting of the gate is meant to represent the breaching of the dike, which keeps a constant width. The bottom of the basin was a smooth surface of concrete, with synthetic fibres reinforced. The water flow was measured with a camera to capture at the spatial flow profile and multiple wave gauges for the water levels. The gauges were located along the centre line of B and at 1, 6, 9, 13, 17, 21 and 23 m from the opening. The dimensions of the used basin can be seen in Figure B.2.

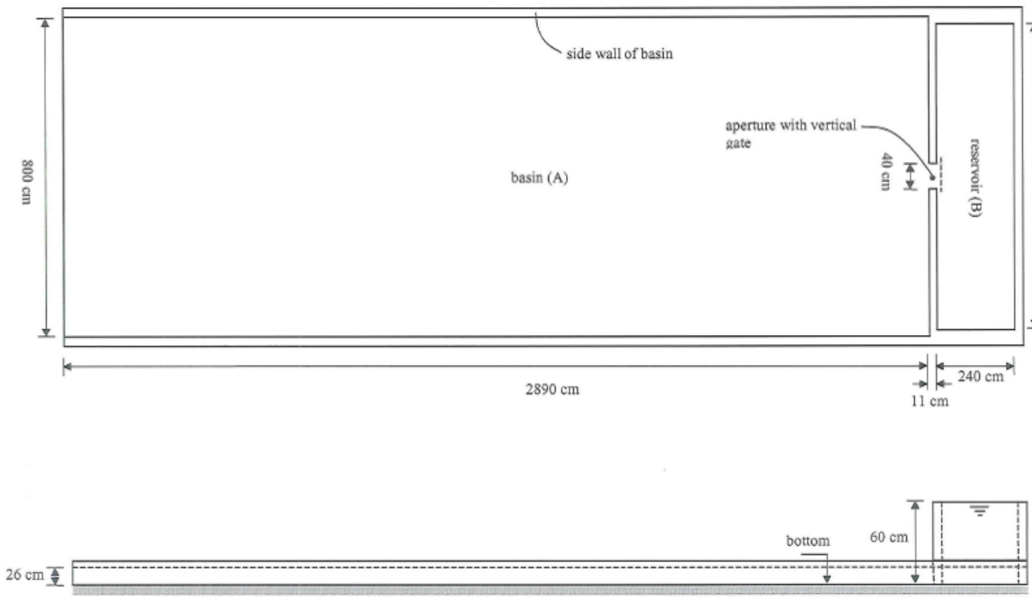

Figure B.2: Top and side view of the experimental setup of the 2D dam break test, directly copied from (Duinmeijer, 2002)

B.4.2. Numerical setup SFINCS

In SFINCS this test is recreated by creating a basin of the same dimensions and making the release of the water in the upstream basin instantaneous instead of with a rising gate. The dam is recreated by 'turning off' the grid cells at the location, done by specifying zeroes in the masker file (sfincs.msk). All boundaries can be seen as vertical walls because in the rest off the domain the masker file contains ones. For the grid the resolution is set the same as Stelling and Duinmeijer (2003) and the minimum in the 1D dam break test: $dx = dy = 0.1m$. In the paper was also found that the numerical results are sensitive to the used friction values. The dry bed case was numerically simulated with $n = 0.01$ and $0.012 s/m^{1/3}$, of which the second value is used here. After doing some calibration with the parameters it was found that it was still necessary to use $\alpha = 0.1$ and the flow depth limiter had to be set to $h_{u,thresh} = 0.01m$. For SFINCS the test is run with the versions LIE, SSWE 1D and SSWE 2D.

B.4.3. Numerical setup XBeach

The only difference between the numerical setup with SFINCS is the way the dam is specified. In XBeach there is no way to disable grid cells so the dam is created by elevating the bed level to 1m for one grid cell wide. Boundaries everywhere are set to 'wall'. Models runs are performed for XBSB and XBNH to see the difference regarding the hydrostatic assumption.

B.4.4. Numerical solutions

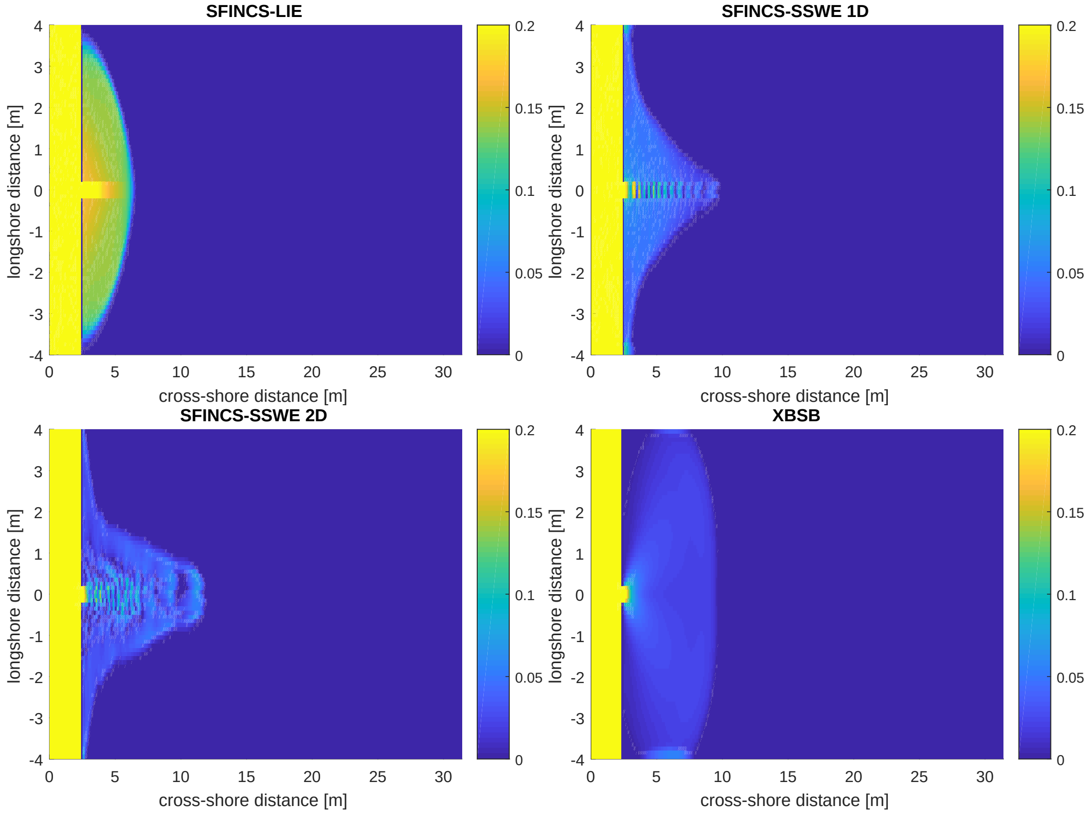

Figure B.3: SFINCS and XBeach solutions for the 2D dam break test with dry bed with $n = 0.03 s/m^{1/3}$ for SFINCS and with $n = 0.012 s/m^{1/3}$ for XBeach, after 4 seconds. Upper left= SFINCS without advection, upper right= SFINCS with 1D advection, lower left= SFINCS with 2D advection, lower right=XBSB, all after 4 seconds

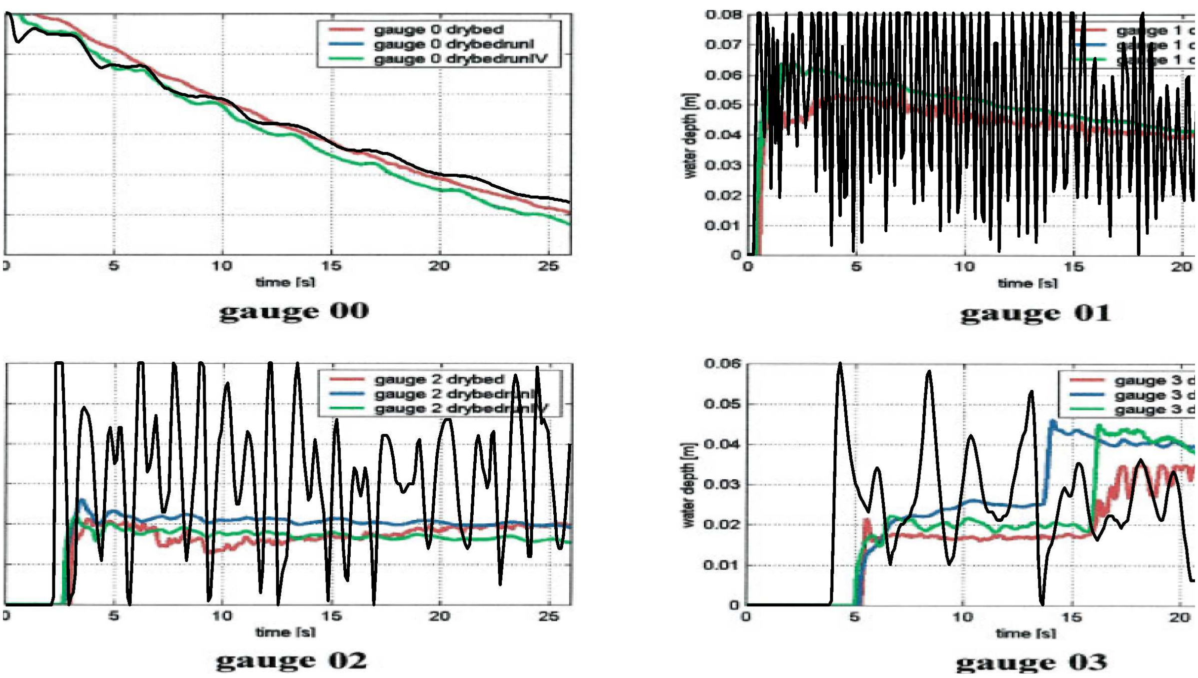

Figure B.4: SFINCS SSWE 2D water levels for the 2D dam break test with dry bed. Black lines are the results of the model runs by SFINCS. The other lines belong to Stelling and Duinmeijer (2003).

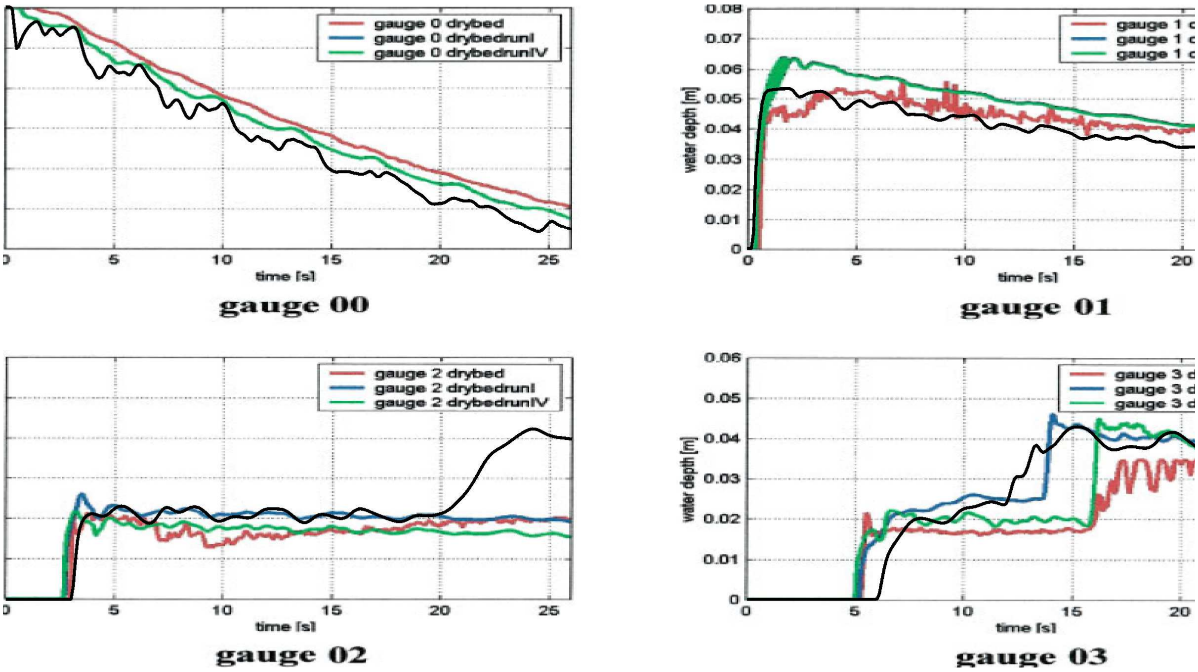

Figure B.5: XBSB water levels for the 2D dam break test with dry bed. Black lines are the results of the model runs by XBeach. The other lines belong to Stelling and Duinmeijer (2003).

B.5. 2D dam break wet bed

The solutions are only shown for the stable SFINCS solutions using $n = 0.12s/m^{1/3}$, while XBeach is run using $n = 0.012$ as used by Stelling and Duinmeijer (2003). Again the high friction value was needed in order to obtain a stable solution. There can be seen in Figures B.6 and B.8 that the forward propagation speed in SFINCS is reasonable, but that the profile in x-direction is off for all runs. This can be explained with Figure B.6, as the region just behind the flow opening with super-critical flow and the hydraulic jump is not modelled correctly. This happens because of the increased friction which was needed for a stable solution.

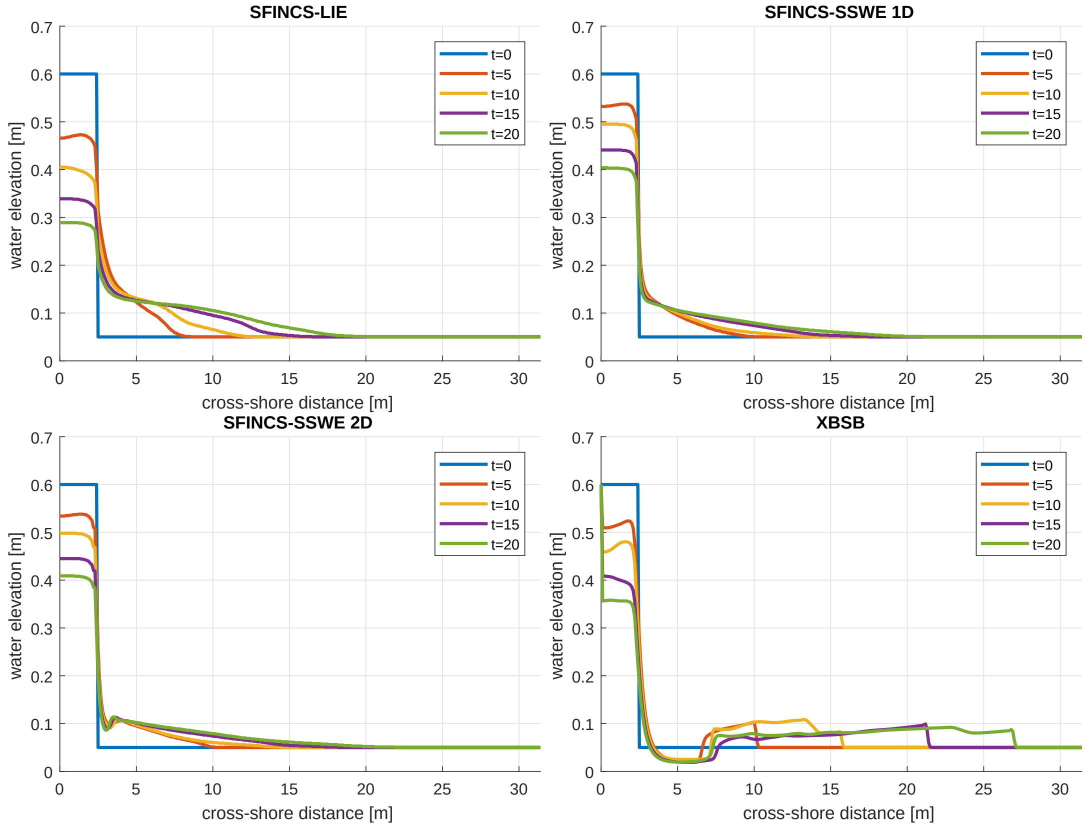

Figure B.6: SFINCS and XBeach propagation fronts for the 2D dam break test with wet bed test. Upper left= SFINCS without advection, upper right= SFINCS with 1D advection, lower left= SFINCS with 2D advection, lower right= XBSB

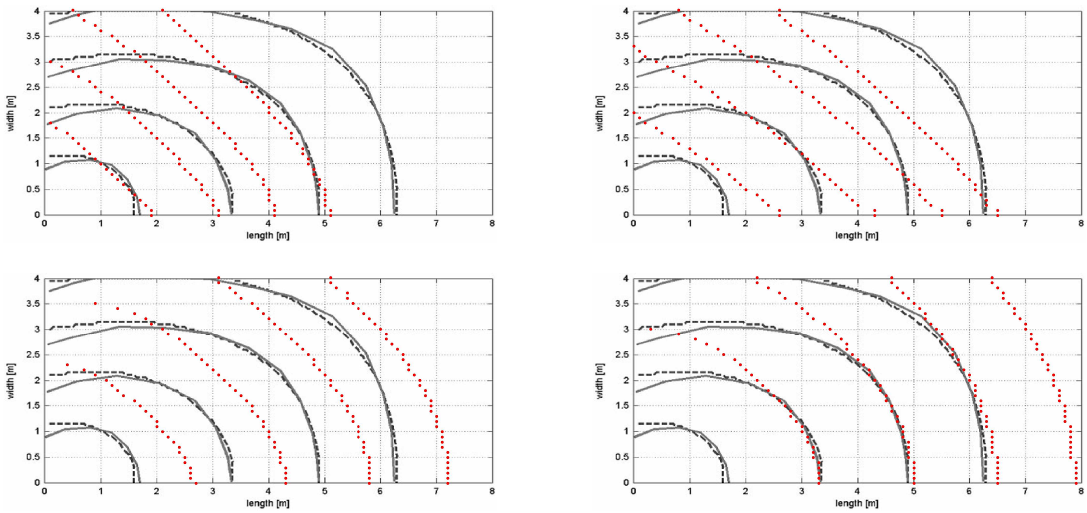

Figure B.7: SFINCS and XBeach propagation fronts for the 2D dam break test with wet bed. Upper left= SFINCS without advection, upper right= SFINCS with 1D advection, lower left= XBSB, lower right= XBNH. Red dots are the results of the model runs by SFINCS/XBeach, the dashed and solid lines are the modelled and measured results of Stelling and Duinmeijer (2003).

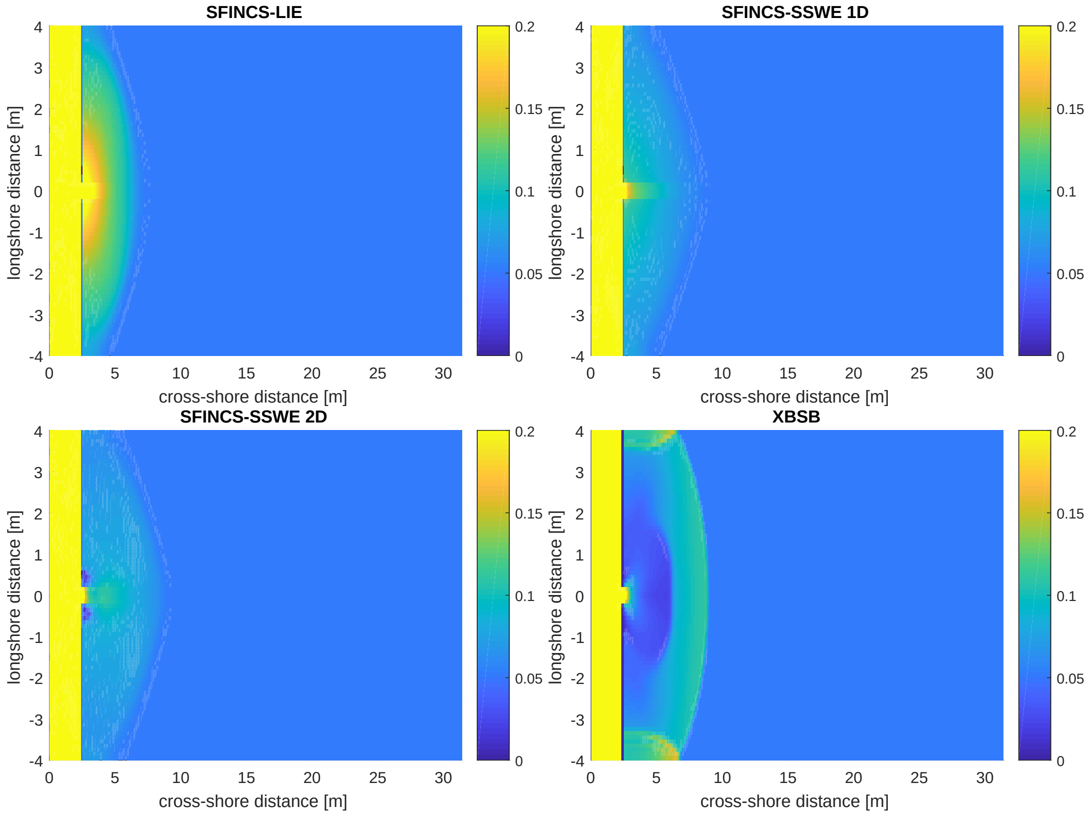

Figure B.8: SFINCS and XBeach propagation fronts for the 2D dam break test with wet bed after 4 seconds. Upper left= SFINCS without advection, upper right= SFINCS with 1D advection, lower left= SFINCS with 2D advection, lower right= XBSB, all after 4 seconds

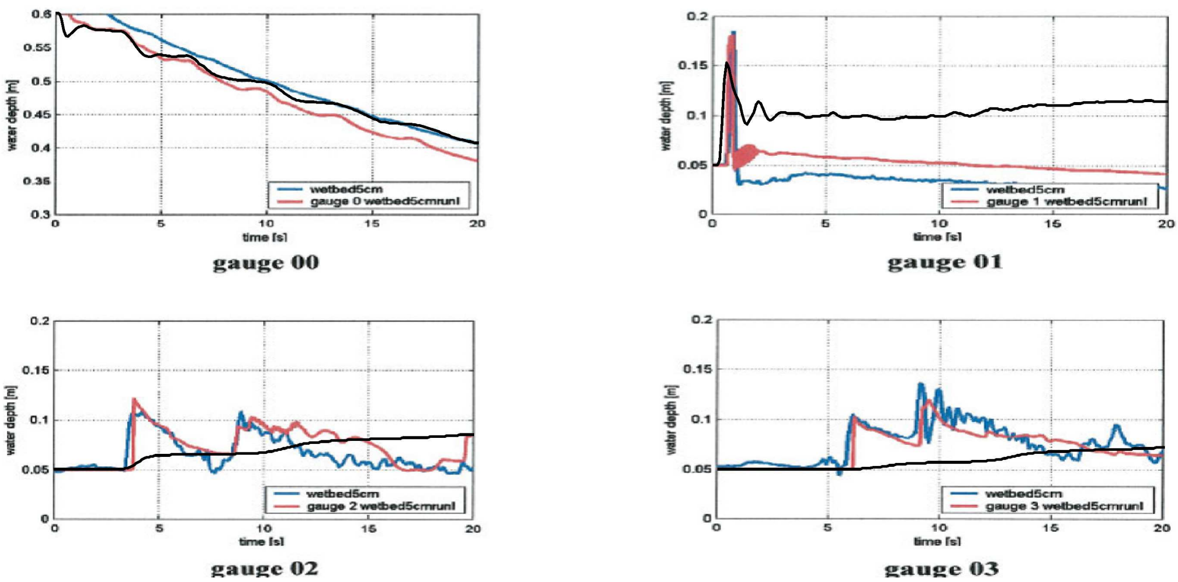

Figure B.9: SFINCS SSWE 2D water levels for the 2D dam break test with wet bed. Black lines are the results of the model runs by SFINCS. The other lines belong to Stelling and Duinmeijer (2003).

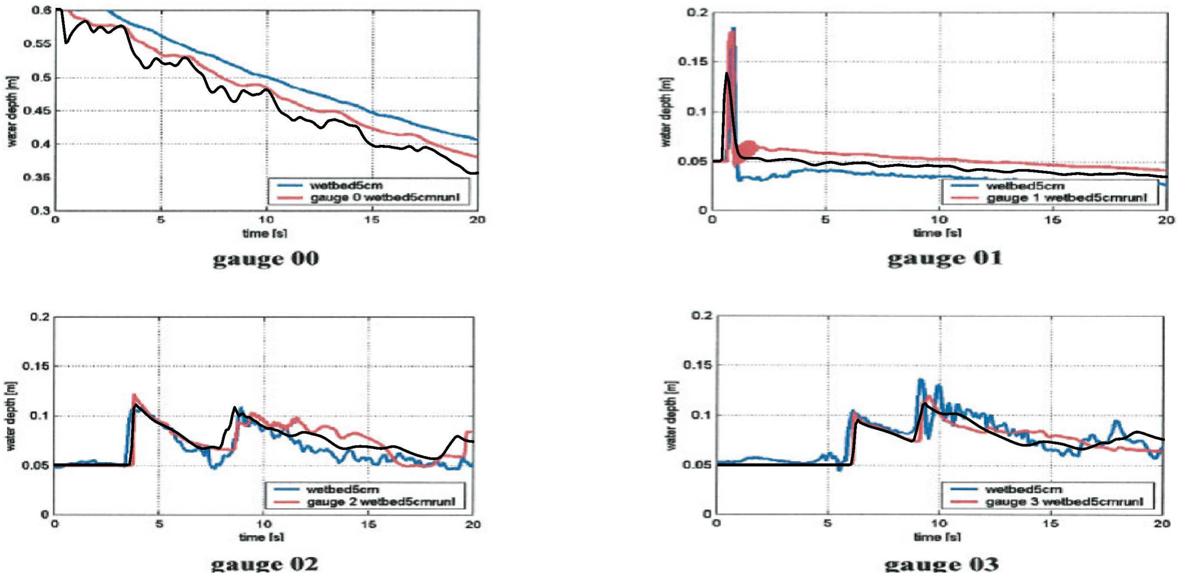

Figure B.10: XBSB water levels for the 2D dam break test with wet bed. Black lines are the results of the model runs by XBeach. The other lines belong to Stelling and Duinmeijer (2003).

B.6. Carrier and Greenspan

B.6.1. Numerical setup

The numerical setup is based on the XBeach setup as embedded in the skillbed of XBeach (Deltares, 2018b). Here a 1D XBSB model is run with a 150 m long domain with a 6 m high linear 1:25 slope. The grid sizes are varying from 1 m offshore to 0.05 m nearshore proportional to the (free) long wave celerity. In SFINCS varying grid sizes are not yet possible, therefore the minimum grid size of 0.05 m is used throughout the whole model. Both models are run without friction. SFINCS and XBeach are run with a minimum flow depth of 10^{-4} m (keywords 'huthresh' and 'eps' respectively). In SFINCS the time-step is reduced by using an α-factor of 0.1. For the default value of 0.75 the results for SFINCS LIE and SSWE are both stable, but the results are a bit smoother and closer to the analytical solution with a lower value of α. The boundary condition for the XBeach model is a harmonic sinusoidal water level variation based on the analytical solution by Carrier and Greenspan (1958). To keep the input for both models exactly the same, the output of the offshore boundary cell of XBeach is used as input for SFINCS. For more settings see the skillbed report of XBeach (Deltares, 2018b).

B.6.2. Analytical solution

The analytical solution is based on the skillbed report of XBeach, of which the following is directly copied. A more theoretical description can for instance be found in Kroon (2009). A free long wave with a wave period of 32 seconds and wave amplitude of half the wave breaking amplitude ($a_{in} = 0.5 \cdot a_{br}$) propagates over a beach with constant slope equal to 1:25. The wave breaking amplitude is computed as $a_{br} = \frac{1}{\sqrt{128 \cdot \pi^3}} \cdot s^{2.5} \cdot T^{2.5} \cdot g^{1.25} \cdot h_0^{-0.25} = 0.0307$ m, where s is the beach slope, T is the wave period and h_0 is the still water depth at the seaward boundary. To compare XBeach output to the analytical solution of Carrier and Greenspan (1958), the first are non-dimensionalised with the beach slope s, the acceleration of gravity g, the wave period T, a horizontal length scale L_x and the vertical excursion of the swash motion A. The horizontal length scale L_x is related to the wave period via $T = \sqrt{\frac{L_x}{g \cdot s}}$ and the vertical excursion of the swash motion A is expressed as: $A = a_{in} \cdot \frac{\pi}{\sqrt{0.125 \cdot s \cdot T \cdot \sqrt{\frac{g}{h_0}}}}$.

B.6.3. Additional figures

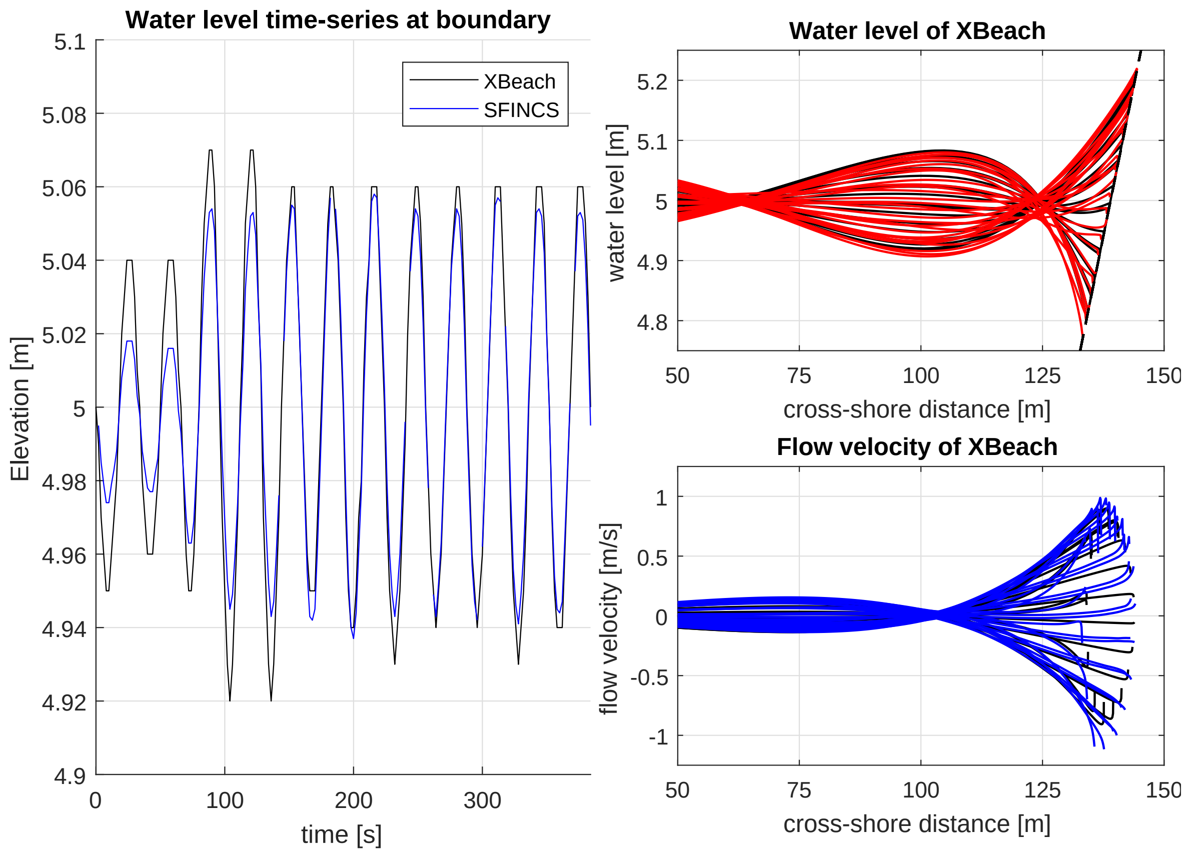

Figure B.11: Additional results Carrier and Greenspan test. Left: SFINCS-SSWE and XBeach input, Right: Water levels and flow velocity of XBeach.

C

Conceptual tests wave processes

This appendix discusses multiple details of the conceptual tests for waves. The numerical setup with the chosen XBeach version, model runtime, grid generation, additional grid cells SFINCS and sensitivity of the SFINCS results are discussed in Section C.1. Thereafter the different steps of the post-processing of the results with the splitting of incoming waves, determining of the wave spectra, significant wave height, setup, swash and runup are discussed in Section C.2. Also the swash zone and runup characteristics are discussed, as well as additional statistical definitions and the definitions of asymmetry and skewness. There is concluded with Section C.3 where additional results of the wave tests are presented.

C.1. Numerical setup

C.1.1. XBeach version

An important decision is whether to run XBeach in incident wave averaged (XBSB) or incident wave solving mode (XBNH+). For the non-hydrostatic version of XBeach it was advised to use the XBNH+ version over XBNH. XBNH+ has an implementation with less numerical dissipation and the second (hydrostatic) layer improves dispersion and reduces numerical wiggles. To make a well-founded decision the limited dataset is run for XBSB as well as XBNH+, comparing multiple swash and runup characteristics of which the R2% is shown in the right panel of Figure C.1. It can be seen that for steeper slopes where incident waves become important, XBSB naturally underestimates the runup because only the IG waves are solved within the model. However, for milder slopes it can also be seen that XBSB underestimates the runup compared to XBNH+, which theoretically should give the same results. Do note here that the comparison would have been more accurate if exactly the same grid were used for XBSB and XBNH+. The general pattern of XBSB under-predicting the runup was also observed in (De Beer, 2017) for milder wave conditions. The differences in the results of the two XBeach versions basically illustrate the uncertainty in the model-model comparison between SFINCS and XBeach. In the end there is chosen to continue with the XBNH+ version, because it is wanted to have a boundary implementation that also performs well for non-dissipative conditions. Because incident waves are and turn out to be important for those conditions, there is chosen to model with XBNH+ since then the individual incident waves can be solved.

C.1.2. Model runtime

Another important decision is what the required runtime is to come up with representative runup characteristics. From an engineering point of view it is not wanted to run models for 24 hours or more, but as short as possible while still holding representative statistical results compared to the long runtime. To assess what the runtime of an XBeach model should be in order to come up with a representative cumulative runup distribution function one wave condition is run for multiple runtimes (1,3,6,9,12,24 hours), while updating the random wave signal every $rt = 3600s$. This is done so that the wave signal does not repeat itself every hour which produces a runup distribution that is not smooth. Furthermore the setup consists of a slope of $\beta = 0.02[-]$ and deep water wave characteristics $H_s = 6m$ and $T_p = 15s$. When the runup distributions are plotted over each other, Figure C.1 is obtained. There can be seen with runtimes of 1 and 3 hours the results are far from their Gaussian fit. For longer runtimes this converges towards the result of 24 hours, which is assumed to be fully Gaussian (which is pretty close to reality). Because for modelling practice it is wanted to

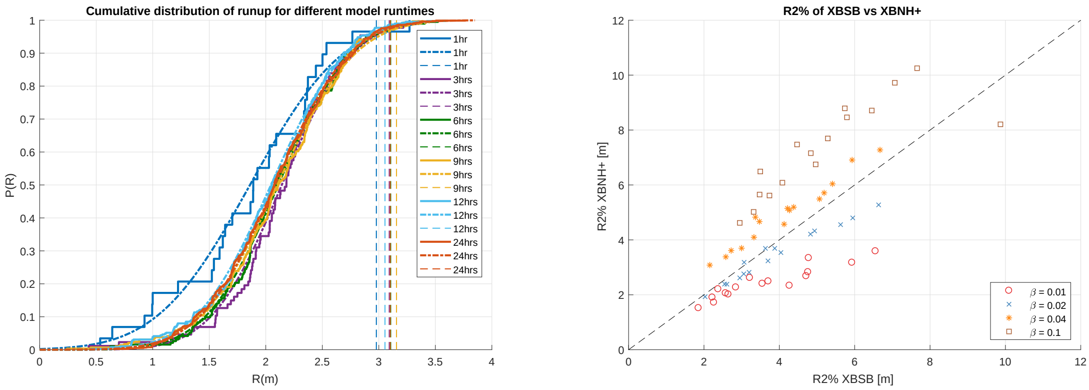

Figure C.1: Left: Comparison of the cumulative runup distributions per model runtime, Right: Comparison of R2% between XBSB and XBNH+

have the shortest possible runtime, the results of 6, 9 and 12 hours are further compared. When calculating $R_{2\%}$, R_{max} and Scatter Index (SI) values compared to the result of 24 hours, a runtime of 6 hours was found to be sufficient. Thereby you have $R_{2\%} = 0.13\%$ (overestimation), $R_{max} = -6.42\%$ (underestimation), $SI = 1.87\%$ and 192 runup peaks were present after removing the spin-up time. The underestimation of R_{max} occurred because of one large runup event in the 24 hour run, also with a runtime of 12 hours this was not captured. At first this test was performed using XBSB because at that time this was considered the desired XBeach version. Later this was changed to XBNH+, but based at the cumulative runup distribution functions of the XBNH+ runs it turned out that 6 hours was still a good choice for a representative runtime. A general rule of thumb is that you need approximately 1000 waves for a good runup distribution, and running six hours with incident waves of around $T_p = 10s$ includes more than 2000 waves.

C.1.3. Grid generation

The grids of the XBeach runs have been made automatically based on the linear slopes as described earlier. For the grid resolutions there has been made use of Matlab scripts of the Open Earth Toolbox (OET, Deltares (2018a)) where point per point the required grid resolution is calculated based on the dispersion relationship using the input of representative wave period, water depth, Courant number and the ratio of grid sizes between two adjacent cells. It also takes into account whether you are solving incident or only IG waves and what the desired number of PPWL is. For XBNH+ it is must be quite high (PPWL=40) with grid resolutions in the range of 5m offshore and 1m nearshore. The offshore boundary is situated at 20m water depth or deeper, depending on the requirement that $kh < 3[-]$ and $n < 0.8[-]$. Based on the offshore slope and wave conditions the offshore boundary water depth varied between 20 and 50 meters. The grids have 3 additional horizontal cells at the offshore side. Figure C.2 gives an example of the model setup. Hereby also the total significant wave height Hm0 over distance is showed, there can be seen that a significant amount of energy is already dissipated at 2 m water depth.

C.1.4. Additional grid cells SFINCS

It was found during steep slopes with strong energetic conditions that the rundown comes very close to the model boundary. Therefore a flat area of 10 m was added at the SFINCS area, the amount of grid cells depends on the bottom slope and is rounded up. Hereafter, the rundown is further away from the boundary, see Figure C.3. Note that both runs are forced with a different random boundary signal. To make sure that the water level at the boundary itself does not drop below the bed level, there was specified that the water level of the created random water level time-series cannot drop below 0.5 m above the bed level. This does not reduce the significant wave height at the boundary significantly. For the real XBNH+ time-series at 2 m water depth the water level also does not seem to become lower than 0.5 m from the bed.

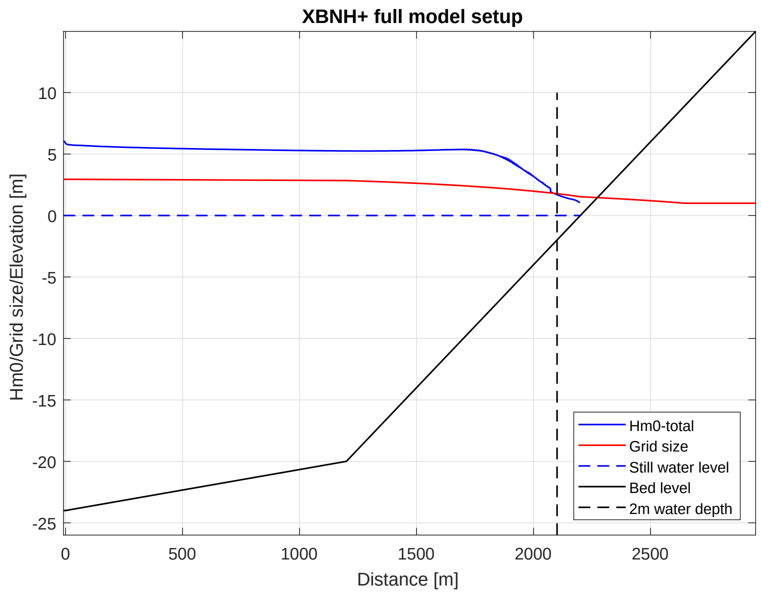

Figure C.2: Example of XBNH+ full model setup with slope 1:50, $H_s = 6m$, $T_p = 10s$ Given are the total Hm0 over distance, grid size over distance and the bed level

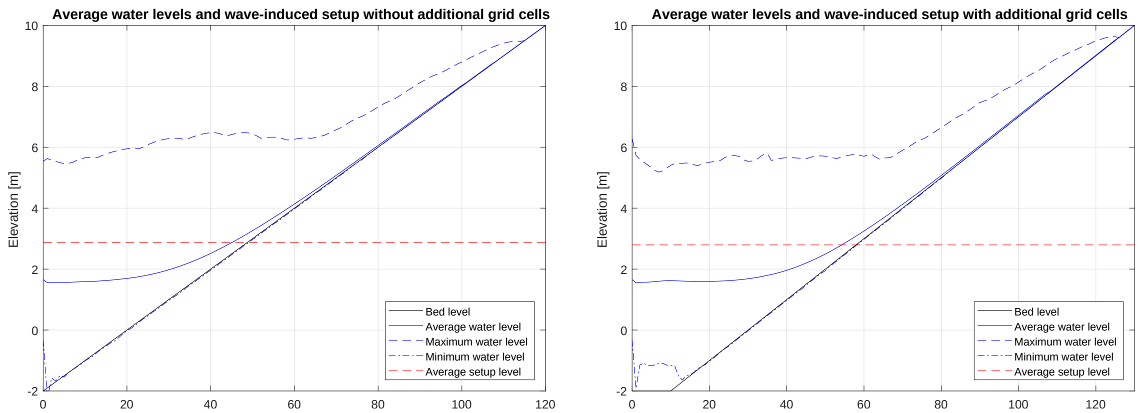

Figure C.3: Illustration of effect added grid cells, both with slope 1:10, $H_s = 10m$, $T_p = 12s$. Left: without added grid cells, Right: with added grid cells

C.1.5. Sensitivity results SFINCS

There is analysed what the sensitivity of the SFINCS results is for the flow depth limiter, the runup gauge flow depth, the friction and the grid resolution. During reduction of the above parametrisation it was already found that the SFINCS results are sensitive to the boundary water level. However for the flow depth limiter value $h_{u,thresh}$ SFINCS was not that sensitive, so this is set to the default value of 0.05m instead of the default value of 0.005m of XBeach (parameter 'eps' (Roelvink et al., 2010)). The flow depth for the runup gauge ('rugdepth' in XBeach (Roelvink et al., 2010)) was more sensitive since during a downrush of a wave always a little bit of water would stay behind, which you do not necessarily want to mark as the actual shoreline at that moment. Therefore the flow depth value of the runup gauge is increased from 0.005 m (default in XBeach) to 0.05 m. The exact friction value made a difference in SFINCS, but the default value of $n = 0.04 s/m^{1/3}$ instead of the used 0.02 did not immediately lead to completely wrong results. However the results of XBeach turned out to be sensitive to the used friction formula. By default XBeach uses the Chèzy formula with a value of $C = 55 s/m^{1/3}$, but this was later changed to the Manning formula with a value of 0.02 as in SFINCS. The depth-dependent Manning formula does decrease the runup since this introduced more friction during the uprush of the waves when the water depth is small. There is also analysed at how sensitive the results are when the grid size is increased from 1 m to a larger value. For milder slopes the SFINCS results do not vary much, but for the 1:10 slope it does affect the outcome.

C.2. Post-processing

C.2.1. Splitting incoming waves

The first step of the post-processing of the results of the wave tests, is the retrieval of the water level and velocity time-series of an observation point in the full XBNH+ model at a bed level of -2 m. Thereafter these are used for the Guza-method for splitting incoming and outgoing waves (Guza et al., 1984). The output of the water level time-series of the incoming waves are used as input for the SFINCS models. For the XBeach swash zone models also the velocity time-series of the incoming wave are used for the boundary conditions. More information regarding the Guza-method can be found in Van Engelen (2016). An example of the result of the method is shown in Figure C.4.

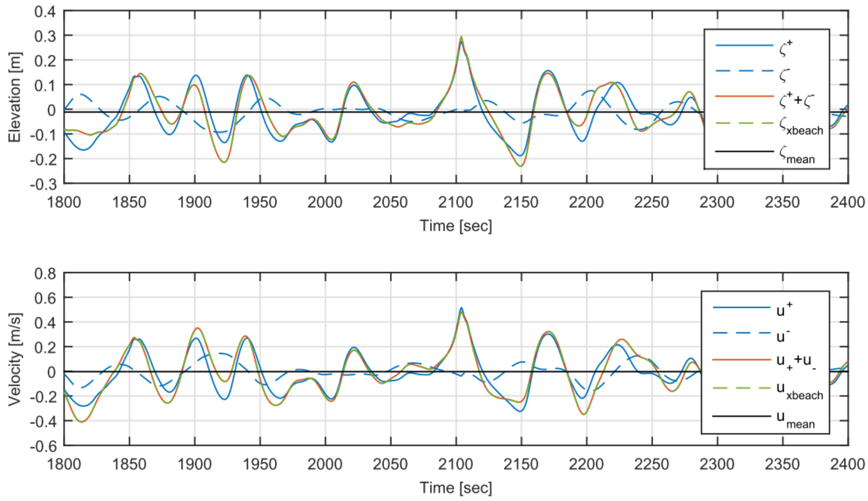

Figure C.4: Example of Guza-method with decomposed signals of the surface elevation and depth-averaged flow velocity from XBeach. Directly copied from Van Engelen (2016)

C.2.2. Determining wave spectra

For the SFINCS runs where an indirect forcing is used, the boundary conditions are not supplied using the incoming water level time-series but are based on the wave spectra. Using the script 'spectrumsimple.m' of the OET a simple spectrum of the incoming water signal is made with the Hann filter and Welch method. Hereby the desired resolution is set to $df = 5.56 \cdot 10^{-4} Hz$ as described in Section 3.3.3. The output is an array of frequencies and an array of corresponding variance densities. An example of such a spectrum is given in Figure C.5. Based on this spectrum, the significant wave heights are determined.

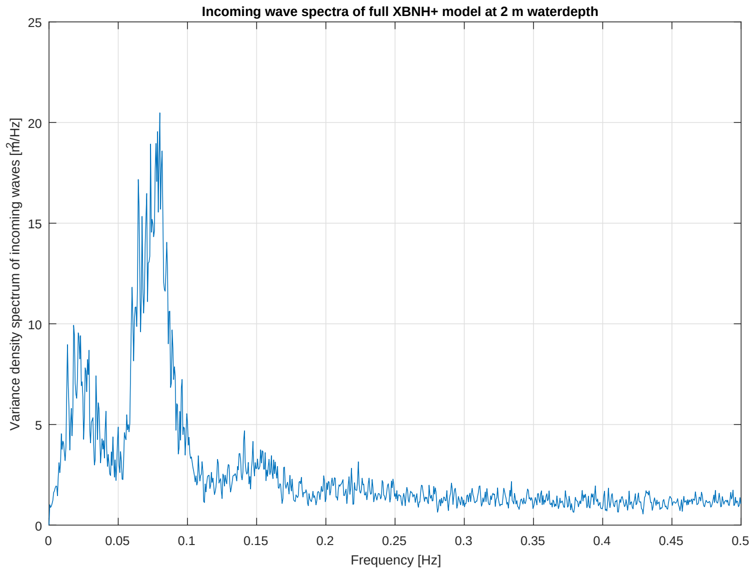

Figure C.5: Example of incoming wave spectra for full XBNH+ model at 2 m water depth with slope 1:10 and offshore $H_s = 10m$ and $T_p = 12$

C.2.3. Determining significant wave height

The significant wave heights are divided into a IG part ($H_{m0,IG}$) and an incident part ($H_{m0,inc}$), separated used the frequency of 0.04 Hz (Quataert et al., 2015). Using the script 'swan_hs.m' of the OET the significant wave height of both parts is calculated as in SWAN.

C.2.4. Determining setup, swash and runup

After all the full and swash zone models have run, characteristics like the setup, swash and runup can be determined. This is illustrated in Figure C.6. At the boundary of the swash zone model the mean water level ζ_b is defined, this is simply the mean value of the incoming water level time-series. Then at the shore there is the shoreline that is varying in time. The vertical water level of this shoreline is called runup and is determined by comparing the water level with the bed level. The last cell with a water depth larger than 0.05 m (analogous with 'rugdepth' in XBeach) is marked as the runup level of that time-step. With this runup time-series also the mean setup at the waterline is determined by taking the mean. This follows the definition of Stockdon et al. (2006). The swash signal is defined as the runup minus the mean setup. From the runup time-series also the runup peaks are retrieved using the Matlab script 'findpeaks.m'. Here the minimum peak distance is set to 60 s and the minimum peak height at 0 m (so no peaks below the mean sea level). This is showed in Figure C.7.

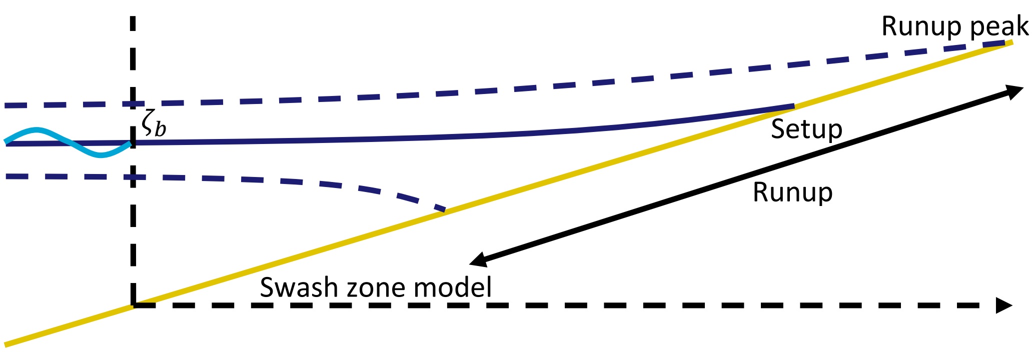

Figure C.6: Illustration of definitions in the swash zone with the mean water level at the boundary, runup and setup at the water line

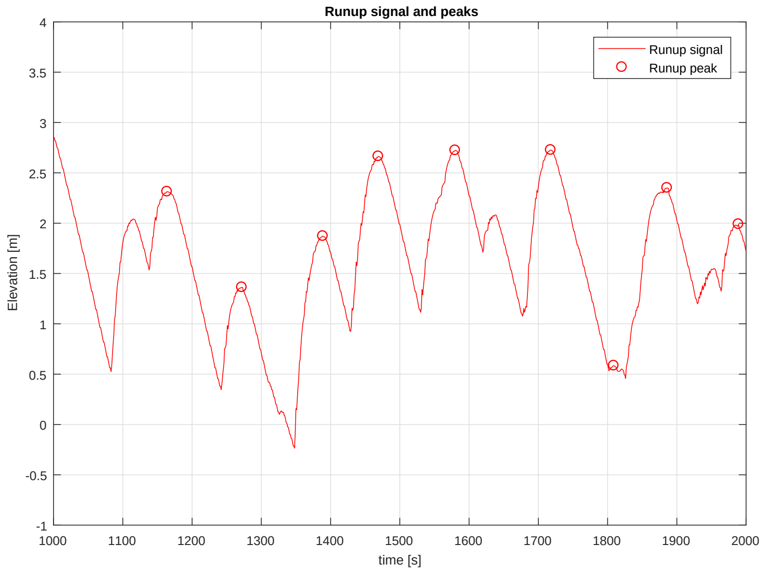

Figure C.7: Example of runup signal and runup peaks for a XBNH+ full model run with slope 1:50 and offshore $H_s = 10m$ and $T_p = 12s$

C.2.5. Swash zone characteristics

After subtracting the setup from the showed runup signal, the remaining swash signal is used to determine the swash zone characteristics. The significant swash S_{ig} and S_{inc} are determined by using the same 'simple-spectrum.m' and 'swan_hs.m' scripts. Again an IG and incident part is distinguished, an example of a swash spectra is showed in Figure C.8. Generally you can see that the swash spectra contains more IG energy than the wave spectra. This is for instance visible when comparing Figures C.5 and C.8. Via bore merging energy from the incident waves is transferred to longer waves.

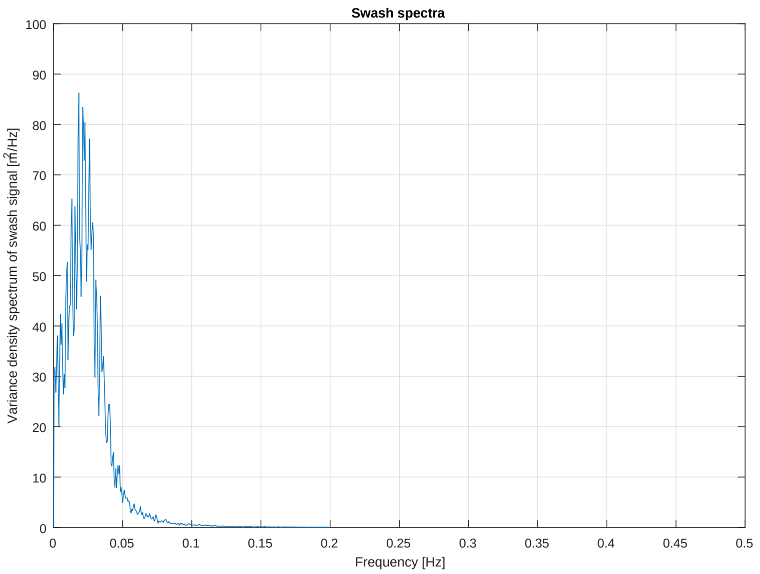

Figure C.8: Example of swash spectra for full XBNH+ model with slope 1:10 and offshore $H_s = 10m$ and $T_p = 12$

C.2.6. Runup characteristics

Using the determined runup peaks also the runup characteristics can be determined. At first a cumulative runup distribution is made from the runup peaks, which is close to a Gaussian distribution (e.g. Stockdon et al. (2006)). From this distribution the runup value with $P(R) = 0.98[-]$ is retrieved. If this value does not exist, there is interpolated between the two closest data points. This gives the runup characteristic R2%. The characteristic Rmax is simply the maximum runup value that occurred during the simulation.

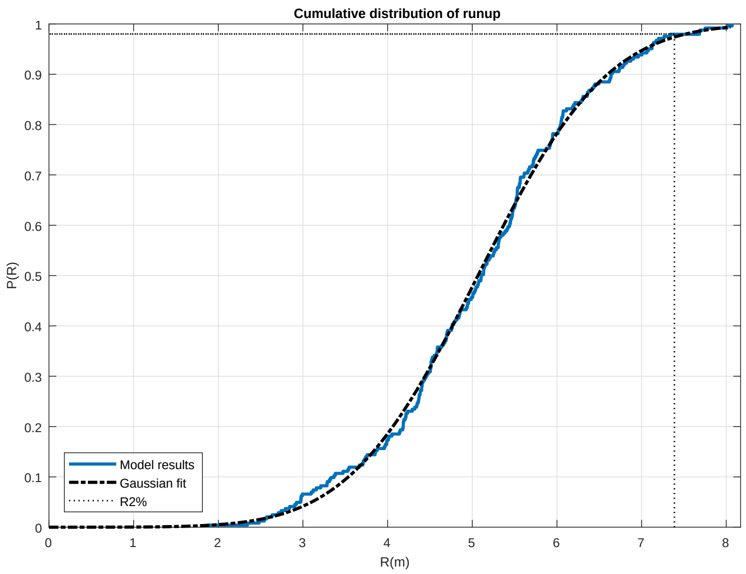

Figure C.9: Example of cumulative distribution of runup for a full XBNH+ model with slope 1:10 and offshore $H_s = 10m$ and $T_p = 12$

C.2.7. Asymmetry and skewness

Also the asymmetry and skewness of the water level time-series is analysed. Asymmetry is defined here as the asymmetry of waves around the vertical axis. Waves pitch forward in shallow water because the wave crest moves faster than the wave crest, since the waves move with $c = \sqrt{gh}$. Very close to the shore the shape of the waves can become close to a saw-tooth shape. Skewness is defined as the asymmetry around the horizontal axis. Waves can get gradual peaking of the wave crest and flattening of the through. The skewness can be described with a factor 's', see Eq C.1. Using the Matlab script 'skewness.m' this factor is calculated for a water level or swash time-series.

$$s = \frac{E(x-\mu)^3}{\sigma^3} \tag{C.1}$$

C.2.8. Statistical definitions

At last some statistical definitions are used when comparing datasets of different swash zone models or settings. Often the least-squared estimators regression line (b), Scatter Index (SI) and relative bias (indicated with 'bias') are calculated. Here f_{full} is used for the results of the full XBNH+ model and f_{swash} for the results of one of the swash zone models. N is the number of data points within at set of f.

Regression line

The regression line is obtained to apply the least-squared estimators to obtain the slope of the regression line.

$$b = \frac{N\sum_{i=1}^{N} f_{full,i} \cdot f_{swash,i} - \sum_{i=1}^{N} f_{full,i} \cdot \sum_{i=1}^{N} f_{swash,i}}{N\sum_{i=1}^{N} f_{full,i}^2 - (\sum_{i=1}^{N} f_{full,i})^2} \tag{C.2}$$

Scatter Index

The scatter index is the standard deviation relative to the mean value of the measured signal.

$$S.I. = \frac{\sqrt{\frac{1}{N-1}\sum_{i=2}^{N}(f_{swash,i} - f_{full,i} - \frac{1}{N}\sum_{i=1}^{N}(f_{swash,i} - f_{full,i}))^2}}{\overline{f_{full}}} \tag{C.3}$$

Relative Bias

The relative bias is the systematic error relative to the mean:

$$Rel.bias = \frac{\sum_{i=1}^{N}(f_{swash,i} - f_{full,i})}{\sum_{i=1}^{N}\overline{f_{full}}} \tag{C.4}$$

C.3. Additional results wave tests

C.3.1. Swash zone processes

Additional figures of the conceptual wave test with direct forcing:

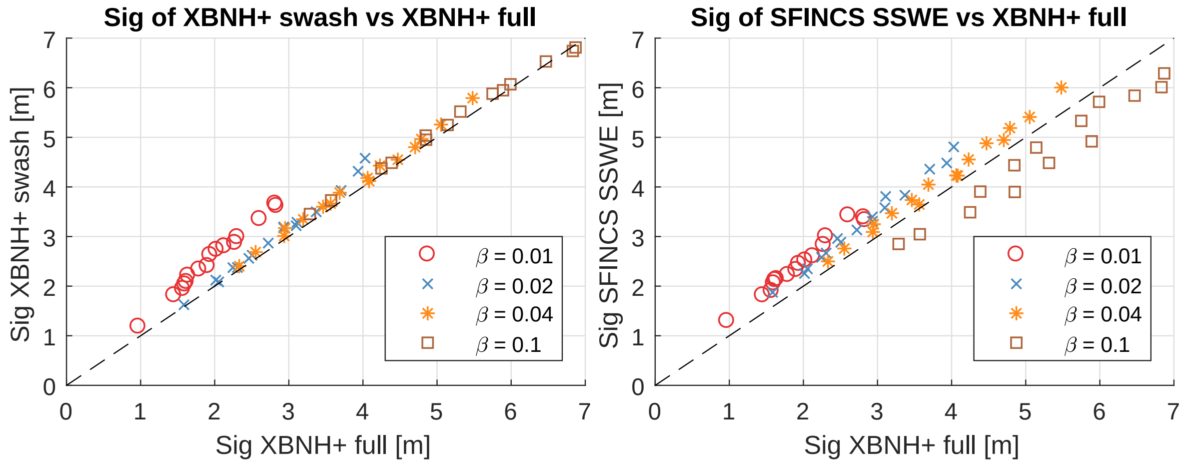

Figure C.10: Significant IG swash of XBNH+ swash and SFINCS-SSWE with real forcing versus XBNH full

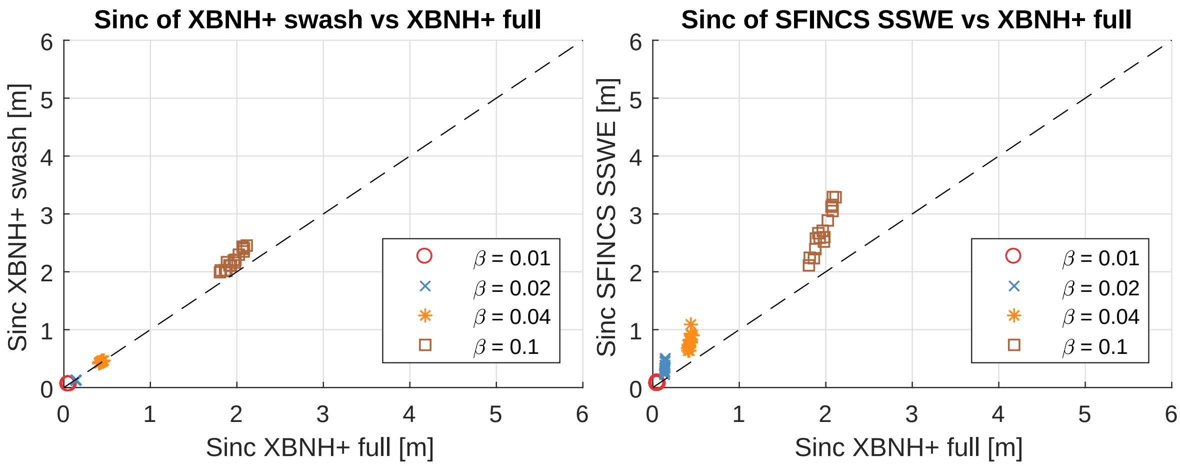

Figure C.11: Significant incident swash of XBNH+ swash and SFINCS-SSWE with real forcing versus XBNH+ full

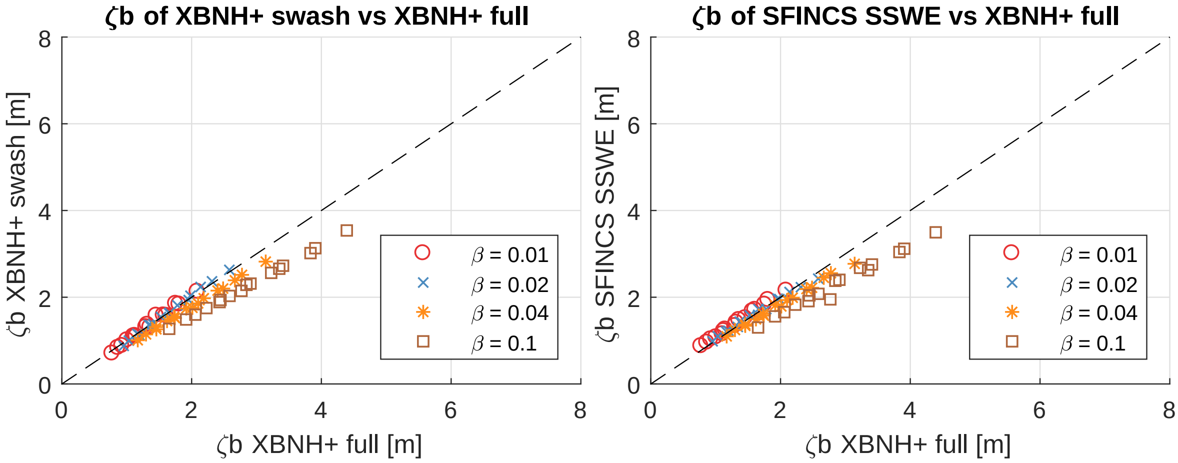

Figure C.12: Mean setup at boundary of XBNH+ swash and SFINCS-SSWE with real forcing versus XBNH+ full

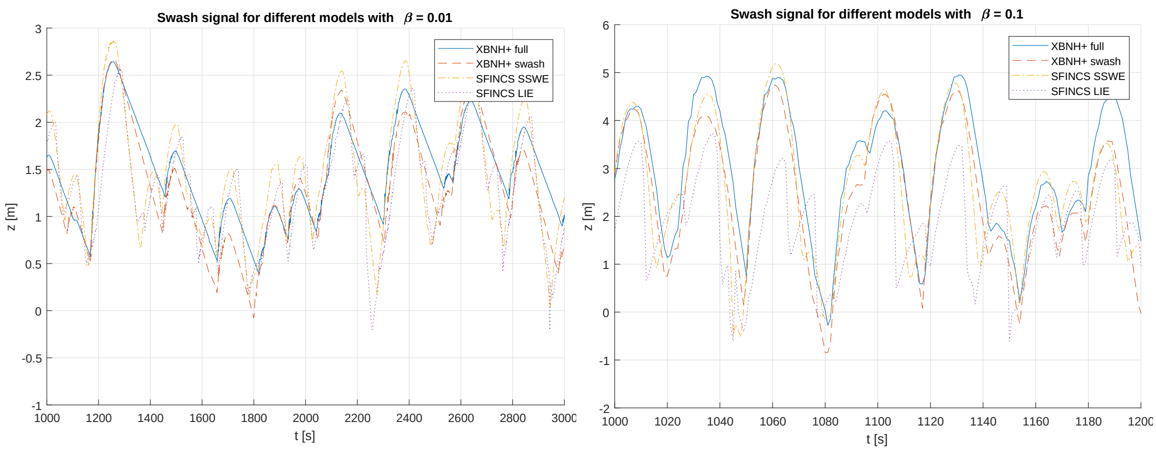

Figure C.13: Examples of swash signals with different swash zone models. Both for offshore conditions $H_s = 10m$ and $T_p = 12s$. Left: $\beta = 0.01$, Right: $\beta = 0.1$

C.3.2. Reduction factor

From comparing the statistics of the R2% for different reduction factor (Table C.1) is was deemed that a 60% reduction (reduction factor 0.4) of the setup parametrisation is best.

Table C.1: Statistics per reduction factor of wave-induced setup parametrisation

Reduction factor	b	si	bias
0	0.7	0.32	-0.23
0.1	0.79	0.24	-0.15
0.2	0.89	0.15	-0.064
0.3	0.98	0.1	0.0082
0.4	1	0.11	0.071
0.5	1.1	0.15	0.13
0.6	1.2	0.2	0.18
0.7	1.2	0.26	0.24
0.8	1.3	0.31	0.3
0.9	1.3	0.37	0.35
1	1.4	0.42	0.4

C.3.3. Optimising grid resolution

In this section the maximum advised grid resolutions per slope are determined based on Table C.3. For the table with all the results per parameter, per slope there is shown what grid resolution is with the lowest absolute scatter index (showed in italic) and the absolute relative bias (showed in bold). For the optimum grid resolution in Table C.2, the grid resolution with the lowest absolute scatter index and relative bias is chosen. If two grid resolutions had the same value, the one with the lowest scatter was chosen. For the final conclusion there was judged what grid resolution per slope gave the overall best performance, which is showed in the last column of Table C.2.

Table C.2: Optimum grid resolution per parameter per slope

	Rmax	R2%	setup	setup>msl	Sig	Sinc	Conclusion
beta	dx,max	dx,max	dx,max	dx,max	dx,max	dx,max	dx,max
0.01	20	10	1	20	50	50	20
0.02	5	10	1	10	20	50	10
0.04	2	2	1	5	5	5	5
0.1	1	2	1	2	2	5	2

Table C.3: Statistical values per parameter per slope per grid resolution

Rmax							R2%							
	dx=1m		dx=2m		dx=5m				dx=1m		dx=2m		dx=5m	
beta	Scattter index	Relative bias	Scattter index	Relative bias	Scattter index	Relative bias		beta	Scattter index	Relative bias	Scattter index	Relative bias	Scattter index	Relative bias
0.01	0.24	0.17	0.22	0.15	0.16	0.08		0.01	0.20	0.18	0.19	0.17	0.13	0.10
0.02	0.17	0.14	0.17	0.07	0.15	**0.03**		0.02	0.21	0.19	0.18	0.15	0.13	0.07
0.04	0.16	0.08	0.16	**0.02**	*0.13*	-0.09		0.04	0.10	0.08	*0.05*	**0.02**	0.12	-0.11
0.1	*0.09*	**0.06**	0.15	-0.10	0.26	-0.23		0.1	0.09	0.07	*0.06*	**-0.05**	0.22	-0.21
	dx=10m		dx=20m		dx=50m				dx=10m		dx=20m		dx=50m	
beta	Scattter index	Relative bias	Scattter index	Relative bias	Scattter index	Relative bias		beta	Scattter index	Relative bias	Scattter index	Relative bias	Scattter index	Relative bias
0.01	0.14	**0.03**	*0.13*	-0.04	0.19	-0.17		0.01	*0.07*	**0.03**	0.08	-0.05	0.18	-0.18
0.02	*0.14*	-0.09	0.18	-0.15	0.30	-0.28		0.02	*0.08*	**-0.04**	0.14	-0.13	0.27	-0.26
0.04	0.22	-0.20	0.31	-0.29	0.45	-0.43		0.04	0.20	-0.20	0.31	-0.30	0.44	-0.43
0.1	0.35	-0.33	0.48	-0.46	0.58	-0.55		0.1	0.34	-0.33	0.47	-0.46	0.55	-0.53
setup							setup>MSL							
	dx=1m		dx=2m		dx=5m				dx=1m		dx=2m		dx=5m	
beta	Scattter index	Relative bias	Scattter index	Relative bias	Scattter index	Relative bias		beta	Scattter index	Relative bias	Scattter index	Relative bias	Scattter index	Relative bias
0.01	*0.06*	**-0.01**	0.07	-0.02	0.11	-0.08		0.01	0.16	0.15	0.15	0.14	0.11	0.09
0.02	0.06	**0.00**	*0.06*	-0.04	0.13	-0.12		0.02	0.18	0.17	0.14	0.13	0.09	0.08
0.04	*0.06*	**-0.03**	0.10	-0.08	0.22	-0.20		0.04	0.16	0.15	0.11	0.10	*0.05*	**0.00**
0.1	*0.09*	**-0.07**	0.18	-0.16	0.33	-0.31		0.1	0.11	0.09	*0.06*	**0.01**	0.13	-0.11
	dx=10m		dx=20m		dx=50m				dx=10m		dx=20m		dx=50m	
beta	Scattter index	Relative bias	Scattter index	Relative bias	Scattter index	Relative bias		beta	Scattter index	Relative bias	Scattter index	Relative bias	Scattter index	Relative bias
0.01	0.17	-0.15	0.26	-0.25	0.35	-0.32		0.01	0.07	0.04	*0.06*	**-0.01**	0.12	-0.10
0.02	0.23	-0.21	0.33	-0.31	0.43	-0.40		0.02	*0.05*	**0.00**	0.08	-0.06	0.18	-0.16
0.04	0.31	-0.30	0.40	-0.38	0.52	-0.49		0.04	0.09	-0.07	0.16	-0.14	0.25	-0.23
0.1	0.42	-0.40	0.54	-0.51	0.61	-0.58		0.1	0.22	-0.20	0.30	-0.28	0.34	-0.32
Sig								Sinc						
	dx=1m		dx=2m		dx=5m				dx=1m		dx=2m		dx=5m	
beta	Scattter index	Relative bias	Scattter index	Relative bias	Scattter index	Relative bias		beta	Scattter index	Relative bias	Scattter index	Relative bias	Scattter index	Relative bias
0.01	0.40	0.37	0.40	0.37	0.34	0.31		0.01	1.83	1.18	1.83	1.47	1.25	1.03
0.02	0.34	0.31	0.29	0.26	0.25	0.20		0.02	2.35	2.01	1.62	1.29	0.65	0.49
0.04	0.21	0.19	0.15	0.12	*0.07*	**0.01**		0.04	1.15	1.07	0.69	0.61	*0.16*	**0.09**
0.1	0.08	0.07	*0.06*	**-0.04**	0.21	-0.20		0.1	0.45	0.42	0.27	0.23	*0.15*	**0.04**
	dx=10m		dx=20m		dx=50m				dx=10m		dx=20m		dx=50m	
beta	Scattter index	Relative bias	Scattter index	Relative bias	Scattter index	Relative bias		beta	Scattter index	Relative bias	Scattter index	Relative bias	Scattter index	Relative bias
0.01	0.29	0.26	0.24	0.21	*0.11*	**0.04**		0.01	1.16	0.98	0.99	0.94	*0.86*	**0.84**
0.02	0.15	0.10	*0.10*	**0.03**	0.17	-0.15		0.02	0.64	0.33	0.23	0.11	*0.22*	**0.03**
0.04	0.11	-0.09	0.21	-0.20	0.37	-0.36		0.04	0.17	-0.12	0.24	-0.22	0.32	-0.24
0.1	0.34	-0.33	0.46	-0.45	0.57	-0.56		0.1	0.18	-0.09	0.29	-0.24	0.24	-0.17

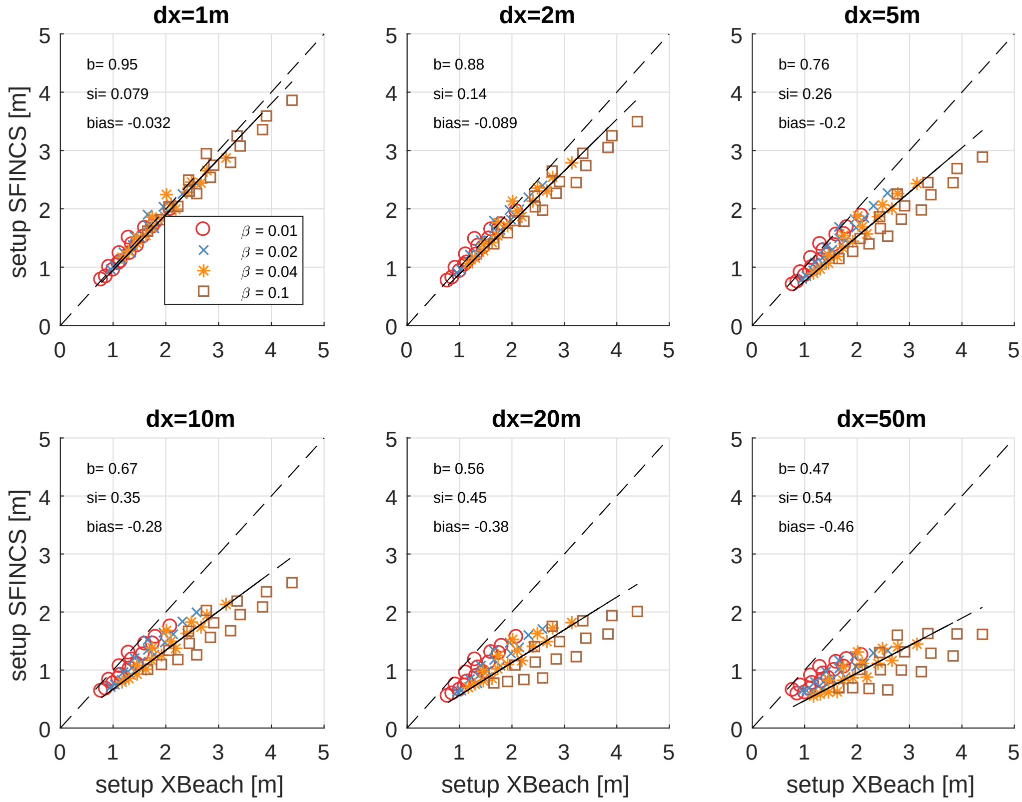

Figure C.14: Setup of SFINCS compared to XBeach for the limited data set, per grid resolution

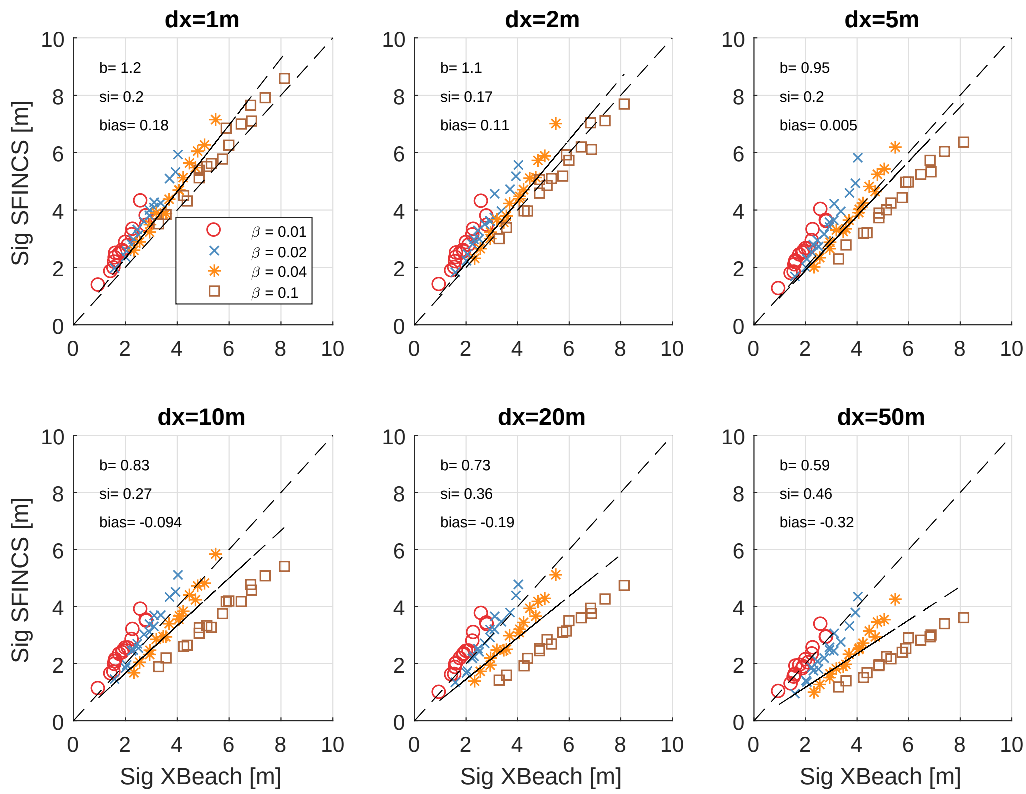

Figure C.15: Significant infra-gravity swash Sig of SFINCS compared to XBeach for the limited data set, per grid resolution

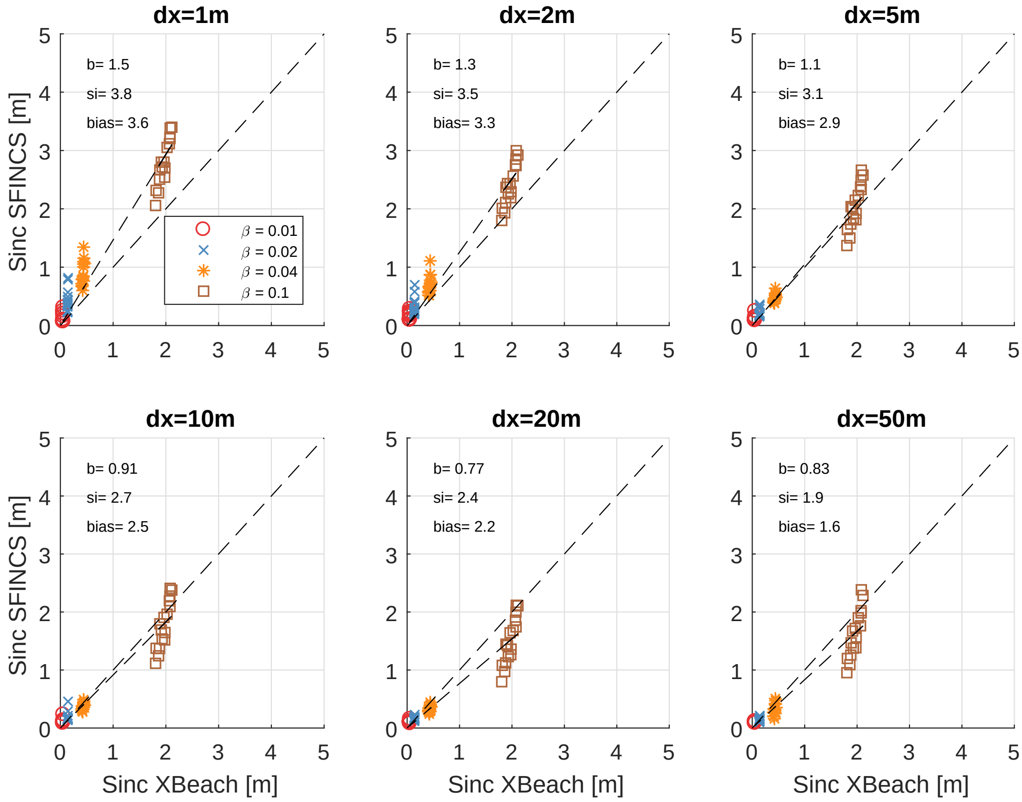

Figure C.16: Significant incident swash Sinc of SFINCS compared to XBeach for the limited data set, per grid resolution

D Conceptual tests other processes

A few simple tests are performed to check whether the implementation of infiltration (Section D.1), discharge (Section D.2), precipitation (Section D.3) and wind-induced setup (Section D.4) are working correctly.

D.1. Infiltration

D.1.1. Numerical setup

A test is performed using a 100 x 100 m basin with a grid size of 1 m. The domain contains vertical boundaries without flux and an initial water level of 1 m is introduced. As a realistic infiltration rate $q_{inf} = -20 mm/hr = -5.55 \cdot 10^{-5} m^3/s$ is used which means that the basin should be empty in 5 hours.

D.1.2. Accuracy

With the output from an observation point in the middle of the domain is shown and compared to the theoretical water level using the same q_{inf}, the following is obtained:

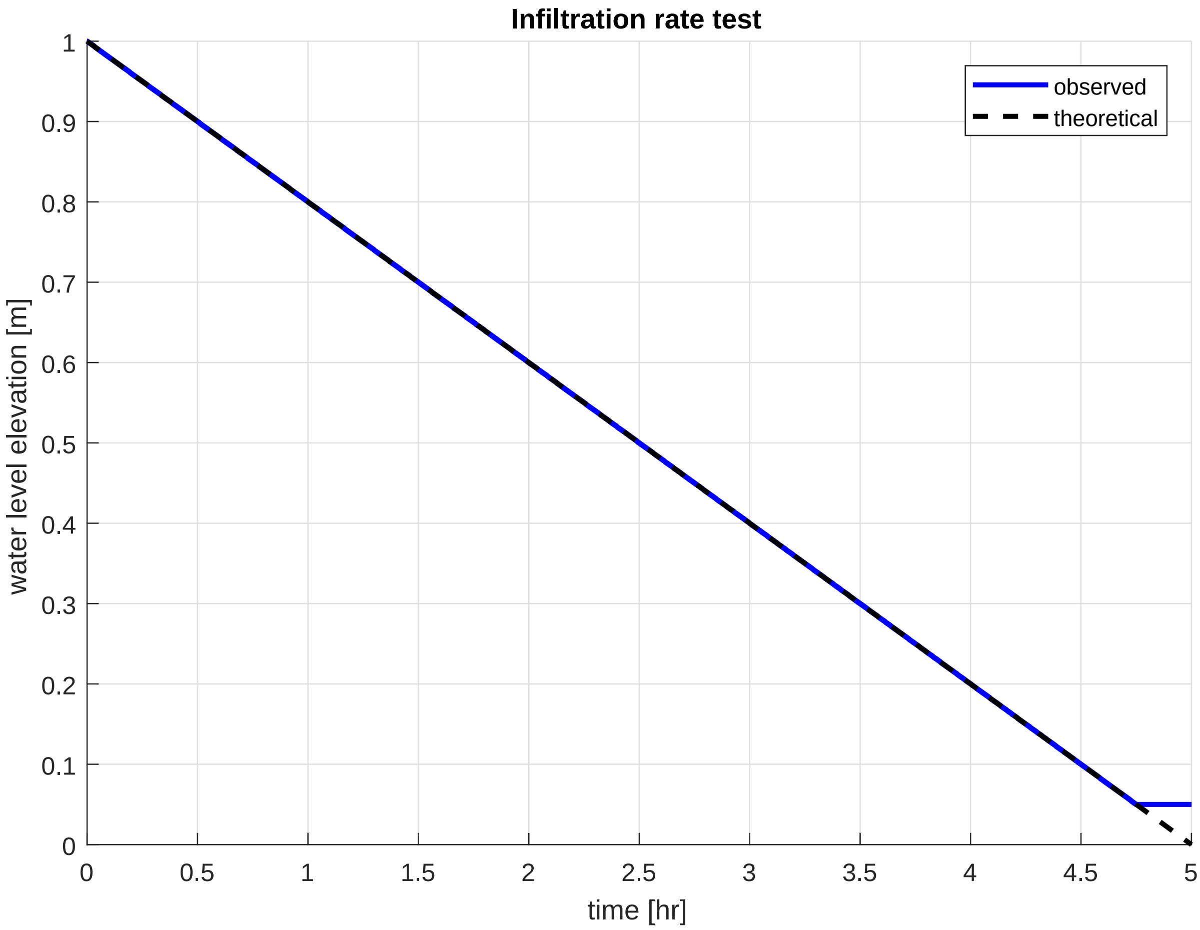

Figure D.1: Observed and theoretical water levels for the infiltration test

There can be seen in FIgure D.1 that the water level in SFINCS is reduced as intended until a water level of 0.05 m. This is equal to the value of the limiter $h_{u,thresh}$ (see Section 3.4.1), which means that this is implemented correctly.

D.2. Discharge points

In the end the implementation of discharge points is not used within the Jacksonville case study, but it is tested anyhow.

D.2.1. Numerical setup

A test has been performed using the same 100 x 100 m basin with a grid size of 1 m. The domain contains vertical boundaries without flux and an initial water level of 0 m is present. Four discharge points with a discharge rate of $q_{src} = 100 * 100/(5 * 3600 * 4) = 0.14 m^3/s$ are used which means that the basin should be filled to 1 m height in 5 hours.

D.2.2. Accuracy

With a observation point in the middle of the domain (so not at the location of a discharge point), it can be observed in Figure D.2 that it takes some time before the water reaches the observation point.

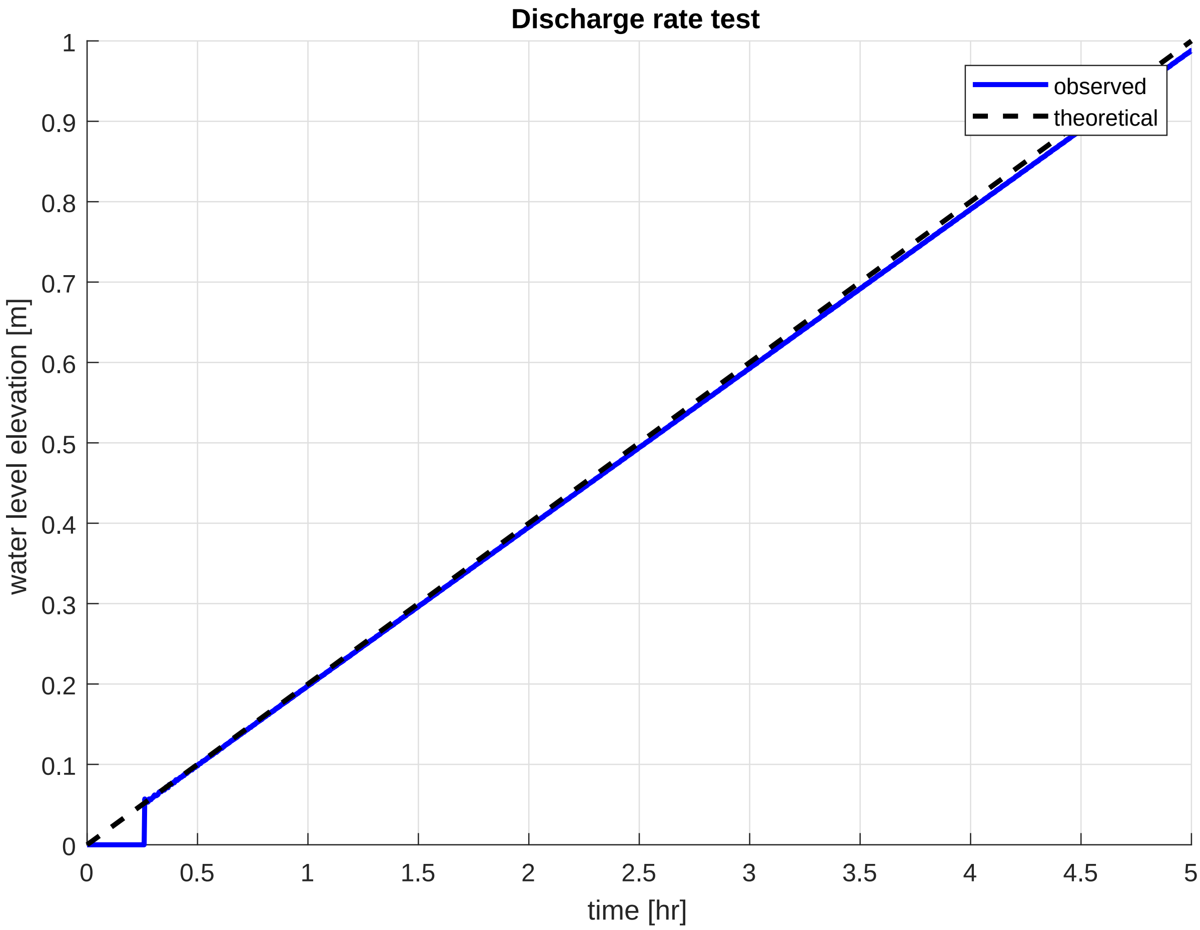

Figure D.2: Observed and theoretical water levels for the discharge test

The filling of the basin starts at the discharge points where immediately the water level is higher then the flow limiter $h_{u,thresh} = 0.05m$ (default). From those points the water starts spreading into the rest of the model where it reaches the middle of the domain after some time. After the disturbance from the initial wetting fades away and the whole model starts filling almost uniformly. Hereby the water level at the middle of domain has a slight lag compared to the water level at the discharge points. Therefore the discharge points are implemented correctly, but for implementation in real cases it has to be taken into account that the current implementation does not included momentum fluxes (see Section 3.4.3).

D.3. Precipitation

D.3.1. Numerical setup

A test has been performed using a 100 x 100 m basin with a grid size of 1 m. The domain contains vertical boundaries without flux and the initial water level is 0 m. In this case a constant precipitation rate of $w_{prcp} = 20mm/hr$ is introduced, which means that the water level should be at 1 m after 5 hours.

D.3.2. Accuracy

When now the output from an observation point in the middle of the domain is shown and compared to the theoretical water level using the same w_{prcp}, the following is obtained:

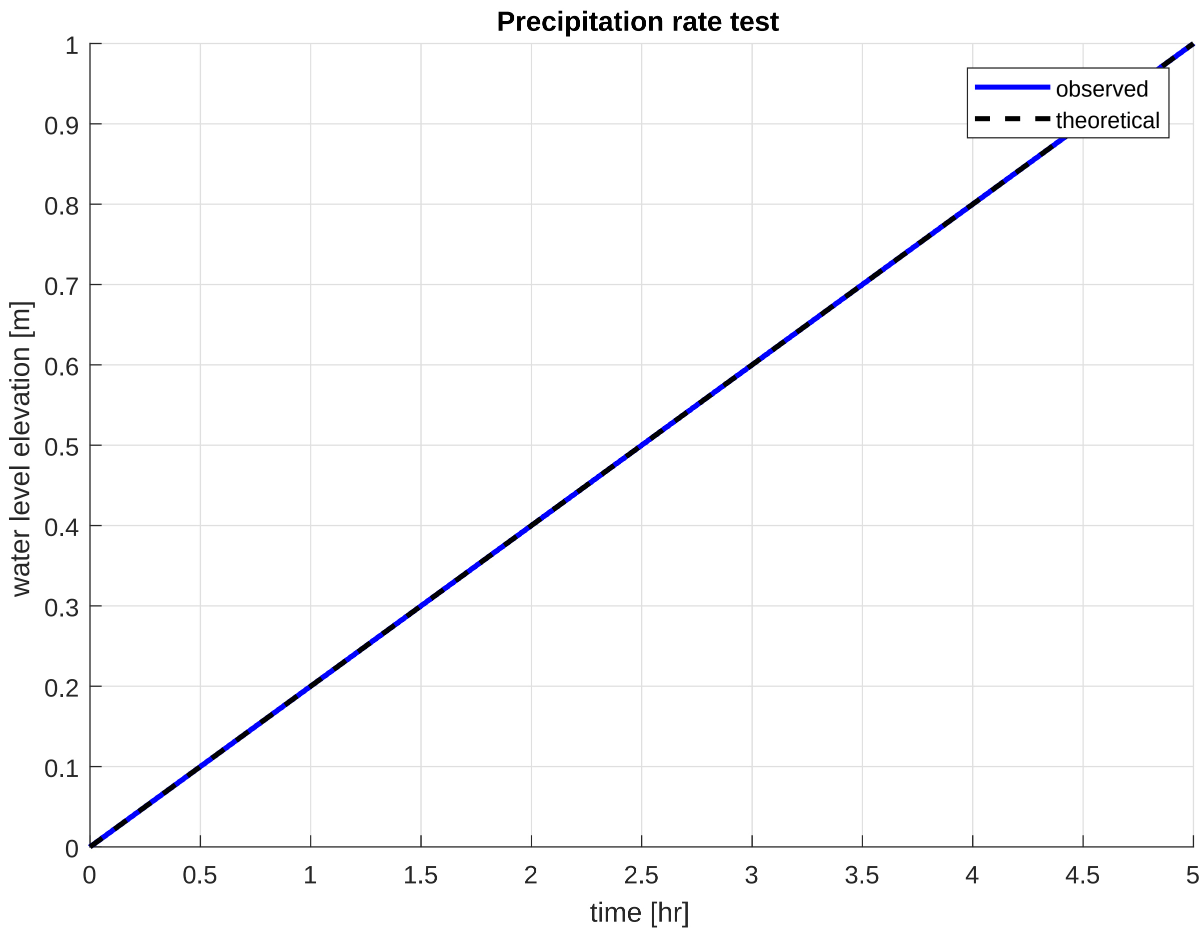

Figure D.3: Observed and theoretical water levels for the precipitation test

There can be seen in Figure D.3 that the water level in SFINCS rises to 1 m height, which means that this is implemented correctly.

D.4. Wind-induced setup

A test is performed comparing the wind-induced setup in a long, shallow basin between the analytical solution, SFINCS and XBeach. In the sequential section the analytical solution and the numerical setup of both models is discussed. Thereafter the model results are shown.

D.4.1. Analytical solution

The equilibrium condition is given as follows (Bosboom and Stive, 2015):

$$\rho_w g h \frac{d\bar{\eta}}{dx} = \tau_{wind,x} \tag{D.1}$$

The equation shows that the wind set-up is inversely proportional to the water depth. Hence, in for shallow water depths water can pile up to great heights (storm surge). The shear stress by the wind on a water body generally speaking consists of a drag force coefficient, the density of air and the wind speed W squared:

$$\tau_{wind,x} = C_d \rho_a W^2 \tag{D.2}$$

D.4.2. Numerical setup SFINCS

The numerical setup of the test in SFINCS is a 10 km long, 100 m wide and 5 m deep rectangular basin with a grid resolution of 10 m. The model consists of vertical walls so the water level can pile up and create a wind-induced setup. It was found that it is important to increase the wind speed vary gradually to reach the equilibrium condition. The maximum applied wind speed is 25 m/s and is spatially uniform. The air density is set by default to $\rho_a = 1.25 kg/m^3$ and the water density to $\rho_w = 1024 kg/m^3$. For both cases a bed friction coefficient of $n = 0.03 s/m^{1/3}$ is used and the total runtime is 12 hours.

D.4.3. Numerical setup XBeach

The same setup is included in XBeach, with the only difference the way C_d is specified. Differently then in SFINCS you have to directly specify a value for the coefficient yourself. This is done with $C_d = 0.0028(-)$ (default normally is $C_d = 0.002$), which is the value in SFINCS for a wind speed of 25 m/s. In XBeach it is not possible to impose spatially varying wind speeds if you wanted to.

D.4.4. Accuracy

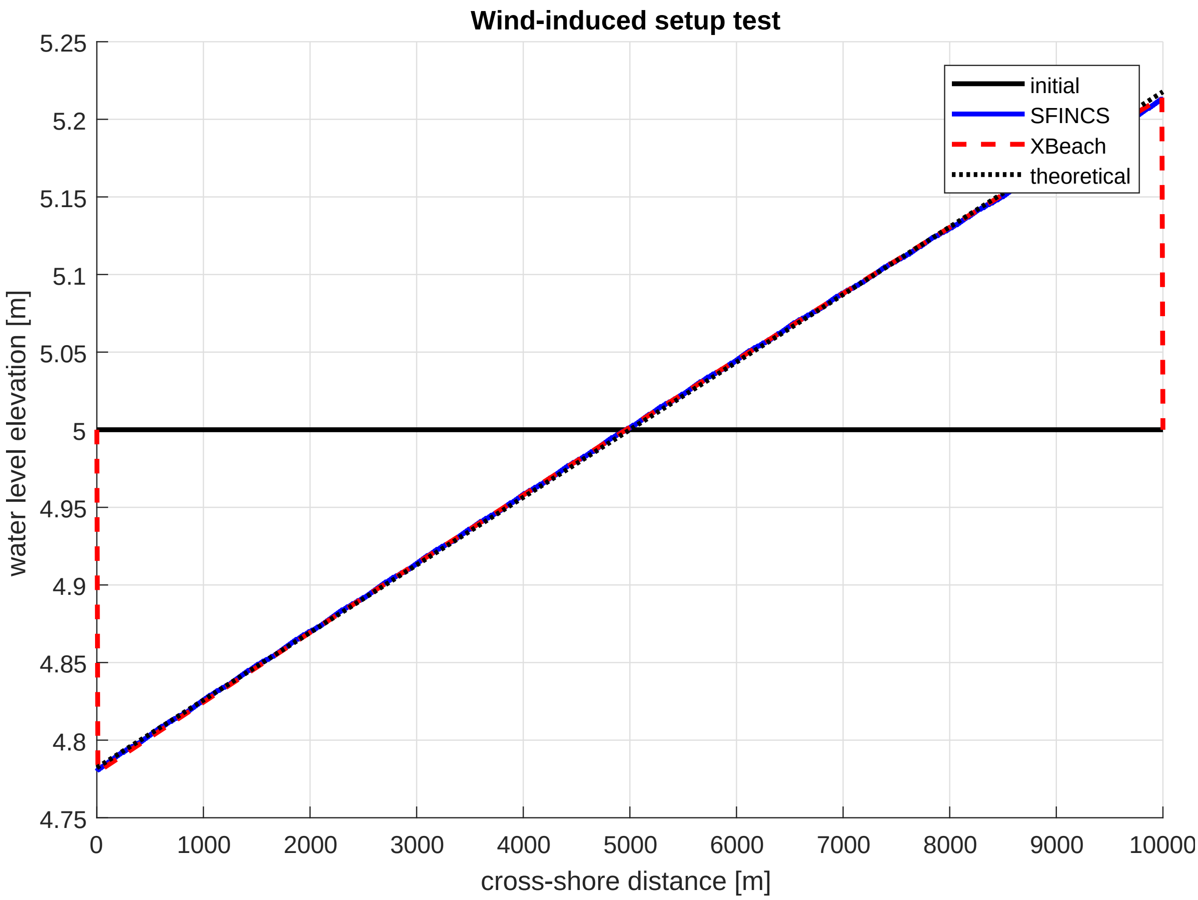

Figure D.4: Observed and theoretical water levels in time for the wind-induced setup test

Figure D.4 shows that the water levels modelled by SFINCS and XBeach both give the same wind-induced setup (0.223 m) as one would expect from the analytical solution. The results vary very slightly compared to the analytical solution, but that is an artefact of the wind setup/stress that is building up and not spread immediately through the whole domain. Thereby there is a little bit of reflection at the end of the domain. Also you can notice that for XBeach you have red vertical lines on both sides of the domain, this is because the water level is kept at the initial water level for the boundary grid points.

E

Hernani case study

This appendix contains additional figures regarding the model setup and results of the Hernani case study of the 1D transect in Section E.1 and of the 2D model in Section E.2.

E.1. 1D transect

Figure E.1 shows on the left the location of the 1D transect on the left side, the location is chosen similar to Roeber and Bricker (2015). On the right hand side the bathymetry of the full XBNH model is showed, as well as the SFINCS model that starts at 0 m+MSL.

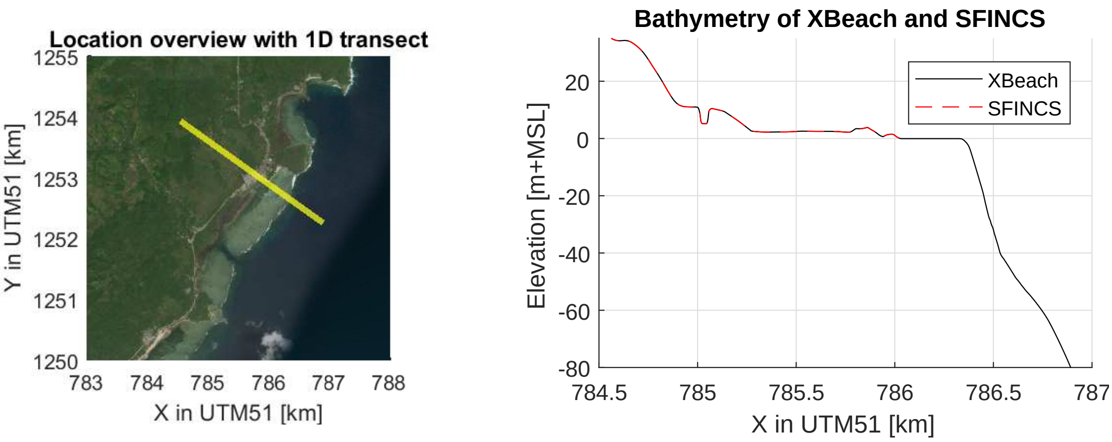

Figure E.1: Location and bed levels of 1D transect for Hernani case study. Left: location of the 1D transect, Right: bathymetry of XBeach and SFINCS models

Figure E.2 shows on the left the input water level time-series of SFINCS, as retrieved from the 1D XBeach model at the location of the SFINCS boundary. On the right the corresponding wave spectra is shown. It can be seen the wave spectrum solely consists of IG waves ($f < 0.04Hz$).

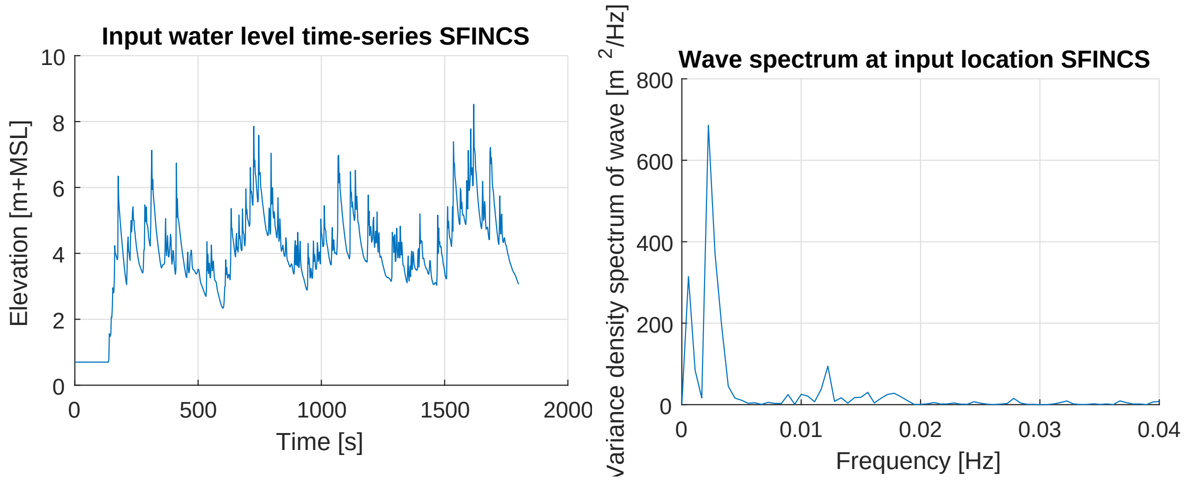

Figure E.2: Input time-series and waves spectra of SFINCS for the 1D transect. Left: water level time-series at the SFINCS boundary, Right: corresponding wave spectrum.

E.2. 2D model

Figure E.3 shows the created input time-series for the 2D SFINCS models with indirect forcing. Hereby the time-series of all input locations are shown (see Figure 5.2). On the left the time-series is shown of the variant where every time-series at every location has different sets of random phases 'random phase'. On the right the same figure is shown, but there the phases per bin are kept the same for every time-series and every location 'uniform phase'. Hereby only the amplitudes are different between the time-series of the different locations.

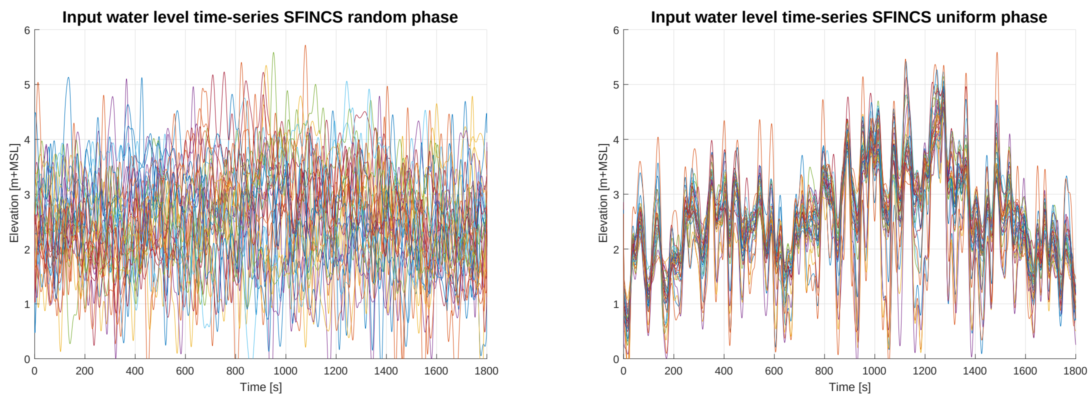

Figure E.3: Input time-series of SFINCS for the 2D model. Left: indirect forcing with random phase, Right: indirect forcing with uniform phase

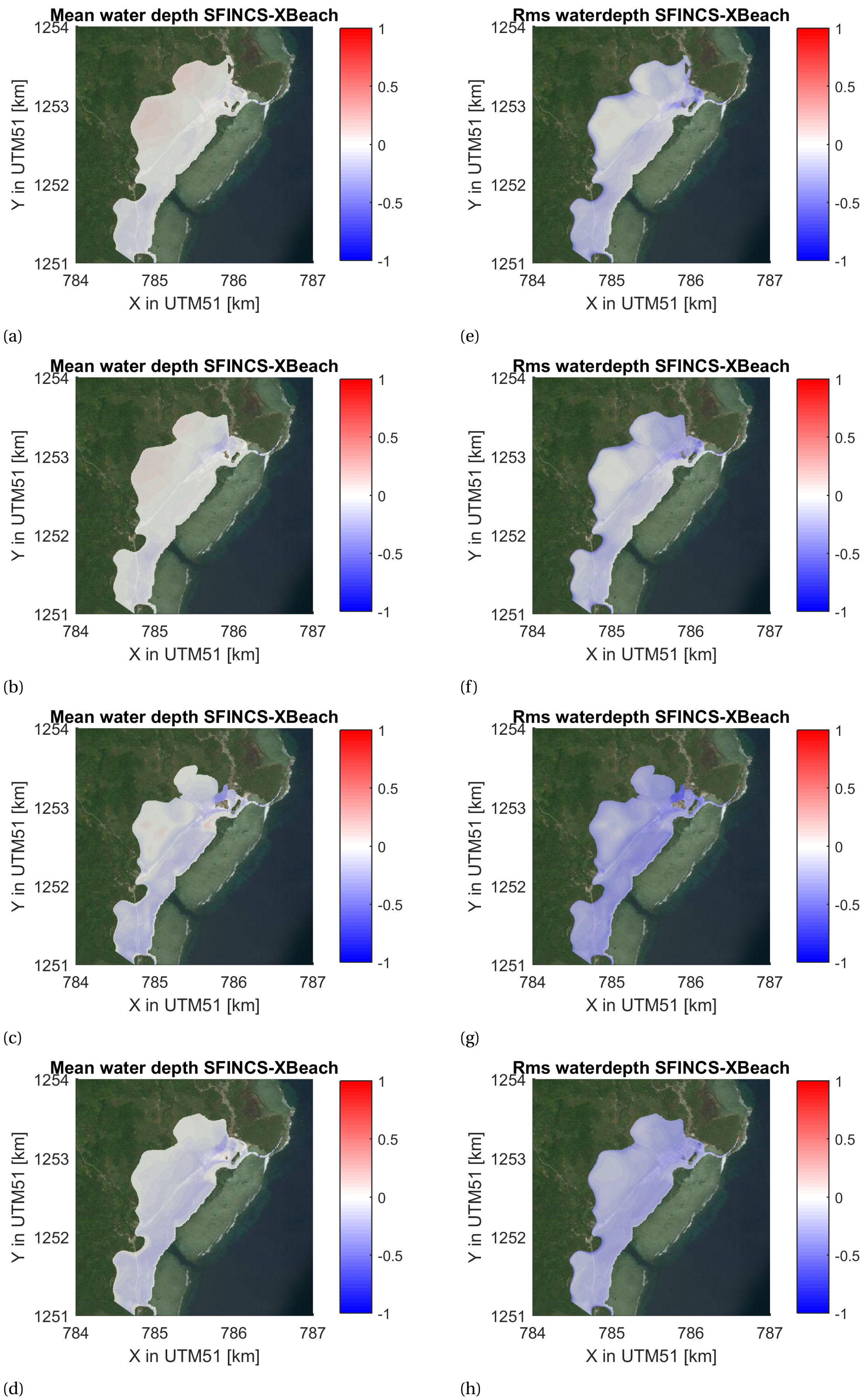

Figure E.4: Mean and rms of water depths SFINCS and compared to XBeach. a & e: SFINCS-LIE with real forcing, b & f: SFINCS-SSWE with real forcing, c & g: SFINCS-SSWE with completely random indirect forcing and d & h SFINCS-SSWE with random indirect forcing but equal phases.

F

Jacksonville case study

This appendix contains more information regarding the model setup of the Jacksonville case study in Section F.1 and the figures of the model validation of the overall and intermediate Delft3D models in Section F.2. There is concluded with figures regarding the detailed models in Section F.3.

F.1. Model setup

F.1.1. Delft3D

Overall model:

- Delft3D-FLOW and -WAVE (SWAN non-stationary)
- Offshore forcing: water levels via tidal re-analysis, no waves
- Wind: NARR + NHC spiderweb of best track. Wind drag coefficient as is Vatvani et al. (2012)(see Section 3.4.4), same for all models including SFINCS.
- Pressure: NARR
- Bathymetry: Coastal Relief Model (CRM) + General Bathymetric Chart of Oceans (GEBCO) through Delft Dashboard (van Ormondt et al., 2017)
- Grid: equidistant, 0.1 x 0.1 degrees (10 km), 350 x 200 cells
- Roughness: spatially varying; manning $n = 0.08 s/m^{1/3}$ on land (bed level>0m+MSL) and $n = 0.024 s/m^{1/3}$ elsewhere
- Numerical settings: dryflc=0.1 m, Dpsopt= MAX, Dpuopt= MEAN_DPS, Cyclic solver
- Duration model: September 01 to September 15, 2017

Intermediate model:

- Delft3D FLOW and WAVE (SWAN non-stationary)
- Offshore forcing: water levels nested from overall model, waves nested from overall model (toch?)
- Precipitation: NARR + 40%
- Wind: NARR + NHC spiderweb of best track
- Pressure: NARR
- Bathymetry: CRM + National Elevation Dataset (NED)
- Grid: equidistant, 0.01 x 0.01 degrees (1 km), 610 x 910 cells

- Roughness: spatially varying; manning $n = 0.06 s/m^{1/3}$ on land (bed level>0m+MSL) and $n = 0.02 s/m^{1/3}$ elsewhere
- Numerical settings: dryflc=0.02 m, Dpsopt= MAX, Dpuopt= MEAN_DPS, Cyclic solver
- Duration model: September 05 to September 15, 2017

Detailed model:

- Delft3D FLOW (4)
- Offshore forcing: water levels nested from intermediate model
- Precipitation: spatially varying, NARR
- Wind: spatially varying, NARR + spiderweb NHC
- Pressure: NARR
- River forcing: water level nested from intermediate model
- Infiltration: 5 mm/hr
- Bathymetry: CRD + NED + navigation charts between Jacksonville and the mouth of the St. Johns river
- Grid: equidistant, 100 x 100 m, 1100 x 1300 cells
- Roughness: spatially varying; manning $n = 0.06 s/m^{1/3}$ on land (bed level>0m+MSL) and $n = 0.02 s/m^{1/3}$ elsewhere
- Numerical settings: dryflc=0.02 m, Dpsopt= MEAN, Dpuopt= MEAN_DPS, Cyclic solver
- Duration model: September 09 to September 15, 2017

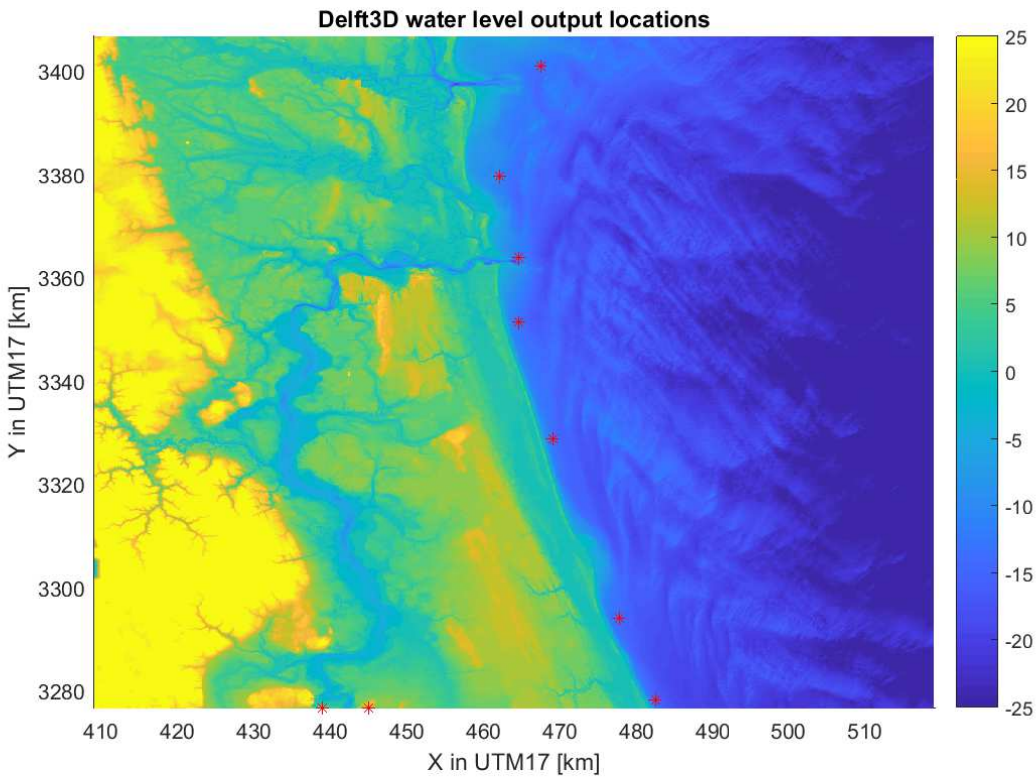

Figure F.1: Depth-file of Delft3D with water level output locations

F.1.2. SFINCS

Detailed model:

- SFINCS-LIE, no advection
- Offshore forcing: water levels nested from detailed Delft3D model close to the coast (see Figure F.1)
- Precipitation: spatially varying, NARR
- Wind: spatially varying, spiderweb NHC
- River forcing: water level nested from detailed Delft3D model (see Figure F.1)
- Infiltration: 5 mm/hr
- Bathymetry: CRD + NED + navigation charts between Jacksonville and the mouth of the St. Johns river
- Grid: equidistant, 100 x 100 m, 1102 x 1302 cells, hereby the offshore points lower than 2m with respect to MSL are not used (see Figure F.2). The number of active cells is 745126.
- Roughness: spatially varying; manning $n = 0.06s/m^{1/3}$ on land (bed level>0m+MSL) and $n = 0.02s/m^{1/3}$ elsewhere
- Numerical settings: $h_{u,thresh} = 0.02m$, $\alpha = 0.75$, $\theta = 0.9$
- Duration model: September 09 to September 15, 2017

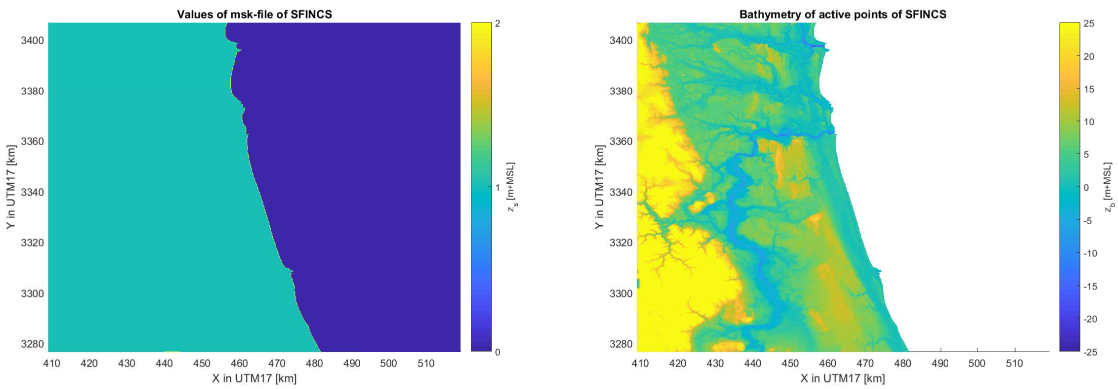

Figure F.2: Masker-file and depth-file of active points of SFINCS

F.1.3. Rain

NARR

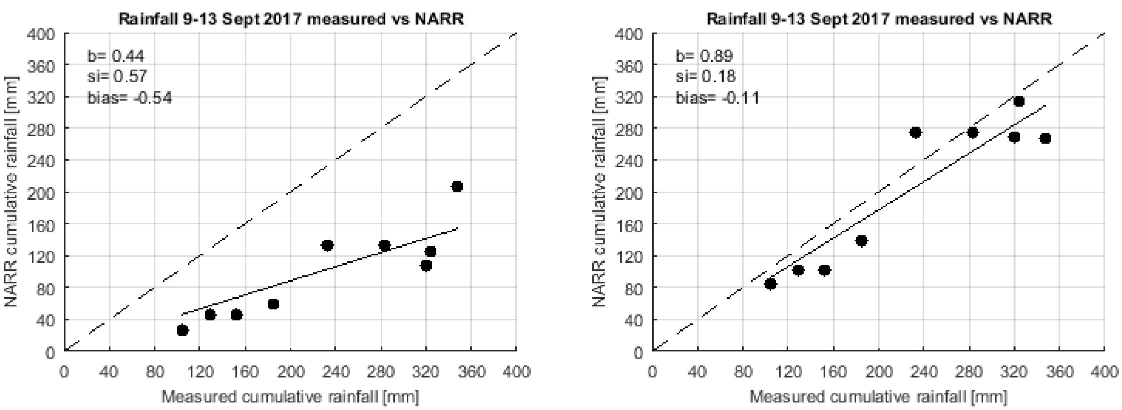

Figure F.3: Cumulative rainfall of NARR compared to measurements. Left: original NARR data, Right: NARR data with 40% more rain

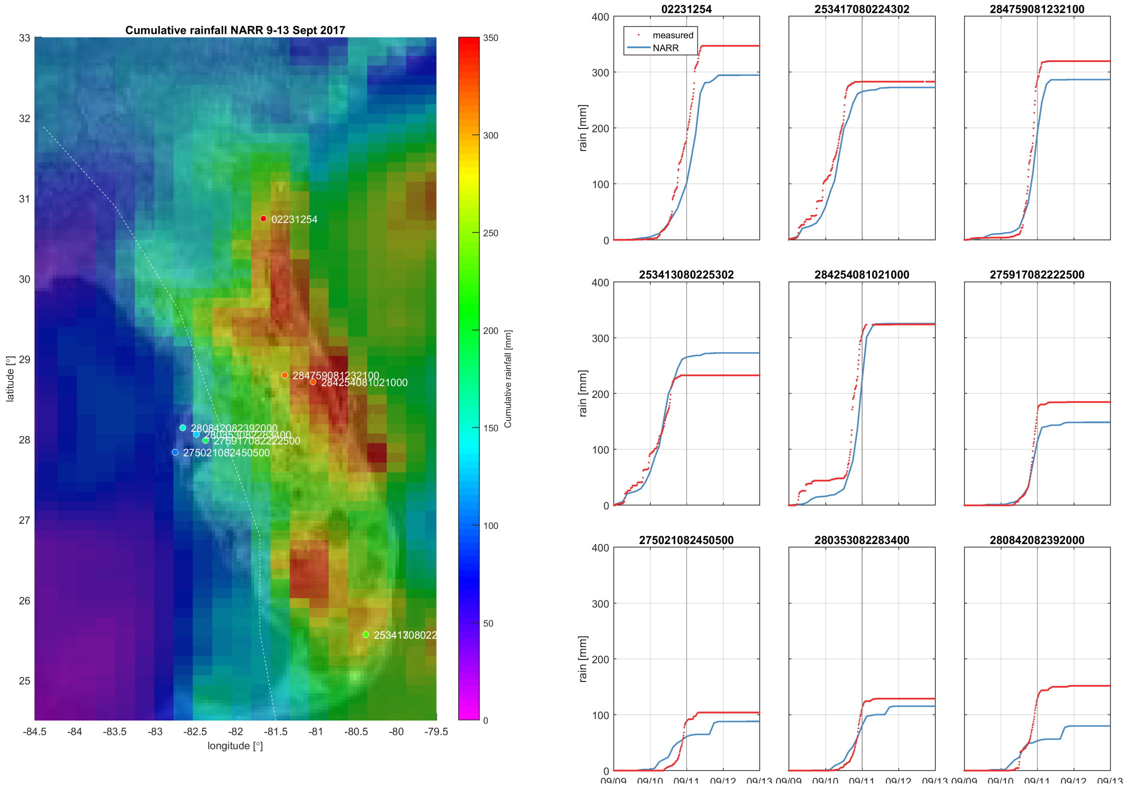

Figure F.4: Cumulative rainfall in intermediate from NARR data

F.2. Model validation Delft3D

Here all the figures of the validation of the wind, pressure, water levels and waves are displayed of the overall and intermediate model are displayed. Thereafter the maximum water levels of the detailed model are given

F.2.1. Wind

Overall model

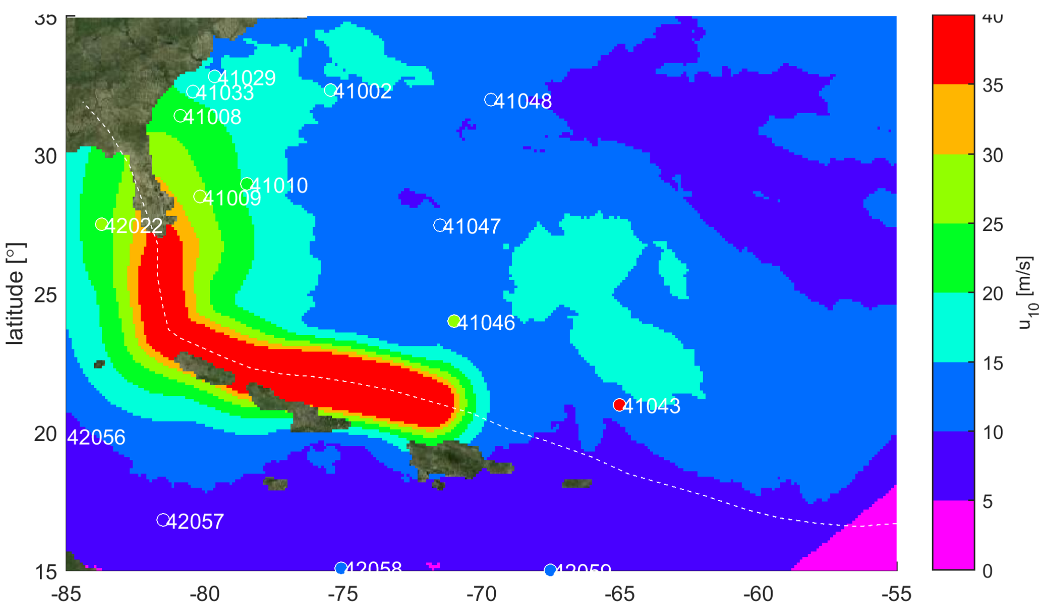

Figure F.5: Wind swath of overall model

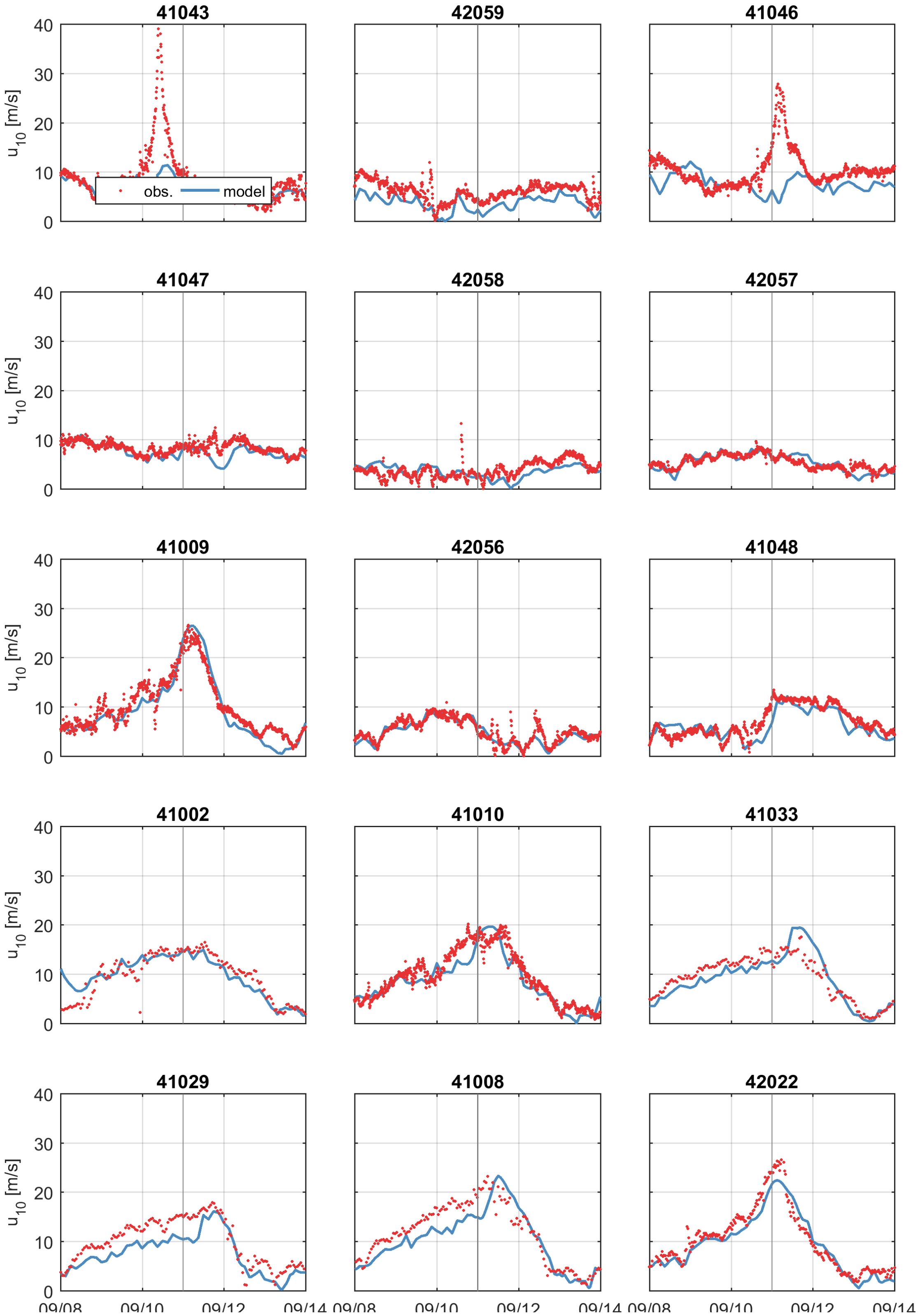

Figure F.6: Time-series of wind speeds of overall model

Intermediate model

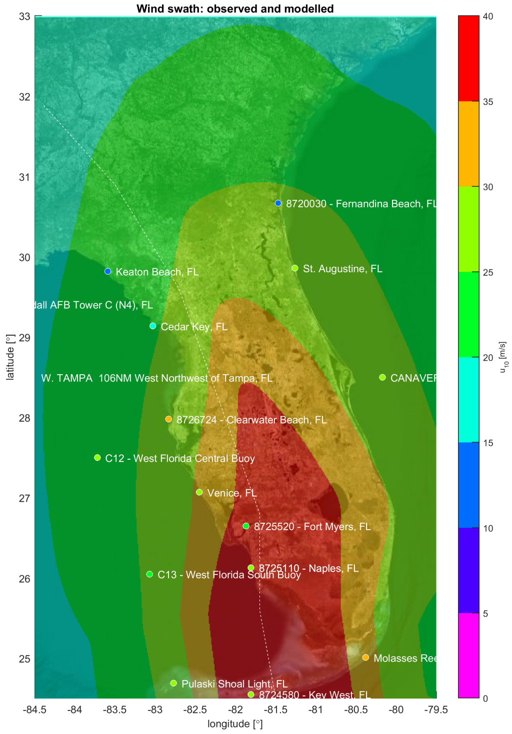

Figure F.7: Wind swath of intermediate model

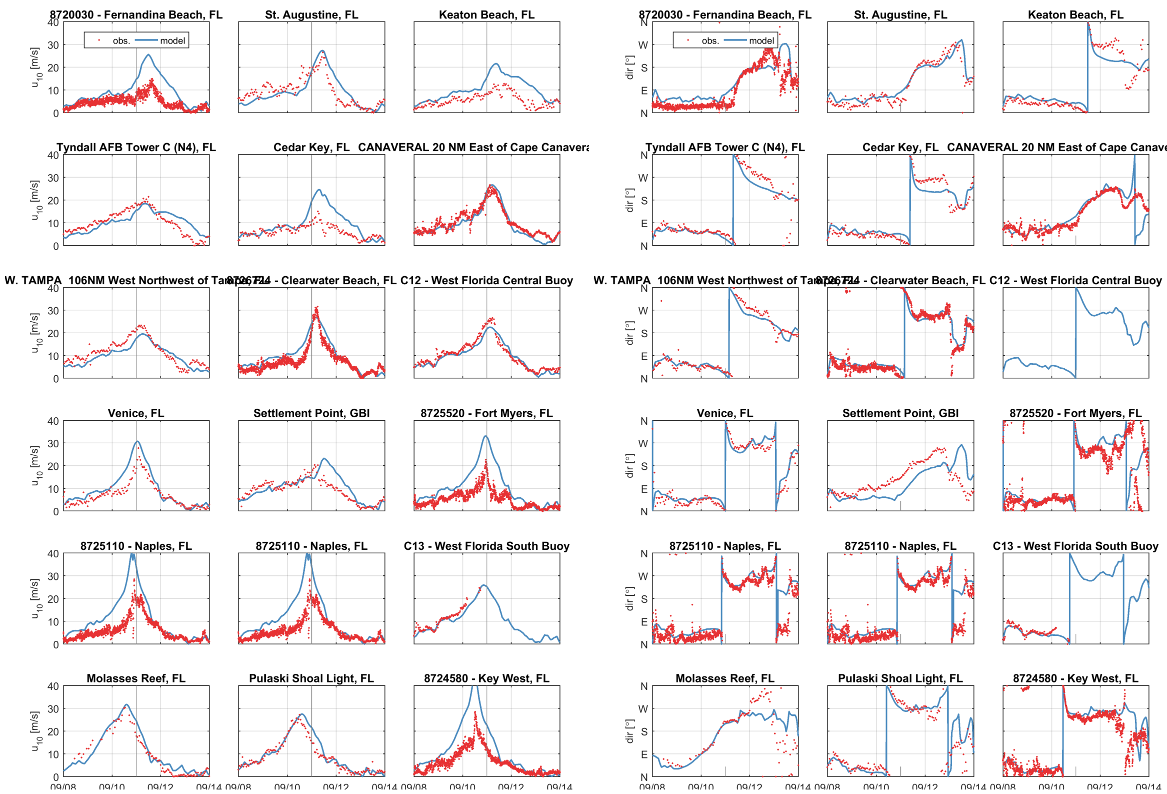

Figure F.8: Time-series of wind speeds and directions of intermediate model

F.2.2. Pressure

Overall model

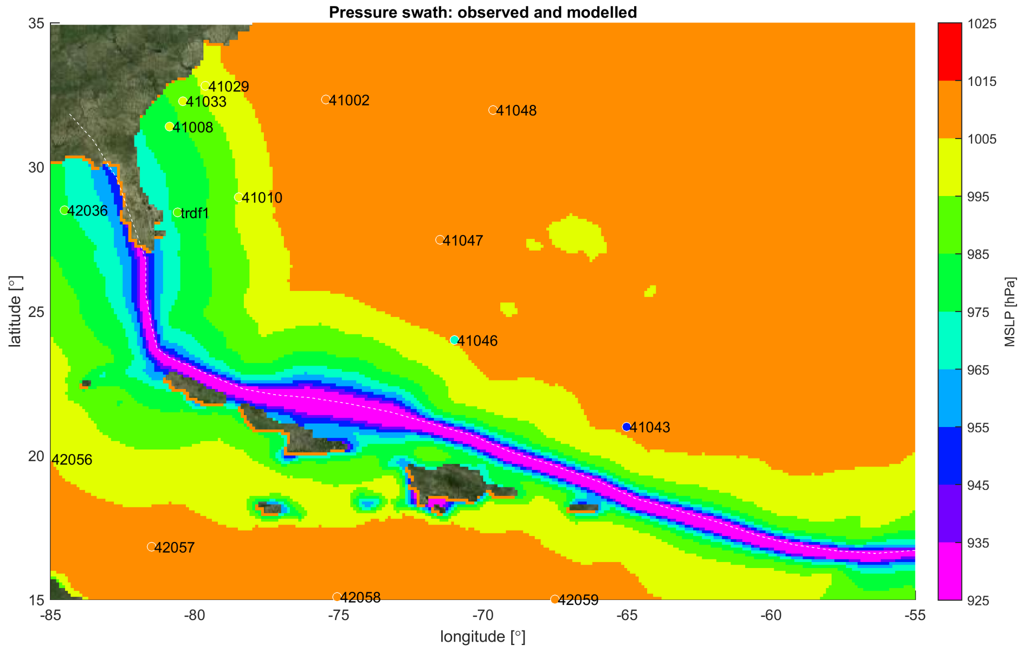

Figure F.9: Pressure swath of overall model

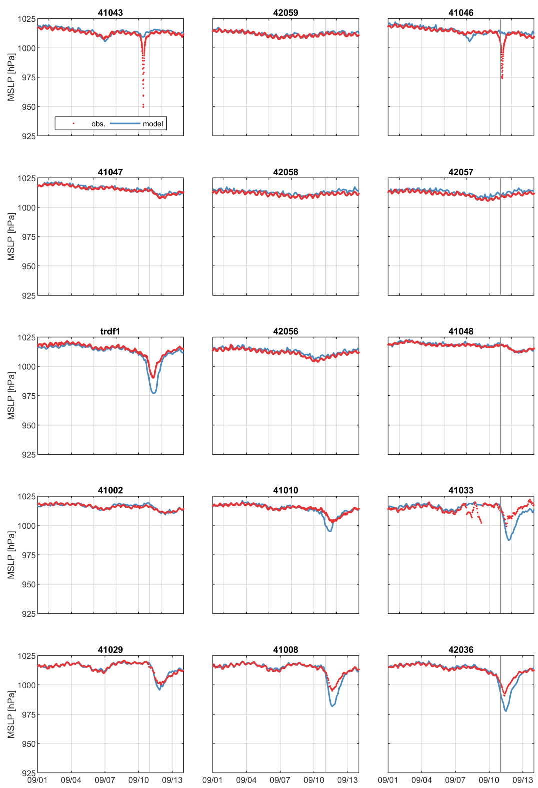

Figure F.10: Time-series of pressure swath of overall model

Intermediate model

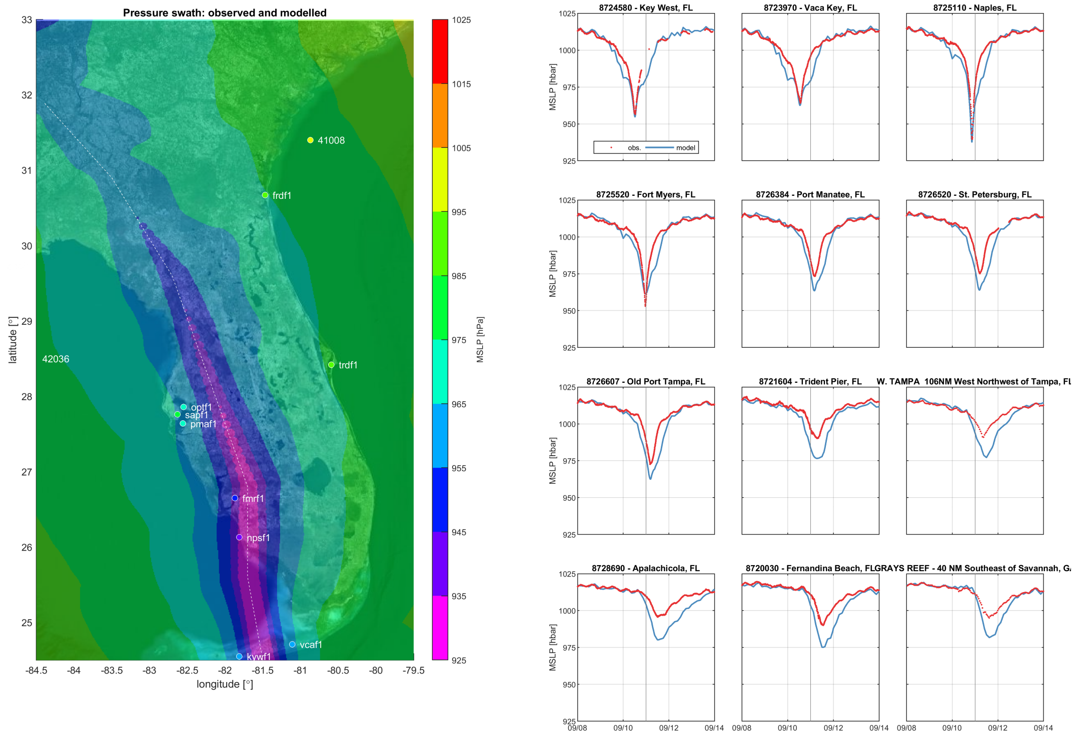

Figure F.11: Pressure swath of intermediate model

F.2.3. Water levels

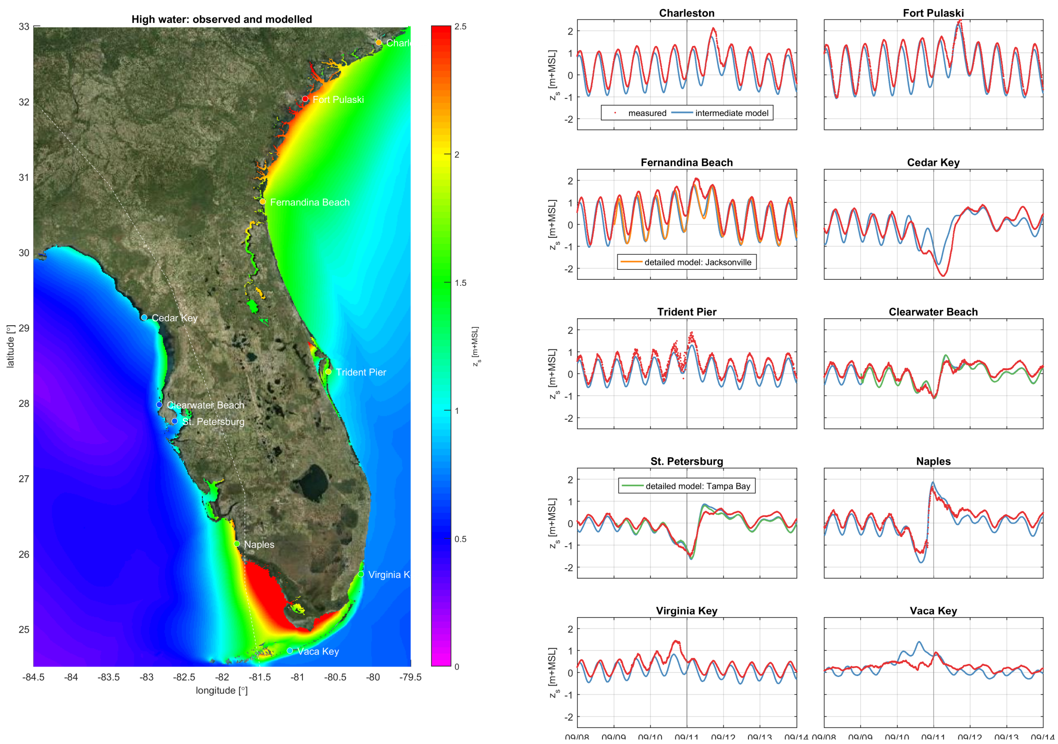

Figure F.12: Water levels intermediate model

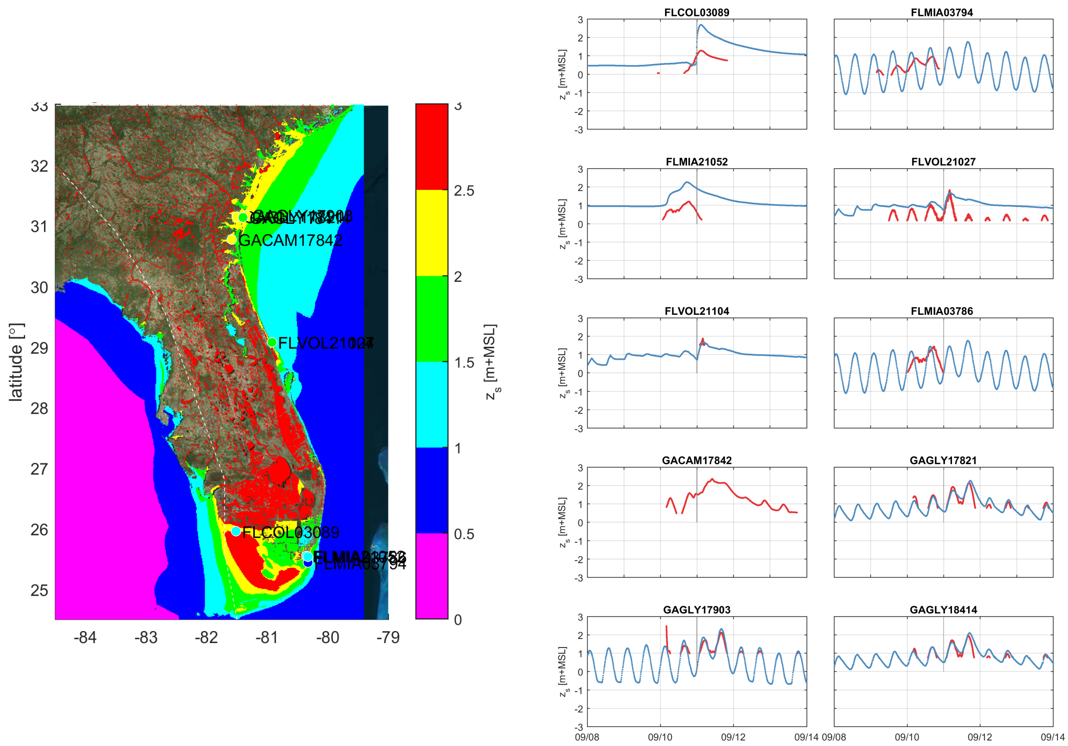

Figure F.13: Water levels intermediate model temporary USGS stations

F.2.4. Waves

Overall model

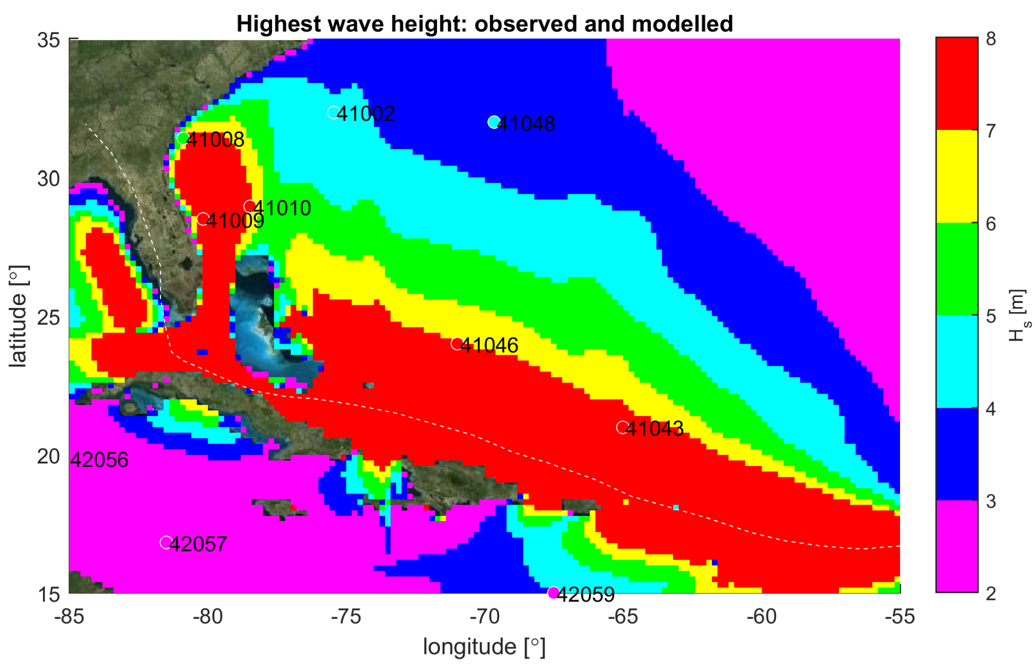

Figure F.14: Waves of overall model

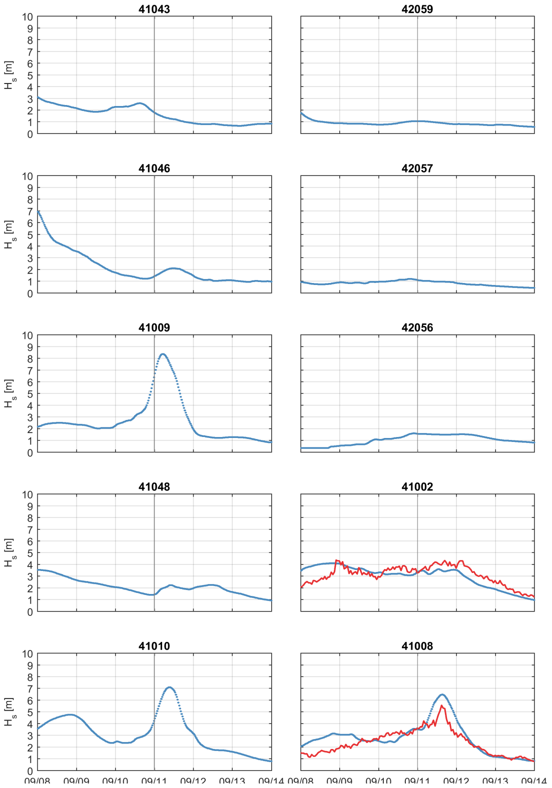

Figure F.15: Time-series of waves of overall model

Intermediate model

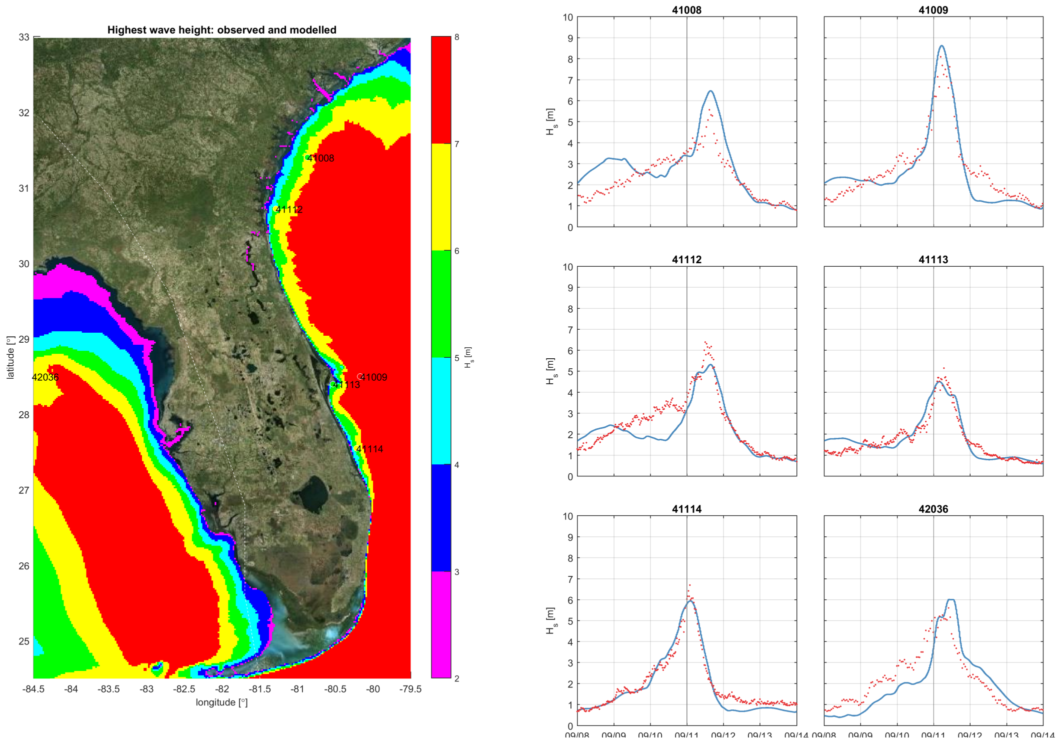

Figure F.16: Waves of intermediate model

F.3. Water levels detailed models

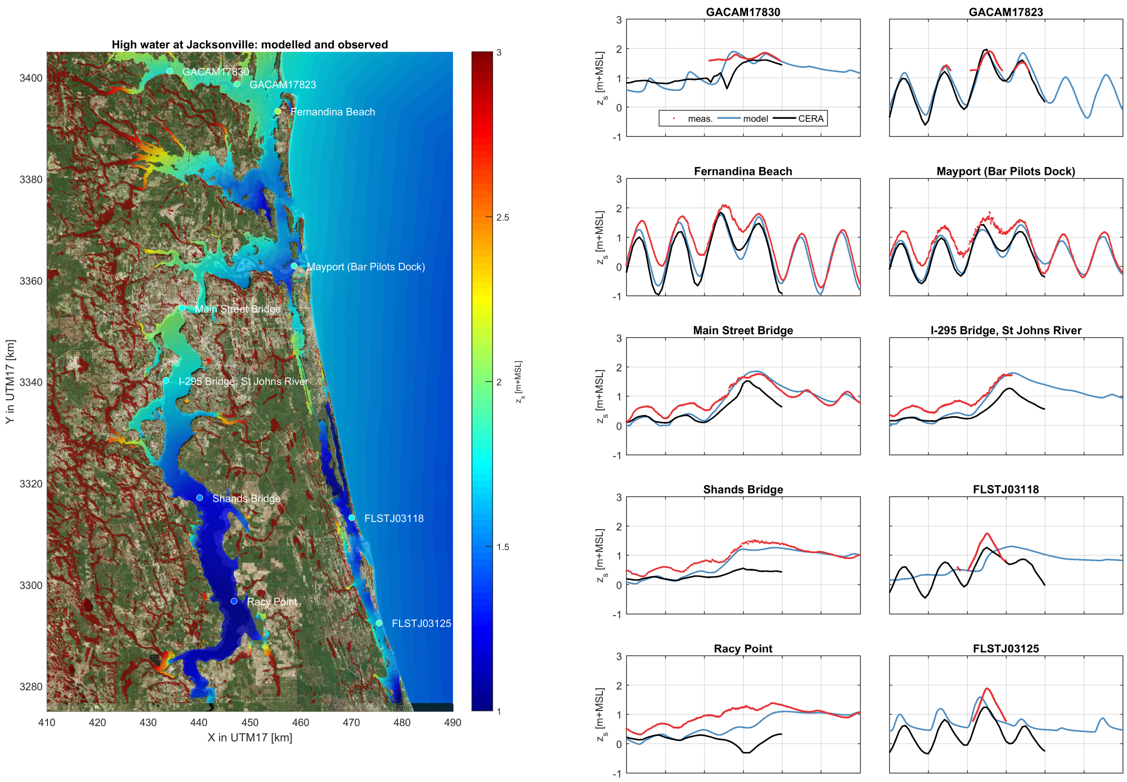

Figure F.17: Maximum water levels of detailed Delft3D model. The black line is of the CERA forecasting system (CERA, 2018)

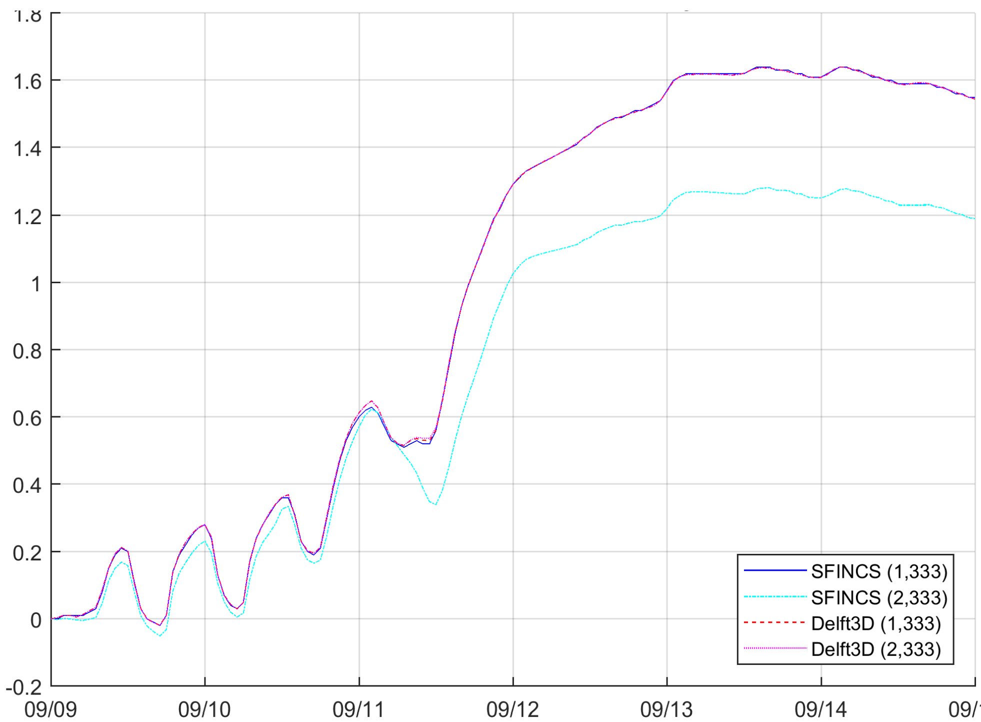

Figure F.18: Time-series of water levels at the southern boundary for Delft3D and SFINCS. Displayed are the boundary cell (1,333) and one cell north of that (2,333).